APEM *journal*

Advances in Production Engineering & Management

University of Maribor

Advances in Production Engineering & Management

Identification Statement

APEM Editorial

OPEN ACCESS

Statements and opinions expressed in the articles and communications are those of the individual contributors and not necessarily those of the editors or the publisher. No responsibility is accepted for the accuracy of information contained in the text, illustrations or advertisements. Chair of Production Engineering assumes no responsibility or liability for any damage or injury to persons or property arising from the use of any materials, instructions, methods or ideas contained herein.

Published by CPE, University of Maribor.

Advances in Production Engineering & Management

Contents

Scope and topics

Advances in Production Engineering & Management (*APEM journal*) is an interdisciplinary refereed international academic journal published quarterly by the *Chair of Production Engineering* at the *University of Maribor*. The main goal of the *APEM journal* is to present original, high quality, theoretical and application-oriented research developments in all areas of production engineering and production management to a broad audience of academics and practitioners. In order to bridge the gap between theory and practice, applications based on advanced theory and case studies are particularly welcome. For theoretical papers, their originality and research contributions are the main factors in the evaluation process. General approaches, formalisms, algorithms or techniques should be illustrated with significant applications that demonstrate their applicability to real-world problems. Although the *APEM journal* main goal is to publish original research papers, review articles and professional papers are occasionally published.

Fields of interest include, but are not limited to:

Additive Manufacturing Processes	Machine Learning in Production
Advanced Production Technologies	Machine-to-Machine Economy
Artificial Intelligence in Production	Machine Tools
Assembly Systems	Machining Systems
Automation	Manufacturing Systems
Big Data in Production	Materials Science, Multidisciplinary
Block Chain in Manufacturing	Mechanical Engineering
Computer-Integrated Manufacturing	Mechatronics
Cutting and Forming Processes	Metrology in Production
Decision Support Systems	Modelling and Simulation
Deep Learning in Manufacturing	Numerical Techniques
Discrete Systems and Methodology	Operations Research
e-Manufacturing	Operations Planning, Scheduling and Control
Evolutionary Computation in Production	Optimisation Techniques
Fuzzy Systems	Project Management
Human Factor Engineering, Ergonomics	Quality Management
Industrial Engineering	Risk and Uncertainty
Industrial Processes	Self-Organizing Systems
Industrial Robotics	Smart Manufacturing
Intelligent Manufacturing Systems	Statistical Methods
Joining Processes	Supply Chain Management
Knowledge Management	Virtual Reality in Production
Logistics in Production	

Supply chain information coordination based on blockchain technology: A comparative study with the traditional approach

Yan, K.[a,b], **Cui, L.**[b], **Zhang, H.**[b,*], **Liu, S.**[c], **Zuo, M.**[a,b]

[a]National Engineering Laboratory for Agri-Product Quality Traceability, Beijing Technology and Business University, Beijing, P.R. China
[b]School of E-Business and Logistics, Beijing Technology and Business University, Beijing, P.R. China
[c]School of Economics and Management, Beijing Jiaotong University, Beijing, P.R. China

A B S T R A C T

Blockchain technology has subverted traditional supply chain operational models and transformed information interactions along supply chains. This paper examines the impact of blockchain technology on supply chain information collaboration and operating costs. This paper develops a three-level supply chain model based on blockchain technology that incorporates retailer sensitivity to information. First, the manufacturer's profit function is developed, and the optimal information-sharing quantity and supply chain pricing decisions are analysed. Then, cost models for both the traditional supply chain and the novel supply chain using blockchain technology are developed and the impact of blockchain technology on supply chain operating costs is determined. The results demonstrate that blockchain technology can effectively reduce supply chain operating costs. In addition, this study has an interesting finding that if blockchain adoption is valuable for the supply chain, the quantity of information-sensitive should be moderate. Too many or too few information-sensitive retailers can reduce the value of the blockchain's use. This is because blockchain is implementation will increase the privacy concerns of supply chain companies.

1. Introduction

One of the most prominent advantages of the blockchain is its ability to increase data interactivity [1]. Companies can more easily share information and data with manufacturers and suppliers by employing blockchain technology [2, 3]. The transparency of the blockchain can also reduce delays by preventing products from stalling on the supply chain [4]. With blockchain-based supply chains, every product can be tracked in real time. At present, there are many applications of blockchain technology in the supply chain, for example, cold chain logistics and transportation [2]. Blockchain technology can also solve the problem of verifying the transportation conditions of food because it enables the real-time tracking of the production and sales process of products from the source. In coffee, pharmaceutical, and automotive supply chains, for example, blockchain technology has exhibited excellent performance.

Due to technical limitations, traditional supply chain management has always experienced some managerial drawbacks. For example, in traditional supply chain management, the data streams are more dispersed. Supply chains often employ enterprise resource planning (ERP) systems that are usually only used for submitting orders and completing transactions; they cannot be extended to other functions such as data collection, induction, and analysis. The non-circulation of information on the supply chain affects the fluency of supply chain operations.

Supply chain information collaboration refers to the integration of information between members of the supply chain with Internet technology. Its goal is to achieve the real-time sharing and transmission of operational and market data [5]. However, the degree of information coordination in traditional supply chains is low and the compatibility of information technology between various enterprises is weak. Furthermore, differences in enterprise size and financial strength negatively impact technological compatibility. Another important factor that influences supply chain information collaboration is the existence of weak trust relationships between members of the supply chain. Blockchain technology can effectively alleviate these problems and promote more efficient supply chain information collaboration.

However, there are important issues to address concerning the use of blockchain technology with supply chains. First, what are the boundaries of supply chain information-sharing? Although the blockchain can guarantee information privacy, complete information transparency might not be conducive to an enterprise's strategic decisions. Secondly, what impact does a company's information sensitivity have on supply chain operations? Will information sensitivity hinder the broad application of blockchain technology? Finally, the application of blockchain technology requires capital investment, but will this technology ultimately reduce supply chain operating costs?

Motivated by observing supply chain operations with blockchain technology and clarifying the general supply chain operating rules, in this paper, we analytically explore the effect of blockchain technology on supply chain collaboration considering the operation costs, information-sensitivity level, and optimal supply chain price strategy. We develop a supply chain profit model and a supply chain cost model to investigate the effect of the blockchain on information coordination along supply chains. To capture the characteristics of supply chain operation based on blockchain technology, we consider the information-sensitivity level of, and supply chain information-sharing quality among, supply chain members. Finally, we examine the impact of blockchain technology on supply chain costs. Having analysed the model, we derive some critical results on various issues regarding blockchain-based supply chain operation and formulate managerial insights drawn from our findings.

This original study makes two crucial contributions. First, to the best of our knowledge, this is the first analytical study that presents the impact of platform operation on supply chain operation costs when blockchain technology is employed. Second, we enlarged the current literature on the blockchain and supply chains by capturing the features of information sensitivity. The information sensitivity of supply chain members will affect the investment in blockchain technology for the supply chain.

We organize the paper as follows. Section 2 provides an overall review of the related studies to recognized gaps in the research and appropriately position our work. In Section 3, we draw the problem, develop the model, and make its assumptions. In Section 4, we explore different supply chain models considering blockchain technology. In Section 5, we provide the results of simulation analysis to examine the impact of blockchain technology. Finally, in Section 6, we conclude the results and give some essential suggested topics for future relevant research.

2. Literature review

Blockchain technology has transformed supply chain management. Many articles have discussed these changes [6, 7]. The management of information flows in the supply chain is essential to achieve supply chain coordination [8-10]. In general, modern information technologies are required to achieve information synergy in supply chains [10, 11]. In modern supply chain management, many firms use advanced technologies to increase the transparency and improve the efficiency of supply chain information transfer [12, 13]. Blockchain, as an effective technological tool, can help supply chains achieve synergy goals.

2.1 The impact of blockchain on a supply chain

Our research involves the changes brought about by the application of blockchain technology in supply chain operations management. First, blockchain technology has significantly changed agricultural product supply chains [7]. Figorilli [14] examined the application of blockchain technology in the lumber supply chain. They considered integrating traceable information related to product quality into an online information system and using blockchain technology to record transactional data. Kamble *et al*. [15] analysed the strategy of implementing blockchain technology in the agricultural supply chain to ensure food safety and sustainability. Salah *et al*. [10] believed that blockchain technology can provide creative solutions for improved traceability of agricultural and other food products. The author proposed using smart contracts to trace the soybean transactional process. Behnke *et al*. [16] supposed that, before implementing blockchain technology, the organizational structure of the supply chain must be changed and information-sharing among members must be voluntary. Kumar and Iyengar [18] constructed a rice supply chain system based on the blockchain to ensure its safety during the supply chain management process. The above research has performed a sufficient analysis of the means for ensuring the safety of agricultural product supply chains and information traceability. This is necessary for analysing the combination of blockchain technology and supply chain operation management from a macro perspective.

2.2 Operation of a supply chain with blockchain

Many articles have previously investigated how to use blockchain technology in the supply chain. Perboli *et al.* [19] proposed that the blockchain be regarded as a distributed ledger database that can permanently record transactional information and ensure its security. Dolgui *et al.* [20] designed a new model of smart contracts using dynamic control theory. Tseng *et al.* [21] investigated medical supply chain governance based on blockchain technology. Verhoeven *et al.* [22] explored a supply chain management case based on the blockchain. The authors emphasized that the premise of the application of blockchain technology is to fully understand it. Abeyratne and Monfared [23] reviewed the development status and application of blockchain technology and then explained the value of blockchain technology in the manufacturing supply chain and detailed its use in global supply chain governance. The above research fully explains, from a technical point of view, that blockchain technology ensures the information security of the supply chain. Our research is also related to supply chain information. However, we explore how blockchain technology enhances supply chain collaboration from the perspective of supply chain operating costs.

2.3 Information collaboration in a supply chain with blockchain

Blockchain technology can improve information security on the supply chain, reduce supply chain risk, and increase supply chain flexibility [24-27]. Zhu and Kouhizadeh [28] discussed the fact that blockchain technology effectively prevents the deletion of product information. The blockchain also enhances rational decision-making for product information management. Francisco and Swanson [29] developed a conceptual model to determine how the blockchain increases supply chain transparency. Toyoda *et al.* [30] designed a product trading platform based on blockchain technology by using research on radio frequency identification (RFID) technology. Choi *et al.* [31] explored how blockchain technology reduces the risk of aviation logistics. Fu and Zhu [32] analysed how blockchain technology decreases the supply chain risk of large production enterprises. Min [33] discussed ways to use blockchain technology to enhance supply chain resilience when risk and uncertainty increases. Saberi *et al.* [34] explored how blockchain technology and smart contracts can promote supply chain flexibility and proposed four obstacles to the implementation of blockchain technology. Hu *et al.* [35] designed a blockchain-based smart contract to collaborate in supply chains.

In this article, unlike previous research, we focus on how blockchain technology can reduce supply chain operating costs and methods to achieve supply chain information collaboration. At the same time, we also consider supply chain pricing decisions when blockchain technology is introduced.

3. Problem statement

Consider a supply chain consisting of two suppliers, a manufacturer, and a group of retailers. The number of information-sensitive retailers is μ, where $0 \leq \mu \leq 1$, and all other actors are information-insensitive. If blockchain technology is introduced into supply chain operations, manufacturers will decide to share α quantity of information to retailers through blockchain technology at cost c_B, where $c_B = k\alpha$ and k is the cost coefficient of information-sharing [25]. If blockchain technology is not introduced, the manufacturer incurs a fixed cost, c_T. The manufacturer purchases raw materials from the two suppliers. The retailer's wholesale price is w_i and manufacturer demand is D_i. Note that $i = B, T$, where B represents a supply chain using blockchain technology and T represents a traditional supply chain. The structure of the supply chain using blockchain technology is illustrated in Fig. 1.

To capture the impact of blockchain technology on supply chain costs, we later consider more complex cost components in Section 4.2. We summarize the notations used throughout this paper in Table 1. Specifically, we consider a monopoly market in which the manufacturer provides a product to retailers and manufacturers can fully meet the needs of all retailers. Without any loss of generality, we assume that retailers are rational actors who make decisions with the goal of achieving the maximum level of profit. In addition, we assume that all members of the supply chain are risk-neutral, which means that the optimal decision of the entire supply chain will not be affected by the risk preferences of suppliers, manufacturers or retailers. These assumptions are not only reasonable, but also help us simplify the problem and get general management enlightenment.
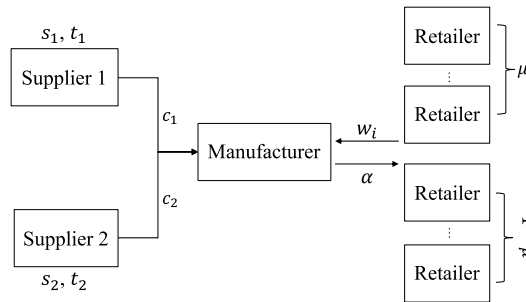
Fig. 1 The structure of a supply chain using blockchain technology

Table 1 Symbols throughout this paper

Symbols	Explanation
D_B	The manufacturer's demand with blockchain technology
D_T	The manufacturer's demand without blockchain technology
d	Basic demand
μ	The proportion of information-sensitive retailers
$1 - \mu$	The proportion of information-insensitive retailers
α	The amount of manufacturer information
w_B	The manufacturer's wholesale price with blockchain technology
w_T	The manufacturer's wholesale price without blockchain technology
k	The cost coefficient of information-sharing
c_B	The manufacturer's cost with blockchain technology, $c_B = k\alpha$
c_T	The manufacturer's cost without blockchain technology
β	Price-sensitive coefficient
π_B	The manufacturer's profit with blockchain technology
π_T	The manufacturer's profit without blockchain technology
s_j	The quality of raw materials provided by supplier j
t_j	The arrival time of raw materials
c_j	The storage cost
n	The unit production delay cost

4. The model

In this section, we first develop profit models for two types of supply chains—the traditional supply chain and the blockchain-based supply chain. We first analyse the optimal pricing strategy, the optimal information-sharing quantity, and the optimal profit of the manufacturer under those two conditions and then determine the impact of information-insensitivity on supply chain operation strategy. Next, we compare the operation costs of the two types of supply chains.

We denote manufacturer demand with a blockchain-based supply chain as Eq. 1 shown:

$$D_B = \mu d + (1 - \mu)d\alpha - \beta w_B \tag{1}$$

Total demand comes from all retailers, including both information-sensitive and information-insensitive retailers. However, it will be negatively affected by rising wholesale prices.

We denote manufacturer demand with a traditional supply chain as:

$$D_T = d - \beta w_T \tag{2}$$

These linear demand functions are used extensively in operations management research [36-38]. To simplify the analysis, we consider only the case in which manufacturer demand with the traditional supply chain is negatively affected by an increase in wholesale prices.

To study the impact of blockchain technology on manufacturers' profits, we obtain the profit function of the manufacturer with different supply chains as:

$$\pi_B = (w_B - k\alpha)D_B \tag{3}$$

$$\pi_T = w_T D_T \tag{4}$$

Differentiating Eq. 3 once with respect to w_B and α, respectively, and then considering the first-order condition yields:

$$w_B = \frac{\mu d + (1 - \mu)d\alpha + \beta k\alpha}{2\beta} \tag{5}$$

$$\alpha = \frac{(1 - \mu)w_B - \mu k}{2(1 - \mu)k} \tag{6}$$

Obviously, it is easy to derive the results of the optimal wholesale price $w_B{}^*$ and the optimal amount of manufacturer's information α^* by combining Eqs. 5 and 6.

Differentiating Eq. 4 once with respect to w_T and considering the first-order condition yields the optimal wholesale price of the traditional supply chain, as follows:

$$\pi_T{}^* = \frac{d^2}{4\beta} \tag{7}$$

Next, we substitute $w_B{}^*$ and α^* and into Eq. 3, substitute Eq. 7 into Eq. 4, yielding the following result.

Lemma 1: The manufacturer's optimal wholesale price with blockchain technology is $w_B{}^* = \frac{k\mu[d(1-\mu)+\beta k]}{(1-\mu)[3k\beta - d(1-\mu)]}$ and the manufacturer's optimal profit with blockchain technology is $\pi_B{}^* = \frac{k\beta\mu(2(1-\mu)-\beta k)}{(1-\mu)[3k\beta - d(1-\mu)]}$.

Lemma 2: The manufacturer's optimal wholesale price without blockchain technology is $w_T{}^* = \frac{d}{2\beta}$ and the manufacturer's optimal profit without blockchain technology is $\pi_T{}^* = \frac{d^2}{4\beta}$.

Lemma 3: The optimal amount of manufacturer information $\alpha^* = \frac{\mu[d(1-\mu)-\beta k]}{(1-\mu)[3k\beta - d(1-\mu)]}$.

By analysing the equilibrium solutions of the profit functions of the manufacturers with the different supply chains, we obtain the optimal price decisions of manufacturers and the optimal amounts of manufacturer information.

4.1 The effect of information sensitivity

To investigate how blockchain technology affects supply chain operation, we consider the relationship between information-sensitivity and the manufacturer's optimal equilibrium strategy. The purpose of the introduction of blockchain technology is to achieve supply chain information

collaboration. Therefore, on the supply chain, the number of information-sensitive retailers has a meaningful and important influence on a manufacturer's decision to implement blockchain technology.

Analysing the above equilibrium solution yields the following proposition.

Proposition 1: When blockchain technology is employed in a supply chain, the proportion of information-insensitive retailers should be satisfied by $\frac{1}{d} < 1 - \mu < \frac{3}{d}$.

Proposition 1 demonstrates that the quantity of information-sensitive retailers ensures the best information-sharing results within a certain range. In addition, the number of information-sensitive suppliers is related to the basic demand of the manufacturer.

Proposition 2: The manufacturer's optimal wholesale price $w_B{}^*$ increases with the proportion of information-sensitive retailers μ when $k(d\beta - \sqrt{\beta(d + 3)}) < t < k(d\beta + \sqrt{\beta(d + 3)})$, otherwise, it decreases with μ.

Proposition 2 illustrates that the manufacturers' wholesale price is non-monotonically related to the quantity of information-sensitive retailers. When the number of information-insensitive retailers is within a certain range, the more sensitive the retailer is to information, the more pricing power the manufacturer wields. This is because blockchain technology increases the possibility and security of information-sharing. If the retailer is sensitive to information, the more likely he or she is to accept the introduction of blockchain technology into the supply chain. Currently, the manufacturer has strong bargaining power.

Proposition 3: The manufacturer's optimal profit $\pi_B{}^*$ increases with the proportion of information-sensitive retailers μ when $t < \frac{2d + 3k^2\beta}{2\beta k}$, otherwise, it decreases with μ.

Proposition 3 illustrates that the manufacturers' profits are affected non-monotonically by the quantity of information-sensitive retailers. When the number of information-insensitive supply chains is small, the more sensitive retailers are, the more profitable the manufacturer is. If a manufacturer wants to increase profits by using blockchain technology, it is necessary to consider not only the retailer's information sensitivity, but also the number of downstream information-sensitive retailers.

4.2 The effect on cost

In Section 4.1, we intentionally ignored the manufacturer's cost because the impact of blockchain technology on supply chain cost is comprehensive. In this section, we specifically discuss manufacturer cost.

In a traditional supply chain, we consider a case in which there are two suppliers that provide raw materials s_j (where $j = 1, 2$) to the manufacturer. However, because of delayed supply and undisclosed information, the manufacturer cannot receive those two suppliers' raw materials at the same time, which leads to production delays. The arrival time of each raw material is t_j (where $j = 1, 2$). Moreover, the manufacturer will incur storage cost c_j (where $i = 1, 2$) for the raw material arriving first and unit production delay cost n for the raw material arriving second.

Consequently, we obtain the total cost c_T to the manufacturer under the condition of using a supply chain without blockchain technology, as follows.

$$c_T = \begin{cases} nt_1, & if\ t_1 > t_2. \\ nt_2, & if\ t_1 < t_2. \\ n(D_T - s_1)^+, & if\ s_1 < s_2. \\ n(D_T - s_2)^+, & if\ s_1 > s_2. \\ (s_i - \min(s_i, D_T))^+ \sum_{i=1}^{2} c_i, & \\ (t_1 - t_2)^+ \sum_{i=1}^{2} c_i s_i, & \\ s_i, t_i, c_i > 0. & \end{cases} \tag{8}$$

In Eq. 8, the first and second items represent the production delay costs. The third and fourth items denote the out-of-stock costs. Note that the above two kinds of costs are caused by the differential between the arrival times of the two suppliers' raw materials. The fifth item is the cost of storing surplus materials. The sixth item is the total storage cost for the raw materials that arrive first. The last item is the constraint to ensure that the model has practical meaning.

Next, we investigate a supply chain using blockchain technology. When the blockchain technology is employed by the supply chain, the manufacturer and supplier can each obtain complete information. The two suppliers can then supply the manufacturer at the same time, thus eliminating the storage cost for the material that arrives first and the cost of storing surplus materials.

Consequently, we obtain the total cost c_B to the manufacturer under the condition of using the blockchain-based supply chain, as follows.

$$c_B = \begin{cases} nt_1, & if\ t_1 > t_2. \\ nt_2, & if\ t_1 < t_2. \\ n(D_T - s_1)^+, & if\ s_1 < s_2. \\ n(D_T - s_2)^+, & if\ s_1 > s_2. \\ (\min\ s_i - D_T)^+ \sum_{i=1}^{2} c_i, \\ s_i, t_i, c_i > 0. \end{cases} \tag{9}$$

In Eq. 9, the first four items are same as Eq. 8. Since the two suppliers have achieved a coordinated supply, the fifth item represents the storage cost for surplus materials. The last item is the constraint to ensure that the model has practical meaning.

After analysing the total costs of the two supply chains, Lemma 4 is provided, as follows.

Lemma 4: Blockchain technology has a great impact on supply chain costs. The cost of the traditional supply chain is c_T and the cost of the blockchain-based supply chain is c_B.

To explore the impact of blockchain technology on supply chain costs in detail, we use the Monte Carlo (MC) method to simulate the costs of the different supply chains.

5. Simulation

We assume that the quality of the raw materials provided by suppliers is denoted as s_j, which is uniformly distributed in [0, 0.3], i.e., $s_1 \sim U[0, 0.3]$ and $s_2 \sim U[0, 3]$. The arrival time of the two different raw materials is denoted as t_j, which is uniformly distributed in [0,0.4], $t_1 \sim U[0, 0.4]$ and $t_2 \sim U[0, 4]$. Using the MC method, we randomly generate 1000 sets s_j and t_2. In addition, let $D_T = 1000$, $c_1 = 100$, and $c_2 = 150$. We consider n ranges from 100 to 180, with an interval of 20. After the simulation, the manufacturer's cost changes are obtained, as shown in Figs. 2 and 3.
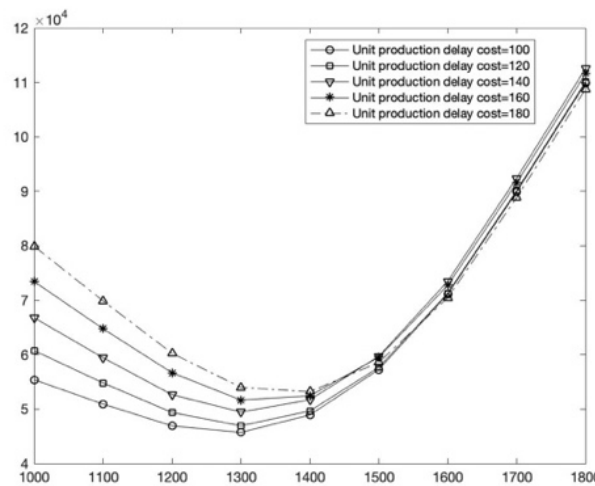
Fig. 2 Changes in manufacturers' costs with traditional supply chains
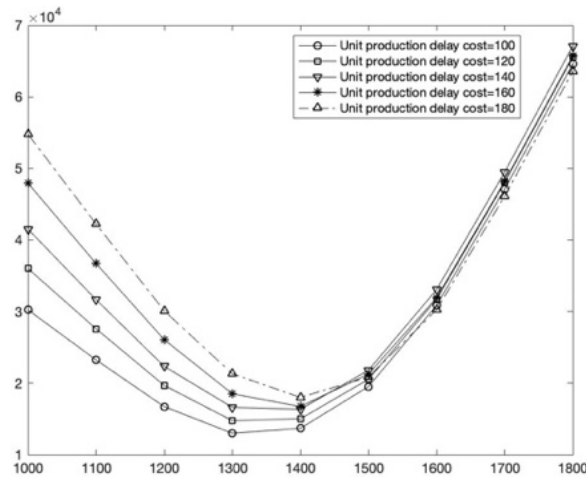
Fig. 3 Changes in manufacturers' costs with blockchain-based supply chains

By simulating the cost models of traditional supply chains and blockchain supply chains, we discover that there is a minimum cost for both types of supply chains under the aversion cost. Moreover, the cost of supply chain changes with delay costs is not monotonous.

The simulation results in Fig. 2 and Fig. 4 show that regardless of the type of supply chain (traditional or blockchain-enabled), an increase in the per unit cost of delay has the potential to increase the total cost of both supply chains. Therefore, manufacturers need to keep a tight rein on the per unit cost of delay. The use of blockchain, on the other hand, increases the transparency of the supply chain and allows the manufacturer to have information on the availability of raw materials. This further illustrates the value of blockchain in collaborating on supply chain information. To better determine how blockchain helps supply chains to achieve information collaboration, we need to compare the total costs of the two supply chains (as shown in Fig. 4).

To study the impact of blockchain technology on supply chain costs, we compared the simulation data of the minimum costs of two supply chains under different delay costs, as illustrated in Fig. 4. The results demonstrate that under any delay cost, the minimum cost of the blockchain supply chain is lower than the minimum cost of the traditional supply chain, which indicates that blockchain technology can effectively reduce supply chain operating costs.

As a whole, the implementation of blockchain has significant value for information collaboration in the supply chain. Our simulation results confirm this value numerically. For blockchain-enabled supply chains, the increased transparency of the supply chain means that manufacturers can produce on demand, order on demand, and do not need higher safety stock levels. Thus, blockchain implementation has practical implications for the efficient collaborative supply chain management.
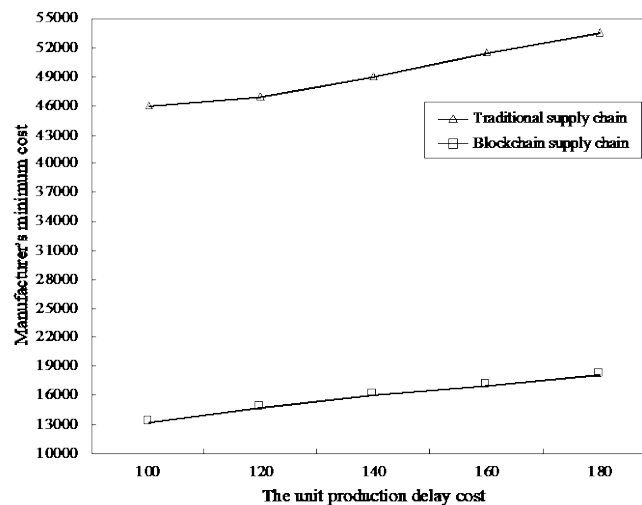
Fig. 4 Comparison of manufacturers' minimum costs with different types of supply chains

6. Conclusion

In traditional supply chains, various entities independently maintain their own supply chain information and the lack of transparency results in higher temporal and informational costs. Blockchain technology has been proven to provide a transparent and reliable unified information platform that is able to reduce logistical costs and trace the entire production and delivery process, thereby improving supply chain management efficiency. In this paper, we considered a three-level supply chain using blockchain technology to analyse the impact of information sensitivity on supply chain operations when blockchain technology was introduced into supply chain management. Our research reached the following conclusions.

- Although the introduction of blockchain technology into the supply chain allows supply chain information to be more effectively shared, it is not the case that the more information is shared, the more beneficial it is to the supply chain. The optimal quality of information-sharing is directly related to the information sensitivity of the supply chain members.
- In the supply chain, there is a non-monotonic relationship between manufacturers' wholesale prices and profits and the number of information-sensitive retailers. Therefore, manufacturers' pricing decisions should consider the cost of information-sharing.
- Simulation research found that blockchain technology could effectively reduce the supply chain operating costs. Therefore, blockchain technology is better used for improving the supply chain governance level.

This study generates insightful guidelines regarding the optimal operational strategies of a supply chain considering blockchain technology, especially when the blockchain technology is introduced into the supply chain, how can the supply chain maintain a reduced operating cost? For further research, it would be interesting to explore a case in which supply chains have different channel structures and determine how blockchain technology affects channel structures. In addition, further research should also consider the impact of information traceability from a management perspective. Another topic we are more interested in is when the members of the supply chain have inconsistent risk appetites for information disclosure, (that is, some members of the supply chain are risk-averse), what should be the optimal decision of the supply chain? In future studies, we will conduct in-depth research on this interesting problem. In addition, future research can consider supply chain risks [38, 39] with blockchain adoption.

Acknowledgement

References

[1] Fosso Wamba, S., Kala Kamdjoug, J.R., Epie Bawack, R., Keogh, J.G. (2020). Bitcoin, blockchain and fintech: A systematic review and case studies in the supply chain, *Production Planning & Control,* Vol. 31, No. 2-3, 115-142, doi: 10.1080/09537287.2019.1631460.

[2] Kim, H.M., Laskowski, M. (2018). Toward an ontology-driven blockchain design for supply-chain provenance, *Intelligent Systems in Accounting, Finance and Management,* Vol. 25, No. 1, 18-27, doi: 10.1002/isaf.1424.

[3] Shahid, A., Almogren, A., Javaid, N., Al-Zahrani, F.A., Zuair, M., Alam, M. (2020). Blockchain-based agri-food supply chain: A complete solution, *IEEE Access*, Vol. 8, 69230-69243, doi: 10.1109/ACCESS.2020.2986257.

[4] Queiroz, M.M., Telles, R., Bonilla, S.H. (2019). Blockchain and supply chain management integration: A systematic review of the literature, *Supply Chain Management,* Vol. 25, No. 2, 241-254, doi: 10.1108/SCM-03-2018-0143.

[5] Montecchi, M., Plangger, K., Etter, M. (2019). It's real, trust me! Establishing supply chain provenance using blockchain, *Business Horizons*, Vol. 62, No. 3, 283-293, doi: 10.1016/j.bushor.2019.01.008.

[6] Tönnissen, S., Teuteberg, F. (2020). Analysing the impact of blockchain-technology for operations and supply chain management: An explanatory model drawn from multiple case studies, *International Journal of Information Management*, Vol. 52, Article No. 101953, doi: 10.1016/j.ijinfomgt.2019.05.009.

[7] Apte, S., Petrovsky, N. (2016). Will blockchain technology revolutionize excipient supply chain management?, *Journal of Excipients and Food Chemicals*, Vol. 7, No. 3, 76-78.

[8]   Babaeinesami, A., Tohidi, H., Seyedaliakbar, S.M. (2020). A closed loop Stackelberg game in multi-product supply chain considering information security: A case study, *Advances in Production Engineering & Management*, Vol. 15, No. 2, 233-246, doi: 10.14743/apem2020.2.361.

[9]   García-Alcaraz, J.L., Maldonado-Macías, A.A., Alor-Hernández, G., Sánchez-Ramírez, C. (2017). The impact of information and communication technologies (ICT) on agility, operating, and economical performance of supply chain, *Advances in Production Engineering & Management*, Vol. 12, No. 1, 29-40, doi: 10.14743/apem2017.1.237.

[10] Fang, I.W., Lin, W.-T. (2021). A multi-objective optimal decision model for a green closed-loop supply chain under uncertainty: A real industrial case study, *Advances in Production Engineering & Management*, Vol. 16, No. 2, 161-172, doi: 10.14743/apem2021.2.391.

[11] Koppenhagen, F., Held, T. (2021). The implications of product modularisation on the development process, supplier integration and supply chain design in collaborative product development, *Advances in Production Engineering & Management*, Vol. 16, No. 1, 82-98, doi: 10.14743/apem2021.1.386.

[12] Homaei, H., Mahdavi, I., Tajdin, A., Khorram, E. (2019). Product quality improvement and air pollutant emission reduction in a mining metal three-stage supply chain under cap-and-trade regulation, *Advances in Production Engineering & Management*, Vol. 14, No. 1, 80-92, doi: 10.14743/apem2019.1.313.

[13] Duan, W., Ma, H., Xu, D.S. (2021). Analysis of the impact of COVID-19 on the coupling of the material flow and capital flow in a closed-loop supply chain, *Advances in Production Engineering & Management*, Vol. 16, No. 1, 5-22, doi: 10.14743/apem2021.1.381.

[14] Figorilli, S., Antonucci, F., Costa, C., Pallottino, F., Raso, L., Castiglione, M., Pinci, E., Del Vecchio, D., Colle, G., Proto, A.R., Sperandio, G., Menesatti, P.A. (2018). A blockchain implementation prototype for the electronic open source traceability of wood along the whole supply chain, *Sensors*, Vol. 18, No. 9, Article No. 3133, doi: 10.3390/s18093133.

[15] Kamble, S.S., Gunasekaran, A., Sharma, R. (2020). Modeling the blockchain enabled traceability in agriculture supply chain, *International Journal of Information Management*, Vol. 52, Article No. 101967, doi: 10.1016/j.ijinfomgt.2019.05.023.

[16] Salah, K., Nizamuddin, N., Jayaraman, R., Omar, M. (2019). Blockchain-based soybean traceability in agricultural supply chain, *IEEE Access*, Vol. 7, 73295-73305, doi: 10.1109/ACCESS.2019.2918000.

[17] Behnke, K., Janssen, M.F.W.H.A. (2020). Boundary conditions for traceability in food supply chains using blockchain technology, *International Journal of Information Management*, Vol. 52, Article No. 101969, doi: 10.1016/j.ijinfomgt.2019.05.025.

[18] Chang, S.E., Chen, Y. (2020). When blockchain meets supply chain: A systematic literature review on current development and potential applications, *IEEE Access*, Vol. 8, 62478-62494, doi: 10.1109/ACCESS.2020.2983601.

[19] Perboli, G., Musso, S., Rosano, M. (2018). Blockchain in logistics and supply chain: A lean approach for designing real-world use cases, *IEEE Access*, Vol. 6, 62018-62028, doi: 10.1109/ACCESS.2018.2875782.

[20] Dolgui, A., Ivanov, D., Potryasaev, S., Sokolov, B., Ivanova, M., Werner, F. (2020). Blockchain-oriented dynamic modelling of smart contract design and execution in the supply chain, *International Journal of Production Research*, Vol. 58, No. 7, 2184-2199, doi: 10.1080/00207543.2019.1627439.

[21] Tseng, J.-H., Liao, Y.-C., Chong, B., Liao, S.-W. (2018). Governance on the drug supply chain via Gcoin blockchain, *International Journal of Environmental Research and Public Health,* Vol. 15, No. 6, Article No. 1055, doi: 10.3390/ijerph15061055.

[22] Verhoeven, P., Sinn, F., Herden, T.T. (2018). Examples from blockchain implementations in logistics and supply chain management: Exploring the mindful use of a new technology, *Logistics*, Vol. 2, No. 3, Article No. 20, doi: 10.3390/logistics2030020.

[23] Abeyratne, S.A., Monfared, R.P. (2016). Blockchain ready manufacturing supply chain using distributed ledger, *International Journal of Research in Engineering and Technology*, Vol. 5, No. 9, 1-10, doi: 10.15623/ijret.2016.0509001.

[24] Kshetri, N. (2018). 1 Blockchain's roles in meeting key supply chain management objectives, *International Journal of Information Management,* Vol. 39, 80-89, doi: 10.1016/j.ijinfomgt.2017.12.005.

[25] Petersen, M., Hackius, N., von See, B. (2018). Mapping the sea of opportunities: Blockchain in supply chain and logistics, *it - Information Technology,* Vol. 60, No. 5-6, 263-271, doi: 10.1515/itit-2017-0031.

[26] Azzi, R., Chamoun, R.K., Sokhn, M. (2019). The power of a blockchain-based supply chain, *Computers & Industrial Engineering,* Vol. 135, 582-592, doi: 10.1016/j.cie.2019.06.042.

[27] Wang, Y., Han, J.H., Beynon-Davies, P. (2019). Understanding blockchain technology for future supply chains: A systematic literature review and research agenda, *Supply Chain Management,* Vol. 24, No. 1, 62-84, doi: 10.1108/SCM-03-2018-0148.

[28] Zhu, Q., Kouhizadeh, M. (2019). Blockchain technology, supply chain information, and strategic product deletion management, *IEEE Engineering Management Review,* Vol. 47, No. 1, 36-44, doi: 10.1109/EMR.2019.2898178.

[29] Francisco, K., Swanson, D. (2018). The supply chain has no clothes: Technology adoption of blockchain for supply chain transparency, *Logistics,* Vol. 2, No. 1, Article No. 2, doi: 10.3390/logistics2010002.

[30] Toyoda, K., Mathiopoulos, P.T., Sasase, I., Ohtsuki, T. (2017). A novel blockchain-based product ownership management system (POMS) for anti-counterfeits in the post supply chain, *IEEE Access,* Vol. 5, 17465-17477, doi: 10.1109/ACCESS.2017.2720760.

[31] Choi, T.-M., Feng, L., Li, R. (2020). Information disclosure structure in supply chains with rental service platforms in the blockchain technology era, *International Journal of Production Economics,* No. 221, Article No. 107473, doi: 10.1016/j.ijpe.2019.08.008.

[32] Fu, Y., Zhu, J. (2019). Big production enterprise supply chain endogenous risk management based on blockchain, *IEEE Access,* Vol. 7, 15310-15319, doi: 10.1109/ACCESS.2019.2895327.

[33] Min, H. (2019). Blockchain technology for enhancing supply chain resilience, *Business Horizons,* Vol. 62, No. 1, 35-45, doi: 10.1016/j.bushor.2018.08.012.

[34] Saberi, S., Kouhizadeh, M., Sarkis, J., Shen, L. (2019). Blockchain technology and its relationships to sustainable supply chain management, *International Journal of Production Research,* Vol. 57, No. 7, 2117-2135, doi: 10.1080/00207543.2018.1533261.

[35] Hu, W., Hu, Y.W., Yao, W.H., Lu, W.Q., Li, H.H., Lv, Z.W. (2019). A blockchain-based smart contract trading mechanism for energy power supply and demand network, *Advances in Production Engineering & Management*, Vol. 14, No. 3, 284-296, doi: 10.14743/apem2019.3.328.

[36] Liu, S., Hua, G., Cheng, T.C.E., Dong, J. (2021). Unmanned vehicle distribution capacity sharing with demand surge under option contracts, *Transportation Research Part E: Logistics and Transportation Review,* Vol. 149, Article No. 102320, doi: 10.1016/j.tre.2021.102320.

[37] Liu, S., Hua, G., Cheng, T.C.E., Choi, T.-M., Dong, J.-X. (2021). Pricing strategies for logistics robot sharing platforms, *International Journal of Production Research*, avaliable online, doi: 10.1080/00207543.2021.2009138.

[38] Zhang, H., Shi, Y., Yang, X., Zhou, R. (2021). A firefly algorithm modified support vector machine for the credit risk assessment of supply chain finance, *Research in International Business and Finance*, Vol. 58, Article No. 101482, doi: 10.1016/j.ribaf.2021.101482.

[39] Zhang, H., Liu, Y., Zhang, Q., Cui, Y., Xu, S. (2020). A Bayesian network model for the reliability control of fresh food e-commerce logistics systems, *Soft Computing,* Vol. 24, 6499-6519, doi: 10.1007/s00500-020-04666-5.

Appendix A

Proof of lemmas: we have $\pi_B = w_B(\mu d + (1-\mu)d\alpha + \beta k\alpha) - \beta w_B^2 - \mu dk\alpha - (1-\mu)dk\alpha^2$, differentiating Eq. 3 once with respect to w_B and α, respectively, and then considering the first-order condition yields: $\frac{\partial \pi_B}{\partial w_B} = \mu d + (1-\mu)d\alpha + \beta k\alpha - 2\beta w_B = 0$ and $\frac{\partial \pi_B}{\partial \alpha} = (1-\mu)dw_B - \mu dk - 2(1-\mu)dk\alpha = 0$. Solving this system of equations, the optimal wholesale price as $w_B^* = \frac{k\mu[d(1-\mu)+\beta k]}{(1-\mu)[3k\beta-d(1-\mu)]}$ and the optimal amount of manufacturer's information as $\alpha^* = \frac{\mu[d(1-\mu)-\beta k]}{(1-\mu)[3k\beta-d(1-\mu)]}$ are obtained. Thus, the manufacturer's optimal profit with blockchain technology as $\pi_B^* = \left(\frac{2\mu\beta k^2}{(1-\mu)[3k\beta-(1-\mu)d]}\right)\left(\frac{\mu d(1-\mu)[3k\beta-d(1-\mu)]}{(1-\mu)[3k\beta-d(1-\mu)]} + \frac{d\mu(1-\mu)[d(1-\mu)-k\beta]}{(1-\mu)[3k\beta-d(1-\mu)]} - \frac{k\mu\beta[d(1-\mu)+\beta k]}{(1-\mu)[3k\beta-(1-\mu)d]}\right) = \frac{k\beta\mu(2(1-\mu)-\beta k)}{(1-\mu)[3k\beta-d(1-\mu)]}$. Similarly, we have $\pi_T = w_T(d - \beta w_T) = w_T d - \beta w_T^2$, differentiating Eq. 4 once with respect to w_B and α, respectively, and then considering the first-order condition yields: $\frac{\partial \pi_B}{\partial w_T} = d - 2\beta w_T = 0$, then we have the manufacturer's optimal wholesale price without blockchain technology as $w_T^* = \frac{d}{2\beta}$. Thus, the manufacturer's optimal profit without blockchain technology as $\pi_T^* = \left(\frac{2d^2}{4\beta} - \frac{d^2}{4\beta}\right) = \frac{d^2}{4\beta}$.

Proof of Proposition 1: We have $\alpha^* = \frac{\mu[d(1-\mu)-\beta k]}{(1-\mu)[3k\beta-d(1-\mu)]} > 0$, thus, there must be $3k\beta - d(1-\mu) > 0$ and $d(1-\mu) - \beta k > 0$ or $3k\beta - d(1-\mu) < 0$ and $d(1-\mu) - \beta k < 0$. Solving this inequality, we obtain $\frac{1}{d} < 1 - \mu < \frac{3}{d}$.

Proof of Proposition 2: Let $\frac{\partial w_B^*}{\partial \mu} = \frac{k\mu(3k^2\beta - 2dk\beta(1-\mu) - d^2(\mu-1)^2)}{(3k\beta + d(\mu-1))^2(\mu-1)^2} > 0$, yielding $3k^2\beta - 2dk\beta(1-\mu) - d^2(\mu-1)^2 > 0$. Then, let $d(1-\mu) = t$. We thus obtain $k(d\beta - \sqrt{\beta(d+3)}) < t < k(d\beta + \sqrt{\beta(d+3)})$. Note that t represents the quantity of information-insensitive retailers.

Proof of Proposition 3: Let $\frac{\partial \pi_B^*}{\partial \mu} = -\frac{k\beta\mu(3k^2\beta - 2d(1-\mu)(\mu-1+\beta k))}{(3k\beta + d(\mu-1))^2(\mu-1)^2} > 0$, yielding $3k^2\beta - 2d(1-\mu)(\mu-1+\beta k) < 0$. Then, let $d(1-\mu) = t$. We thus obtain $t < \frac{2d+3k^2\beta}{2\beta k}$.

A new multi-objective optimization approach for process parameters optimization during numerical simulation of quenching steel parts

Hrnjica, B.[a,*], Behrem, Š.[a]

[a]Faculty of Technical Engineering, University of Bihać, Bihać, Bosnia and Herzegovina

ABSTRACT

The paper presents the numerical simulation of quenching cylindrical steel sample immersed in three different quenchants: water, 5 % aquatensid solution, and isorapid oil. The quenching process starts from the initial temperature of the cylinder at 850 °C and moves through the air until it reaches the quenching bath. The quenchant is held at constant temperature of 40 °C. The cylinder is made of carefully selected steel which does not change its structure during quenching and heating. Cylindrical samples were manufactured in three different dimensions (R, H), (mm): (12.5 × 100), (25 × 150) and (37.5 × 225), so that four measuring points were installed in each sample. Each measuring point consists of thermocouple installed beneath the cylinder surface, capable of measuring the temperature every half second. Based on the experiment, the numerical simulation is recognized as transient and nonlinear two-dimensional heat conduction problem consisting of the two main tasks: direct heat transfer problem (DHTP) and inverse heat transfer problem (IHTP). The paper proposes a new multi-objective optimization approach for the estimation of heat transfer coefficients during the numerical simulation of quenching cylindrical steel sample. The proposed approach gained better results and less convergence time compared to the results from the literature. The paper includes methods, algorithms and the source code for the calculation of the temperature fields in time and heat transfer coefficient estimation of the IHTP. The simulation software has been implemented in C# programming language and can be found at *http://github.com/bhrnjica/quenching_simulation*.

1. Introduction

Quenching is the key of the heat treatment process which improves the material properties. However, when not controlled, the quenching can significantly damage the material in form of cracks and distortions. For this reason, the quenching process should be carefully controlled to gain optimal quenching process with expected material properties [1]. These two consequences of the quenching process are opposite to each other which means that the higher quenching intensity achieves greater depth of hardening but also increases possibilities of the deformation and size change [2]. This demonstrates the complexity of the quenching process and indicates the need for the optimization of process parameters to control the quenching intensity. From the mathematical point of view, the quenching is transient nonlinear process where all variables could be changed in time. The quenching temperature field ϑ is a function of the coordinates and time as well as the material properties, e.g. density of material ρ, thermal capacity c, and conductivity coefficient λ.

During quenching, the temperature change cannot be measured at the surface of the workpiece which indicates inability to calculate the heat transfer coefficient needed for the boundary conditions for the partial differential equation of the heat transfer. This limits the formulation of the quenching process and the optimization of the quenching parameters [3, 4]. To successfully perform numerical simulation, the determination of the heat transfer coefficients on the workpiece surface must be known at any time of the quenching process. There are many approaches to the estimation of the heat transfer coefficient in the literature, and almost all are based on the principle to measure the temperature inside the computational domain [5, 6].

Once the temperature in the computational domain is known, the parameters calculation can be estimated by using the IHTP procedure [7]. Since the quenching process goes through three different phases: film boiling, nucleate boiling and convection [8], the heat transfer coefficient passes through three different value ranges [9]. In case of the first and the third phase of the quenching process, the heat transfer coefficient can be identified with stable value range, while the second phase indicates very unstable value ranges with high gradients up to 20000 W/cm (Fig. 1).

Most of the available literature estimate the heat transfer coefficient only for the side of the cylinder, while the heat transfer coefficients of the bases are neglected. This state is assumed when height of the cylinder is much greater than the cylinder radius (H >> R). This paper considers heat transfer coefficient for all three cylinder's surfaces which increased the complexity of the quenching numerical model. The heat transfer coefficients at all sides show different behaviour since they pass different quenching conditions at the same time. Moreover, the heat transfer coefficient at the side of the cylinder is not constant, and depends of the height of the cylinder.

Fig. 1 Heat transfer coefficient around the cylinder when all quenching phases are presented

This is obvious because the immersion of the cylinder goes vertically (Fig. 1). However, the heat transfer of the cylinder bases can be considered constant at the time since the area of the base surface is affected with the same boundary condition.

2. Methods

2.1 Mathematical description of DHTP

Quenching process is a typical transient problem, thus the temperature field of any point in the body can be expressed as a function of coordinates and time [10]:

$$\vartheta = f(x, y, z, t) \tag{1}$$

In general form, Fourier's heat transfer differential equation describes a nonlinear three-dimensional nonstationary conduction of heat through an orthotropic solid in space and time:

$$\rho\, c\, \frac{\partial \vartheta}{\partial t} = \frac{\partial}{\partial x}\left(\lambda_x \cdot \frac{\partial \vartheta}{\partial x}\right) + \frac{\partial}{\partial y}\left(\lambda_y \cdot \frac{\partial \vartheta}{\partial y}\right) + \frac{\partial}{\partial z}\left(\lambda_z \cdot \frac{\partial \vartheta}{\partial z}\right) + \Phi_v \tag{2}$$

The computational domain of the presented work is the cylinder, so the temperature field is better expressed in the cylindrical coordinates. The previous expression can be transformed into cylindrical coordinates by involving transformation matrix, hence it assumes the following transformed expression [11]:

$$\rho\, c\, \frac{\partial \vartheta}{\partial t} = \frac{1}{r} \cdot \frac{\partial}{\partial r}\left(r\, \lambda_r \cdot \frac{\partial \vartheta}{\partial r}\right) + \frac{1}{r^2} \cdot \frac{\partial}{\partial \varphi}\left(r\, \lambda_\varphi \cdot \frac{\partial \vartheta}{\partial \varphi}\right) + \frac{\partial}{\partial z}\left(\lambda_z \cdot \frac{\partial \vartheta}{\partial z}\right) + \Phi_v \tag{3}$$

in which $\rho, c, \lambda_r, \lambda_\varphi, \lambda_z$ are material properties: density, thermal coefficient and thermal conductivity in r, φ and z directions of the cylindrical coordinates respectively, ϑ temperature of a point, t time and Φ_v – volumetric heat source.

For isotropic solid ($\lambda = \lambda_r = \lambda_\varphi = \lambda_z$) without internal source ($\Phi_v = 0$), the temperature gradient in circular direction is neglected ($\partial \vartheta / \partial \varphi = 0$), and the final equation of axisymmetric problem becomes:

$$\rho\, c\, \frac{\partial \vartheta}{\partial t} = \left[\lambda_r \frac{\partial^2 \vartheta}{\partial r} + \lambda_r \frac{1}{r} \cdot \frac{\partial \vartheta}{\partial r} + \lambda_z \frac{\partial^2 \vartheta}{\partial z}\right] \tag{4}$$

Due to high temperature of the quenching process, the variables $\lambda(\vartheta)$ and $c(\vartheta)$ are dependent of the current temperature ϑ which makes the quenching process nonlinear transient problem. Due to the geometrical beauty of the cylinder, computational domain of the partial differential Eq. 4 can be reduced to the rectangle ($R \times H$) (Fig. 2).

Fig. 2 shows discretisation of the computational domain and transition from the 3D into 2D axisymmetric problem. The new computational domain is the rectangle consisting of 4 edges. The first three edges (boundaries) (Γ_1, Γ_2 and Γ_3) are involved in heat transfer with specific heat transfer coefficient (HTC), while the fourth boundary (Γ_4) is symmetric axis where the heat flux is equal to zero. Heat transfer across boundaries Γ_1, Γ_2, and Γ_3 is defined by the balance of Fourier's and Newton's laws of conduction and heat transfer.
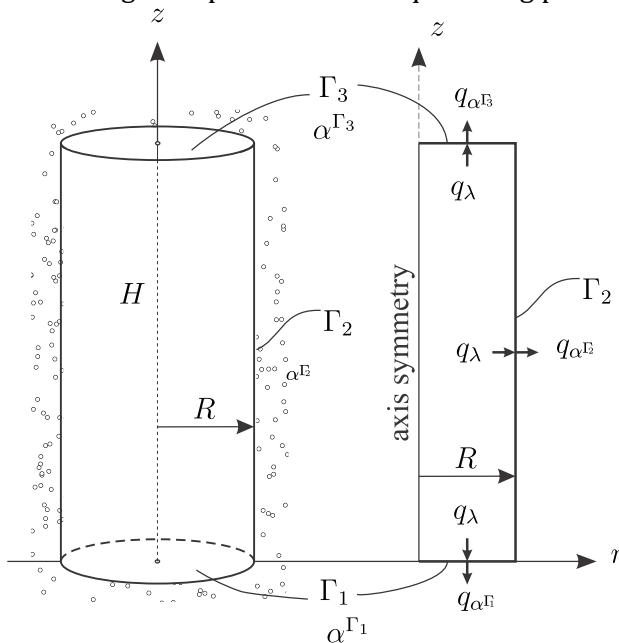
Fig. 2 Computational domain of the cylinder as axisymmetric domain rectangle

2.2 Initial and boundary conditions of the axisymmetric heat transfer

Due to the second order of the partial differential Eq. 4, the initial and the boundary conditions must be defined to completely define the equation.

The initial condition defines the initial temperature on any points in the computational domain:

$$\vartheta(r, \varphi, z) = \vartheta_0, \text{ for } t = 0 \tag{5}$$

The boundary conditions are defined on each edge of the rectangle. They are boundary conditions of third kind. The bottom edge Γ_1, where $z = 0$ and $0 \leq r \leq R$, the boundary conditions can be expressed as:

$$-\lambda(\vartheta)\, \frac{\partial \vartheta}{\partial z} = \alpha^{\Gamma_1}(\vartheta - \vartheta_\infty) \tag{6}$$

where α^{Γ_1} is the HTC at the bottom edge, ϑ is the temperature at the edge, and ϑ_∞ is the ambient temperature.

The upper edge Γ_3, where $z = H$ and $0 \leq r \leq R$, the boundary conditions are expressed as:

$$-\lambda(\vartheta)\,\frac{\partial\vartheta}{\partial z} = \alpha^{\Gamma_3}(\vartheta - \vartheta_\infty) \tag{7}$$

in which α^{Γ_3} is the HTC at the upper edge. Along the bottom and top edges, the HTCs are constant at time t_i.

The boundary conditions at the right edge Γ_2, where $r = R$ and $0 \leq z \leq H$, can be expressed as:

$$-\lambda(\vartheta)\,\frac{\partial\vartheta}{\partial r} = \alpha^{\Gamma_2}\,(\vartheta - \vartheta_\infty) \tag{8}$$

in which α^{Γ_2} is the HTC at the right edge. Note that the α^{Γ_2} is not constant, but rather a function of z coordinate ($\alpha^{\Gamma_2} = f(z)$).

At the left edge Γ_4 where $r = 0$ and $0 \leq z \leq H$, the boundary represents the adiabatic border ($q_{(r=0)} = 0$) where the temperature gradient is equal to zero (Fig. 2):

$$\left(\frac{\partial\vartheta}{\partial r}\right)_{(r=0)} = 0 \tag{9}$$

2.3 HTC calculation of the computational domain

By defining the boundary conditions (Eqs. 6 to 9), the HTCs of the three edges are unknown and must be resolved to compute DHTP. The computation of the HTCs is usually performed experimentally. To compute the HTC, the ambient and the temperature at the edges of the rectangle domain must be measured. However, measurement of the temperature at the edge cannot be performed because the measuring thermo-couples would be directly exposed to the heat source during heating phase. Instead of measuring the temperature at the edges, the thermo-couples can be installed beneath the cylindrical surfaces, so that they can measure the temperatures at some points in the computational domain. One such layout of installed thermo-couples is depicted in Fig. 3.

The three thermo-couples are installed 1.5 mm beneath the right edge Γ_2, spreading equally along the height. The fourth thermo-couple is installed at the midpoint of the symmetry axes. With such layout of the measuring points, the HTCs still cannot be computed directly, and the boundary conditions cannot be resolved. However, the inverse form of the problem can be stated, so that instead of calculating the HTC at edges, the values are computed by minimizing the value of the objective function which is usually squared error between measured and calculated temperatures. In this paper, the calculation of the HTCs at edges is performed by using three measuring points, and bilinear interpolation.
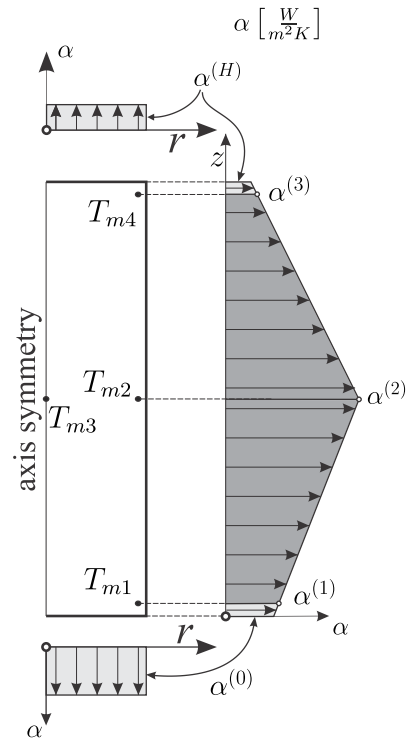
Fig. 3 Approximated HTC distributions along edges of the computational domain

In case of the bilinear interpolation the HTC value is expressed as (Fig. 3):

$$\alpha(z) = \begin{cases} \alpha^{(1)} + \dfrac{\left(\alpha^{(2)} - \alpha^{(1)}\right)}{z_2 - z_1}, 0 \leq z \leq \dfrac{H}{2} \\[4mm] \alpha^{(2)} + \dfrac{\left(\alpha^{(3)} - \alpha^{(2)}\right)}{z_3 - z_2}, \dfrac{H}{2} < z \leq H \end{cases} \tag{10}$$

The HTC values at the bottom and top edges α^{Γ_1} and α^{Γ_2} are calculated by using Eq. 10 for $z = 0$ and $z = H$, respectively. The HTC value at the right edge $\alpha^{\Gamma_3}(z)$ directly depends on the z coordinate.

2.4 Variational form and finite element method of the heat transfer differential equation
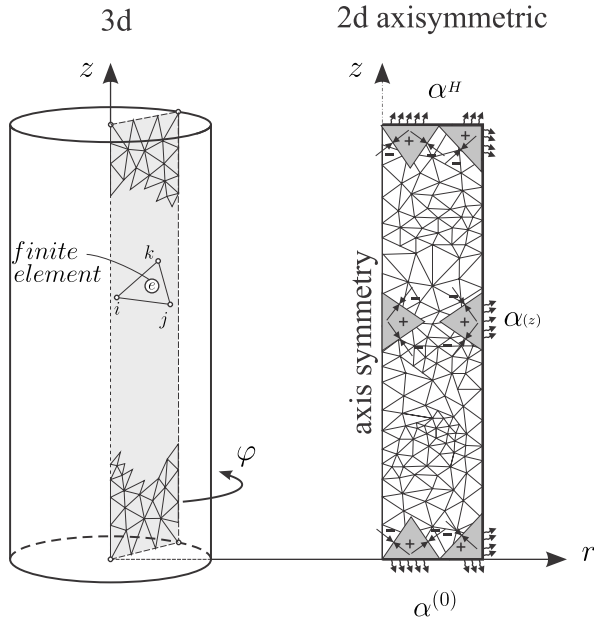
Fig. 4 Discretization of the cylinder profile (right)

The presented problem is completely defined with the Eq. system 4 to 9. In order to solve the differential Eq. 4 using finite element method (FEM) the variational form of the Eq. 4 must be derived. Variational form can be derived by using procedure described in three steps [13]. The first step is performed by taking the scalar product of the weighted function and the Eq. 4, and taking the integral over the computational domain. In the next step, the partial integration and Green Theorem are used in order to evaluate the integral over the boundary. In the last step, the weighted function is replaced with the variation of the temperature field function, and the integrals are evaluated over the boundary. After performing all three steps, the final expression of the variational form of the Eq. 4, including the boundary conditions (Eqs. 6 to 9), is shown as:

$$I = \frac{1}{2} \iiint_{\Omega} \left[\lambda\, r \left(\frac{\partial \vartheta}{\partial r} \right)^2 + \lambda\, r \left(\frac{\partial \vartheta}{\partial z} \right)^2 + 2 \left(\rho c r \cdot \frac{\partial \vartheta}{\partial t} \right) \vartheta \right] d\Omega + \frac{1}{2} \iint_{\Gamma_1} r\, \alpha^{\Gamma_1} (\vartheta - \vartheta_\infty)^2 \, d\Gamma_1$$

$$+ \frac{1}{2} \iint_{\Gamma_2} r\, \alpha^{\Gamma_2} (\vartheta - \vartheta_\infty)^2 \, d\Gamma_2 + \frac{1}{2} \iint_{\Gamma_3} r\, \alpha^{\Gamma_3} (\vartheta - \vartheta_\infty)^2 \, d\Gamma_3 \tag{11}$$

The FEM procedure starts by dividing the computation domain Ω into N nodes which define E finite elements and minimize the functional of the Eq. 11 for each finite element. Discretization of the computational domain is performed by using triangle finite elements with three nodes i, j and k (Fig. 4).

The spatial approximation of the temperature field $\vartheta^{(e)}$ above a triangle e is defined as matrix product of the shape functions $[N]$ and the nodal temperatures $\{\vartheta\}$ of a triangular finite element $e(i, j, k)$:

$$\vartheta^{(e)} = [N_i \quad N_j \quad N_k] \begin{Bmatrix} \vartheta_i \\ \vartheta_j \\ \vartheta_k \end{Bmatrix} = [N]\{\vartheta\} \tag{12}$$

The shape functions for the 3-node triangle finite element are:

$$N_i = \frac{1}{2A} (a_i + b_i r + c_i z), N_j = \frac{1}{2A} (a_j + b_j r + c_j z), N_k = \frac{1}{2A} (a_k + b_k r + c_k z) \tag{13}$$

where A is area of the triangle, and a, b and c are coefficients [12].

Combining the Eqs. 11 and 12, the variational form of any finite element in the computation domain (Fig. 4) can be expressed as:

$$I^{(e)} = \frac{1}{2} \iiint\limits_{\Omega^{(e)}} \left[\lambda\, r \left(\frac{\partial \vartheta^{(e)}}{\partial r} \right)^2 + \lambda\, r \left(\frac{\partial \vartheta^{(e)}}{\partial z} \right)^2 + 2 \left(\rho c r \cdot \frac{\partial \vartheta^{(e)}}{\partial t} \right) \vartheta^{(e)} \right] d\Omega$$

$$+ \frac{1}{2} \iint\limits_{\Gamma_1^{(e)}} r\, \alpha^{\Gamma_1} \left(\vartheta^{(e)} - \vartheta_\infty \right)^2 d\Gamma_1 \tag{14}$$

$$+ \frac{1}{2} \iint\limits_{\Gamma_2^{(e)}} r\, \alpha^{\Gamma_2} \left(\vartheta^{(e)} - \vartheta_\infty \right)^2 d\Gamma_2 + \frac{1}{2} \iint\limits_{\Gamma_3^{(e)}} r\, \alpha^{\Gamma_3} \left(\vartheta^{(e)} - \vartheta_\infty \right)^2 d\Gamma_3$$

The minimization process starts by taking the derivative of the Eq. 14 by nodal temperature ϑ_i, ϑ_j and ϑ_k of every finite element.

$$\frac{\partial I^{(e)}}{\partial \vartheta_i} = 0 \tag{15}$$

Combining the Eqs. 15 and 14 the minimization of the functional $I^{(e)}$ for a particular node temperature ϑ_i of the finite element e is expressed as:

$$\frac{\partial I^{(e)}}{\partial \vartheta_i} = \int\limits_{\Omega^{(e)}} \left[\lambda \cdot r \cdot \frac{\partial \vartheta^{(e)}}{\partial r} \frac{\partial}{\partial \vartheta_i} \left(\frac{\partial \vartheta^{(e)}}{\partial r} \right) + \lambda \cdot r \cdot \frac{\partial \vartheta^{(e)}}{\partial z} \frac{\partial}{\partial \vartheta_i} \left(\frac{\partial \vartheta^{(e)}}{\partial z} \right) \right.$$

$$\left. + 2 \left(\rho \cdot c \cdot r \cdot \frac{\partial \vartheta^{(e)}}{\partial t} \right) \frac{\partial \vartheta^{(e)}}{\partial \vartheta_i} \right] d\Omega$$

$$+ \int\limits_{\Gamma_1^{(e)}} r \cdot \alpha^{\Gamma_1} \left(\vartheta^{(e)} - \vartheta_\infty \right) \frac{\partial \vartheta^{(e)}}{\partial \vartheta_i} \, d\Gamma_1 \tag{16}$$

$$+ \int\limits_{\Gamma_2^{(e)}} r \cdot \alpha^{\Gamma_2} \left(\vartheta^{(e)} - \vartheta_\infty \right) \frac{\partial \vartheta^{(e)}}{\partial \vartheta_i} d\Gamma_2 + \int\limits_{\Gamma_3^{(e)}} r \cdot \alpha^{\Gamma_2} \left(\vartheta^{(e)} - \vartheta_\infty \right) \frac{\partial \vartheta^{(e)}}{\partial \vartheta_i} \, d\Gamma_3$$

Line integrals in the Eq. 16 are equal to zero for nodes that do not lie on surfaces $\Gamma_1^{(e)}, \Gamma_2^{(e)}, \Gamma_3^{(e)}$ (Fig. 4).

The Eq. 16 can be further simplified into:

$$\frac{\partial I^{(e)}}{\partial \vartheta_i} = \int\limits_{\Omega^{(e)}} \left[\frac{\partial N_i}{\partial r} \cdot \lambda \cdot r \cdot \frac{\partial}{\partial r} ([N]) \cdot \{\vartheta\}^e + \frac{\partial N_i}{\partial z} \cdot \lambda \cdot r \cdot \frac{\partial}{\partial z} (N) \cdot \{\vartheta\}^e \cdot + 2 \cdot \rho \cdot c \cdot r \cdot N_i \cdot [N] \right.$$

$$\left. \cdot \frac{\partial}{\partial t} \{\vartheta\}^e \right] d\Omega^{(e)}$$

$$+ \int\limits_{\Gamma_1} N_i \cdot r \cdot \alpha^{\Gamma_1} \left(\vartheta^{(e)} - \vartheta_\infty \right) d\Gamma_1 \tag{16a}$$

$$+ \int\limits_{\Gamma_2} N_i \cdot r \cdot \alpha^{\Gamma_2} \left(\vartheta^{(e)} - \vartheta_\infty \right) d\Gamma_2 + \int\limits_{\Gamma_3} N_i \cdot r \cdot \alpha^{\Gamma_3} \left(\vartheta^{(e)} - \vartheta_\infty \right) d\Gamma_3$$

Similar expression is obtained when using j and k nodes of the triangle finite element e. By grouping nodes i, j and k into the finite element e, the expressions can be transformed into final matrix equation:

$$\frac{\partial I^{(e)}}{\partial \{\vartheta\}^{(e)}} = \left(\left[K_1^{(e)} \right] + \left[K_2^{(e)} \right] \right) \{\vartheta\} + \left[K_3^{(e)} \right] \frac{\partial}{\partial t} \{\vartheta\}^{(e)} - \{f^{(e)}\} = 0 \tag{17}$$

The Eq. 17 is defined with stiffens matrix $\left[K_1^{(e)}\right]$, convective matrix $\left[K_2^{(e)}\right]$, the capacitance matrix $\left[K_3^{(e)}\right]$ and the vector of nodal loads $\{f^{(e)}\}$ which have the following forms:

$$\Omega^{(e)} = 2r\pi \cdot A^{(e)} = r \cdot \pi\left[r_i \cdot (z_j - z_k) + r_j \cdot (z_k - z_i) + r_k \cdot (z_i - z_j)\right],$$

$$\left[K_1^{(e)}\right] = \int_{\Omega^{(e)}} \begin{bmatrix} \dfrac{\partial N_i}{\partial r} & \dfrac{\partial N_i}{\partial z} \\ \dfrac{\partial N_j}{\partial r} & \dfrac{\partial N_j}{\partial r} \\ \dfrac{\partial N_k}{\partial r} & \dfrac{\partial N_k}{\partial z} \end{bmatrix} \cdot \lambda \cdot r \begin{bmatrix} 1 & 0 \\ 0 & 1 \end{bmatrix} \cdot \begin{bmatrix} \dfrac{\partial N_i}{\partial r} & \dfrac{\partial N_j}{\partial r} & \dfrac{\partial N_k}{\partial r} \\ \dfrac{\partial N_i}{\partial z} & \dfrac{\partial N_j}{\partial z} & \dfrac{\partial N_k}{\partial z} \end{bmatrix} \cdot d\Omega^{(e)},$$

$$\left[K_2^{(e)}\right] = \left[\int_{\Gamma_1} \alpha^{\Gamma_1} \cdot [N]^T[N] \cdot \begin{Bmatrix} r_i \\ r_j \\ r_k \end{Bmatrix} d\Gamma_1 + \int_{\Gamma_2} \alpha^{\Gamma_2} \cdot [N]^T \cdot [N] \cdot \begin{Bmatrix} r_i \\ r_j \\ r_k \end{Bmatrix} d\Gamma_2 \right.$$

$$\left. + \int_{\Gamma_3} \alpha^{\Gamma_3} \cdot [N]^T \cdot [N] \cdot \begin{Bmatrix} r_i \\ r_j \\ r_k \end{Bmatrix} d\Gamma_3 \right],$$

(18)

$$\left[K_3^{(e)}\right] = \int_{\Omega^{(e)}} \left(2 \cdot \rho \cdot c \cdot r \cdot \begin{bmatrix} N_i \\ N_j \\ N_k \end{bmatrix} \cdot [N_i \quad N_j \quad N_k] \right) \cdot d\Omega^{(e)}$$

$$= \left[\int_{\Omega^{(e)}} 2 \cdot \rho \cdot c \cdot r \cdot [N]^T \cdot [N] \cdot d\Omega^{(e)} \right],$$

$$\{f^{(e)}\} = \left[\int_{\Gamma_1} r \cdot \alpha^{\Gamma_1} \cdot \vartheta_\infty \cdot \begin{bmatrix} N_i \\ N_j \\ N_k \end{bmatrix} \cdot d\Gamma_1 + \int_{\Gamma_2} r \cdot \alpha^{\Gamma_2} \cdot \vartheta_\infty \cdot \begin{bmatrix} N_i \\ N_j \\ N_k \end{bmatrix} \cdot d\Gamma_2 \right.$$

$$\left. + \int_{\Gamma_3} r \cdot \alpha^{\Gamma_3} \cdot \vartheta_\infty \cdot \begin{bmatrix} N_i \\ N_j \\ N_k \end{bmatrix} \cdot d\Gamma_3 \right]$$

The final form of the finite element equation is given when the first two matrices are combined and the third is renamed as $\left[K_3^{(e)}\right] = M^{(e)}$, so that:

$$M^{(e)} \frac{\partial}{\partial t}\{\vartheta\}^{(e)} + K^{(e)}\{\vartheta\} = f^{(e)}$$

(19)

Final form of the matrices in terms of shape functions with coordinates of the triangle centroid are given in the literature [12]

By assembling all finite elements back into the domain, the global matrix equation is expressed as:

$$\sum_{e}^{E} \left(M^{(e)} \frac{\partial}{\partial t}\{\vartheta\} + K^{(e)}\{\vartheta\} - f^{(e)} \right) = 0$$

(20)

To numerically solve the system of matrix Eq. 20, the time derivative has to be discretized by using finite difference method (FDM). The discretization starts by defining the variation of the temperature in time. Using the Taylor series, the temperature at the $n + 1$ time step can be expressed by using the previous time steps [10]:

$$\vartheta^{n+1} = \vartheta^n + \Delta t \frac{\partial \vartheta^n}{\partial t} + \frac{\Delta t^2}{2} \cdot \frac{\partial^2 \vartheta^n}{\partial t^2} + \cdots, \tag{21}$$

Assuming the second and higher order terms of the series (21) are neglected, the final form of the time discretization is shown as:

$$([M] + \Delta t[K])\{\vartheta\}^{n+1} = [M]\{\vartheta\}^n + \Delta t \{f\}^{n+1} \tag{22}$$

The matrix Eq. 22 is complete set of equations used to solve the unknow nodal temperatures in time $n + 1$. To calculate the nodal temperatures $\{\vartheta\}^{n+1}$ previous nodal temperatures must be known. The procedure goes to the initial temperature field which is defined by the Ex. 5, so that the nodal temperatures of the time step 1 can be calculated:

$$([M] + \Delta t[K])\{\vartheta\}^1 = [M]\{\vartheta\}^0 + \Delta t \{f\}^1 \tag{23}$$

At any time step, the nodal temperatures can be estimated using the Eq. 23 and the initial conditions (Eq. 5). The Eq. 23 represents the implicit method of the time discretization, which is much better for the computer implementation than explicit approach [4]. Unlike implicit, the time can be discretized by using different methods described in the literature [4]. Convergence criteria for both FEM and FDM is beyond the scope of the paper but can be found in the referenced literature [4-6].

2.5 Inverse heat transfer calculation using Levenberg-Marquardt approach

Typically, the heat transfer problem is defined as the calculation of the temperature field for known boundary and initial conditions. Often the boundary conditions are not known and cannot be resolved due to practical reasons [24]. In such cases, the problem of the calculation of the boundary conditions is part of the integrated problem such that the temperature field is solved based on prior estimation of the boundary conditions. A possible way of estimating the boundary conditions is to have measuring points inside the computational domain. For every estimated value of the boundary conditions the calculated and measured temperature field are compared at the measuring points. Once the residual is computed and the squared error is calculated, the values of the boundary conditions are corrected for certain amount and the calculation process continue until the result reaches the satisfied accuracy. This process is known as Inverse Heat Transfer Problem [5, 7, 15-17]. Since the solutions of the IHTP are unstable, the problem is recognized as ill-posed. The existence and uniqueness of the solution for IHTP can be proved only for specific cases, since it is very sensitive to random errors. This leads to the use of specific approaches in order to minimize the error influence and satisfy the stability of the solution. In general, the IHTP can be defined as the optimization problem, but there are some critical differences that distinguish these two methods from each other [14, 18, 19].

Every inverse problem starts by defining the objective function C. Usually, the objective function is square error (SE) between actual (measured) and calculated field variable. The field variable for this paper is the temperature, so the objective function is expressed:

$$C = (Y - \vartheta)^2 \tag{24}$$

where Y is the vector of the measured temperatures, and ϑ the vector of the calculated temperatures.

The measured temperatures are obtained during the experimental phase and the calculated temperatures are obtained by using the DHTP. The objective function C_t at any time t of the quenching process presented in the paper can be defined as modified version of the Eq. 23 as:

$$C_t(\alpha^\Gamma) = \sum_{j=1}^{m} \left(Y_t^j - \vartheta_t^j(\alpha^\Gamma) \right)^2 \tag{25}$$

where m is number of measuring points, Y_t^j - measured temperature in point j at time t, ϑ_t^j calculated temperature in point j at time t. The calculated temperature field is the solution of Eq. 4. The temperature field ϑ (r, z, t) satisfies the boundary and initial conditions given by Eqs. 5 to 9 for

every point in the computational domain (R, H). To solve the Eq. 4, the boundary conditions must be resolved at any time. To resolve the boundary conditions, the heat transfer coefficients α^{Γ_1}, α^{Γ_2}, α^{Γ_3} from the Eqs. 5 to 9 must be known. In fact, the heat transfer coefficients become the unknown parameters of the IHTP. The Eq. 25 can be defined so that at any time t the objective function C_t depends on the current calculation of the vector of unknown parameters α^{Γ}.

The procedure of the unknown parameters' optimization starts by minimizing the least square norm of the Eq. 25. The minimization of the expression can be estimated by equating the partial derivatives of the objective function to zero by every unknown parameter.

At any time t, the gradient ∇ of the objective function C_t in terms of the unknown vector α^{Γ} can be expressed as:

$$\nabla C_t = 2 \sum_{j=1}^{m} \left[-\frac{\partial \vartheta^j}{\partial \alpha^{\Gamma}} \right] \left(Y_t^j - \vartheta_t^j \right) = 0 \tag{26}$$

Assuming there are m measuring points, the sensitivity matrix J of unknown parameters α^{Γ} at time t is expressed as:

$$J(\alpha^{\Gamma}) = \begin{bmatrix} \dfrac{\partial \vartheta^1}{\partial \alpha^{\Gamma_1}} & \dfrac{\partial \vartheta^1}{\partial \alpha^{\Gamma_2}} & \dfrac{\partial \vartheta^1}{\partial \alpha^{\Gamma_3}} \\ \dfrac{\partial \vartheta^2}{\alpha^{\Gamma_1}} & \dfrac{\partial \vartheta^2}{\partial \alpha^{\Gamma_2}} & \dfrac{\partial \vartheta^2}{\partial \alpha^{\Gamma_3}} \\ \vdots & \vdots & \vdots \\ \dfrac{\partial \vartheta^m}{\alpha^{\Gamma_1}} & \dfrac{\partial \vartheta^m}{\partial \alpha^{\Gamma_2}} & \dfrac{\partial \vartheta^m}{\partial \alpha^{\Gamma_3}} \end{bmatrix} \tag{27}$$

By using Eqs. 27 and 25 the procedure of finding the unknown parameters is described in the literature [7, 14-20]. Since the quenching process is transient and nonlinear, the solution of the system equations derived from Eq. 26 can be obtained by iterative process based on the parameter values from the previous step α_k^{Γ}:

$$\alpha_{k+1}^{\Gamma} = \alpha_k^{\Gamma} + \Delta \alpha_k^{\Gamma} \tag{28}$$

The value $\Delta \alpha_k^{\Gamma}$ is given as [20]:

$$\Delta \alpha_k^{\Gamma} = [[J_k]^T \cdot J_k + \mu_k \, \Omega_k]^{-1} [J^k]^T \left[Y - \vartheta_k(\alpha_k^{\Gamma}) \right] \tag{29}$$

where μ_k is positive real number called dumping parameter, and Ω_k is the diagonal matrix of real numbers. They called Levenberg-Marquardt stability parameters.

The parameters (μ_k, Ω_k) dump the oscillations and instabilities due to ill-conditioned behaviour of the problem, so that they become large at the beginning of the iteration process, after which they decrease as the matrix $[J^T \cdot J]$ becomes larger. Different initial values are proposed for the stability parameters. Usually, the matrix Ω_k is initialized with $\Omega_k = diag[[J_k]^T \cdot J_k]$, while the dumping parameter is initialized at the beginning of the iteration process as $\mu_k = 10^{-3}$, and then gradually increased or decreased by factor 10 or 0.1 respectively [7]. The calculation of the sensitivity matrix (Eq. 27) and stopping criteria of the Levenberg-Marquardt algorithm are described in the literature [7].

3. Application

3.1 Experimental setup

The experiment setup consists of a cylindrical probe made of the steel AISI 304. The main property of the material is no crystal conversion during the heating and quenching. The probe is heated at 850 °C using electric furnace. Once the probe reached the temperature, it moved down toward the quenching bath with constant velocity until immersed in cooling fluid completely. Throughout the entire quenching process, the temperature of the cooling fluid is 40 °C. To maintain the constant temperature, the cooling fluid is constantly flowing upwards. The main aim of such kind of an

experiment is to provide axisymmetric heating and quenching, so that the mathematical description of the process would be as simplified as possible. There are 5 mayor components of the experiment [21, 22, 24], (Fig. 5).

During quenching process, temperature values are continuously measured in four points (1, 2, 3, 4) by using thermocouples described in Fig. 3. Due to their many advantages, the thermocouples have long been used successfully in temperature metrology [2, 9]. They are practically composed of only two wires of different metals, joined together at one end, which produce a small voltage, depending on the temperature. Therefore, they are very easy to use, cheap, small in size, carefully designed, and can be used to measure a wide range of temperatures (–270-3000 °C) in different environmental conditions. An important property is that many combinations of thermocouples give an almost linear voltage output in a wide range of temperatures, which is important in calibration and measurement process. The number of potential combinations of thermocouples is practically infinite because any two different metals can be used. The positions of the measured points in the cylindrical probe are depicted in Fig. 5 [21, 24]. Once the thermocouples are installed in the probe, the process of collection the data is controlled from the datalogger. The datalogger sends the data to the PC for further clean-up and preparation of the experimental results. The process of heating a probe took up to 4 hours. However, the process of quenching was completed in 100 to 700 seconds depending of the quenchant.
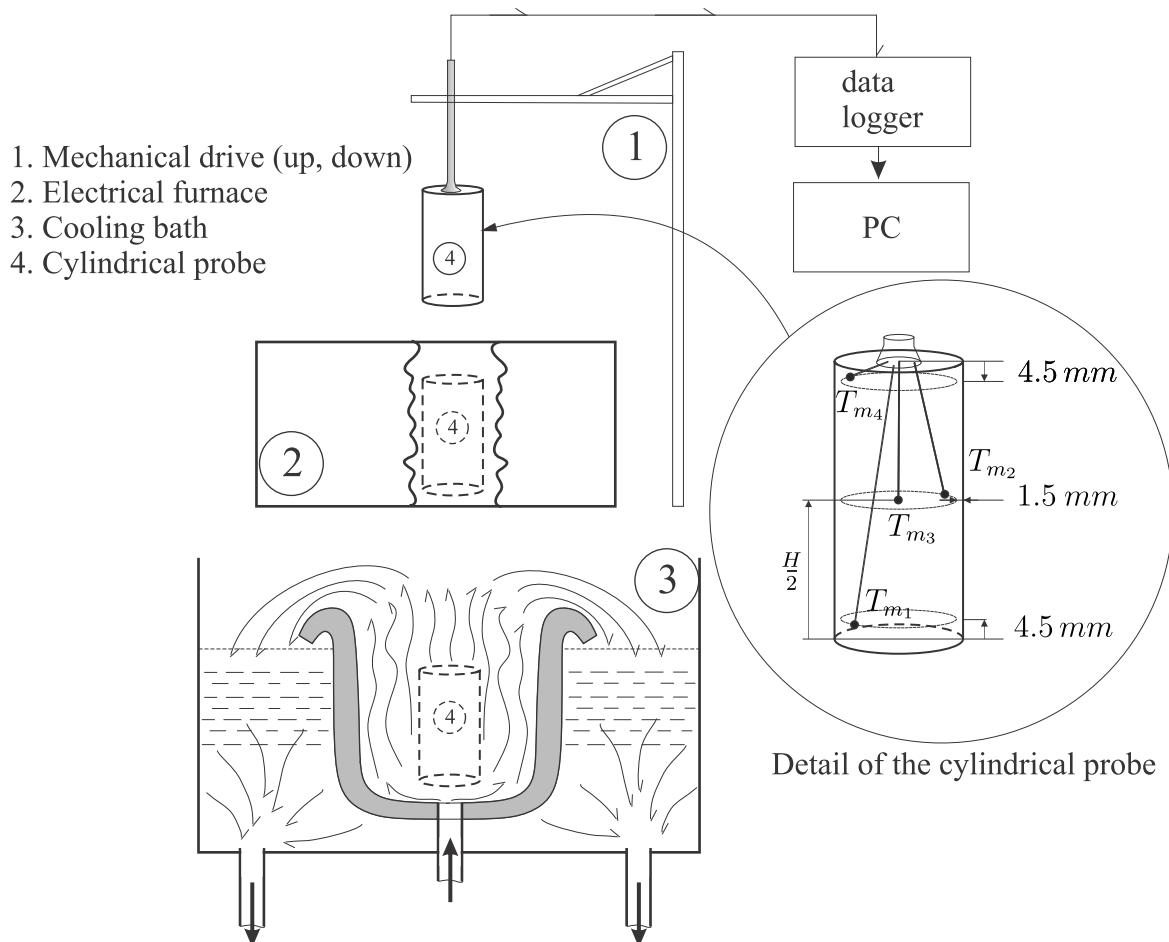
Fig. 5 Schematic view of the experiment with the main components. The details show the layout of the measuring points

3.2 Numerical simulation of the quenching process

Once the experimental results are collected, the computer simulation starts by preparing the numerical model for the IHTP. The computational domain is the cylinder of three different radii 12.5, 25 and 37.5 mm and heights 100, 150 and 220 mm respectively, with 4 temperature sensors recording at every half second. Three sensors are directly used in the IHTP, while the thermocouple

located at the symmetry axis was used as control point. As previously stated, the IHTP is defined as the estimation of the heat transfer coefficients at cylinder surfaces: α^{Γ_1} – bottom base, α^{Γ_2} – cylinder shell around bases, and α^{Γ_3} – top base.

Previously, the IHTP of the cylinder quenching was solved by using Levenberg-Marquart method (LMM) and NSGA II [21, 24], where the DHTP was solved using COMSOL Multiphysics®. The reason of using NSGA II in combination with LMM is due to ill-conditioned problem and inability to solve the multi-objective optimization problem by using LMM only. Some of the disadvantages of this approach is slow convergence time and the complexity of the method as well as the nature of the NSGA II [24].

This paper presents a new approach for parameter optimization by using modified version of the LMM and implemented 1D and 2D axisymmetric solver for DHTP by using FEM (line and triangle finite elements). To overcome ill-conditioned nature of the presented quenching process, the paper proposes two improvements of the LMM:

1. Estimation of the initial values of the HTC by using 1D LMM, and
2. Modified version of the calculation of the sensitivity matrix.

3.3 Estimation of the initial values of the unknown parameters

As can be seen throughout the literature, the initial parameter values of the LMM optimization are very important. The closer the initial values of the HTC parameter to the exact solution, the faster the convergence achieved [7, 19, 18, 14]. In order to estimate the initial HTC values ($\alpha^{(1)}$, $\alpha^{(2)}$ and $\alpha^{(3)}$), 1D LMM is performed for the three points in the computational domain separately, which is depicted in Fig. 3. Each of the 1D optimization process was performed for time $t = 1$ to T, so that every time step has it own initial values.

Once the initial values of the HTC were estimated, the main multi-objective LMM optimization is performed. As can be seen in Fig.1, the HTC values along the cylinder shell have nonlinear distribution. By knowing HTC values at three points along the cylinder height, one can interpolate the HTC values by using a known interpolation function. In order to interpolate the distribution of the HTC along the cylinder, bi-linear function through three points was used. Regarding the HTC distribution along the cylinder bases, the constant value is assumed. By using the interpolation function, the IHTP can be reduced to the estimation of the HTC parameters $\alpha^{(1)}$, $\alpha^{(2)}$ and $\alpha^{(3)}$ (see Fig. 4).

3.4 Calculation of the sensitivity matrix

Since the HTC parameters are not independent of each other, the calculation of the sensitivity matrix (27) in the multi-objective LMM optimization produces the unstable equation system such that the iteration process falls into the local optimum. To overcome this problem, the sensitivity matrix (27) is calculated only for parameter which produces the highest error. The rest of parameters are not changed for the current iteration. In order words, inter-dependency of the unknown parameters in the sensitivity matrix is avoided by considering the most dominant parameter only, while the other parameters are not changed for the current iteration.

The calculation of the most dominant HTC is expressed as:

$$\alpha_{md} = Argmax(Y_t - \vartheta_t(\alpha^{\Gamma})) \tag{29}$$

where *Argmax* function returns the HTC parameter α_{md} which produces the maximum squared error.

Once the most dominant parameter is determined, the sensitivity matrix (27) becomes:

$$J(\alpha_{md}) = \left[\frac{\partial \vartheta^j}{\partial \alpha_{md}}\right] = \left[\frac{\partial \vartheta^1}{\partial \alpha_{md}} \quad \cdots \quad \frac{\partial \vartheta^m}{\partial \alpha_{md}}\right]^T \tag{29}$$

The rest of the LMM procedure remains as originally proposed [7].

3.5 The algorithm for the estimation of the unknown parameters

The classic Levenberg-Marquart method (LMM) and related computational algorithm can be found in many books [7]. The difference of the algorithm variations can be identified in determination of the stability parameters, and the calculation of the sensitivity matrix. The paper presents the modified LMM version in the estimation of the initial parameter values, the determination of the most dominant parameters in the objective function, and the calculation of the sensitivity matrix.

The following listing present 1D LMM algorithm for the estimation of the initial parameter values:

Algorithm 1 Estimation of the initial parameter values by using 1D LMM

Step 1: Read initial value files:
Y_t^m - experimental results
$1D$ mesh - finite element mesh
$c(\vartheta), \rho, \lambda(\vartheta)$ - material properties.

Inputs: Y_t^i, $\alpha_0^i = 0$ and $\vartheta_0^i = 850^0 C$, $\mu_0 = 0.001$
Step 3: Start iteration process of time $k = 1$ to T. $if(t = T)$ GOTO **Step 13**
Step 4: Solve 1D DHTP given by equation (5), with available α_k^i
Step 5: Calculate objective function $C(\alpha_k)$ given by (53).
Step 6: Calculate sensitivity according to (55), then calculate dumping matrix $\Omega_k = diag\left[\boldsymbol{J}_k^T \cdot \boldsymbol{J}_k\right]$.

Step 7: Solve matrix equation (61) to obtain $\Delta\alpha_k^i$.
Step 8: Calculate new estimate $\alpha_{k+1}^i = \alpha_k^i + \Delta\alpha_k^i$
Step 9: Solve 1D DHTP given by equation (5), with the new value sof α_{k+1}^i. Then calculate objective function $C(\alpha_{k+1})$ given by (53).
Step 10: $if C(\alpha_{k+1}) \geq C(\alpha_k) \implies \mu_k = 10\mu_k$ and $GOTO$ **Step 7**
Step 11: $if C(\alpha_{k+1}) < C(\alpha_k) \implies \mu_k = 0.1\mu_k$ and accept the value of α_{k+1}^i

Step 12: if (63) OR (64) OR (65) $= TRUE$ $k = k + 1$ GOTO **Step 4**
$else$ GOTO **Step 6**
Step 13 Store the estimated values and stop the program.

Three executions of the 1D LMM algorithm are performed in order to estimate three HTC parameters ($\alpha^{(1)}$, $\alpha^{(2)}$ and $\alpha^{(3)}$) depicted in Fig. 3.

The multi objective LMM starts by accepting the initial values of $\alpha^{(1)}$, $\alpha^{(2)}$ and $\alpha^{(3)}$ for every time step:

Algorithm 2 Multi-objective LMM algorithm for parameter estimation

Step 1: Read initial value files:
Y_t^m - experimental results
$2D$ mesh - triangle finite element mesh
$c(\vartheta), \rho, \lambda(\vartheta)$ - material properties.

Inputs: Y_t^m and $\vartheta_0^i = 850^0 C$, $\mu_0 = 0.001$
Step 3: For $k = 1$ to T. Set initial values $\alpha_k^1, \alpha_k^2, \alpha_k^3$ $if(t = T)$ GOTO **Step 13**
Step 4: Solve 2D DHTP given by equation (5), with available $\alpha_k^1, \alpha_k^2, \alpha_k^3$
Step 5: Calculate objective function $C(\boldsymbol{\alpha}_k^\Gamma)$ given by (53).
Step 6: Determine the most dominant parameters α_{md} by using expression (66)
Step 7: Calculate sensitivity according to (67), then calculate dumping matrix $\Omega_k = diag\left[\boldsymbol{J}_k^T \cdot \boldsymbol{J}_k\right]$.

Step 8: Solve matrix equation (61) to obtain $\Delta\alpha_k^i$.
Step 9: Calculate new estimate $\alpha_{k+1}^i = \alpha_k^i + \Delta\alpha_k^i$
Step 10: Solve 1D DHTP given by equation (5), with the new value sof α_{k+1}^i. Then calculate objective function $C(\alpha_{k+1})$ given by (53).
Step 11: $if C(\alpha_{k+1}) \geq C(\alpha_k) \implies \mu_k = 10\mu_k$ and $GOTO$ **Step 8**
Step 12: $if C(\alpha_{k+1}) < C(\alpha_k) \implies \mu_k = 0.1\mu_k$ and accept the value of α_{k+1}^i

Step 13: if (63) OR (64) OR (65) $= TRUE$ $k = k + 1$ GOTO **Step 4**
$else$ GOTO **Step 5**
Step 14 Store the estimated values and stop the program.

The computer implementation of both algorithms as well as direct solver has been implemented in C# programming language and can be found at *http://github.com/bhrnjica/quenching_simulation*. The Daany – DAta ANalYtics on .NET [23] library was used for the HTC interpolations, matrix algebra, and system of equations solver.

The simplified flowchart of the computer implementation is shown in Fig 6.
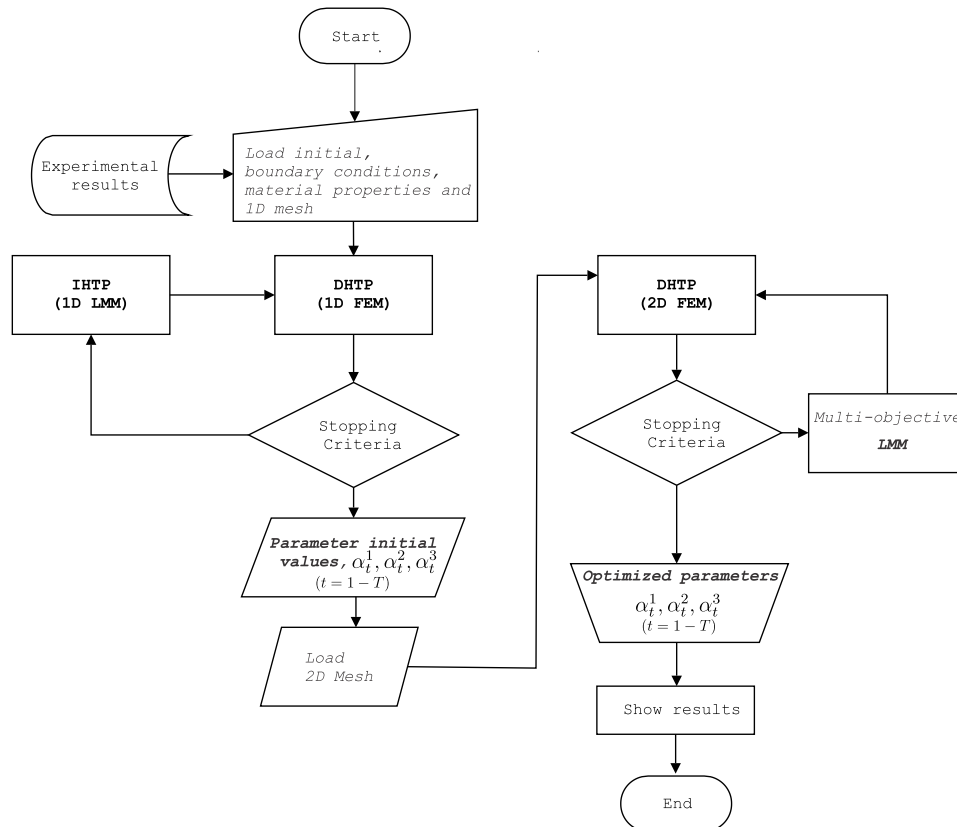
Fig. 6 Flowchart of the computer implementation of the numerical simulation

4. Results of the numerical simulation

With the modified implementation of the LMM, the numerical simulation of quenching process was performed on different cylinder geometries and different quenching fluids. In total, nine different numerical simulations were performed and compared with the experimental results. Table 1 shows different cylinder geometries and related statistics of the finite element model.

Table 2 shows combination of the cylinder dimension and quenchants used in the numerical simulation. Nine different numerical simulations were performed with different cylinder geometry and quenchant types. Each numerical simulation included estimation of the HTC parameters by solving IHTP of multi-objective function.

Table 3 shows the overview of the error summary of each numerical simulation at every measured point. In total, 36 different error measures were performed by calculating minimum, maximum and average of the absolute and relative errors respectively.

The nine different numerical simulations were performed to estimate the HTC at three cylindrical edges (Γ_1, Γ_2 and Γ_3). The HTC at Γ_2 was changing along the cylinder height, hence it is interpolated by using bi-linear interpolation (Fig. 3).

Table 1 Cylinder probe dimensions and corresponding FEM mesh used in the numerical simulation

Cylinder (R, H), (mm)	# of nodes	# finite elements	finite element type
(25, 100)	660	1164	triangle
(50, 150)	1213	2195	triangle
(75, 225)	1949	3560	triangle

Table 2 Overview of the numerical simulations

Numerical simulation Id	Cylinder dim. (Φ, H), (mm)	Quenchant type
NS1	(25, 100)	Water
NS2	(50, 150)	Water
NS3	(75, 225)	Water
NS4	(25, 100)	Aquatensid solution 5 %
NS5	(50, 150)	Aquatensid solution 5 %
NS6	(75, 225)	Aquatensid solution 5 %
NS7	(25, 100)	Isorapid oil
NS8	(50, 150)	Isorapid oil
NS9	(75, 225)	Isorapid oil

Table 3 Overview of absolute and relative errors at measuring points

Id	MP	AEmax	AEavg	AEmin	REmax (%)	REavg (%)	Remin (%)
NS1	Tm1	1.8	0.8	0.0	3.2	0.9	0.0
	Tm2	2.0	0.5	0.0	2.2	0.4	0.0
	Tm3	9.2	3.8	0.2	11.0	1.7	0.0
	Tm4	2.1	0.9	0.0	3.7	0.6	0.0
NS2	Tm1	2.0	0.8	0.0	2.5	0.7	0.0
	Tm2	1.9	0.5	0.0	3.2	0.3	0.0
	Tm3	50.6	11.5	0.1	14.8	3.3	0.0
	Tm4	1.6	0.6	0.0	1.7	0.3	0.0
NS3	Tm1	2.0	0.6	0.0	2.9	0.5	0.0
	Tm2	2.1	0.7	0.0	3.4	0.5	0.0
	Tm3	33.6	6.2	0.1	5.4	1.6	0.1
	Tm4	1.9	0.6	0.0	3.5	0.4	0.0
NS4	Tm1	2.1	0.7	0.0	4.3	0.8	0.0
	Tm2	2.1	0.6	0.0	3.6	0.5	0.0
	Tm3	21.8	7.5	0.5	14.3	3.4	0.1
	Tm4	2.0	0.6	0.0	3.9	0.4	0.0
NS5	Tm1	4.4	0.8	0.0	4.9	0.8	0.0
	Tm2	1.9	0.5	0.0	1.8	0.4	0.0
	Tm3	37.7	8.5	0.4	14.8	3.6	0.0
	Tm4	4.1	0.7	0.0	3.0	0.3	0.0
NS6	Tm1	4.4	0.8	0.0	4.6	0.6	0.0
	Tm2	2.0	0.9	0.0	2.8	0.4	0.0
	Tm3	22.1	6.3	0.3	6.3	2.1	0.0
	Tm4	3.8	0.7	0.0	3.7	0.4	0.0
NS7	Tm1	2.1	0.8	0.0	4.0	0.7	0.0
	Tm2	2.0	0.8	0.0	1.8	0.5	0.0
	Tm3	27.3	7.7	0.1	11.1	2.5	0.0
	Tm4	2.1	0.8	0.0	1.5	0.3	0.0
NS8	Tm1	34.6	1.5	0.0	4.5	1.0	0.0
	Tm2	8.9	0.7	0.0	1.4	0.4	0.0
	Tm3	21.8	6.7	0.4	9.2	2.0	0.0
	Tm4	10.4	0.8	0.0	1.2	0.3	0.0
NS9	Tm1	12.8	0.7	0.0	1.5	0.2	0.0
	Tm2	2.1	0.8	0.0	0.4	0.2	0.0
	Tm3	23.4	8.0	0.3	6.5	1.7	0.0
	Tm4	8.5	0.7	0.0	1.0	0.2	0.0

The following 3 figures show the results of the numerical simulations for NS1, NS2 and NS3. Each figure consists of 4 images: a) comparison between experimental and numerical temperatures at four measured points, b) residual plots of the measured and calculated temperatures, c) optimized values of the HTC parameters α_1, α_2, α_3, and d) temperature filed calculated at five different times of quenching.
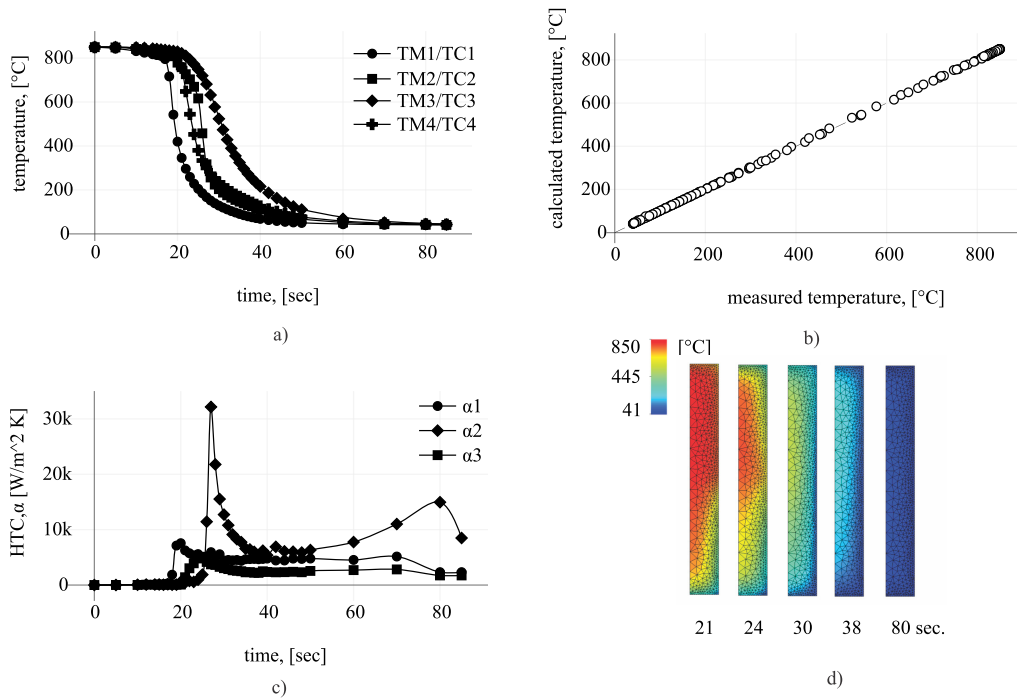
Fig. 7 Numerical results for cylinder 25 × 100 mm immersed in water
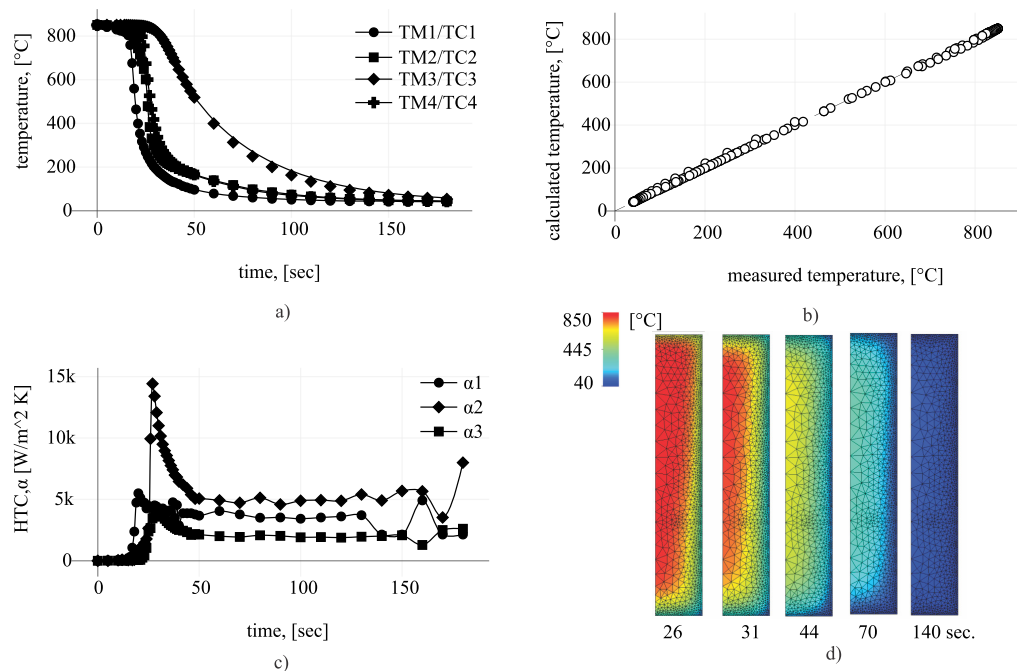
Fig. 8 Numerical results for cylinder 25 × 100 mm immersed in 5 % aquatensid solution

The greatest local deviations between measured and calculated temperatures can be identified at the location of the Tm3 thermocouple at the time when boiling phase of the quenching process is presented. The presented results in Table 3 are in all cases closer than the results in the cited literature [21, 24]. When comparing the results for the control point Tm3, the results show inconsistency e.g., NS2 has 50 °C deviation, while the results from the [24] has 40 °C. Other results of the control points are approximately the same.

Regarding the optimization algorithms, the presented algorithms reduced the optimization time significantly and showed superiority to the algorithms cited in the literature [21, 24]. The whole optimization process at regular PC took less than 25 minutes for all 9 simulations, while compared algorithms took several hours only for one simulation [21, 24].

Fig. 8 Numerical results for cylinder 25 × 100 mm immersed in Isorapid oil

5. Conclusion

The paper presents methods, algorithms, and results of the numerical simulation of quenching cylindrical steel probe. In the first part the derivation of partial differential equation of the heat transfer in cylindrical coordinates for axisymmetric problem domain was presented. In addition, the variational form of the partial differential equation was derived as the starting point of derivation of the finite element procedure for DHTP. Subsequently, the IHTP was introduced and applied for the 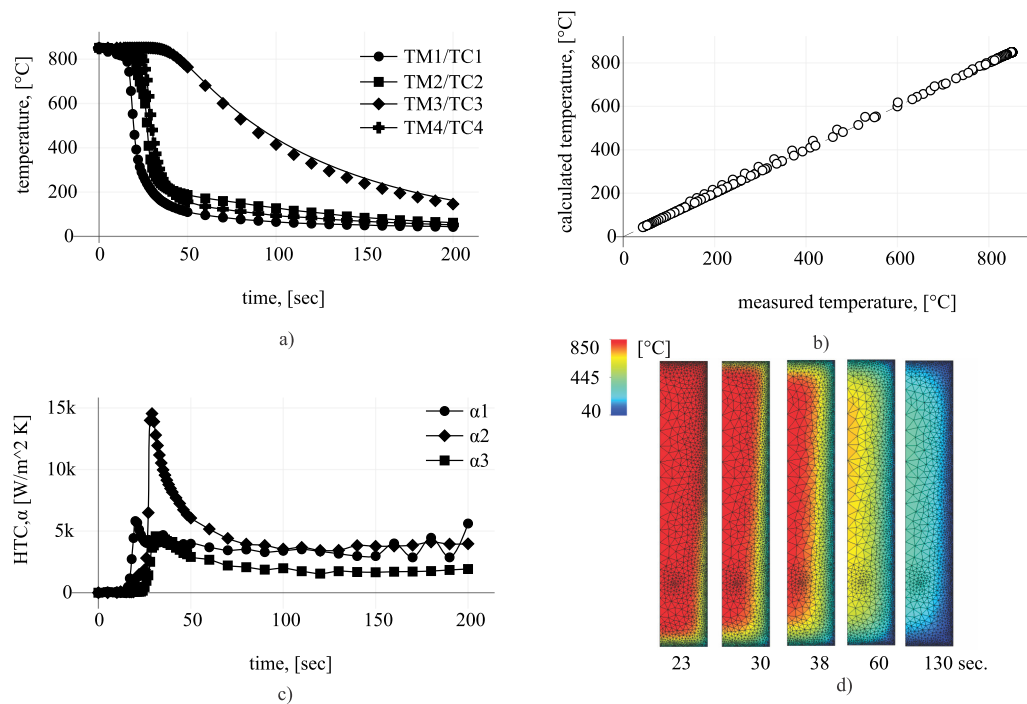quenching of the cylinder which is immersed in three different quenchant. Since the multi-objective optimization of the HTC parameters is required, the paper present the modified version of the LMM in terms of parameter initial value calculation and determination of the most dominant parameter for sensitivity matrix calculation. To test the numerical simulation, three measuring points are installed beneath the cylinder surface and one measuring point in the centre of the cylinder. As the results show, in all cases of the measuring points beneath the cylinder surface (Tm1, Tm2 and Tm4), the absolute and relative error are minimal and show great accuracy.

However, for some cases at the measuring location Tm3, the results deviate up to 50 °C or 14.8 % of the relative error. Analysis shows that the deviation of the results appeared in the "bubble boiling" phase of the quenching where the gradients are very large and the applied approximation of the HTC was not good enough to estimate the temperature field. This can also be recognized in Fig. 1 where the real HTC distribution along the cylinder height differs from the interpolation function used in the numerical simulation.

By comparing the presented results with the results from the literatures [21, 24], it can be concluded that the calculated results are closer to measured results. The presented optimization algorithm has significantly reduced the optimization process up to 25 minutes in comparison to the several hours in the literature [21, 24].

References

[1] Ramesh, G., Prabhu, K.N. (2014). Wetting and cooling performance of mineral oils for quench heat treatment of steels, *ISIJ International,* Vol. 54, No. 6, 1426-1435, doi: 10.2355/isijinternational.54.1426.

[2] Liščić, B., Singer, S. (2014). 12.05 - Calculation of the heat transfer coefficient based on experiments by the liscic probes comprehensive materials processing, In: Hashmi, S., Batalha, G.F., Van Tyne, C.J., Yilbas, B.S. (eds.), *Comprehensive Materials Processing,* Elsevier, Amsterdam, Netherlands, 123-176, doi: 10.1016/B978-0-08-096532-1.01205-X.

[3] Song, M., Pu, Y., Liu, Q., Wang, R., Wang, B. (2019). Numerical simulation and experimental verification of the quenching temperature field of grinding balls, *Materiali in tehnologije/Materials and technology,* Vol. 53, No. 4, 515-520, doi: 10.17222/mit.2018.226.

[4] Carlone, P., Palazzo, G.S., Pasquino, R. (2010). Finite element analysis of the steel quenching process: Temperature field and solid–solid phase change, *Computers & Mathematics with Applications,* Vol. 59, No. 1, 585-594, doi: 10.1016/j.camwa.2009.06.006.

[5] Jahedi, M., Berntsson, F., Wren, J., Moshfegh, B. (2018). Transient inverse heat conduction problem of quenching a hollow cylinder by one row of water jets, *International Journal of Heat and Mass Transfer,* Vol. 117, 748-756, doi: 10.1016/j.ijheatmasstransfer.2017.10.048.

[6] Carasso, A. (1982). Determining surface temperatures from interior observations, *SIAM Journal on Applied Mathematics,* Vol. 42, No. 3, 558-574, doi: 10.1137/0142040.

[7] Özisik, M.N., Orlande, H.R.B. (2021). *Inverse heat transfer: Fundamentals and applications,* Second edition, CRC Press, Boca Raton, Florida, USA, doi: 10.1201/9781003155157.

[8] Totten, G.E., Tensi, H.M. (2002). Using conductance data to characterize quenchants, *Heat Treating Progress,* Vol. 2, No. 5, 39-42.

[9] Liščić, B., Singer, S., Beitz, H. (2011). Dependence of heat transfer coefficient at quenching on diameter of cylindrical workpieces, *International Heat Treatment and Surface Engineering,* Vol. 5, No. 3, 101-105, doi: 10.1179/174951411X13051201040910.

[10] Rao, S.S. (2017). *The finite element method in engineering,* Fifth edition, Elsevier, Amsterdam, Netherlands, doi: 10.1016/C2009-0-04807-7.

[11] Nithiarasu, P., Lewis, R.W., Seetharamu, K.N. (2016). *Fundamentals of the finite element method for heat and mass transfer,* Second edition, John Wiley & Sons, Hoboken, New Jersey, USA.

[12] Taler, J., Ocłoń, P. (2014). Finite element method in steady-state and transient heat conduction, In: Hetnarski, R.B. (eds.), *Encyclopedia of Thermal Stresses,* Springer, Dordrecht, Netherlands, 1604-1633, doi: 10.1007/978-94-007-2739-7_897.

[13] Reddy, J.N. (2019). *An introduction to the finite element method,* Third edition, McGraw-Hill Education, New York, USA.

[14] Press, W.H., Teukolsky, S.A., Vetterling, W.T., Flannery B.P. (2007). *Numerical recipes : The art of scientific computing,* Third edition, Cambridge University Press, New York, USA.

[15] Özisik, M.N. (1993). *Heat conduction,* Second edition, John Wiley & Sons, New York, USA.

[16] Wang, S., Jia, H., Sun, X., Zhang, L. (2017). Two-dimensional steady-state boundary shape inversion of CGM-SPSO algorithm on temperature information, *Advances in Materials Science and Engineering,* Vol. 2017, Article ID 2461498, doi: 10.1155/2017/2461498.

[17] Colaço, M.J., Orlande, H.R.B., Dulikravich, G.S. (2006). Inverse and optimization problems in heat transfer, *Journal of the Brazilian Society of Mechanical Sciences and Engineering*, Vol. 28, No. 1, 1-24, doi: 10.1590/S1678-58782006000100001.

[18] Bard, Y. (1974). *Nonlinear parameter estimation,* Academic Press, New York, USA.

[19] Beck, J.V., Arnold, K.J. (1977). *Parameter estimation in engineering and science,* John Wiley & Sons, New York, USA.

[20] Marquardt, D.W. (1963). An algorithm for least-squares estimation of nonlinear parameters, *Journal of the Society for Industrial and Applied Mathematics,* Vol. 11, No. 2, 431-441, doi: 10.1137/0111030.

[21] Behrem, Š., Hrnjica, B., (2018). Estimate of heat transfer coefficient during quenching steel in water, *Transactions of FAMENA,* Vol. 42, 61-73, doi: 10.21278/TOF.42Si106.

[22] Behrem, Š., Hrnjica, H., (2021). Results of heat transfer coefficient estimation during the quenching of cylindrical samples in aqueous solutions, *Transactions of FAMENA,* Vol. 45, 49-58, doi: 10.21278/TOF.SI1008421.

[23] Hrnjica, B. (2021). Daany – DAta ANalYtics on .NET, *Software Engineering,* from *http://arxiv.org/abs/2107.03733*, accessed November 27, 2021.

[24] Behrem, Š. (2015) *The influence of the wetting kinematics and cylindrical probe diameters on the heat transfer coefficient during steel quenching,* PhD Thesis, University of Bihac, Faculty of Technical Engineering, Bihac, Bosnia and Herzegovina.

Appendix A

A list of abbreviations

Abbreviation	Description
DHTP	Direct Heat Transfer problem
IHTP	Inverse Heat Transfer Problem
HTC	Heat Transfer Coefficient
FEM	Finite Element Method
FDM	Finite Difference Method
LMM	Levenberg-Marquart Method
NSGA	Nondominated Sorting Genetic Algorithm II

Modelling and simulation of hot direct extrusion process for optimal product characteristics: Single and multi-response optimization approach

Elplacy, F.[a,*], Samuel, M.[b], Mostafa, R.[b]

[a]Mechatronics Department, Faculty of Engineering, Horus University, New Damietta, Egypt
[b]Production Engineering & Mechanical Design Department, Faculty of Engineering, Mansoura University, Mansoura, Egypt

A B S T R A C T

The study of eccentricity minimization in cylindrical products helps to reduce the mechanical vibrations and wear of related mechanical parts such as bearings, columns and gears which positively affects in maintenance costs savings and increasing production quality reliability. The main purpose of this paper is to investigate the effect of the eccentricity between the billet material and the die parts on the quality of the final product in the direct extrusion process. The input parameters to produce a cylindrical product shape are optimized in MINITAB based on Taguchi method and ANOVA. The selected material of the billet is the aluminium alloy AA2024, and the die material is Steel H13. The inputs parameters are the temperature, the die angle, the ram speed, and the presumed eccentricity. The finite element model of the process is simulated in DFORM-3D for providing the extrusion information such as the pressure, the effective stress and strain, the final product eccentricity, and the roundness error. The study is carried out on two cases of the presumed eccentricity in addition to a case of zero eccentricity. The single and multi-response optimizations are executed to obtain the optimum parameters for the minimum product eccentricity and roundness error.

1. Introduction

Extrusion process is used to create different and complex cross-sectional areas with a good surface finish. It is utilized in multiple shapes production such as strips, bars, tubes, hollow and solid profiles, and it could achieve the energy and material savings [1]. Aluminium alloys (Al-alloy) are the most popular materials that provide a lot of valuable properties such as light metal weight, high process ability, rust resistance, eco-friendly and high strength with good ductility and toughness [2]. Al-extrusion is a widespread metal forming process for producing long and durable parts. Hot Al-extrusion process depends on forcing a preheated billet into a steel die with a specific design. Proper selection of the extrusion initial parameters such as billet temper-

ature, ram pressure, die angle and ram pressure is the main aid to obtain a right extruded product. However, during hot Al-extrusion process, various defects may happen and are responsible for reducing the quality of the final product and rising the scrap percentage and the product cost. These defects such as internal cracking, Pipe Formation, subsurface defects, Funnel formation, centre burst and the eccentricity whereas it is a common defect in the extrusion process [3]. Studying and optimizing the Al-extrusion parameters may help in improving the product quality, minimizing the defects, and decreasing the cost.

In the past, extrusion parameters were selected according to the experience and consequently, the researchers tried to investigate the process parameters to obtain the optimum setting of the initial conditions. Yanran *et al.* [4] used the Finite-Element (FE) method to analyse the deformation stage of extrusion process according to the principle of minimum deformation force for optimizing the angle of the die. Jang *et al.* [5] aimed to study the numerical analysis of radial extrusion process combined with direct extrusion to investigate the forming properties of an AA 2024 alloy in terms of material flow into the direct can and radial flange sections. Jurković *et al.* [6] determined the optimal direct extrusion parameters to minimize the extrusion load using Taguchi approach. Many researchers studied the effects of Al-extrusion parameters (billet temperature, ram speed, die angle, etc.) that simulated through different finite element analysis solvers on the output responses. Zhang *et al.* [7] simulated the Al-extrusion process using HYPERXTRUDE to optimize the symmetry of the metal flow and the extrusion force using Taguchi and ANOVA. Jajimoggala [8] studied the effect of the extrusion parameters of AL6061 on the extrusion load and the effective stress using DOE and the analysis of variance. Bressan *et al.* [9] modelled the hot direct extrusion process of AL6060 through FVM and compared the results with the experimental results. Mai *et al.* [10] determined the ram speed and billet temperature in bars of Al-alloy to obtain the optimum of the surface roughness and the extrusion pressure. Francy *et al.* [11] dealt with the input parameters of the extrusion process such as half die angle, coefficient of friction, logarithmic strain and ram velocity using DEFORM-3D software and Taguchi approach to minimize the power consumption. Fernández *et al.* [12] studied the influence of the extrusion parameters on the manufacturing of Bimetallic cylinders combining of Ti-Alloy sleeve and Mg-Alloy core using DOE by Taguchi Method. Medvedev *et al.* [13] developed an approach to increase productivity rate of the Al-extrusion by optimizing of extrusion dies design coupled with subsequent optimizing of extrusion parameters such as extrusion ratio, ram speed, lubrication using FM simulation. Few researchers have dealt with the defects of the aluminium extrusion process such as centre burst, surface cracking, eccentricity, and product roundness. Parghazeh and Haghighat [14] investigated the prediction of the central bursting defects in the extrusion process through Conical-Die. Ngernbamrung *et al.* [15] determined the extrudability of Aluminium alloy is by tearing appearance under extrusion parameters (temperature and speed). Yang *et al.* [16] used the velocity-transformed central-flow model for analysing the centre-shifted of punch of the backward-extrusion for eccentric tubes from circular billets. The work hardening is considered, and the extrusion pressure is computed.

Most of the pre-existing works carried on developing the optimized design with some variations in the input process parameters under different optimization techniques. There have been no reports on the attempts in the numerical studying of the effects of main input parameters including the misalignment between the billet and the extrusion on the eccentricity and the roundness of an extruded aluminium tubes.

In this work, a combination of Finite Element Modelling (FEM) and Design of Experiments (DOE) is employed to study the effects of main extrusion process inputs on the eccentricity of a cylindrical product and its roundness. As a FEM for Hot-Direct-Extrusion process of AA2024 by DEFORM-3D software is applied to simulate the input parameters such as the billet temperature, the ram speed, the die angle, and the pre-eccentricity between the billet and the die. The outputs of the process such as the extrusion pressure, the stress and strain distribution, the eccentricity of the produced cylinder and its roundness are investigated. Taguchi Method is employed for DOE and an orthogonal array L9 is constructed by using a statistical software MINITAB 18. The multi-response of the outputs is discussed as the objectives are to minimize the extrusion pressure, the product eccentricity and the roundness error and obtain the effective stress and strain.

Also, the ANOVA is adopted to verify and identify the sequence of importance of input parameters on the final product quality.

2. Materials and method

Optimization of production parameters is a desirable research field in the recent eras [17]. To perform the modelling and simulation in this study for the experimental design of the certain cases of the hot extrusion process, the Taguchi-technique [18] using the statistical program MINITAB 18 is applied, the process elements (billet and die) are modelled in SolidWorks platform and the Finite Element Analysis (FEA) for the process in each experiment is simulated in DEFORM-3D software. Finally, the ANOVA is adopted to identify and verify the importance of extrusion parameters that affected on the eccentricity and the roundness error of the final product.

2.1 Materials selection

In this work, AA2024 alloy is selected as the billet-material. AA2024 has a high strength, lightweight, a good fatigue and corrosion resistance and it is ranked as one of an optimal selected material for the aircraft and vehicle applications. The billet has a dimension with 64 mm Dia. and 100 mm long. While H13 tool steel that offers High hardenability, excellent wear resistance and high toughness is selected as the die-material. Tables 1, 2 and Table 3 illustrate the chemical composition and the mechanical properties of the billet and the die materials, respectively. Fig. 1 represents the SolidWorks 2018 modelling of the billet, the container, the ram, and the die with its proposed dimensions.

Table 1 Chemical composition of AA2024 [19]

Element	Cu	Mg	Mn	Fe	Zn	Si
Wt.%	4.45	1.57	0.56	0.17	0.16	0.06

Table 2 Chemical composition of H13 steel [20]

Element	C	Si	Mn	Cr	Mo	V	P	S
Wt.%	0.32-0.45	0.80-1.20	0.20-0.50	4.74-5.50	1.10-1.75	0.80-1.20	≤ 0.030	≤ 0.03

Table 3 Mechanical and physical properties of AA2024 and H13 [21]

Mechanical properties	Density (g/cm³)	Melting point (°C)	Modulus of elasticity (GPa)	Poisson ratio	UTS (MPa)
AA2024	2.78	538-602	73.1	0.33	437
H13 steel	7.80	1427	215	0.27-0.30	446

a) Billet	b) Container	c) Ram	d) Die
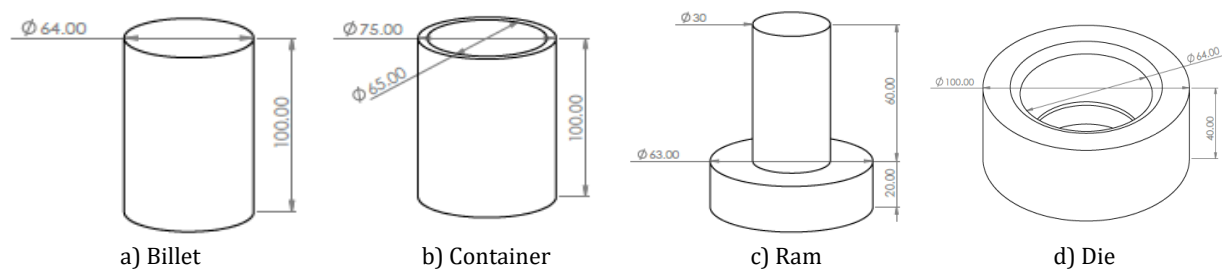
Fig. 1 SolidWorks geometrical models of the Billet, Container, Ram, and the Die with dimensions in mm (±0.05)

2.2 Methodology

For studying the effect of presumed eccentricity E_{pre} in the hot extrusion process of AA2024, four input parameters namely, the billet temperature T, ram speed Rs, die angle α and the presumed eccentricity are considered in an optimization problem whereas the coveted responses will be the pressure p, stress σ, strain ε, the extruded product eccentricity E_c, and its roundness Ro. The levels of parameters are shown in Table 4. A L9 Taguchi orthogonal array for the selected parameters is constructed in MINITAB 18 and it is illustrated in Table 5.

To study the effect of the presumed eccentricity on the quality of the final product, two cases of presumed eccentricity are adopted, and the results are compared to a zero case (E_{pre} = 0). The supposed two cases are (1) eccentricity between the ram and billet (the billet, container and die have the same enter line) (2) eccentricity between the container and the billet (the ram, container and die have the same centreline) as shown in Fig. 2. So, Finite Element Models for each experiment in the designed cases are constructed to study the optimum parameters for minimum pressure, stress, strain, eccentricity in the extrude and the roundness error. the FEA of the modelled process is carried through in DEFORM-3D software whereas the material properties are selected from the software database. The Boundary Conditions (BCs) and the Mesh Procedures (MP) for the simulated problem are introduced in Table 6. The outputs (pressure, stress, strain, the product eccentricity, and its roundness) for each experiment are exported to MINITAB to optimize the input parameters for the multi-responses in each case of eccentricity. Fig. 3 illustrates the simulation of extrusion steps in DEFORMTM-3D. The flowchart in Fig. 4 displays the procedures of the applied methodology and the steps sequence that are performed throughout the research.

Table 4 Hot extrusion process input parameters and its levels

Process parameter	Level 1	Level 2	Level 3
T (°C)	300	350	400
Rs (mm/s)	1	2	3
α (°)	12	16	18
E_{pre} (mm)	0.3	0.5	0.7

Table 5 Taguchi orthogonal array L9

No. of experiments	T (°C)	Rs (mm/s)	α (°)	E_{pre} (mm)
1	300	1	12	0.3
2	300	2	16	0.5
3	300	3	18	0.7
4	350	3	12	0.3
5	350	1	16	0.5
6	350	2	18	0.7
7	400	2	12	0.3
8	400	3	16	0.5
9	400	1	18	0.7
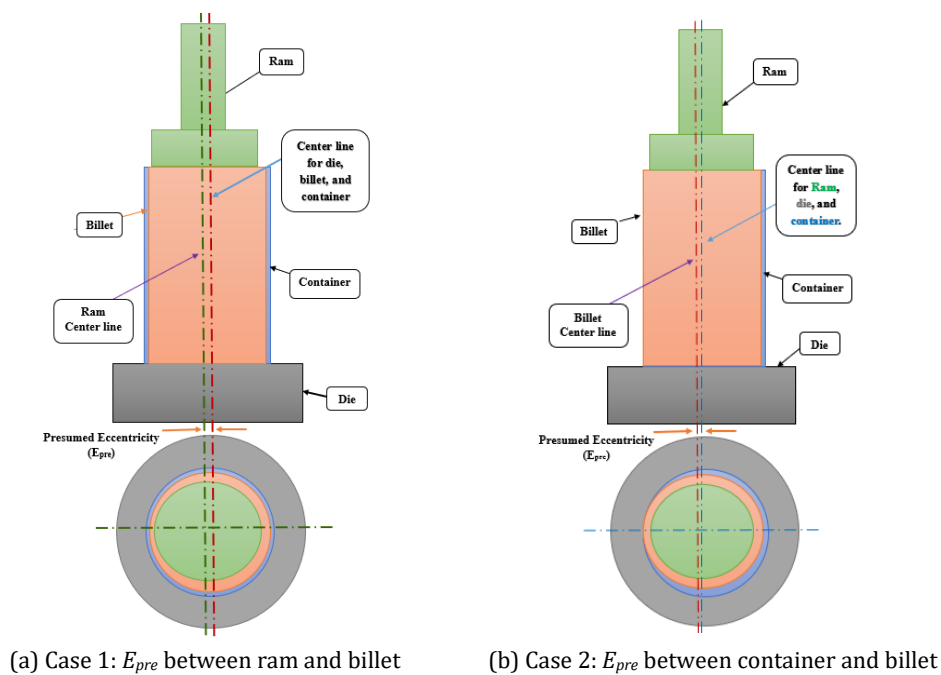
(a) Case 1: E_{pre} between ram and billet   (b) Case 2: E_{pre} between container and billet
Fig. 2 Presumed eccentricity (E_{pre}) cases in the simulated extrusion process

(a)	(b)	(c)	(d)	(e)	(f)

Fig. 3 Schematic demonstration of the extrusion simulation at different steps during the process

Table 6 Boundary conditions of the simulated problem

Meshing element type	Tetrahedral	Starting step number	-1	Step increment	5
Mesh elements	8000 (elements)	No. of simulation steps	500, 250, 1000		
Coefficient of friction	0.4	Room temperature	20 °C		

2.3 Product eccentricity calculation

The axis eccentricity of any cylindrical part may have much influence on the measurement results and the quality of its performance. Because of this came the importance of detecting the eccentricity of the final extruded product in this work. So, the eccentricity of the extruded product is calculated by taking an image of each model from the DEFORM-3D platform and exporting it into SolidWorks platform. The tracking setting is used to identify the model and its dimensions. Then, the billet axis is determined, as well as the axis of the extruded product. The axial eccentricity is computed by detecting the horizontal distance between the billet-centre and the product-centre as shown in Fig. 5.
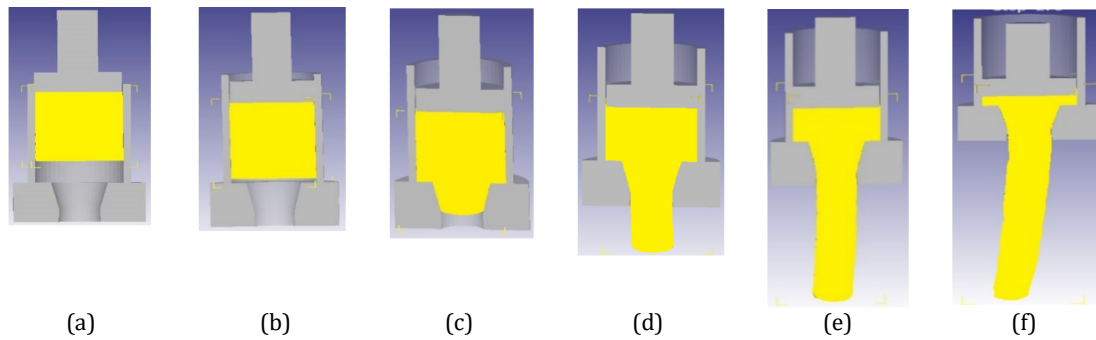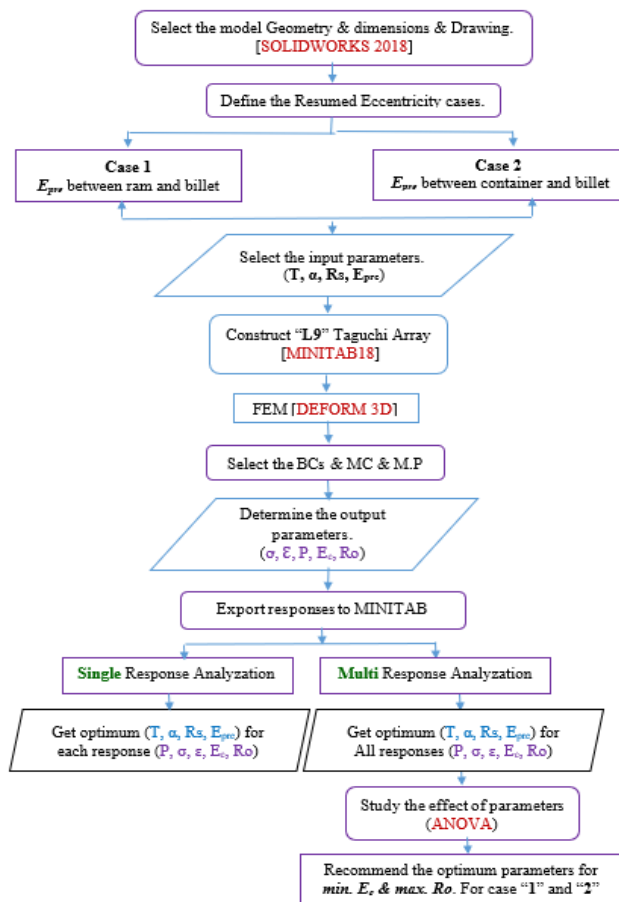

Fig. 5 Extruded Product Eccentricity

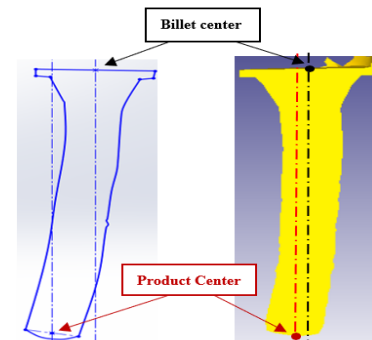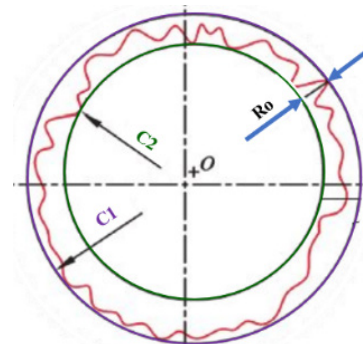**Fig. 4** The flowchart of the procedures of the applied methodology and the steps sequence

Fig. 6 Roundness Error using MZC method

2.4 Roundness error calculation

Roundness means to how tightly an object's shape resembles that of an accurately ideal circle. It is generally measured by rotational techniques by calculating radial deviations from a rotating fixed axis that becomes the main reference for all measurements. Roundness error can measure by four methods: Least Squares Circles, Maximum Inscribed Circle, Minimum Circumscribed Circle and Minimum Zone circle [22]. In this work, a Minimum Zone circle (*MZC*) is used to measure the roundness error by utilizing two circles as references. One circle (*C1*) is depicted outside the rounded product profile just to contain the whole of it and the second circle (*C2*) is drawn inside so that it only addresses the profile of the product. The roundness error (*Ro*) here is the difference between the radius of the two circles outside and inside as shown in Fig. 6.

3. Results and discussion

As earlier mention, the input parameters in the simulated extrusion process problem include (*T, Rs, α and E_{pre}*) and the output responses are (*P, σ, ε, E_c and Ro*). In this work, the single and multi-response optimization using Taguchi approach are applied for catching the optimum parameters to minimize the normal pressure, the product eccentricity, and the roundness-error in the suggested cases of eccentricity. ANOVA analysis is also applied to study the effect of inputs on the required responses.

As known, the statistical optimization has three types for optimizing data, they are (1) Nominal-the-best "N-type" (2) Larger-the better "L-type" and (3) Smaller-the-better "S-type". The objectives of "S-type & L-type" attempts are to identify the level of the optimal parameters to reach the smallest or greatest value of quality-characteristics. So, the smaller-the-better "S-type" is planned to use in this optimization problem.

3.1 Ideal case of eccentricity (No-presumed eccentricity)

In this step of the research, the problem has no-presumed eccentricity (*E_{pre}* = 0) while the billet and die parts are coaxial. After completion the simulation process in DEFORM-3D of nine experiments (L9) of input parameters and the implementation of the statistical optimization in Minitab platform, it found that the optimum parameters are 400 ℃ as the temperature, 2 mm/s as the ram speed, and 16° as the die angle while the outputs are 59.9 MPa as the normal pressure, 22.7 MPa as the stress and 10.8 as the strain. It was noted that the values of the product eccentricity *E_c* and the roundness error Ro were constant in all experiments. Their values are 0.02 mm as the product eccentricity and 0.03 mm as the roundness. And this is logical while there is no presumed eccentricity between the die parts and the billet. Fig. 7 illustrates the main effects of means of the process parameters and Fig. 8 represents the simulation of the process and the values of the optimum outputs (pressure, stress and strain).
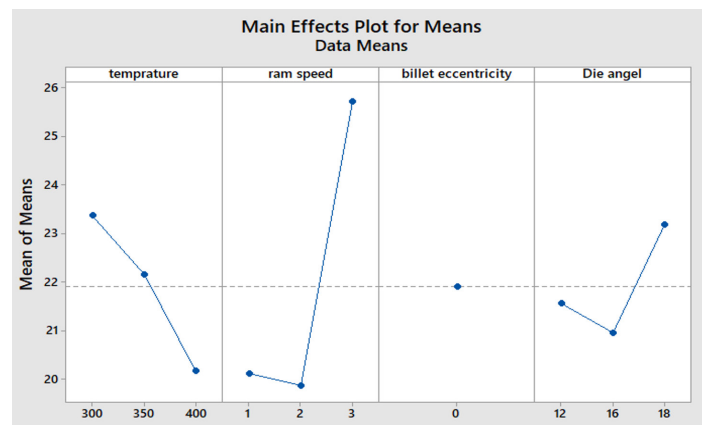

Fig. 7 Main effects plot for means of process parameters in Ideal Case of Eccentricity
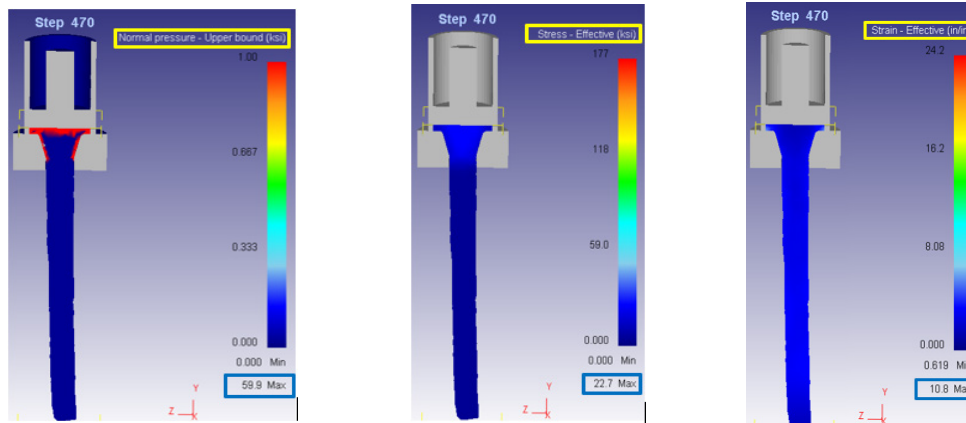
Fig. 8 Simulation of the process and the values of optimum responses in Ideal case of Eccentricity

3.2 Presumed eccentricity cases

The proposed eccentricity cases in this research are:

Case (1): The presumed eccentricity E_{pre} is between the billet and the ram while the billet, the container and the die have the same centreline.
Case (2): The presumed eccentricity E_{pre} is between the billet and the container while the ram, the container and the die have the same centreline.

3.3 Single response optimization and ANOVA technique

In this step, a single response optimization using MINITAB 18 is performed for both suggested eccentricity cases to realize the effect of the presumed eccentricity on the responses for each experiment. Then, ANOVA technique is applied to assess the competences of the input process parameters while extruding the AA2024.

In the case (1), and by observing the results of the optimization problem, it was found that the increasing in E_{pre} has an active impact on all outputs as the responses (P, Ec) are increased while σ, ε, and Ro decreases. In the case (2), it was observed that the increase in E_{pre} was accompanied by a decrease in P, σ, and ε, and an increase in Ec and Ro.

In the case (1), and by studying the one-way ANOVA results for each parameter, it was noticed that the most effective parameter on the final product eccentricity Ec is the ram speed Rs with the contribution percentage about 37.81 % then the die angle α with the contribution percentage about 26.09 %. The results also showed that the most influential parameter on the roundness error Ro is the temperature T with the contribution percentage about 51.48 % then the ram speed Rs with the contribution percentage about 38.59 %.

In the case (2), it was noted that the most effective parameter on Ec is the Rs with the contribution percentage about 44.63 % then the presumed eccentricity E_{pre} with the contribution percentage about 41.51 %. For the roundness error Ro response, the most influential parameter is T with the contribution percentage about 40.82 % then the die angle α with the contribution percentage about 27.79 %.

3.4 Multi response optimization

Under the situations of the single pattern of process parameters that may be optimal for certain specific characteristic however the same settings may have negative consequences for other quality aspects, the multi-characteristics-response-optimization may be the key. Since the multi-response in Taguchi method is a common technique that can deal with multi-data at the same time, it will be used in this work. and it will be followed by ANOVA technique to get the contribution percentage of the input parameters as it reveals the influence of each parameter on the responses.

In this statistical optimization problem, and for the nine proposed experiments (L9), the Signal to Noise ratio (S/N) plots are studied to determine the optimal parameters values for minimizing the objectives.

In the case (1), by using the responses data that is represented in Table 7, and by applying the multi response technique, it was found that the experiment No. 3 has the optimum process parameters that lead to obtaining the desired objectives of optimizing the responses $P, Ec, \sigma, \varepsilon,$ and Ro. The parameters are the temperature $T = 300$ °C, the ram speed $Rs = 3$ mm/s, presumed eccentricity $E_{pre} = 0.7$ mm, and the die angle $\alpha = 18°$. The optimal values of output responses are the pressure $P = 376$ MPa, the effective stress $\sigma = 85.6$ MPa, the effective strain $\varepsilon = 6.75$, the product eccentricity $Ec = 0.46$ mm and the roundness $Ro = 2.61$ mm. Fig. 9 shows the main effects of means for the input process parameters and Fig. 10 represents the DEFORM-3D simulation of the extrusion process of the experiment No. 3 for the optimum responses $P, \sigma,$ and ε.

Table 7 Input parameters and output responses data of L9 Taguchi array for case (1)

No.	T (°C)	Rs (mm/s)	E_{pre} (mm)	α (°)	P (MPa)	σ (MPa)	ε	Ec (mm)	Ro (mm)
1	300	1	0.3	12	937	89.9	7.43	7.71	3.09
2	300	2	0.5	16	757	122.0	6.78	0.76	1.84
3	300	3	0.7	18	376	85.6	6.75	0.46	2.61
4	350	1	0.5	18	1260	91.0	7.75	8.77	5.13
5	350	2	0.7	12	621	88.0	8.19	3.55	4.49
6	350	3	0.3	16	586	96.0	6.45	2.51	3.07
7	400	1	0.7	16	1170	79.5	6.66	2.74	2.38
8	400	2	0.3	18	759	83.0	5.30	3.96	2.74
9	400	3	0.5	12	499	72.6	6.06	8.35	2.96
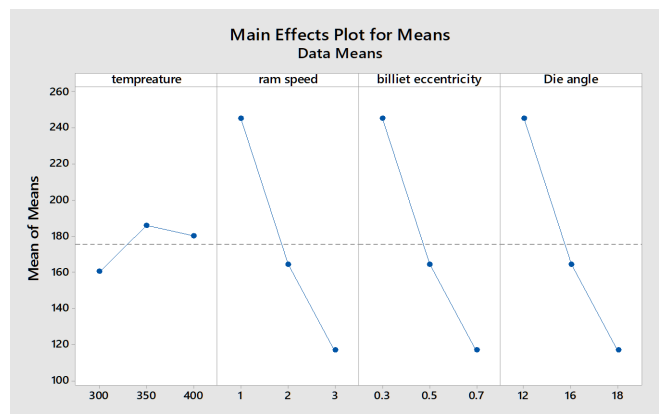
Fig. 9 Main effects plot for means of process parameters in Case (1)

Fig. 10 Simulation of the Extrusion process of the optimal responses in Case (1) using multi-response optimization

In the case (2), by using the responses data that is represented in Table 8, and by applying the multi- response optimization, it was noticed that the experiment No. 4 has the optimum process parameters that get the objective. The optimum responses are found at $T = 350$ °C, $Rs = 1$ mm/s, $E_{pre} = 0.5$ mm, and $\alpha = 18°$. The optimal values of output responses are the pressure $p = 575$ MPa, the effective stress $\sigma = 90.6$ MPa, the effective strain $\varepsilon = 8.74$, the product eccentricity $E_c = 0.92$ mm, and the roundness $Ro = 6.42$ mm. Fig. 11 shows the main effects of means for the input pro-

cess parameters of case (2), and Fig. 12 represents the DEFORM-3D simulation of the extrusion process of the optimum experiment No. 4 for the optimum responses (P, σ, ε) and that obtains the minimum product eccentricity E_c.

Table 8 Input parameters and output responses data of L9 Taguchi array for case (2)

| No.	T (°C)	Rs (mm/s)	E_{pre} (mm)	α (°)	P (MPa)	σ (MPa)	ε	E_c (mm)	Ro (mm)
1	300	1	0.3	12	284	70.9	10.20	11.24	2.96
2	300	2	0.5	16	536	89.9	9.76	23.94	1.10
3	300	3	0.7	18	291	76.8	6.55	47.59	7.18
4	350	1	0.5	18	575	90.6	8.74	0.92	6.42
5	350	2	0.7	12	358	83.2	9.22	51.01	13.92
6	350	3	0.3	16	519	73.4	11.80	10.06	3.17
7	400	1	0.7	16	325	90.9	6.53	12.89	1.81
8	400	2	0.3	18	308	81.9	9.14	35.84	4.81
9	400	3	0.5	12	526	88.4	14.80	5.25	1.30

Fig. 11 Main effects plot for means of process parameters in case (2)

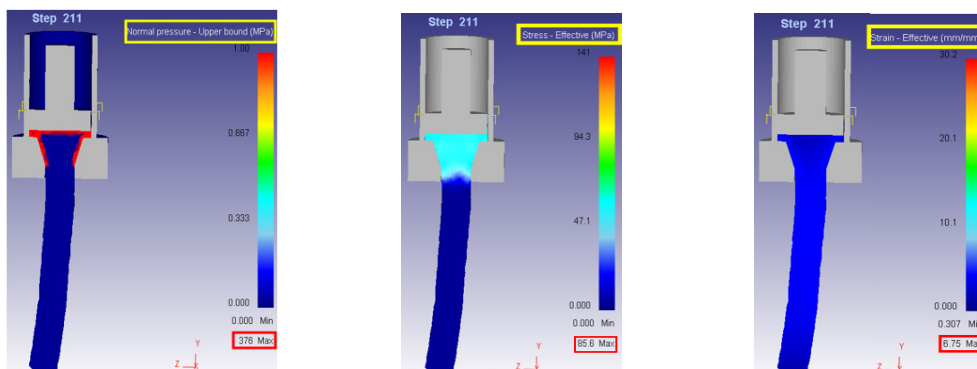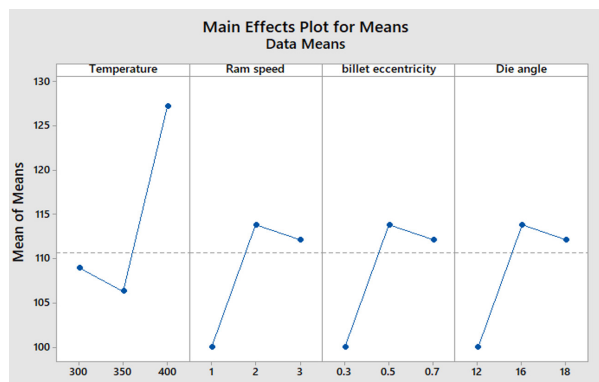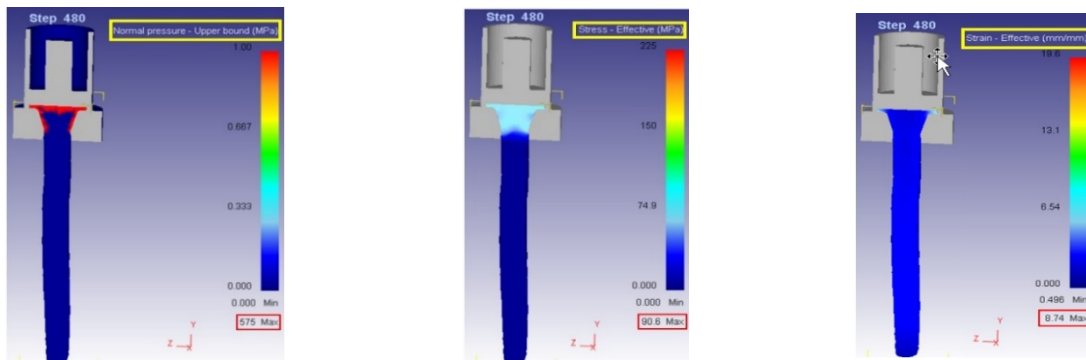**Fig. 12** Simulation of the Extrusion process of the optimal responses in case (2) using multi-response optimization

3.5 Study the effect of process parameters on the responses

It is important to study the cause-effect relationships among inputs to understand the multivariate nature of the simulated extrusion process. Frequently in the extrusion process, the temperature, the ram speed, and the die angle are the vital and basic process parameters that have a great influence on the product quality and the amount of the energy consumption. Additionally, the extruded product and the process productivity often depend on the die parts accuracy and the coaxially between these parts and the billet material. So, the study of the eccentricity effect must be inserted in the crib of the effective extrusion parameters. In this section the impact of input parameters on the responses that lead to high productivity and performance is discussed.

In the case (1): The optimum experiment (Exp. No. 3) shows that the highest value of Ram Speed (Rs = 3 mm/s) has a significant effect in reducing the pressure response which means savings in the energy consumption. Consequently, the extrusion rate increases with increase in the value of the ram speed. This happens due to the work hardening of the billet material during

the process. The selected value of ram speed leads to an appropriate effective stress and strain for the deformation occurrence. The Higher the ram speed also obtains the minimum the product eccentricity and an acceptable value of roundness error while comparing with its values in the other experiments.

Die Angle plays a central role in the hot extrusion. In Exp. No. 3, Die angle recorded the maximum ($\alpha = 18°$). Concurrently, the higher the die angle produces more metal flow. It is expected that while a die angle increases, the extrusion pressure will increase, but here it is combined with other parameters and a multi response optimization is executed, and the result is to obtain the lowest value of the pressure. The maximum value of the die angle also helps to obtain the minimum product eccentricity and an acceptable roundness error.

It is known that the high billet temperatures will reduce the extrusion pressure and the producer must decrease the ram speed to avoid the press and die parts deterioration. In this case of research, the lowest value of Temperature ($T = 300$ °C) is selected in the optimum group of input parameters. It successfully leads to obtain the lowest pressure and product eccentricity and a suitable effective stress and strain to deform the billet material.

The Presumed Eccentricity achieves its highest value ($E_{pre} = 0.7$ mm) in the optimum experiment. This parameter is combined with other optimum inputs to obtain the minimum pressure, product eccentricity, an acceptable roundness and a suitable stress and strain to produce the plastic deformation. So, this means that it has slight effect on the output responses while comparing with other parameters in the optimum experiment.

In the case (2): By studying the values of input parameters that represent the optimum experiment (Exp. No. 4), it is found that the Ram Speed achieves the lowest level ($Rs = 1$ mm/s) which will occur a larger torque. This is exhibited in the corresponding value of pressure response as it reaches the maximum whenever compared to the other values of pressure. The effective stress is also reached the highest which is desirable especially in the start of the forming region. Concurrently, the effective strain increases drastically, which helps to cause more billet deformation. As while the product eccentricity may achieve the lowest value with the selected optimum parameters the roundness error yields a relatively large value. The increase in the Temperature ($T = 350$ °C) and the achievement of the die angle to its highest level ($\alpha = 18°$) helped in obtaining these responses value. The effect of the Presumed eccentricity appears here effectively on the quality of the final product and its ability to negatively affect the outputs if its value increases. This is evident by comparing the value of the product eccentricity and roundness error at the optimum experiment with its other values.

3.6 Comparison between ideal and eccentricity cases

The main target of this research is to study the presence of the presumed eccentricity whether between the die parts or with the billet and its effect on the extrusion product quality (product eccentricity and roundness error). And based on the idea that there must be an initial eccentricity, even if it is very small, between the extrusion process parts, the basis of the comparison between cases is to obtain the optimum value of product eccentricity. By observing the optimum experiment in the ideal and both eccentricity cases, it is found that the global minimum product eccentricity is ($Ec = 0.46$ mm). It occurs while the eccentricity is between the billet and the ram, case (1). Table 9 illustrates the responses values for the three cases of eccentricity at the optimum parameters of case (1), as $T = 300$ °C, $Rs = 3$ mm/s, $E_{pre} = 0.7$ mm and $\alpha = 18°$. Table 10 shows the increase and decrease in the responses where the optimal parameters are used while comparing each two cases separately. Also, by noticing the results of comparison in the Table 10 and, it is found that the run time of simulated process under a selected optimum parameter of the case (1) is suitable and acceptable for achieving the simulation.

Table 9 Responses Data and Run Time consuming of DEFORM-3D simulation at the selected input parameters ($T = 300$, $Rs = 3$, $E_{pre} = 0.7$, $\alpha = 18°$) for all Eccentricity Cases

Eccentricity Case	P (MPa)	σ (MPa)	ε	E_c (mm)	Ro (mm)	Time (min)
Ideal Case ($E_{pre} = 0$)	106	29.7	7.34	0.02	0.03	50
Case (1)	376	85.6	6.75	0.46	2.61	25
Case (2)	291	76.8	6.55	47.59	7.18	15

Table 10 Status of Responses while comparing between Ideal case and Eccentricity cases (1 and 2)

No.	Cases	P	σ	ε	Ec	Ro	Run Time
1	Ideal-Case1	↑	↑	↓	↑	↑	↓
2	Ideal - Case2	↑	↑	↓	↑	↑	↓
3	Case1- Case2	↓	↓	↓	↑	↑	↓

3.7 ANOVA analysis of extrusion process parameters

ANOVA is a statistical technique for detecting the process parameters that notably affected the product quality. In this section, the ANOVA results of product eccentricity E_c and roundness error Ro responses are analysed for the optimum parameters in both cases of eccentricity. The Degree of Freedom (DF), the Sum of Squares (SS), the Mean Square (MS), F-value, P-value and the Contribution percentage are calculated and tabulated.

In the case (1), by noticing the *results of* ANOVA, it found that the most effective parameter on the product eccentricity E_c is the presumed eccentricity E_{pre} with 37.8 % contribution percentage. The ram speed Rs with the contribution of 26.09 % is ranked the second most influential parameter and it is. followed by the die angle α with 11.27 %. The least affecting parameter is the temperature T with the contribution percentage 9.84 %.

Moreover, the most effective parameter on the roundness Ro is the temperature T with 51.48 % contribution percentage. The presumed eccentricity E_{pre} with the contribution of 5.13 % is ranked the second most influential parameter and it is followed by the ram speed Rs with 4.77 %. The least affecting parameter is the die angle α with the contribution percentage 0.024 %.

In the case (2), by observing the ANOVA results, it found that the most effective parameter on E_c is the Rs with 44.62 % contribution percentage. The E_{pre} with the contribution of 41.52 % is the second most influential parameter and it is followed by the T with 5.33 %. The least affecting parameter is the α with the contribution percentage 0.63 %.

Additionally, the most effective parameter on the roundness Ro is the temperature T with 40.82 % contribution percentage. The presumed eccentricity E_{pre} with the contribution of 22.55 % is the second most influential parameter and it is followed by the ram speed Rs with 8.83 % then the α is come with the minimum contribution percentage 0.056 %.

4. Conclusion

This research addresses the input parameters in a hot direct extrusion process of AA2024 to explore the minimization of the final product eccentricity and its roundness error.

The statistical and numerical study is successfully executed by using MINITAB 18 and DFORM-3D software. The single and the multi-response optimizations based on Taguchi method and the Analysis of Variance are applied effectively to obtain the optimum parameters for minimum objectives in both suggested cases of eccentricity in addition to the case of zero eccentricity.

In the first case of eccentricity (the eccentricity between the billet and the ram), the multi-response results displayed that the optimal input parameters are T = 300 °C, a = 18°, E_{pre} = 0.7 mm and Rs = 3 mm/s to obtain the minimum final product eccentricity E_c that equal to 0.46 mm and while the roundness Ro is equal to 2.61 mm.

In the second case of eccentricity (the eccentricity between the billet and the container), the multi response results showed that the optimal input parameters are T = 350 °C, a=18°, E_{pre} = 0.5 mm and Rs = 1 mm/s to obtain the minimum final product eccentricity E_c that equal to 0.92 mm and while the roundness Ro is equal to 6.42 mm.

In the case (1), the results of the ANOVA analysis exhibited that the most effective input parameter on E_c is E_{pre} with 37.8 % contribution percentage, then Rs with 26.09 %, then α with 11.27 % and T with 9.84 %. The most effective parameter on the roundness Ro is T with 51.48 % contribution percentage, then E_{pre} with 5.13 %, Rs with 4.77 %, and α with 0.024 %.

In the case (2), the results of the ANOVA analysis demonstrated that the most effective parameter on E_c is Rs with 44.62 % contribution percentage, then E_{pre} with 41.52 %, T with 5.33 %, and α with 0.63 %. The most effective parameter on the roundness Ro is T with 40.82 % contribution percentage, then E_{pre} with 22.55 %, Rs with 8.83 % and α with 0.056 %.

References

[1] Jabbar, J.K. (2010). Calculation of relative extrusion pressure for circular section by local coordinates system by using finite element method F.E.M, *Diyala Journal of Engineering Sciences,* Vol. 3, No. 2, 80-96.

[2] Summers, P.T., Chen, Y., Rippe, C.M., Allen, B., Mouritz, A.P., Case, S.W., Lattimer, B.Y. (2016). Overview of aluminium alloy mechanical properties during and after fires, *Fire Science Reviews,* Vol. 4, Article No. 3, doi: 10.1186/s40038-015-0007-5.

[3] Arif, A.F.M., Sheikh, A.K., Qamar, S.Z., Raza, M.K., Al-Fuhaid, K.M. (2002). Product defects in aluminium extrusion and its impact on product defects in aluminium extrusion and its impact on operational cost, In: *Proceedings of 6th Saudi Engineering Conference,* Dammam, Saudi Arabia.

[4] Yanran, Z., Wang, Z.R., Weimin, C. (1995). Numerical simulations for extrusion and ironing and die-angle optimization, *Journal of Materials Processing Technology,* Vol. 55, No. 1, 48-52, doi: 10.1016/0924-013(95)01811-5.

[5] Jang, D.H., Ok, J.H., Lee, G.M., Hwang, B.B. (2006). The forming characteristics of AA 2024 aluminium alloy in radial extrusion process combined with backward extrusion, *Materials Science Forum,* Vol. 519-521, 955-960, doi: 10.4028/www.scientific.net/MSF.519-521.955.

[6] Jurkovic, Z., Jurkovic, M., Buljan, S. (2006). Optimization of extrusion force prediction model using different techniques, *Journal of Achievements in Materials and Manufacturing Engineering,* Vol. 17, No. 1-2, 353-356.

[7] Zhang, C., Zhao, G., Chen, H., Guan, Y., Li, H. (2012). Optimization of an aluminium profile extrusion process based on Taguchi's method with S/N analysis, *International Journal of Advanced Manufacturing Technology,* Vol. 60, No. 5-8, 589-599, doi: 10.1007/s00170-011-3622-x.

[8] Jajimoggala, S. (2019). Optimization of hot extrusion process parameters using Taguchi based grey relation analysis: An experimental approach, *International Journal of Materials Forming and Machining Processes,* Vol. 6, No. 1, 1-18, doi: 10.4018/IJMFMP.2019010101.

[9] Bressan, J.D., Martins, M.M., Bandini, C. (2019). Validation of Finite volume method by hot extrusion analysis of aluminium alloy, *Materials Today: Proceedings,* Vol. 10, Part 2, 234-241, doi: 10.1016/j.matpr.2018.10.401.

[10] Mai, N.T., Trung, D.D., Quy, T.D., Nghe, P.V. (2019). Determining RAM speed and billet temperature to ensure two indicators of surface roughness and extrusion pressure when extruding aluminium alloy, In: Fujita, H., Nguyen, D., Vu, N., Banh, T., Puta, H. (eds.), *Advances in Engineering Research and Application, ICERA 2018, Lecture Notes in Networks and Systems,* Vol 63, Springer, Cham, 253-260, doi: 10.1007/978-3-030-04792-4_34.

[11] Francy, K.A., Srinivasa Rao, C., Gopalakrishnaiah, P. (2019). Optimization of direct extrusion process parameter on 16MnCr5 and AISI1010 using DEFORM-3D, *Procedia Manufacturing,* Vol. 30, 498-505, doi: 10.1016/j.promfg.2019.02.070.

[12] Fernández, D., Rodríguez-Prieto, A., Camacho, A.M. (2020). Effect of process parameters and definition of favourable conditions in multi-material extrusion of bimetallic AZ31B–Ti6Al4V billets, *Applied Sciences*, Vol. 10, No. 22, Article No. 8048, doi: 10.3390/app10228048.

[13] Medvedev, A., Bevacqua, A., Molotnikov, A., Axe, R., Lapovok, R. (2020). Innovative aluminium extrusion: Increased productivity through simulation, *Procedia Manufacturing,* Vol. 50, 469-474, doi: 10.1016/j.promfg.2020.08.085.

[14] Parghazeh, A., Haghighat, H. (2016). Prediction of central bursting defects in rod extrusion process with upper bound analysis method, *Transactions of Nonferrous Metals Society of China,* Vol. 26, No. 11, 2892-2899, doi: 10.1016/S1003-6326(16)64418-7.

[15] Ngernbamrung, S., Suzuki, Y., Takatsuji, N., Dohda, K. (2018). Investigation of surface cracking of hot-extruded AA7075 billet, *Procedia Manufacturing,* Vol. 15, 217-224, doi: 10.1016/j.promfg.2018.07.212.

[16] Yang, D.Y., Kim, Y.U., Lee, C.M. (1992). Analysis of centre-shifted backward extrusion of eccentric tubes using round punches, *Journal of Materials Processing Technology,* Vol. 33, No. 3, 289-298, doi: 10.1016/0924-0136(92)90214-D.

[17] Ojstersek, R., Javernik, A., Buchmeister, B. (2021). The impact of the collaborative workplace on the production system capacity: Simulation modelling vs. real-world application approach, *Advances in Production Engineering & Management,* Vol. 16, No. 4, 431-442, doi: 10.14743/apem2021.4.411.

[18] Crnjac, M., Aljinovic, A., Gjeldum, N., Mladineo, M. (2019). Two-stage product design selection by using PROMETHEE and Taguchi method: A case study, *Advances in Production Engineering & Management,* Vol. 14, No. 1, 39-50, doi: 10.14743/apem2019.1.310.

[19] Saud, H.M., Abdulrazzaq, M.A. (2020). Study the effect of cold working on the mechanical properties of aluminium alloy 2024 T4, *IOP Conference Series: Materials Science and Engineering,* Vol. 928, Article No. 022125, doi: 10.1088/1757-899X/928/2/022125.

[20] Zhang, M., Li, C., Gao, Q., Fang, J., Wu, T.L., Wang, K.H. (2020). The effect of heat treatment on microstructure and properties of laser-deposited TiC reinforced H13 steel matrix composites, *Optik,* Vol. 206, Article No. 164286, doi: 10.1016/j.ijleo.2020.164286.

[21] Mat Web. Material Property Data – Databases, from *http://www.matweb.com,* accessed May 26, 2021.

[22] Sui, W., Zhang, D. (2012). Four methods for roundness evaluation, *Physics Procedia,* Vol. 24, Part C, 2159-2164, doi: 10.1016/j.phpro.2012.02.317.

Optimization approaches for solving production scheduling problem: A brief overview and a case study for hybrid flow shop using genetic algorithms

Xu, W.[a], **Sun, H.Y.**[a], **Awaga, A.L.**[a], **Yan, Y.**[a], **Cui, Y.J.**[b,*]

[a]School of Management, Shenyang University of Technology, Shenyang, P.R. China
[b]School of Finance, Dongbei University of Finance and Economics, Dalian, P.R. China

A B S T R A C T

The aim of this paper is to investigate scheduling problems in manufacturing. After a brief introduction to the modelling approach to the scheduling problem, the study focuses on the optimization approach to the scheduling problem. Firstly, the different optimization approaches are categorised and their respective advantages and disadvantages are shown. This is followed by a detailed analysis of the characteristics and applicability of each of the commonly used optimization approaches. Finally, a case study is presented. A mathematical model is developed with the objective of minimising the maximum completion time for a mixed flow shop scheduling problem, and a genetic algorithm is used to solve the problem. The validity of the model is verified through the case study, which can provide a reasonable scheduling solution for actual manufacturing. This provides a reference for the selection and use of methods for solving scheduling problems in practical production.

1. Introduction

In today's rapidly developing technology, manufacturing plays an important role in the development of the national economy. How to reduce manufacturing costs is often the primary issue that manufacturing companies need to consider, and how to strengthen production management capabilities, improve production efficiency and reduce production and operating costs is attracting increasing attention. These problems can be solved by optimising the production scheduling arrangements [1, 2]. Production scheduling is the efficient arrangement of production processes based on certain scheduling objectives to achieve job scheduling and optimal allocation of resources within the constraints of time and other conditions [3]. The level of scheduling decisions often determines the ability of the business to achieve cost reductions and respond quickly to market demands. Scheduling optimisation on the manufacturing floor is therefore a key concern for modern manufacturing companies.

Scholars have used different algorithms to model and optimise different job shop scheduling problems such as single-machine scheduling and multi-machine scheduling. This paper firstly reviews and summarises the optimization approaches used by scholars for scheduling problems in the past, and analyses the advantages and disadvantages of different approaches and the applicable environment, which can provide reference for subsequent scholars in the selection of optimization approaches for production scheduling problems. The hybrid shop scheduling problem is more complex than the general shop scheduling problem. This is because there are parallel machines for certain processes in the process and machine selection is required for the machining of the workpiece. Therefore, this paper chooses to conduct a case study for the hybrid flow shop scheduling problem. A mathematical model is developed and solved using a genetic algorithm, and the validity of the model is then verified.

2. Literature review

The problem of workshop scheduling has been studied by a very large number of national and international scholars. Song and Yang solved the scheduling problem with a real-time scheduling algorithm based on a branch-and-bound algorithm and an artificial neural network [4]. Yang proposed a multi-objective hybrid genetic algorithm that incorporates local search into evolutionary computation to solve the scheduling problem for flow shops [5]. Zhoudesigned a genetic algorithm-based production scheduling optimization model for multiple processes and machines [6]. Zheng and Pan proposed an improved discrete firefly optimization algorithm combined with a local search algorithm to solve the flexible job shop scheduling problem, and conducted simulations to verify the effectiveness of the algorithm [7]. Li *et al.* solved the dual-objective hybrid flow shop scheduling problem based on genetic algorithms, combining with small habitat techniques [8]. Wang *et al.* established a model for the single-machine scheduling problem considering equipment availability constraints with the optimization objective of minimizing the total delay time, and then solved it with a genetic algorithm, which can effectively cope with the impact of equipment availability on production scheduling [9].

There are always uncertainties in a system that cause project delays [10, 11]. Regarding the uncertainty condition constraint, Chen *et al.* established a fuzzy multi-objective scheduling model to effectively solve the replacement flow shop scheduling problem considering processing time and fuzzy lead time [12]. You *et al.* established a dynamic scheduling method based on game theory, considering machine failures in flexible job shop scheduling, and developed a multi-stage complete information static game model for the scheduling problem under failures [13].

In foreign research, Chen, Y.R. *et al.* developed two mixed integer programming models for the single-machine scheduling problem with flexible maintenance and non-recoverable operations [14]. Grznar *et al.* have developed a simulation model to simulate the logistics system, which can determine the state of the plant layout and effectively suggest solutions to problems in production and supply [15]. Wang *et al.* studied the disassembly of a product and applied an intelligent algorithm to solve the disassembly line balancing problem [16]. Liu *et al.* developed a mathematical model considering constraints such as variable machining times and intermittent machining with an objective of completion time and energy consumption, using a forging shop as a study [17]. Paternina-Arboleda *et al.* presented a heuristic algorithm based on bottleneck stage identification for the flow shop completion time minimization problem, rescheduling the sequence of workpieces on the bottleneck stage [18]. Yang and Wang proposed a novel hybrid method of adaptive neural networks and heuristics in solving the shop floor scheduling problem [19]. Torabi *et al.* presented a new mixed-integer nonlinear programming design for determining machine allocation, sorting, batching, and scheduling decisions, which was solved using an enumeration method [20]. Vincent *et al.* took constraints such as machine capacity and time lag into account and proposed a mixed integer linear programming and constrained programming model, which was solved using a meta-heuristic algorithm [21].

3. A brief overview of methods for solving production scheduling problem

The production scheduling problem can be described as the scheduling of materials, processing time and sequences of operations with the objective of optimising manufacturing time or costs, etc., subject to various conditions. In a shop floor production system, production scheduling problems can be classified into the following types depending on the processing method: single machine scheduling problems, parallel machine scheduling problems, flow shop scheduling problems, hybrid flow shop scheduling problems, job shop scheduling problems and open shop scheduling problems [22, 23]. There are several modelling methods for solving shop floor scheduling problems, comprising three main categories, mathematical programming method, graph and network method and simulation method [24]. The core of the mathematical planning method is that the relationships between variables in a system can be expressed by corresponding mathematical relationships, the diagram and network method mainly includes activity cycle diagrams, critical path method, etc. The simulation method is based on the establishment of a system model to express the system behaviour, which is transformed into a computer simulation program. Each of the three types of methods has its own advantages and disadvantages, and the one that is more frequently used is the mathematical planning method. Once a mathematical model has been built for the shop floor scheduling problem, the problem needs to be solved using the appropriate algorithms, which can be divided into two main categories: exact methods and approximate methods.

Precision methods can be used to solve scheduling optimisation or sub-optimisation problems, with the advantage that the global optimum solution is guaranteed and is suitable for solving problems that require high precision. The precise methods commonly used include mathematical programming method and branch and bound method. Mathematical planning methods can be divided into integer programming, mixed integer programming, Lagrangian relaxation method and decomposition method. However, the disadvantage is that it can only solve small-scale problems and is slow, and its use is limited for complex problems.
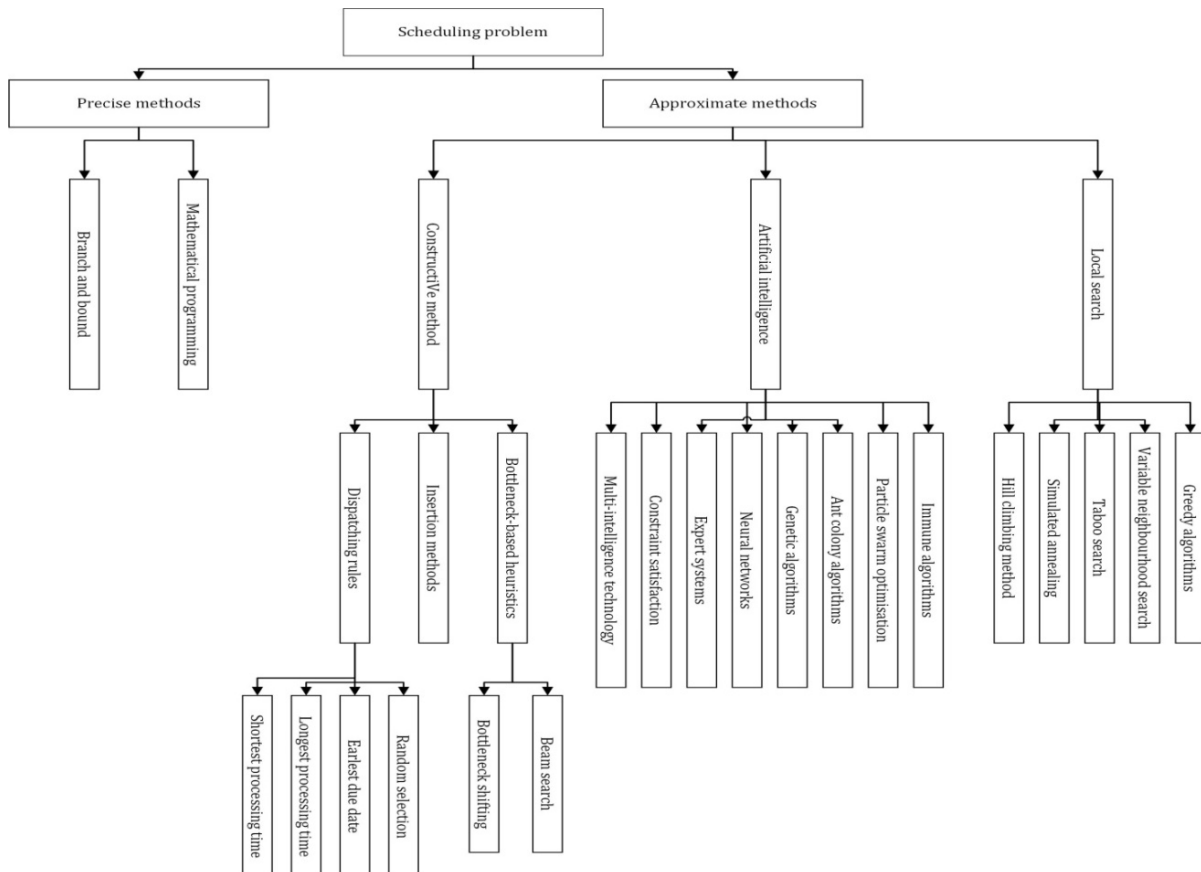

Fig. 1 Methods for solving scheduling problems

The opposite is true of the approximation method, which gives a quick solution to the problem, but has the disadvantage that there is no guarantee of an optimal solution. It is suitable for large-scale problems and better meets the needs of real-world problems. Approximation methods can be further divided into three main categories: construction method, artificial intelligence method and local search algorithm. The construction methods mainly include dispatching rule method, interpolation method and bottleneck-based heuristic method, etc. Artificial intelligence algorithms mainly include constraint satisfaction, expert systems, neural networks, multi-intelligent body techniques, and meta-heuristics (e.g., genetic algorithms, ant colony algorithms, etc.) Finally local search algorithms, mainly represented by simulated annealing method and taboo search, etc. The main structure and some common algorithm features are shown in Figs. 1 and 2.
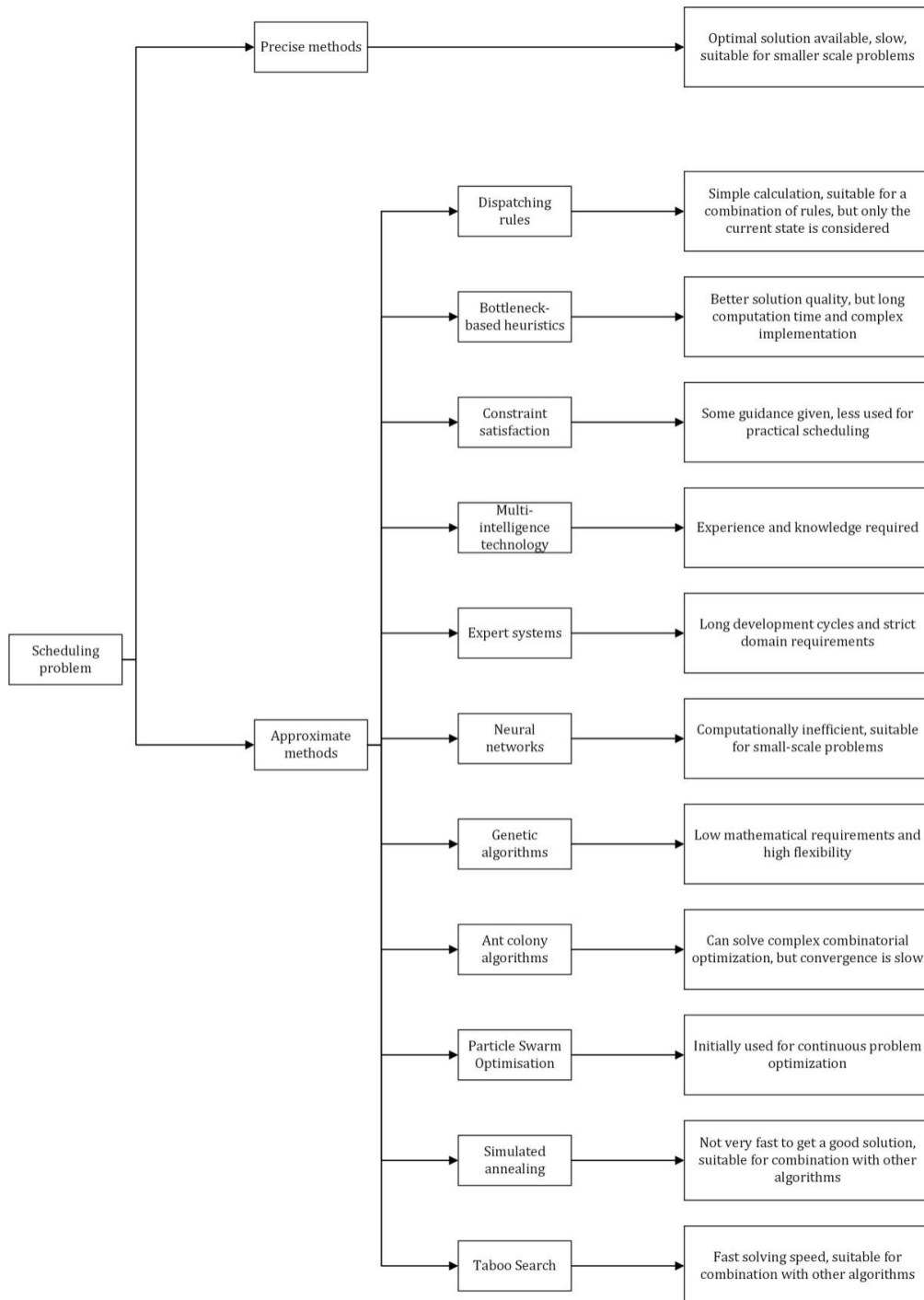

Fig. 2 Characteristics of scheduling problem solving methods

When using exact methods to solve scheduling problems, the optimal solution to the problem can be obtained. However, traditional optimisation methods such as linear programming, dynamic programming and branch-and-bound methods are slow and more suitable for solving small-scale shop floor scheduling problems, while complex shop floor scheduling problems are difficult or impossible to solve quickly. For large-scale scheduling problems, approximate methods are often a better choice. Approximation methods differ from exact methods in that they do not seek the optimal solution to a scheduling optimisation problem, but rather aim to find a more satisfactory solution in a given amount of time.

Among the construction methods, the assignment rule method contains First Come First Served, Shortest Processing Time, Earliest Due Date and so on. They are based on information such as processing times, delivery deadlines, number of parts and workshop conditions, which determine which rules are used to optimise the scheduling solution. They are characterised by their simplicity of calculation and the possibility of obtaining a satisfactory solution, but only the current state is considered. In practice, it can be used in combination with a variety of rules or with other intelligent optimisation algorithms. In addition, the construction method also contains a bottleneck-based heuristic method, which in turn includes the bottleneck shifting method and the shot-beam search method. The advantage of this method is the better quality of the solution, the disadvantage is the long computation time and the complexity of the implementation.

The most popular and widely used algorithms are intelligent optimisation algorithms, which originate from the summary and simulation of certain unique natural phenomena and laws, and involve a wide range of disciplines, and have unique advantages for solving complex scheduling optimisation problems. These algorithms can be divided into artificial intelligence and local search algorithms according to their principles. Commonly used artificial intelligence methods are constraint satisfaction, multi-intelligence techniques, expert systems, neural networks, genetic algorithms, ant colony algorithms and particle swarm optimisation. Constraint satisfaction methods can give guidance on scheduling problems to a certain extent. Multi-intelligent body techniques methods require experience and knowledge. The expert system approach has a long development cycle and is strictly domain specific. Neural network methods are less computationally efficient and more suitable for small-scale problems. Genetic algorithms have low mathematical requirements and are highly flexible in their application. Ant colony algorithms can be used to solve complex combinatorial optimisation but are slow to converge. Particle swarm optimisation methods were originally used for continuous problem optimisation.

Finally, there are local search algorithms. The main local search algorithms commonly used are simulated annealing and taboo search. The simulated annealing method is not able to obtain a good solution very quickly and is suitable for use in combination with other algorithms. The taboo search method is faster and is also suitable for use in combination with other algorithms.

As mentioned above, different types of job shops have different modes of operation, so different models can be built to solve the production scheduling problem for different job shops using different algorithms. This paper selects the mixed flow shop scheduling problem as the research object, establishes the scheduling optimization mathematical model, and solves it by genetic algorithm.

4. Problem statement and research methodology

4.1 Production scheduling model for hybrid flow shop

Hybrid flow shop scheduling, which is also called flexible flow shop scheduling, exists in a wide range of areas and is more complex than the normal flow shop [25]. Its machining structure is shown in Fig. 3. Workpieces are processed in several stages, each of which may have several optional machines, and the workpieces are processed in a fixed sequence. The hybrid flow shop scheduling problem is more closely related to actual manufacturing and is therefore the most used. In this paper, we aim to develop a mathematical model for production scheduling in a hybrid flow shop with the objective of minimising completion time.
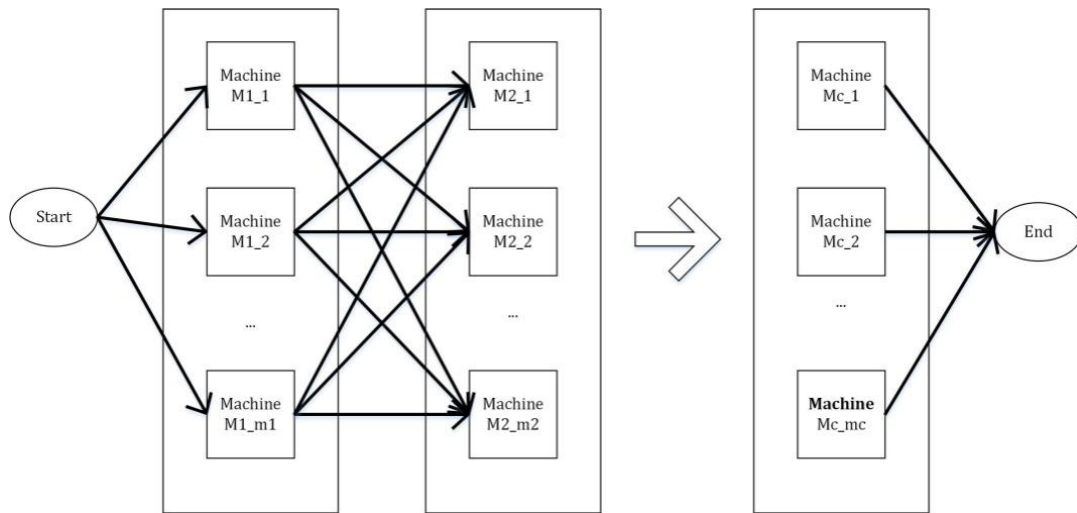
Fig. 3 Processing diagram of the hybrid flow shop

The scheduling problem in a mixed flow shop can be characterised as follows: there are n parts to be machined $\{N_1, N_2,..., N_n\}$ on m machines $\{M_1, M_2,..., M_m\}$, where at least one machine exists for each process and parallel machines exist for at least one process, and any of the parallel machines can be selected to process the process. The purpose of scheduling is to find the sequence of workpieces in the overall production plan and to select the most suitable equipment for each process so that the scheduling solution is optimal.

Model hypothesis:

1) Only a maximum of one workpiece can be machined on one machine at any one time.
2) A workpiece can only be processed by one machine at any one time.
3) Once the machine has started working on the workpiece, it cannot be interrupted and must complete the process.
4) Each workpiece is processed strictly in its own sequence.
5) Each workpiece is processed in each process in strict accordance with the optional equipment.
6) Equal machining priority between different workpieces.

Model building:

The objective function is as follows.

$$min\, f = min\{max\, T_k\}, \qquad 1 \le k \le m \tag{1}$$

The constraints are as follows.

$$\sum_{p=1}^{n} x_{ip} = 1, \qquad p = 1,2,...,n \tag{2}$$

$$\sum_{i=1}^{n} x_{ip} = 1, \qquad i = 1,2,...,n \tag{3}$$

$$\sum_{j=1}^{m} M_j > m \tag{4}$$

$$\sum_{k=1}^{M_j} O_{ijk} = 1, j = 1,2,...,m, k = 1,2,...,M_j \tag{5}$$

$$T_{ij} - T_{i(j-1)} \ge t_{ijk} O_{ijk}, 2 \le j \le n \tag{6}$$

Where T_k is the time of completion of the k-th machine. x_{ip} indicates that the i-th workpiece is assigned to be processed at the p-th location. M_j indicates the number of machines available for the j-th process. O_{ijk} is a 0/1 variable that takes the value of 1 when the j-th process of workpiece i is processed on the j-th machine and 0 otherwise. T_{ij} indicates the completion time of the j-th process of workpiece i and t_{ijk} indicates the time spent by workpiece i on the k-th machine for the j-th process.

Eq. 1 indicates the minimised maximum completion time, $k = 1,2,...,m$. Eqs. 2 and 3 show that a machine can only be used to machine one workpiece at a time and that a workpiece can only be machined by one machine at a time. Eq. 4 shows that there are concurrent machines for at least one process. Eq. 5 indicates that only one machine can process each process of the same workpiece. Eq. 6 means that the current process is completed before moving on to the next process and cannot be interrupted.

4.2 Algorithm design

This paper applies a genetic algorithm to optimize the hybrid flow shop scheduling problem with the target of minimising the maximum completion time.

Step 1: Coding design

Considering the specificity of the hybrid flow shop model, in order to be able to describe both the processing sequence of the workpiece and the assigned machine information, this paper adopts a two-layer coding approach, containing both the process sequence and the machine sequence. The first layer is based on the workpiece process coding, and the other chromosome coding layer numbers the processing machines for each process. Each two-layer code then corresponds to a scheduling scheme based on the known set of available machines and their corresponding processing schedules.

Let $M\{a, b\}$ denote the set of machines that process the b-th process of workpiece a, and let $T\{a, b\}$ denote the set of time spent on the different machines that process the b-th process of workpiece a. Now suppose that a job shop has four machines to process three workpieces, each of which has to go through three processes, and that the corresponding M and T are shown in Tables 1 and 2.

In the chromosome code shown, each gene in the process sequence represents a workpiece number, where the number of times it appears in the chromosome indicates the number of processes it represents. As shown in the Fig. 4.

The sequence of execution of each workpiece process and the arrangement of machines for the scheduling scheme corresponding to this chromosome is derived as shown in the Fig. 4. The Gantt chart of the processing corresponding to this chromosome code can be obtained as shown in Fig. 5. A chromosome can be obtained using the two-layer coding method as shown in Table 3.

Table 1 Optional set of machines for machining workpieces

Workpiece	Working procedure 1	Working procedure 2	Working procedure 3
N_1	M_4	M_1, M_3	M_3
N_2	M_2, M_4	M_1	M_2, M_3
N_3	M_4	M_1, M_4	M_2

Table 2 Time set for machining of workpieces

Workpiece	Working procedure 1	Working procedure 2	Working procedure 3
N_1	3	[3,4]	5
N_2	[5,3]	4	[3,2]
N_3	4	[5,1]	2

Table 3 Chromosome coding

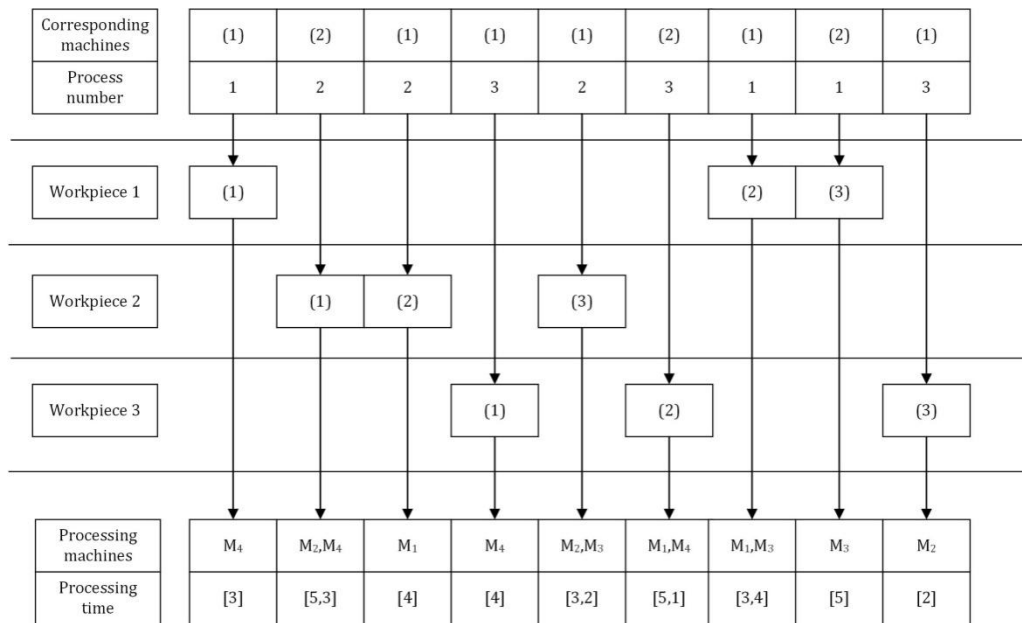| Process sequence	1	2	2	3	2	3	1	1	3
Machine sequence	1	2	1	1	1	2	1	2	1

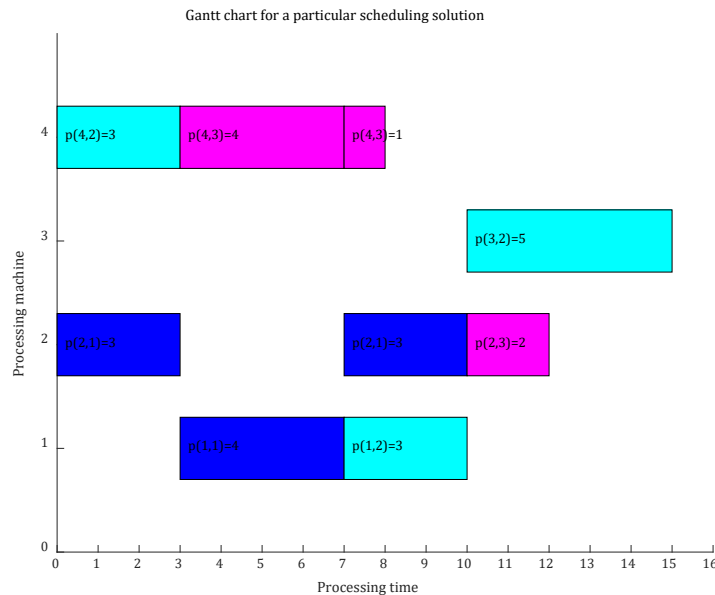**Fig. 4** Schematic representation of the double-layered chromosome code

Fig. 5 Processing Gantt chart corresponding to chromosome codes

Step 2: Select design

In genetic algorithms, the higher the fitness level, the higher the probability of being selected. This algorithm design is based on ranked fitness selection. The probability of selection of individuals is determined by ranking individuals in order of fitness. Firstly, the individuals in the population are ranked linearly according to their fitness, and then the values of fitness in the population are selected proportionally using a 'roulette wheel' approach.

Step 3: Crossover and variation

Crossover is the process of replacing and recombining parts of the structure of two parents to create a new individual, and the search power of genetic algorithms can be greatly improved by crossover. The crossover operation starts by selecting two chromosomes at random from the population, crossing the chromosomes at random locations, and then adjusting the crossed chromosomes to match the number of expressions.

Variation is used to give the genetic algorithm the ability to search locally at random and to maintain the diversity of the population [26]. The basic element of the mutation operator is to make changes to gene values. First individuals determine whether or not to mutate based on a pre-determined mutation probability, and then mutations are made to randomly selected mutation sites for those individuals making mutations.

5. Simulation analysis: Results and discussion

5.1 Results

The production scheduling problem is a key issue in manufacturing and a proper scheduling solution can effectively improve the operational efficiency of a manufacturing company. In this case study, the objective is to minimise the completion time and to optimise the scheduling problem in a hybrid shop. There are six workpieces that need to be processed in six stages, and ten machines are responsible for processing them. Some of the workpieces have parallel machines for some of the processes and can be selected to be processed on different machines, with the specific information on the machines available in the Table 4.

The different machine options correspond to different processing time, as shown in the Table 5.

Table 4 Optional machine set for workpieces

	Workpiece1	Workpiece2	Workpiece3	Workpiece4	Workpiece5	Workpiece6
Working procedure 1	3	7	4	[2,8]	[3,6]	5
Working procedure 2	4	[2,8]	9	7	5	[1,10]
Working procedure 3	5	[7,8]	6	[2,1]	10	5
Working procedure 4	3	2	[4,6]	10	[2,5]	[3,7]
Working procedure 5	[4,3]	3	[8,10]	7	2	[3,9]
Working procedure 6	[2,6]	4	[7,8]	6	9	[3,8]

Table 5 Time setting for workpiece processing

Workpiece	Workpiece 1	Workpiece 2	Workpiece 3	Workpiece 4	Workpiece 5	Workpiece 6
Working procedure 1	11	12	7	[4,2]	[2,5]	8
Working procedure 2	5	[3,4]	5	4	3	[4,4]
Working procedure 3	7	[6,5]	4	[4,2]	7	6
Working procedure 4	5	3	[3,3]	7	[7,6]	[4,7]
Working procedure 5	[6,6]	7	[5,2]	7	3	[8,5]
Working procedure 6	[3,1]	5	[7,4]	5	8	[6,9]

This paper uses Matlab software to program and solve the above production scheduling optimisation problem using a genetic algorithm, setting the initial population size to 40 and the maximum number of iterations to 50. The Gantt chart of the optimal scheduling solution obtained after solving using Matlab software is shown in the Fig. 6.
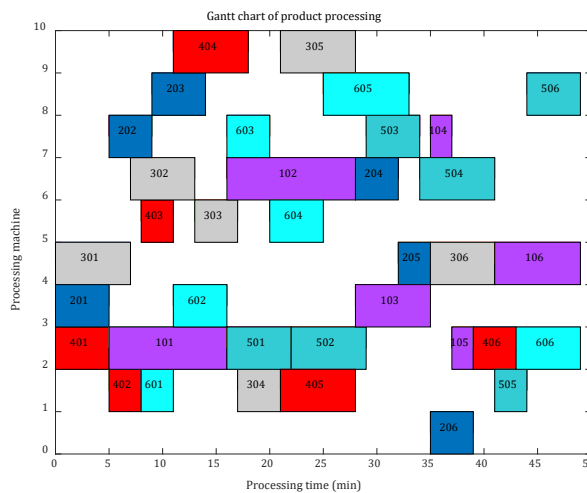

Fig. 6 Gantt chart of the optimal scheduling solution

As shown in Fig. 6, the x-axis shows the processing time of the workpiece and the y-axis shows the machine number corresponding to the workpiece processing. Based on the above Gantt chart, it is clear that in this case of a hybrid flow shop, the selection of machines for the different processes of the different workpieces and the time taken to process them can be seen. Where the number in the rectangle indicates the *j*-th process of the *i*-th workpiece, it can be seen that the final time taken to complete all processes is 49 minutes. In solving the above problem using Matlab, the resulting evolutionary iteration diagram is shown in the Fig. 7.
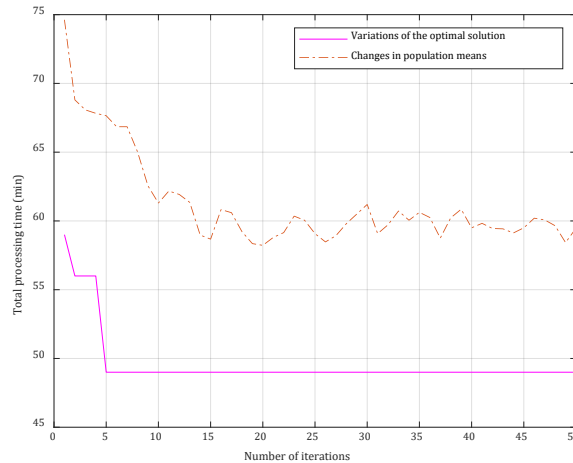

Fig. 7 Evolutionary iteration diagram of the optimal solution

The above images show the variation of the solution and the variation of the population mean in solving the production scheduling optimisation problem for a hybrid shop floor. The results show that the algorithm used in this paper can effectively find the optimal scheduling solution for the hybrid shop floor problem in a short time.

5.2 Discussion

The simulation results show that the genetic algorithm used in this paper can effectively solve the scheduling problem for a hybrid flow shop. Fig. 6 clearly shows the machine and sequence arrangement and the corresponding processing time for scheduling each workpiece process, while Fig. 7 shows the evolutionary iterative process of the optimal solution.

Each algorithm for solving production scheduling problems often has its own advantages and disadvantages, such as global search, local search, speed of solution, accuracy of solution, scale of application, etc. It is usually necessary to choose the right algorithm according to the needs of the problem.

The genetic algorithm used in this paper first encodes the variables to be decided upon, and then operates on their encoding. The sequence is manipulated directly, simulating the process of chromosome evolution. It is based on probabilistic rules that make the search more flexible, as well as its population search feature, which starts from the population and avoids some points that do not need to be searched, allowing for better global search, but at the same time has disadvantages in terms of local search. It can be used in combination with other algorithms when necessary to solve practical problems. And more research could be done in the future on retaining good individuals while maintaining population diversity.

6. Conclusion

Based on the understanding and analysis of different types of job shop production scheduling problems, this paper provides an overview of modelling and solution methods for the optimisation of scheduling problems. The advantages, disadvantages and applicability characteristics of the different methods are analysed, and situations in which the different optimisation methods are applicable are derived. Where necessary, a reasonable combination of different solution

54

methods can be used to cope with complex scheduling problems. This can provide a reference for the choice of modelling and solution methods in the study of scheduling problems. Later, a case study is conducted on the hybrid flow shop scheduling problem. A production scheduling optimisation model with the objective of minimising the maximum completion time is constructed, and a genetic algorithm based on two-layer coding is applied to solve the problem, proving the validity of the model and the algorithm.

Acknowledgement

References

[1] Tian, W., Zhang, H.P. (2021). A dynamic job-shop scheduling model based on deep learning, *Advances in Production Engineering & Management,* Vol. 16, No. 1, 23-36, doi: 10.14743/apem2021.1.382.

[2] Chen, D., Zhao, X.R. (2021). Production management of hybrid flow shop based on genetic algorithm, *International Journal of Simulation Modelling,* Vol. 20, No. 3, 571-582, doi: 10.2507/IJSIMM20-3-CO12.

[3] Guo, Q., Zhang, M.L., Sun, L.X., Liu, X. (2020). Genetic algorithm-based optimization of flexible workshop scheduling, *Science, Technology and Engineering,* Vol. 20, No. 29, 11931-11936.

[4] Song, Y., Yang, G.K. (2008). Real-time scheduling strategy based on branch delimitation and neural networks, *Computer Simulation,* Vol. 25, No. 12, 321-324.

[5] Yang, K.B. (2008). Multi-objective hybrid genetic algorithm for solving flow shop scheduling problems, *Computer and Information Technology,* No. 2, 28-30, doi: 10.19414/j.cnki.1005-1228.2008.02.009.

[6] Zhou, F.L. (2019). Genetic algorithm based multi-process multi-machine scheduling optimization research, *Software,* Vol. 40, No. 6, 123-126.

[7] Zheng, J., Pan, D.Z. (2021). Improved discrete firefly optimization algorithm for solving flexible job shop scheduling problems, *Computers and Modernisation,* No. 8, 11-15.

[8] Li, W.T., Tao, Z., Chen, X.F. (2019). Research on dual-objective flow-shop scheduling problem based on genetic algorithm, *Journal of Shenyang University of Technology,* Vol. 38, No. 4, 52-57.

[9] Wang, J.F., Chen, L., Yang, W.H. (2021). Single machine scheduling problem considering equipment availability constraints, *Journal of Shanghai Jiaotong University,* Vol. 55, No. 1, 103-110, doi: 10.16183/j.cnki.jsjtu.2019.173.

[10] Emon, M.B. (2018). Study on construction delay and the factors of delay in construction project, *Journal of Logistics, Informatics and Service Science,* Vol. 5, No. 2, 42-54.

[11] Ahmed, S., Hoque, I. (2018). Investigation of the causes of accident in construction projects, *Journal of System and Management Sciences,* Vol. 8, No. 3, 67-89.

[12] Chen, K.J., Duan, R.M., Liu, B.Y., Zhou, X.M. (2021). A multi-objective model for fuzzy replacement flow shop scheduling, *Operations and Management,* Vol. 30, No. 8, 28-36.

[13] You, Y.C., Wang, Y., Ji, Z.C. (2021). A study on dynamic scheduling of flexible job shops based on game theory, *Journal of Systems Simulation,* Vol. 33, No. 11, 2579-2588.

[14] Chen, Y., Huang, C., Chou, F.-D., Huang, S. (2020). Single-machine scheduling problem with flexible maintenance and non-resumable jobs to minimise makespan, *IET Collaborative Intelligent Manufacturing,* Vol. 2, No. 4, 174-181, doi: 10.1049/iet-cim.2020.0014.

[15] Grznar, P., Gregor, M., Gaso, M., Gabajova, G., Schickerle, M., Burganova, N. (2021). Dynamic simulation tool for planning and optimisation of supply process, *International Journal of Simulation Modelling,* Vol. 20, No. 3, 441-452, doi: 10.2507/IJSIMM20-3-552.

[16] Wang, Y.J., Wang, N.D., Cheng, S.M., Zhang, X.C., Liu, H.Y., Shi, J.L., Ma, Q.Y., Zhou, M.J. (2021). Optimization of disassembly line balancing using an improved multi-objective Genetic Algorithm, *Advances in Production Engineering & Management,* Vol. 16, No. 2, 240-252, doi: 10.14743/apem2021.2.397.

[17] Liu, Z., Yan, J., Cheng, Q., Yang, C., Sun, S., Xue, D. (2020). The mixed production mode considering continuous and intermittent processing for an energy-efficient hybrid flow shop scheduling, *Journal of Cleaner Production,* Vol. 246, Article No. 119071, doi: 10.1016/j.jclepro.2019.119071.

[18] Paternina-Arboleda, C.D., Montoya-Torres, J.R., Acero-Dominguez, M.J., Herrera-Hernandez, M.C. (2008). Scheduling jobs on a *k*-stage flexible flow-shop, *Annals of Operations Research,* Vol. 164, 29-40, doi: 10.1007/s10479-007-0257-2.

[19] Yang, S., Wang, D. (2001). A new adaptive neural network and heuristics hybrid approach for job-shop scheduling, *Computers & Operations Research,* Vol. 28, No. 10, 955-971, doi: 10.1016/S0305-0548(00)00018-6.

[20] Torabi, S.A., Karimi, B., Fatemi Ghomi, S.M.T. (2005). The common cycle economic lot scheduling in flexible job shops: The finite horizon case, *International Journal of Production Economics,* Vol. 97, No. 1, 52-65, doi: 10.1016/j.ijpe.2004.05.005.

[21] Boyer, V., Vallikavungal, J., Cantú Rodríguez, X., Salazar-Aguilar, M.A. (2021). The generalized flexible job shop scheduling problem, *Computers & Industrial Engineering,* Vol. 160, Article No. 107542 doi: 10.1016/j.cie.2021. 107542.

[22] Lebbar, G., El Abbassi, I., Jabri, A., El Barkany, A., Darcherif, M. (2018). Multi-criteria blocking flow shop scheduling problems: Formulation and performance analysis, *Advances in Production Engineering & Management,* Vol. 13, No. 2, 136-146, doi: 10.14743/apem2018.2.279.

[23] Modrák, V., Pandian, R.S. (2010). Flow shop scheduling algorithm to minimize completion time for n-jobs m-machines problem, *Tehnički Vjesnik – Technical Gazette,* Vol. 17, No. 3, 273-278.

[24] Li, C.P., Wang, G.C., Cui, H.Y. (2012). Current status and trends of research on flexible job shop scheduling, *Combined machine tools and automated machining technology,* No. 11, 109-112.

[25] Ištoković, D., Perinić, M., Borić, A. (2021). Determining the minimum waiting times in a hybrid flow shop using simulation-optimization approach, *Tehnički Vjesnik – Technical Gazette,* Vol. 28, No. 2, 568-575, doi: 10.17559/ TV-20210216132702.

[26] Liu, T., Xu, W., Wu, Q. (2008). Modeling and optimization of production scheduling system based on genetic algorithm, *East China Economic Management*, No. 2, 152-154, doi: 10.19629/j.cnki.34-1014/f.2008.02.037.

The role of agility in responding to uncertainty: A cognitive perspective

Kim, Minkyun [a], **Chai, Sangmi** [b,*]

[a]Sogang University, Sogang Business School, Seoul, Republic of Korea
[b]Ewha Womans University, Ewha School of Business, Seoul, Republic of Korea

ABSTRACT

This research investigates the impact of external environment, cognitive factors, and behavioral dimensions in the context of implementing supply chain agility. It applies social cognitive theory to establish a link between various environments including business uncertainty and supply chain disruption risk, cognitive factors such as supply chain agility self-efficacy, trust, and supply chain cooperation, coordination, and communication attitude, and actions such as implementing supply chain agility as well as behavior to explain the decision-making process in implementation. Based on the survey data collected from 254 supply and purchasing managers in the Korean manufacturing industry, AMOS software with structural equation method was used for data analysis Our results support the concept that business uncertainty reduces self-efficacy in supply chain agility although both business uncertainty and supply chain disruption risk boosted trust in the supply chain as well as buyers' positive attitude toward supply chain cooperation, coordination, and communication. The concept of supply chain agility, self-efficacy, trust, and supply chain cooperation, coordination, and communication attitude have a positive impact on firm performance. Supply chain agility, self-efficacy, and trust in suppliers positively affects implementation of supply chain agility as well as firms' financial, operational, and supply chain performance. This research provides meaningful insights for considering external environments and cognitive factors while making decisions in implementing supply chain agility.

1. Introduction

Competition has intensified in the market and business environments have become dynamic. As customer requirements for organizations have increased, the ability to adjust to shorter product lifecycles, longer lead times, higher supply volatility, and unpredictable demand has become essential [1]. Organizations must have agility to respond quickly to changes in the industry as well as markets. In managing a supply chain, agility has emerged as a solution for improving flexibility in the market. Organizations with supply chain agility provide higher service levels although their inventories are lower [2]. More importantly, due to increased complexity, business uncertainty has been considered as one of the most important factors for managers to deal with and generate solutions. With increased levels of turbulence as well as unpredictability, organizations emphasize on the need to develop agility to offer superior value to customers in

managing flow of materials and services without any disruptions [3]. Therefore, supply chain agility has emerged as an important issue in the management and operation of supply chains in both academia and industry.

The concept of supply chain agility has recently been discussed in supply chain and operations management from a different perspective. The concept of supply chain agility is considered as the capability of firms to respond to market changes [4]. Supply chain agility is defined as firms' ability to determine and quickly respond to market changes in their supply chain from an internal supply chain perspective [3]. Gligor and Holcomb [1] provide a similar definition of supply chain agility recognizing it as the ability of the supply chain network to align its operations with the market quickly and proactively. Based on this definition, the research efforts of Gligor *et al.* [5] culminated in establishing five dimensions of supply chain agility: alertness, accessibility, decisiveness, swiftness, and flexibility. This research applies the definition of supply chain agility, namely firms' ability to adjust supply chain operations quickly, based on the study of Gligor and Holcomb [1], Gligor *et al.* [5] Gligor *et al.* [6] and the approach that supply chain agility is closely tied to effectiveness in managing supply chains [6].

Social cognitive theory (SCT) has been applied to various fields, but mainly to explain individual and group behavior by interacting with cognitive factors as well as external environments. The theory attempts to identify people's behavior based on a framework of interactions between cognitive factors, environmental factors, and human behavior [7]. Thus, based on the interplay between these factors, this theory predicts that human behavior is influenced by cognitive, affective, personal factors, and external environments [7]. By applying SCT, this research investigates the relationship between a firm's cognitive decisions in implementing supply chain agility by reacting to external environments. As this study considers cognitive factors as the focal point of these relationships, it examines the role of supply chain agility, self-efficacy, trust, supply chain cooperation, coordination, and communication attitude in the implementation of supply chain agility as well as firm performance in response to business uncertainties and supply chain disruption risk.

Applying social cognitive theory and definition of supply chain agility, firms' ability to adjust supply chain operations quickly, this research established self-efficacy in the context of supply chain agility. Thus, supply chain agility self-efficacy is defined as a confidence on managing supply chain with agility. When supply chain managers deal with business uncertainty and risk, their confidence make a critical impact on their decision makings. Therefore, supply chain agility self-efficacy is considered as one of the most important cognitive factors in explain managerial behaviors.

Based on SCT, this study identifies the antecedents of supply chain agility and explains how managers' cognitive, affective, personal factors in events such as self-efficacy in supply chain agility, achieving trust in supply chain relationships, supply chain cooperation, coordination, and communication affect actual implementation of supply chain agility as well as firm performance. Although prior studies investigate the antecedents of supply chain agility as well as performance, this research attempts to identify the cognitive aspects of the antecedents in the implementation of supply chain agility and investigates the relationships between cognitive factors and supply chain agility including the relationship between implementation of supply chain agility and firm performance.

2. Theoretical background and literature review

2.1 Theoretical background

Social cognitive theory establishes a theoretical framework to understand the interactions between human behavior and personal and environmental factors [7, 8]. According to SCT, personal and environmental factors closely interact with each other and influence human behavior. Environmental factors modify and involve human beliefs, while cognitive and personal factors affect individual actions. Therefore, SCT can be used to explain human behavior depending on personal and environmental factors [7, 8]. This research applies SCT to explain the behavioral

intention of supply managers and executives in implementing supply chain agility and improving firm performance. Thus, our study investigates how environmental and cognitive factors impact managerial decision making for supply chain agility.

This research considered business uncertainty and supply chain disruption risk as the business environmental factors affecting managers' cognitive and personal factors [9, 10]. Supply chain self-efficacy, trust, and supply chain cooperation, coordination, and communication attitude as cognitive and personal factors influencing managerial behavior. This study selected implementation of supply chain agility as well as firm performance as actual behavior and outcomes relating to personal factors.

2.2 Literature review

In a supply chain, firms need to establish a strategy to deal with unexpected disruptions as well as uncertainties. Supply chain disruption is defined as an event that disrupts flows of goods and services, information, and money in a supply chain [11]. Supply chain disruptions generate financial difficulties for suppliers as well as downstream members of the supply chains [12]. Those disruptions are caused by various disturbances such as disease like COVID-19, environmental disasters like tsunami, hurricane and earthquake, and international conflicts like the local wars. These disturbances contain the expectancy and lead to potential risk of disruptions in the supply chain. Since they are coming from outside of the supply chain, the risk of supply chain disruptions interacting with market and technology turbulence and unexpected events such as natural disasters inclines supply chain disruption risk to external environmental factors [13].

Business uncertainty refers to environmental factors and may be interpreted as uncertainties of effect, condition, name, and response and generated by various sources [14]. Business uncertainty is considered a critical factor because it forms the basis for making a cognitive decision [15]. Since this study considers business uncertainty as an environmental factor, it applies the measurement of level of unpredictability in business environments following the research of Kocabasoglu *et al.* [16]. Further, their research established four dimensions of business uncertainty: munificence, dynamism, hostility, and heterogeneity [17]. This research adopts business uncertainty and supply chain disruption risk as external environmental factors because managers need to consider and deal with those two factors when making cognitive decisions based on SCT.

Trust has been widely discussed in supply chain management literature and has been defined as willingness to rely on supply chain partners the organization is confident about [18]. In inter-firm settings of the supply chain, trust is considered as an expected action that is desired by supply chain partners; therefore, trust plays a key role in firm behavior when there is uncertainty in the supply chain [19]. Trust must be necessary for supply chain members to increase asset-specific investments [20]. It also reduces minimal requirement and monitors and controls partners' actions, reduces conflict in supply chain relationships leading to successful supply chain management [18]. Thus, trust is considered an important antecedent for establishing good supply chain relationships as well as boosting collaboration in the supply chain [21].

Supply chain cooperation generates various benefits in the supply chain, especially reducing stock holdings for retailers, manufacturers, and distributors [22]. Supply chain coordination has a positive impact on supply chain performance [23]. Communication within a supply chain boosts integration, thereby increasing collaboration in the supply chain [24]. These mechanisms (cooperation, coordination, and communication) are empirically validated to show that they have a positive impact on supply chain agility [1]. Although actual implementation of supply chain cooperation, coordination, and communication are examined in the context of supply chain agility, this research investigates the role of trust and attitude toward supply chain cooperation, coordination, and communication as cognitive, affective, and personal factors in the context of SCT affecting actual implementation of supply chain agility as well as performance.

Supply chain agility (SCA) is defined as a supply chain's ability to respond quickly to changes in business environments [4]. However, since supply chain agility focuses on outcome measures, it applies to the focal firm's capability. Therefore, a firm's supply chain agility is its ability to work with suppliers and customers and adjust to and respond quickly to changing market dynamics by improving its supply chain capabilities [3]. Gligor and Holicomb [1] also emphasized

the importance of supply chain agility in the context of a firm's ability to adjust its operations proactively. The research of Gligor *et al.* [25] summarized supply chain agility into six themes: ability to quickly change directions, ability to speed/accelerate operations, ability to scan the environment/anticipate, ability to empower the customer/customize, ability to adjust tactics and operations, and ability to integrate process and within across firms. More importantly, environmental uncertainty also is closely linked to the concept of supply chain agility [25].

While the definition of supply chain agility has been discussed from the perspective of quick response, the research of Gligor *et al.* [5] classified firms' supply chain agility into two distinct dimensions: cognitive and physical. Notably, the concept of supply chain agility includes the cognitive ability to respond swiftly to changes as well as actions [6, 26]. Thus, this research investigates the impact of supply chain agility from the cognitive perspective as self-efficacy in supply chain agility, and the physical dimension as implementation of supply chain agility.

Based on the definition of supply chain agility, cognitive ability to make a quick respond quickly to market dynamics [3, 5], this research developed the concept of supply chain agility self-efficacy by reflecting Bandura's social cognitive theory. Self-efficacy represents that it promotes positive outcome due to more confidence in their skills [27]. Self-efficacy has been applied in various decision making contexts. Career decision-making self-efficacy means the level of individuals' confidence of their ability to perform the tasks [28]. Computer self-efficacy indicates individuals' beliefs regarding using computers to solve problems [29]. By applying self-efficacy in supply chain agility, this research applied self-efficacy in supply chain agility to supply chain managers' cognitive perspective. Therefore, our study defined supply chain agility self-efficacy as managers' confidence level on managing supply chain with agility in a cognitive perspective. This research investigates the managers' confidence level in supply chain agility in order to deal with supply disruption risk as well as business uncertainty.

3. Research model and hypotheses

Business uncertainty leads to the establishment of multiple communication channels among firms for the smooth flow of goods and information, resulting in more frequent interactions in the supply chain [30]. Additionally, supply chain managers quickly establish and implement supply chain strategies in response to environmental changes and to survive in highly competitive markets [9]. Further, managers' cognitive, affective, and personal factors in decision making are critical to business uncertainty.

A significant impact of business uncertainty is that it prevents managers from making risky investment decisions from the cognitive, affective, and personal perspectives [31]. Although previous research posits that business uncertainty encourages supply chain managers to implement supply chain practices such as integration [9], business uncertainty increases the risk propensity inherent in a supply chain [16]. This cognitive process has helped managers to avoid risks in their decisions and adopt new practices such as implementation of supply chain agility.

In SCT, external environmental factors such as business uncertainty influence managers' beliefs or self-efficacy as well as cognitive competencies that require quick response in decision making like self-efficacy in supply chain agility [7]. Cognitive hesitation caused by business uncertainty as well as lack of control reduces confidence in decision making. Thus, lack of control on the external environment is negatively related to self-efficacy in a start-up business [32]. Business uncertainty is negatively associated with changes in managers' perceived self-efficacy [33]. Thus, this research proposes hypothesis 1 as negative association between business uncertainty and managers' supply chain agility self-efficacy as follows:

H1. Business uncertainty is negatively associated with buyers' supply chain agility self-efficacy.

Firms encounter business uncertainty from demand variations and technology development. To ease business uncertainty, firms in a supply chain seek stable relationships with their partners [34]. Business uncertainty is considered an unpredictable factor in supply chain relationships. In a volatile business environment, buyers find it difficult to estimate the outcome of purchasing decisions and from maintaining healthy relationships so that good business exchanges generate

positive results with trust [35]. By fostering trust, supply chain relationships can build mutual commitment and shared values [36]. Increased business uncertainty strengthens trust between organizations [34]. When business uncertainty escalates in a supply chain, buyers strengthen trust with suppliers to maintain a close relationship in the supply chain. Therefore, this study posits the positive relationships between businesses uncertainty and buyers, and perceived trust in suppliers in hypothesis 2:

H2. Business uncertainty positively affects buyers' trust in suppliers.

Business uncertainty generates an inherent situation where interactions among firms are caused due to the involvement of multi-channel communications. Further, higher business uncertainty forces supply chain members to increase collaboration and coordination with more information [30]. In the context of uncertainty in demand, supply, and technology, increasing business uncertainty reinforces supply chain relationships, including cooperation and communications [37]. In supply chain environmental management, cooperation strengthens if business uncertainty increases [38]. As business uncertainty emerges in supply chains, buyers' efforts to improve supplier involvement to increase supply chain cooperation, coordination, and communication, results in motivating a positive mindset and attitude for working with suppliers. Thus, to overcome business uncertainty, this research proposes positive association between business uncertainty and buyers' attitude toward supply chain cooperation, coordination, and communication in hypothesis 3:

H3. Business uncertainty has a positive impact on buyers' attitude toward supply chain cooperation, coordination, and communication.

Firms use two dimensions to evaluate and measure supply chain disruption risk: probability and magnitude of risk, as perceived and judged by buyers [39]. To manage supply chain disruption risk, firms develop infrastructure and strategies for risk management and quick response [11]. However, perceived supply chain disruption risk interacts with supply and purchasing managers' confidence for making quick decisions. Managers with high self-efficacy tend to take higher risks [33]. On the opposite direction between risk and confidence, managers with high risk-tolerance levels tend to show greater confidence in their decision making, indicating that higher risk reduces confidence in decision making [40]. Meanwhile, Christopher and Lee [41] show that supply chain disruption risk reduces confidence in the supply chain, requiring responsive action. High supply chain disruption risk reduces the confidence in making a quick response action for supply chain agility. Thus, our study posits a negative relationship between supply chain disruption risk and buyers' supply chain agility self-efficacy in hypothesis 4:

H4. Supply chain disruption risk is negatively associated with buyers' supply chain agility self-efficacy.

Adding to the negative impact on confidence in supply chain agility, perceived supply chain disruption risk affects the entire supply chain network. Supply chain disruption risk demonstrates that exposure to disruption affects the relationship between members of the supply chain [42]. However, in high-risk environments, firms attempt to use integration with suppliers to mitigate supply chain disruption risk and improve cost and innovation performance [43]. The foundation of this relationship is trust. If trust increases in supplier relationships, the effect of sharing risk information with suppliers will help in improving firms' financial performance [44]. Perceived supply chain disruption risk leads to increased trust by generating many opportunities for strengthening relationships with supply chain members, as proposed in hypothesis 5

H5. Supply chain disruption risk positively affects buyers' trust in suppliers.

In dealing with supply chain disruption risk, firms use risk management strategies and practices for mitigation. Juttner [42] pointed out that firms tend to increase open discussion, communication, as well as cooperation with supply chain members. Riche and Bradely [45] also emphasized close collaboration, effective communication, and strong relationships in mitigating supply chain disruption risk. The study of Blos *et al.* [46] mentioned the importance of better communications

as well as coordination of business processes in a supply chain. As a risk management solution, firms attempt to increase supply chain cooperation, coordination, and communication to deal with perceived supply chain disruption risk. Such trials help to generate positive attitude toward supply chain cooperation, coordination, and communication. Thus, this research proposes hypothesis 6:

H6. Supply chain disruption risk has a positive impact on buyers' attitude toward supply chain cooperation, coordination, and communication.

In management studies, many researchers investigate the relationship between self-efficacy and actions. Entrepreneurial self-efficacy is considered to be one of the most important antecedents in establishing the entrepreneurship process [47]. To facilitate entrepreneurship, developing entrepreneurial capabilities helps to improve self-efficacy and pursue it as a career choice [48]. In computer usage, self-efficacy plays a significant role as it leads to easy use of computers from a user perspective [49]. If managers have high confidence in supply chain agility, it leads to action on implementing supply chain agility. Thus, firms with self-efficacy in supply chain agility tend to implement supply chain agility for better results, as proposed in hypothesis 7:

H7. Self-efficacy in supply chain agility is positively associated with buyers' implementation of supply chain agility.

Self-efficacy is considered a predictor of future performance, especially in the context of task [50], and is applied to improve employees' job performance. Job self-efficacy and creative self-efficacy are key attributes associated with workplace performance [51]. In using computers, self-efficacy has a direct impact on both intentional behavior of computer usage and ease of use, thereby helping to use computers [52]. Self-efficacy in computers improves performance in learning and using computers and is positively associated with learning engagement [29]. Self-efficacy in supply chain agility as managers' cognitive factor positively affect firms' comprehensive performance like implementation of supply chain agility self-efficacy as an action. Thus, this research proposes hypothesis 8 to show that self-efficacy in supply chain agility improves firms' performance including financial, operational, and supply chain:

H8. Self-efficacy in supply chain agility positively affects buyers' financial, operational, and supply chain performance.

Trust plays a positive role in supply chain management. Although trust has a cognitive form, it is expressed as a behavioral dimension. Notably, in supply chain relationships, trust creates more frequent exchange of communication and motivates suppliers to receive royalty from buyers so that buyers' trust in suppliers improves the responsiveness in a supply chain [53]. In the context of strategic sourcing, trust is considered a critical factor in improving supply chain agility [54]. Prior studies emphasized that trust is a strong driver in improving supply chain agility [55]. Thus, in hypothesis 9, our study proposes that buyers' trust in suppliers leads to buyers' decision in implementing supply chain agility:

H9. Buyers' trust in suppliers is positively associated with buyers' implementation of supply chain agility.

Trust has a positive impact on firms conducting various supply chain practices. Trust is positively associated with alliance performance due to the fact that it strengthens the relationship between allied companies [56]. Trust is also a very important mechanism in improving the performance of joint research and development projects [57]. However, a few studies have attempted to investigate the direct association between trust and firms' performance including financial, operational, and supply chain aspects. Capaldo and Giaannoccaro [58] used a simulation model to show that trust has a positive impact on supply chain performance and a moderating effect on the relationship between supply chain interdependence and supply chain performance. Thus, buyers' trust is positively associated with the total aspects of performance, as proposed in hypothesis 10:

H10. Buyers' trust in suppliers positively affects buyers' financial, operational, and supply chain performance.

Broadly, supply chain agility is positively affected by internal integration, and integration among suppliers including cooperation, coordination, and communication, and integration with suppliers [3]. While cooperation in a supply chain is considered one of the most important antecedents for improving supply chain agility [59], communication and cooperation also improve agility in a supply chain [60]. Supply chain cooperation, coordination, and communication are positively associated with supply chain agility [1]. Thus, this study proposes in hypothesis 11 that buyers' positive attitude toward supply chain cooperation, coordination, and communication leads to actual implementation of supply chain agility:

H11. Buyers' positive attitude toward supply chain cooperation, coordination, and communication are positively associated with implementation of supply chain agility.

Prior studies mentioned the positive impact of supply chain cooperation, coordination, and communication on firm performance. In green supply chain management, supplier partnerships have a positive impact on the firm's environmental and organizational performance [61]. Investments in supply chain coordination improve a firm's delivery performance [62]. Supply chain information exchange, coordination, and integration improve a firm's financial and market performance [63]. Based on these discussions, this research attempts to establish a positive association between buyers' positive attitude toward supply chain cooperation, coordination, and communication and the various aspects of firm performance, as in hypothesis 12:

H12. Buyers' positive attitude toward supply chain cooperation, coordination, and communication positively affects buyers' financial, operational, and supply chain performance.

In the context of supply chain management, supply chain agility positively affects both operational and relational performance [1]. Besides, supply chain agility is positively associated with a firm's financial performance and return on assets through cost efficiency and effective customer response, given the advantage of responding quickly to customers [6]. More importantly, supply chain agility generates positive outcomes in supply chain relationship as well as firms' performance. Our study proposes in hypothesis 13 that buyers' implementation of supply chain agility improves firms' financial, operational, and supply chain performance:

H13. Buyers' implementation of supply chain agility has a positive impact on their financial, operational, and supply chain performance.

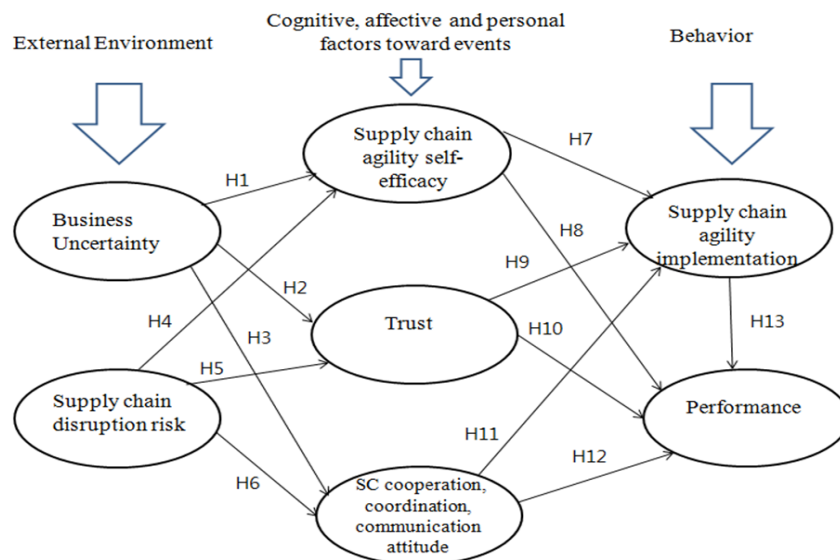Figure 1 describes our research model.

Fig. 1 A research model

4. Methodology

4.1 Instrument development

For validating our research hypotheses with industry data, survey questionnaires were developed by reviewing prior literature. All questionnaires in the measurements were revised to reflect the context of supply chain management. Business uncertainty, representing the dynamics of business environments, is measured with 6 items [16, 30]. Supply chain disruption risk indicating perceived risk of disruption in the supply chain is measured using 7 items [11, 39]. Supply chain agility self-efficacy, representing confidence levels regarding supply chain agility, is measured with 11 items [3, 4, 6]. This construct is based on supply chain agility combining self-efficacy concept that measured degree of managers' confidence toward supply chain agility in their cognitive perspective. In other words, all 11 items captured managers' confidence level on 11 items of definition of supply chain agility which are used in measuring implementation of supply chain agility in this survey questionnaires at the same time. Trust in suppliers, representing buyers' trust in suppliers in a supply chain relationship, is measured with 6 items [19, 20]. Supply chain cooperation, coordination, and attitude to communication are measured by 6 items indicating buyers' attitude and willingness to cooperate, coordinate, and communicate with suppliers [1, 64]. Implementation of supply chain agility as the actual behavioral dimension of implementing supply chain agility is measured using 11 items and these are consistent with supply chain agility self-efficacy items [3, 4, 6]. Finally, performance of three dimensions: financial, operational, and supply chain is measured in 12 items and compared with industry averages [65, 66].

After completing the first version of the survey, based on the literature review of previous studies, this research conducted intensive interviews with five supply, purchasing, and supply chain managers, including supply and purchasing executives from manufacturing industries. During the interviews, we received feedbacks on the measurement items as well as the survey for content validation, helping the survey to use proper terms in the industry. Using the modified survey, we executed a pilot study with a group of 31 experts (supply, purchasing, supply chain managers, and supply and purchasing executives) to improve a level of reliability and validity in the contents of the survey. All the statistical results, Cronbach's alpha, of the pilot study on measurement reliability were greater than 0.7, which was high enough to ensure that no measurement items were necessary to be eliminated.

After the pilot study, we finalized the survey such as scale, content, wording, and length. Our research utilized a 7-point Likert scale with response categories from 1 (strongly agree) to 7 (strongly disagree). For measurement purification, confirmatory factor analysis (CFA) with the maximum likelihood estimation (MLE) method was conducted with AMOS 20. This research also evaluated unidimensionality, reliability, convergent validity, and discriminant validity. They are presented in Tables 1 and 2.

4.2 Study sample

The target subjects of this research were supply, purchasing, and supply chain managers, including supply and purchasing executives who were capable of answering all questions properly in the survey designed for manufacturing firms in Korea. Firm level was the unit of analysis. We collected the surveys from various firms that manufactured automobiles, automobile components, various electronic products, various electronic product components textiles, clothing and related products, heavy equipment as well as its components, chemicals, healthcare products and equipment, furniture, metal products, and numerous consumable goods.

This research used firm size as a control variable since smaller firms need to deal with fewer resources for implementing supply chain management practices. A company's annual sales were used to measure firm size [6]. 50 firms with annual sales of firms less than $500 million, 39 firms from $500 million to $1 billion, 41 firms with $1 billion to $2 billion, 39 firms from $2 billion to $3 billion, 43 firms with $3 billion to $4 billion and finally, 40 firms with more than $ 4 billion among 252 firms.

Further, 900 paper-based survey questionnaires were randomly distributed to supply, purchasing, and supply chain managers, including supply and purchasing executives in Korean manufacturing firms on April, 2017. Nearly 260 responses were returned with a response rate of 28.88 % on May, 2017. However, 8 surveys were incomplete as they were marked with a single answer, resulting in 252 completed responses, which were used for data analysis. One respondent from each manufacturing company, a buyer in a supply chain as a focal firm did not complete one survey.

This research assessed the non-response bias following the approach outlined in the study of Mentzer and Flint [67]. About 111 non-respondents were randomly contacted by email and statistically no significant differences were found between the answers given by respondents and non-respondents. Although we received responses for only two weeks, our study compared the answers of early and late respondents and found no statistical differences. We conducted the Harman's single factor test to identify if the common method bias exists. By conducting an un-rotated factor analysis, this research checked all the eigenvalues according to the research of Doty and Glick [68] and Podsakoff and Organ [69]. This result ensures that no single factor, including no first factor, has a value greater than 20 % of the variances in our research data, which confirms the no common method bias.

5. Results

5.1 Measurement model

Using AMOS, this research examined various aspects of unidimensionality, reliability, convergent validity, and discriminant validity relatability in the measurement items. Cronbach's alpha and composite relatability for our measurement items are greater than 0.7, which presents satisfactory reliability in Table 1. For assessing both convergent validity and discriminant validity, we conducted confirmatory factor analysis with AMOS and checked the comparative fix index (CFI). Our research represents a goodness of fit model with a Chi-square of 411.66 and 194 degrees of freedom, CFI = 0.920, RMSEA = 0.052, and NFI = 0.936. If CFI is greater than 0.80 and the root mean square error of approximation (RMSEA) is less than 0.08, we can conclude that the model is satisfactory [70].

For examining convergent validity, our study checked the estimated parameters between the latent variables and their indicators and the values were above 0.50 in Table 1, indicating acceptable convergent validity [71]. For assessing discriminant validity, this research compared the square root values of the average variance extracted (AVE) with correlations of constructs and observed that the square root of AVEs were greater than the correlation values suggesting adequate discriminant validity in Table 2 [72].

Table 1 Reliability results

	Item loadings	Cronbach Alpha	Composite reliability	Item to total correlation	Average variance extracted
BU1	0.808	0.845	0.852	0.785	0.739
BU2	0.789			0.766	
BU3	0.816			0.795	
BU4	0.863			0.843	
BU5	0.794			0.771	
BU6	0.799			0.759	
SCR1	0.798	0.823	0.861	0.769	0.675
SCR2	0.863			0.844	
SCR3	0.883			0.862	
SCR4	0.818			0.800	
SCR5	0.805			0.784	
SCR6	0.817			0.792	
SCR7	0.748			0.722	
ASE1	0.848	0.851	0.880	0.801	0.702
ASE2	0.879			0.855	
ASE3	0.813			0.802	

Table 1 (Continuation)

ASE4	0.881			0.861	
ASE5	0.739			0.715	
ASE6	0.794			0.773	
ASE7	0.877			0.856	
ASE8	0.859			0.836	
ASE9	0.772			0.758	
ASE10	0.797			0.756	
ASE11	0.890			0.881	
TRU1	0.913	0.820	0.869	0.900	0.729
TRU2	0.894			0.880	
TRU3	0.743			0.722	
TRU4	0.888			0.889	
TRU5	0.897			0.845	
TRU6	0.826			0.811	
SCA1	0.890	0.880	0.910	0.877	0.830
SCA2	0.861			0.856	
SCA3	0.821			0.809	
SCA4	0.782			0.777	
SCA5	0.735			0.736	
SCA6	0.747			0.750	
SCAI1	0.800	0.847	0.879	0.788	0.801
SCAI2	0.821			0.807	
SCAI3	0.921			0.911	
SCAI4	0.837			0.824	
SCAI5	0.802			0.800	
SCAI6	0.778			0.764	
SCAI7	0.814			0.809	
SCAI8	0.816			0.811	
SCAI9	0.886			0.874	
SCAI10	0.882			0.852	
SCAI11	0.850			0.833	
FP1	0.779	0.828	0.860	0.766	0.852
FP2	0.807			0.799	
FP3	0.818			0.805	
FP4	0.824			0.815	
OP1	0.918			0.910	
OP2	0.876			0.845	
OP3	0.881			0.877	
OP4	0.852			0.826	
SCP1	0.896			0.881	
SCP2	0.833			0.822	
SCP3	0.839			0.817	
SCP4	0.883			0.867	

Performance includes financial (FP), operational (OP) and supply chain (SCP) performance.

Table 2 Correlation Matrix for constructs: Discriminant Validity

Variables	BU	SCR	ASE	TRU	SCA	SCAI	PERF
BU	**0.86**						
SCR	0.06	**0.82**					
ASE	0.51	0.23	**0.84**				
TRU	0.45	0.32	0.55	**0.85**			
SCA	0.46	0.52	0.58	0.55	**0.91**		
SCAI	0.51	0.24	0.48	0.48	0.48	**0.89**	
PERF	0.59	0.09	0.59	0.43	0.54	0.52	**0.92**

BU = business uncertainty; SCR = supply chain disruption risk; ASE = supply chain agility self-efficacy; TRU = trust; SCA = supply chain cooperation, coordination and communication attitude; SCAI = supply chain agility implementation; PERF = financial, operational and supply chain performance

5.2 Structural model

By employing structural equation modeling (SEM) to validate our research model, our results indicate a good fit for our research model with a Chi-square of 428.12 and 194 degrees of freedom, CFI of 0.927, RMSEA of 0.061, and NFI of 0.908 [73]. Hypothesis 1: Business uncertainty is

negatively associated with buyers' supply chain agility self-efficacy, was supported (CR = 5.278, $\beta1 = -0.496$, p < 0.001). With increasing levels of business uncertainty, manufactures' confidence toward supply chain agility declines. Our research results also support hypothesis 2: Business uncertainty positively affects buyers' trust in suppliers, (CR = 5.087, $\beta2 = 0.431$, p < 0.001). As business environments become dynamic and competitive, manufacturers' trust in suppliers would reduce. Our results provide empirical evidence for hypothesis 3: Business uncertainty makes a positive impact on buyers' attitude toward supply chain cooperation, coordination, and communication (CR = 5.019, $\beta3 = 0.417$, p < 0.001). A high level of business uncertainty discourages a proactive approach toward cooperation, coordination, and communication with suppliers. However, hypothesis 4: Supply chain disruption risk is negatively associated with buyers' supply chain agility self-efficacy was not supported (CR = 1.165, $\beta4 = 0.043$, p = 0.392).

Our research supports hypothesis 5: Supply chain disruption risk positively affects buyers' trust on suppliers (CR = 3.103, $\beta5 = 0.295$, p < 0.005) and hypothecs 6: Supply chain disruption risk makes a positive impact on buyers' attitude toward supply chain cooperation, coordination, and communication (CR = 4.165, $\beta6 = 0.427$, p < 0.001). As managers' perceived disruption risk in supply chain increases, manufacturers' trust as well as positive attitude toward cooperation, coordination, and communication with suppliers would diminish. Our research results also support Hypothesis 7: Supply chain agility self-efficacy is positively associated with buyers' implementation of supply chain agility (CR = 6.095, $\beta7 = 0.522$, p < 0.001). Hypothesis 8: Supply chain agility self-efficacy positively affects buyers' financial, operational, and supply chain performance (CR = 4.528, $\beta8 = 0.316$, p < 0.001) is also supported. Confidence in supply chain agility is considered as a positive antecedent for implementing supply chain agility and improving the three dimensions of firm performance. Our research results empirically confirmed hypothesis 9: Buyers' trust in suppliers is positively associated with buyers' implementation of supply chain agility (CR = 3.786, $\beta9 = 0.308$, p < 0.001). Similarly, hypothesis 10: Buyers' trust in suppliers positively affects buyers' financial, operational, and supply chain performance (CR = 5.959, $\beta10 = 0.443$, p < 0.001) is confirmed. Trust in supply chain relationships also plays a positive role in implementing supply chain agility and improving firm performance.

On the other hand, hypothesis 11: Buyers' attitude toward supply chain cooperation, coordination, and communication are positively associated with buyers' implementation of supply chain agility was not supported (CR = 1.009, $\beta11 = 0.0089$, p = 0.240). Our research results supported hypothesis 12: Buyers' attitude toward supply chain cooperation, coordination, and communication positively affects buyers' financial, operational, and supply chain performance (CR = 4.236, $\beta12 = 0.388$, p < 0.001p = 0.240). Hypothesis 13: Buyers' implementation of supply chain agility makes a positive impact on their financial, operational, and supply chain performance (CR = 7.012, $\beta13 = 0.558$, p < 0.001) is also supported. Manufacturers' willingness and positive attitude toward supply chain cooperation, coordination, and communication as well as implementation of supply chain agility improves firms' performance.

Table 3 presents direct effects among factors from research results.

Table 3 Direct effects testing results

Hypothesis No.	Path	Relationship direction	Standard weights	Critical Ratios	Supported
H1	BU→ASE	-	0.496	5.378	Yes: p < 0.01
H2	BU→TRU	-	0.431	5.087	Yes: p < 0.01
H3	BU→SCA	-	0.417	5.019	Yes: p < 0.01
H4	SCR→ASE	-	0.043	1.165	No: p = 0.392
H5	SCR→TRU	-	0.295	3.103	Yes: p < 0.05
H6	SCR→SCA	-	0.427	4.165	Yes: p < 0.01
H7	ASE→SCAI	+	0.522	6.095	Yes: p < 0.01
H8	ASE→PERF	+	0.316	4.528	Yes: p < 0.01
H9	TRU→SCAI	+	0.308	3.786	Yes: p < 0.01
H10	TRU→PERF	+	0.443	5.959	Yes: p < 0.01
H11	SCA→SCAI	+	0.089	1.009	No: p = 0.240
H12	SCA→PERF	+	0.388	4.236	Yes: p < 0.01
H13	SCAI→PERF	+	0.558	7.012	Yes: p < 0.01

6. Discussion and conclusion

This research provides meaningful implications for the academic world and the practical industry. It has filled a gap in the literature by identifying external environmental factors such as business uncertainty and supply chain risk as negative antecedents in the cognitive aspects in the context of supply chain agility. In supply chain risk management, uncertainty and risk have been discussed profoundly and prior studies provided various solutions. To mitigate business uncertainty and supply chain risk, information sharing, supply chain collaboration, and supply chain integration have been considered as appropriate solutions for supply chain management [74]. With an empirical approach, our study established an environmental-cognitive-behavioral framework for firms' decision making in implementing supply chain agility.

However, prior studies have not investigated the link between external environments that managers need to deal with such as business uncertainty and supply chain risk and cognitive factors in the context of supply chain agility. Thus, this study has addressed this gap in the literature and shows that business uncertainty reduces managers' confidence in supply chain agility while it strengthens trust and attitude for supply chain collaboration with suppliers. Notably, as business environments become more dynamic and unpredictable, buyers' trust in suppliers and their attitude toward cooperation, coordination, and communication with suppliers becomes more positive for boosting collaboration to overcome the uncertainty although business uncertainty increases uncertainty in supply chain agility.

Similar to business uncertainty, supply chain managers need to deal with supply chain disruption risk. Trust and supply chain collaboration consolidate supply chain relationships that play a positive role in mitigating supply chain risk [75]. Our research contributed to the literature envisaging that as perceived supply chain disruption risk increases, buyers' trust in suppliers and attitude for collaboration also increases as they want to overcome and mitigate disruption in supply chain risk. Thus, this research provides meaningful insights for supply chain disruption risk; managers rely on good supply chain relationships for strengthening trust and positive attitude for collaboration. However, supply chain disruption risk does not have significant relationships with efficacy in supply chain agility because managers' perception of dealing with supply chain disruption risk does not have a direct impact on their confidence in supply chain agility.

Like other applications of SCT in areas such as using computers, adopting innovation, and selecting a career, this study applies self-efficacy in the context of supply chain agility and finds that efficacy in supply chain agility has a positive impact on implementing supply chain agility as well as firm performance. In order to implement supply chain agility, firms need to educate the significance and need for supply chain agility in managing supply chains more effectively. In addition, managers' self-efficacy in supply chain agility is one of the success factors for implementing supply chain agility as it boosts the confidence levels of firms that have the capacity to deal quickly with unexpected events in the supply chain. Just as self-efficacy has a positive influence on computer learning and performance [29, 52], our research results confirm that self-efficacy in supply chain agility improves firm performance. Cognitive aspects of production system would help to adopt new technology and new business approach in the supply chain. More importantly, it gives confidence leading to successful operations in the supply chain networks. Thus, managers need to consider that improving self-efficacy in a supply chain results in successful implementation of supply chain agility and improves performance.

Trust has been receiving heightened attention in literature on supply chain relationships. Our results are consistent with most studies that provide empirical evidence on buyers' trust in supply chain relationships that generate a positive impact on supply chain agility as well as performance [54-58]. However, this study contributes that buyers' trust in suppliers is considered a significant cognitive antecedent for making decisions on implementing supply chain agility. Trust in suppliers is validated as a driving factor in decision making as it leads to the action of implementing supply chain agility from the buyers' perspective. In the context of trust and performance, buyers' trust in suppliers improves buyers' financial, operational, and supply chain performance, or complete firm performance, differentiating from prior literature which posits

that trust has a positive impact on only one dimension of performance, either financial or operational.

In supply chain management, trust is seen as a positive factor improving relationships, integration, agility, and performance. This research also provides consistent insights to supply chain managers suggesting that they need to find a way to establishing supply chain strategies to boost buyers' trust in suppliers so that it can lead an action of implementing supply chain agility and improve the overall buyers' performance. As a cognitive and affective factor, it is not easy to strengthen trust in suppliers. Frequent communication and information sharing can reinforce trust in suppliers. Supply chain managers' efforts to collaborate with suppliers improve trust.

Supply chain cooperation, coordination, and communication are empirically confirmed, and this illustrates the positive association between implementation of supply chain agility and firms' performance [1]. Thus, this research empirically confirmed that a positive attitude toward supply chain cooperation, coordination, and communication improves firm performance. This study contributes to the literature that a positive attitude toward supply chain practices can also play a significant role in improving buyers' performance instead of actual implementation. Firms need to consider educating managers about supply chain practices to boost the positive impact they can generate and provide managers clarity on such supply chain practices. Although information sharing improves supply chain agility [74], the positive attitude of supply chain cooperation, coordination, and communication is not a critical factor in decisions on implementing supply chain agility. With industry 4.0 technologies, decision making process will be improved [76]. In addition, supply chain collaboration would help to design product development process effectively (77).

Finally, supply chain agility implementation improves the firms' performance [1,6]. This research differentiates by measuring three dimensions: financial, operational, and supply chain performance. Implementation of supply chain agility is positively associated with the overall aspects of firm performance. Our study has some limitations due to the characteristics of empirical studies. First, this study applies the buyers' perspective in supply chain management practices. We collected the survey data from buyer firms by considering them as focal firms in a supply chain. This research targeted executives in supply and purchasing functions of buyer firms because they were knowledgeable and capable of answering all the survey questions to overcome this limitation. Second, our survey responses were collected from Korean manufacturing firms. Even though these companies have been doing business worldwide, geographical limitations continue to exist. In addition, future research can apply our research model in the context of service industries. Therefore, future studies could explore supply chain agility in the context of the U.S., China, or Europe or service industry by applying our research model to be tested. Finally, the future study would apply our research model in the context of Covid 19 situation that could generate severe supply disruptions risk as well as business uncertainty.

References

[1] Gligor, D.M., Holcomb, M.C. (2012). Antecedents and consequences of supply chain agility: Establishing the link to firm performance, *Journal of Business Logistics,* Vol. 33, No. 4, 295-308, doi: 10.1111/jbl.12003.

[2] Dubeauclard, R., Kubik, K., Ngali, V. (2015). How agile is your supply chain, from *https://www.mckinsey.com/business-functions/operations/our-insights/how-agile-is-your-supply-chain*, accessed March 14, 2016.

[3] Braunscheidel, M.J., Suresh, N.C. (2009). The organizational antecedents of a firm's supply chain agility for risk mitigation and response, *Journal of Operations Management,* Vol. 27, No. 2, 119-140, doi: 10.1016/j.jom.2008.09.006.

[4] Swafford, P.M., Ghosh, S., Murthy, N. (2006). The antecedents of supply chain agility of a firm: scale development and model testing, *Journal of Operations Management,* Vol. 24, No. 2, 170-188, doi: 10.1016/j.jom.2005.05.002.

[5] Gligor, D.M., Holcomb, M.C., Stank, T.P. (2013). A multidisciplinary approach to supply chain agility: Conceptualization and scale development, *Journal of Business Logistics*, Vol. 34, No. 2, 94-108, doi: 10.1111/jbl.12012.

[6] Gligor, D.M., Esmark, C.L., Holcomb, M.C. (2015). Performance outcomes of supply chain agility: When should you be agile?, *Journal of Operations Management*, Vol. 33-34, No. 1, 71-82, doi: 10.1016/j.jom.2014.10.008.

[7] Bandura, A. (1986). *Social foundations of thought and action: A social cognitive theory*, Prentice-Hall, Englewood Cliffs, New Jersey, USA.

[8] Bandura, A. (2001). Social cognitive theory: An agentic perspective, *Annual Review of Psychology,* Vol. 52, No. 1, 1-26, doi: 10.1146/annurev.psych.52.1.1.

[9] Kim, M., Chai, S. (2016). Assessing the impact of business uncertainty on supply chain integration, *The International Journal of Logistics Management*, Vol. 27, No. 2, 463-485, doi: 10.1108/IJLM-11-2014-0175.

[10] Kim, M., Suresh, N.C., Kocabasoglu-Hillmer, C. (2015). A contextual analysis of the impact of strategic sourcing and E-procurement on performance, *Journal of Business & Industrial Marketing,* Vol. 30, No. 1, 1-16, doi: 10.1108/JBIM-01-2012-0010.

[11] Ambulkar, S., Blackhurst, J., Grawe, S. (2015). Firm's resilience to supply chain disruptions: Scale development and empirical examination, *Journal of Operations Management,* Vol. 33-34, No. 1, 111-122, doi: 10.1016/j.jom.2014.11.002.

[12] Li, Y., Zhen, X., Qi, X., Cai, G. (2016). Penalty and financial assistance in a supply chain with supply disruption, *Omega,* Vol. 61, No. 2, 167-181, doi: 10.1016/j.omega.2015.12.011.

[13] Trkman, P., McCormack, K. (2009). Supply chain risk in turbulent environments – A conceptual model for managing supply chain network risk, *International Journal of Production Economics,* Vol. 119, No. 2, 247-258, doi: 10.1016/j.ijpe.2009.03.002.

[14] Wu, G.-C. (2013). The influence of green supply chain integration and environmental uncertainty on green innovation in Taiwan's IT industry, *Supply Chain Management,* Vol. 18, No. 5, 539-552, doi: 10.1108/SCM-06-2012-0201.

[15] Sitkin, S.B., Weingart. L.R. (1995). Determinants of risky decision-making behavior: A test of the mediating role of risk perceptions and propensity, *Academy of Management Journal,* Vol. 38, No. 6, 1573-1592, doi: 10.2307/256844.

[16] Kocabasoglu, C., Prahinski, C., Klassen. R.D. (2007). Linking forward and reverse supply chain investments: The role of business uncertainty, *Journal of Operations Management*, Vol. 25, No. 6, 1141-1160, doi: 10.1016/j.jom.2007.01.015.

[17] Keats, B.W., Hitt, M.A. (1988). A causal model of linkages among environmental dimensions, macro organizational characteristics, and performance, *Academy of Management Journal,* Vol. 31, No. 3, 570-598, doi: 10.5465/256460.

[18] Zhang, M., Huo, B. (2013). The impact of dependence and trust on supply chain integration, *International Journal of Physical Distribution & Logistics Management,* Vol. 43, No. 7, 544-563, doi: 10.1108/IJPDLM-10-2011-0171.

[19] Cai, S., Jun, M., Yang, Z. (2010). Implementing supply chain information integration in China: The role of institutional forces and trust, *Journal of Operations Management,* Vol. 28, No. 3, 257-268, doi: 10.1016/j.jom.2009.11.005.

[20] Corsten, D., Gruen, T., Peyinghaus, M. (2011). The effects of supplier-to-buyer identification on operational performance – An empirical investigation of inter-organizational identification in automotive relationships, *Journal of Operations Management,* Vol. 29, No. 6, 549-560, doi: 10.1016/j.jom.2010.10.002.

[21] Sahay, B.S. (2003). Understanding trust in supply chain relationships, *Industrial Management & Data Systems,* Vol. 103, No. 8, 553-563, doi: 10.1108/02635570310497602.

[22] Ding, H., Guo, B., Liu, Z. (2011). Information sharing and profit allotment based on supply chain cooperation, *International Journal of Production Economics,* Vol. 133, No. 1, 70-79, doi: 10.1016/j.ijpe.2010.06.015.

[23] Huo, B., Zhang, C., Zhao, X. (2015). The effect of IT and relationship commitment on supply chain coordination: A contingency and configuration approach, *Information & Management*, Vol. 52, No. 6, 728-740, doi: 10.1016/j.im.2015.06.007.

[24] Jacobs, M.A., Yu, W., Chavez, R. (2016). The effect of internal communication and employee satisfaction on supply chain integration, *International Journal of Production Economics,* Vol. 171, Part 1, 60-70, doi: 10.1016/j.ijpe.2015.10.015.

[25] Gligor, D., Gligor, N., Holcomb, M., Bozkurt, S. (2019). Distinguishing between the concepts of supply chain agility and resilience: A multidisciplinary literature review, *The International Journal of Logistics Management,* Vol. 30, No. 2, 467-487, doi: 10.1108/IJLM-10-2017-0259.

[26] Gligor, D.M., Holcomb, M.C., Feizabadi, J. (2016). An exploration of the strategic antecedents of firm supply chain agility: The role of a firm's orientations, *International Journal of Production Economics,* Vol. 179, 24-34, doi: 10.1016/j.ijpe.2016.05.008.

[27] Lent, R.W., Ireland, G.W., Penn, L.T., Morris, T.R., Sappington, R. (2017). Sources of self-efficacy and outcome expectations for career exploration and decision-making: A test of the social cognitive model of career self-management, *Journal of Vocational Behavior,* Vol. 99, 107-117, doi: 10.1016/j.jvb.2017.01.002.

[28] Guan, P., Capezio, A., Restubog, S.L.D., Read, S., Lajom, J.A.L., Li, M. (2016). The role of traditionality in the relationships among parental support, career decision-making self-efficacy and career adaptability, *Journal of Vocational Behavior,* Vol. 94, 114-123, doi: 10.1016/j.jvb.2016.02.018.

[29] Chen, I.-S. (2017). Computer self-efficacy, learning performance, and the mediating role of learning engagement, *Computers in Human Behavior,* Vol. 72, 362-370, doi: 10.1016/j.chb.2017.02.059.

[30] Wong, C.Y., Boon-itt, S., Wong, C.W.Y. (2011). The contingency effects of environmental uncertainty on the relationship between supply chain integration and operational performance, *Journal of Operations Management,* Vol. 29, No. 6, 604-615, doi: 10.1016/j.jom.2011.01.003.

[31] Lee, S.-Y., Klassen. R.D. (2016). Firms' response to climate change: The interplay of business uncertainty and organizational capabilities, *Business Strategy and the Environment*, Vol. 25, No. 8, 577-592, doi: 10.1002/bse.1890.

[32] Chen, C.C., Greene, P.G., Crick, A. (1998). Does entrepreneurial self-efficacy distinguish entrepreneurs from managers?, *Journal of Business Venturing,* Vol. 13, No. 4, 295-316, doi: 10.1016/S0883-9026(97)00029-3.

[33] Krueger, N., Dickson. P.R. (1994). How believing in ourselves increases risk taking: Perceived self-efficacy and opportunity recognition, *Decision Sciences,* Vol. 25, No. 3, 385-400.

[34] Wei, H.-L., Wong, C.W.Y., Lai, K.-H. (2012). Linking inter-organizational trust with logistics information integration and partner cooperation under environmental uncertainty, *International Journal of Production Economics,* Vol. 139, No. 2, 642-653, doi: 10.1016/j.ijpe.2012.05.036.

[35] Lai, K.-H., Bao, Y., Li, X. (2008). Channel relationship and business uncertainty: Evidence from the Hong Kong market, *Industrial Marketing Management,* Vol. 37, No. 6, 713-724, doi: 10.1016/j.indmarman.2007.05.017.

[36] Wang, L., Yeung, J.H.Y., Zhang, M. (2011). The impact of trust and contract on innovation performance: The moderating role of environmental uncertainty, *International Journal of Production Economics*, Vol. 134, No. 1, 114-122, doi: 10.1016/j.ijpe.2011.06.006.

[37] Fynes, B., de Búrca, S., Marshall, D. (2004). Environmental uncertainty, supply chain relationship quality and performance, *Journal of Purchasing and Supply Management,* Vol. 10, No, 4-5, 179-190, doi: 10.1016/j.pursup. 2004.11.003.

[38] Sharfman, M.P., Shaft, T.M., Anex. R.P. (2009). The road to cooperative supply-chain environmental management: Trust and uncertainty among pro-active firms, *Business Strategy and the Environment,* Vol. 18, No. 1, 1-13, doi: 10.1002/bse.580.

[39] Ellis, S.C., Henry, R.M., Shockley, J. (2010). Buyer perceptions of supply disruption risk: A behavioral view and empirical assessment, *Journal of Operations Management,* Vol. 28, No. 1, 34-46, doi: 10.1016/j.jom.2009.07.002.

[40] Ghosh, D., Ray, M.R. (1997). Risk, ambiguity, and decision choice: Some additional evidence, *Decision Sciences,* Vol. 28, No. 1, 81-104, doi: 10.1111/j.1540-5915.1997.tb01303.x.

[41] Christopher, M., Lee, H. (2004). Mitigating supply chain risk through improved confidence, *International Journal of Physical Distribution & Logistics Management,* Vol. 34, No. 5, 388-396, doi: 10.1108/09600030410545436.

[42] Jüttner, U. (2005). Supply chain risk management: Understanding the business requirements from a practitioner perspective, *The International Journal of Logistics Management*, Vol. 16, No. 1, 120-141, doi: 10.1108/09574090 510617385.

[43] Wiengarten, F., Humphreys, P., Gimenez, C., McIvor, R. (2016). Risk, risk management practices, and the success of supply chain integration, *International Journal of Production Economics,* Vol. 171, Part 3, 361-370, doi: 10.1016/j.ijpe.2015.03.020.

[44] Li, G., Fan, H., Lee, P.K.C., Cheng, T.C.E. (2015). Joint supply chain risk management: An agency and collaboration perspective, *International Journal of Production Economics,* Vol. 164, 83-94, doi: 10.1016/j.ijpe.2015.02.021.

[45] Ritchie, B., Brindley, C. (2007). Supply chain risk management and performance: A guiding framework for future development, *International Journal of Operations & Production Management,* Vol. 27, No. 3, 303-322, doi: 10.1108/01443570710725563.

[46] Blos, M.F., Quaddus, M., Wee, H.M., Watanabe, K. (2009). Supply chain risk management (SCRM): A case study on the automotive and electronic industries in Brazil, *Supply Chain Management,* Vol. 14, No. 4, 247-252, doi: 10.1108/13598540910970072.

[47] Boyd, N.G., Vozikis. G.S. (1994). The influence of self-efficacy on the development of entrepreneurial intentions and actions, *Entrepreneurship Theory and Practice,* Vol. 18, No. 4, 63-77, doi: 10.1177/104225879401800404.

[48] Wilson, F., Kickul, J., Marlino, D. (2007). Gender, entrepreneurial self-efficacy, and entrepreneurial career intentions: Implications for entrepreneurship education, *Entrepreneurship Theory and Practice,* Vol. 31, No. 3, 387-406, doi: 10.1111/j.1540-6520.2007.00179.x.

[49] Chau, P.Y. (2001). Influence of computer attitude and self-efficacy on IT usage behavior, *Journal of Organizational and End User Computing,* Vol. 13, No. 1, 26-33, doi: 10.4018/joeuc.2001010103.

[50] Locke, E.A., Frederick, E., Lee, C., Bobko, P. (1984). Effect of self-efficacy, goals, and task strategies on task performance, *Journal of Applied Psychology,* Vol. 69, No. 2, 241-251, doi: 10.1037/0021-9010.69.2.241.

[51] Tierney, P., Farmer, S.M. (2002). Creative self-efficacy: Its potential antecedents and relationship to creative performance, *Academy of Management Journal,* Vol. 45, No. 6, 1137-1148, doi: 10.5465/3069429.

[52] Hsia, J.-W., Chang, C.-C., Tseng, A.-H. (2014). Effects of individuals' locus of control and computer self-efficacy on their e-learning acceptance in high-tech companies, *Behaviour & Information Technology,* Vol. 33, No. 1, 51-64, doi: 10.1080/0144929X.2012.702284.

[53] Handfield, R.B., Bechtel, C. (2002). The role of trust and relationship structure in improving supply chain responsiveness, *Industrial Marketing Management*, Vol. 31, No. 4, 367-382, doi: 10.1016/S0019-8501(01)00169-9.

[54] Khan, K.A., Pillania, R.K. (2008). Strategic sourcing for supply chain agility and firms' performance: A study of Indian manufacturing sector, *Management Decision,* Vol. 46, No. 10, 1508-1530, doi: 10.1108/002517408109 20010.

[55] Agarwal, A., Shankar, R., Tiwari, M.K. (2007). Modeling agility of supply chain, *Industrial Marketing Management.* Vol. 36, No. 4, 443-457, doi: 10.1016/j.indmarman.2005.12.004.

[56] Krishnan, R., Martin, X., Noorderhaven, N.G. (2006). When does trust matter to alliance performance?, *Academy of Management Journal*, Vol. 49, No. 5, 894-917, doi: 10.5465/amj.2006.22798171.

[57] Arranz, N., de Arroyabe. J.C.F. (2012). Effect of formal contracts, relational norms and trust on performance of joint research and development projects, *British Journal of Management,* Vol. 23, No. 4, 575-588, doi: 10.1111 /j.1467-8551.2011.00791.x.

[58] Capaldo, A., Giannoccaro, I. (2015). How does trust affect performance in the supply chain? The moderating role of interdependence, *International Journal of Production Economics,* Vol. 166, 36-49, doi: 10.1016/j.ijpe. 2015.04.008.

[59] Yusuf, Y.Y., Gunasekaran, A., Musa, A., Dauda, M., El-Berishy, N.M., Cang, S. (2014). A relational study of supply chain agility, competitiveness and business performance in the oil and gas industry, *International Journal of Production Economics,* Vol. 147, Part B, 531-543, doi: 10.1016/j.ijpe.2012.10.009.

[60] Wieland, A., Wallenburg, C.M. (2013). The influence of relational competencies on supply chain resilience: A relational view, *International Journal of Physical Distribution & Logistics Management,* Vol. 43, No, 4, 300-320, doi: 10.1108/IJPDLM-08-2012-0243.

[61] Zhu, Q., Sarkis, J., Geng, Y. (2005). Green supply chain management in China: Pressures, practices and performance, *International Journal of Operations & Production Management,* Vol. 25, No. 5, 449-468, doi: 10.1108/01443570510593148.

[62] Da Silveira, G.J.C., Arkader, R. (2007). The direct and mediated relationships between supply chain coordination investments and delivery performance, *International Journal of Operations & Production Management,* Vol. 27, No. 2, 140-158, doi: 10.1108/01443570710720595.

[63] Wu, F., Yeniyurt, S., Kim, D., Cavusgil, S.T. (2006). The impact of information technology on supply chain capabilities and firm performance: A resource-based view, *Industrial Marketing Management,* Vol. 35, No. 4, 493-504, doi: 10.1016/j.indmarman.2005.05.003.

[64] Cao, M., Zhang, Q. (2011). Supply chain collaboration: Impact on collaborative advantage and firm performance, *Journal of Operations Management,* Vol. 29, No. 3, 163-180, doi: 10.1016/j.jom.2010.12.008.

[65] Fullerton, R.R., Kennedy, F.A., Widener, S.K. (2014). Lean manufacturing and firm performance: The incremental contribution of lean management accounting practices, *Journal of Operations Management,* Vol. 32, No. 7-8, 414-428, doi: 10.1016/j.jom.2014.09.002.

[66] Chen, D.Q., Preston, D.S., Xia, W. (2013). Enhancing hospital supply chain performance: A relational view and empirical test, *Journal of Operations Management*, Vol. 31, No. 6, 391-408, doi: 10.1016/j.jom.2013.07.012.

[67] Mentzer, J.T., Flint, D.J. (1997). Validity in logistics research. *Journal of Business Logistics,* Vol. 18, No. 1, 199-216.

[68] Doty, D.H., Glick, W.H. (1998). Common methods bias: Does common methods variance really bias results?, *Organizational Research Methods,* Vol. 1, No. 4, 374-406, doi: 10.1177/109442819814002.

[69] Podsakoff, P.M., Organ, D.W. (1986). Self-reports in organizational research: Problems and prospects, *Journal of Management,* Vol. 12, No. 4, 531-544, doi: 10.1177/014920638601200408.

[70] Byrne, B.M. (2008). *Structural equation modelling using SPSS and AMOS*, Taylor & Francis Group, New York, USA.

[71] Hair, J.F., Sarstedt, M., Ringle, C.M., Mena, J.A. (2012). An assessment of the use of partial least squares structural equation modeling in marketing research, *Journal of the Academy of Marketing Science,* Vol. 40, 414-433, doi: 10.1007/s11747-011-0261-6.

[72] Fornell, C., Larcker, D.F. (1981). Evaluating structural equation models with unobservable variables and measurement error, *Journal of Marketing Research,* Vol. 18, No. 1, 39-50, doi: 10.1177/002224378101800104.

[73] Browne, M.W., Cudeck, R. (1993). Alternative ways of assessing model fit, In: Bollen, K.A., Long, J.S. (eds.), *Testing structural equation models*, Sage Publications, Newbury Park, California, USA, 136-162.

[74] Kim, M., Chai, S. (2017). The impact of supplier innovativeness, information sharing and strategic sourcing on improving supply chain agility: Global supply chain perspective, *International Journal of Production Economics,* Vol. 187, 42-52, doi: 10.1016/j.ijpe.2017.02.007.

[75] Kwon, I.-W.G., Suh, T. (2004). Factors affecting the level of trust and commitment in supply chain relationships, *Journal of Supply Chain Management*, Vol. 40, No. 1, 4-14, doi: 10.1111/j.1745-493X.2004.tb00165.x.

[76] Rosin, F., Forget, P., Lamouri, S., Pellerin, R. (2021). Impact of Industry 4.0 on decision-making in an operational context, *Advances in Production Engineering & Management*, Vol. 16, No. 4, 500-514, doi: 10.14743/apem2021.4.416.

[77] Koppenhagen, F., Held, T. (2021). The implications of product modularisation on the development process, supplier integration and supply chain design in collaborative product development, *Advances in Production Engineering & Management*, Vol.16, No. 1, 82-98, doi: 10.14743/apem2021.1.386.

Appendix A

Survey items and sources

Business uncertainty	**[16, 30]**
Range: strongly disagree-strongly agree (7 Likert scale)	
BU1	In your industry, growth in customer demand is dramatically increased.
BU2	In your industry, rate at which products and service become outdated is very rapid.
BU3	Market activities of your competitors have become more hostile.
BU4	In your industry, success depends on providing a large range of consumer tastes.
BU5	Our customers often change their order in a short period of time
BU6	Our plant uses core production technologies that often change.
Supply chain disruption risk	**[11, 39]**
Range: strongly disagree-strongly agree (7 Likert scale)	
SCR1	It is highly likely that our company will experience an interruption in the supply from our suppliers.

SCR2	We worry that our supplier may not supply the products following our purchasing agreement.
SCR3	Suppliers' inability to supply their products would jeopardize our business performance.
SCR4	An interruption of supplies from our suppliers would have severe negative financial consequences for our business.
SCR5	We recognize that supply chain disruptions are always looming.
SCR6	Supply chain disruptions show us where we can improve.
SCR7	Supply chain disruptions show us where we can improve.
Supply chain agility self-efficacy	**[3, 4, 6]**
Range: strongly disagree-strongly agree (7 Likert scale)	
ASE1	We have a confidence on being able to changes in demand without overstocks or lost sales.
ASE2	We have a confidence on our supply chain being capable of responding to real market demand.
ASE3	We have a confidence on that our supply chain members recognize the importance of information integration.
ASE4	We have a confidence on that our supply chain members recognize the importance of joint planning on purchasing and production.
ASE5	We have a confidence on improving customer service as a high priority including delivery reliability
ASE6	We have a confidence on improving responsiveness to changing market needs as a high priority.
ASE7	We have a confidence that inventory and demand levels are visible through the supply chain.
ASE8	We have a confidence on detecting and responding the changes quickly in our business environments
ASE9	We have a confidence on identifying and making a definite decision toward opportunities in our business environments.
ASE10	We have a confidence on recognizing and dealing with threats swiftly in our business environments
ASE11	We have a confidence on adjusting our short-term capacity and orders whenever needed.
Trust	**[19, 20]**
Range: strongly disagree-strongly agree (7 Likert scale)	
TRU1	Our suppliers are trustworthy.
TRU2	Our suppliers have always been evenhanded in their negotiations with us.
TRU3	Our suppliers never use opportunities that arise to profits at our expense.
TRU4	When sharing our problems with suppliers, we know that they will respond with understandings.
TRU5	When it comes to things that are important to us, we can depend on our suppliers' supports.
TRU6	Whenever our suppliers give us advice on our business operations, we know that they are sharing their best judgement
Supply chain cooperation, coordination and communication attitude	**[1, 64]**
Range: strongly disagree-strongly agree (7 Likert scale)	
SCA1	We have a positive attitude on jointly implementing plans with our key supply chain members
SCA2	We have a positive attitude on coordinating our process and activities with our key supply chain members.
SCA3	There is a cooperative attitude on the relationship between our firm and other key supply chain members.
SCA4	Our supply chain members have a positive attitude on permitting each other to participate in strategic decisions.
SCA5	We have a positive attitude on exchanging information with our supply chain members.
SCA6	We have a positive attitude on exchanging information as soon as it becomes available.
Supply chain agility implementation	**[3, 4, 6]**

Range: strongly disagree-strongly agree (7 Likert scale)	
SCAI1	We are able to changes in demand without overstocks or lost sales.
SCAI2	Our supply chain is capable of responding to real market demand.
SCAI3	Our supply chain members recognize the importance of information integration.
SCAI4	Our supply chain members recognize the importance of joint planning on purchasing and production.
SCAI5	Improving customer service is our firm's high priority including delivery reliability.
SCAI6	Improving responsiveness to changing market needs is our firm's high priority.
SCAI7	Inventory and demand levels are visible through the supply chain.
SCAI8	We detect and respond the changes quickly in our business environments.
SCAI9	We identify and make a definite decision toward opportunities in our business environments.
SCAI10	We recognize and deal with threats swiftly in our business environments.
SCAI11	We adjust our short-term capacity and orders whenever needed.
Performance	**[65, 66]**
Rate your firm's performance comparing with your industry average	
Range: very low–very high (7 Likert scale)	
FP1	Average return on investment
FP2	Average return on assets
FP3	Average income
FP4	Growth on market shares
OP1	Defect rate
OP2	Delivery reliability
OP3	Production and inventory cost
OP4	Lead time
SCP1	Ability to respond to and accommodate periods of poor supplier and delivery performance
SCP2	Ability to respond to and accommodate new products, new markets or new competitors
SCP3	Customer response time in supply chain
SCP4	Total cost of distribution and manufacturing

Modelling of multiple surface roughness parameters during hard turning: A comparative study between the kinematical-geometrical copying approach and the design of experiments method (DOE)

Tomov, M.[a,*], Gecevska, V.[a], Vasileska, E.[a]

[a]Ss. Cyril and Methodius University in Skopje, Faculty of Mechanical Engineering, Skopje, North Macedonia

A B S T R A C T

This paper proposes and applies two different methodologies for modelling the roughness parameters in hard turning. The first method is based on the kinematical-geometrical copying of the cutting tool geometry onto the machined surface including a feedback loop through the parameter of statistic equality of sampling lengths in surface roughness measurements (*SE*). The other method employs the Design of Experiments (DOE) principles expressing the roughness parameters as first order nonlinear function of the input variables: cutting speed v, feed f, depth of cut a_p, and tool nose radius r_ε. The research includes the R_a and R_z roughness parameters which are commonly modelled throughout the research works, and additionally develops models for the R_p, R_v and $R_{mr(c)}$ roughness parameters which are more challenging to model compared to R_a and R_z as they depend more on the shape of the roughness profile and position of its mean line. Both methodologies for all roughness parameters were verified using a CNC lathe and special rings made of steel EN C55 with hardness of 53±1 HRC. Considering that the roughness profile is just a part of the total geometric deviations of the processed surfaces, and it is obtained from the total profile using software filtration, the research also considers the W_a parameter (waviness profile), as well as the deviations from the circularity (out-off-roundness) of the processed rings as indicators for the stability of the machining process.

A R T I C L E I N F O

1. Introduction

The significance of surface roughness in the functioning of the mechanical parts is well known, irrespective of the method and the mechanical processing technique applied to obtain them. C.L. He *et al.* in the research presented in [1] provide a detailed overview of the state-of-the-art of the influential factors and the methods applied in surface roughness modelling in turning, regardless of whether the processed materials have normal or enhanced hardness. In addition, Trung and Thinh [2] propose a novel approach for determining the minimum surface roughness based on four multi-criteria decision-making methods including MAIRCA, EAMR, MARCOS and TOPSIS, however only the R_a parameter is considered. Kramar and Cica [3] employ a Response Surface Methodology (RSM) to obtain the models for the R_a and R_t roughness parameters. Interestingly, they optimize the input parameters of the model for obtaining the lowest roughness

using a cuckoo search (CS) algorithm. The research studies [4-7] present a concurrent use of multiple methods (response surface methodology, artificial intelligence obtained through artificial neural networks, fuzzy logic, genetic algorithms, simulated annealing (SA) algorithm, goal-attainment method, regression response optimization) for modelling the surface roughness attained with milling and turning machining processes, as well as a comparison of the results. Mgwatu [8] develops and computes two machining optimization models to provide inclusive decisions of machining parameters, tool wear and surface quality while maximizing material rate and minimizing production costs. Kang *et al.* [9], using simulation study, investigate the influence of controlled vibration amplitudes and frequencies on the process of shaping the roughness profile and the subsequent values of the R_a and R_t parameters.

On the other hand, it is worth noting that, when processing materials with enhanced hardness, i.e., hardness greater than 45 HRC, increasing efforts are made to replace grinding with turning [10-12]. Therefore, there is considerable research referring to hard turning surface roughness modelling and predicting. Agrawal *et al.* [13] provide a literature review of optimization studies on hard turning. Thus, in [13-17] are described results of the impact of cutting parameters when optimizing and predicting the roughness of the surfaces. The impact of the tool geometry on the surface roughness estimation during hard turning, among other matters, is investigated in [18-20]. The influence of the cutting tool materials and workpiece hardness on the roughness profile formation during hard turning is analyzed in [12, 21-25], while information on the impact of different cooling mediums is provided in the research works in [26, 27].

A detailed analysis suggests that, regardless of the input parameters considered in the research (cutting parameters, tool geometry, cutting tool materials, workpiece hardness etc.), surface roughness optimization and prediction during hard turning is performed for limited number of roughness parameters, typically the R_a and R_z (R_t) parameters. Mite *et al.* in [28, 29] conclude that even though considered surfaces can have nearly identical values of the R_a and R_z (R_t) parameters, their roughness profile forms can be different, leading to a dissimilar behavior during the exploitation process.

This means that, when optimizing and predicting surface roughness as a result of hard turning, multiple roughness parameters need to be considered in order to define the roughness profile shape uniquely and accurately. Thus, unlike the previously referenced studies, this research, in addition to the R_a and R_z parameters, also considers the R_p, R_v and $R_{mr(c)}$ parameters for the same measured roughness profile. The distinctiveness of these parameters is that their values are quite sensitive to the roughness profile shape and the position of the mean line of the profile and therefore, it is more cumbersome to model and predict their values.

Another possible shortcoming of the previously referenced research refers to the fact that the roughness profile is considered as an independent variable, disregarding the fact that it derives from the total profile using software filtration, a procedure described in [30]. Research [31] confirms a tight correlation between the primary, waviness, and roughness profile in a stable hard turning process.

In the presented study, two different methods will be conducted and presented for modelling and predicting multiple roughness profile parameters, i.e., the R_a, R_z, R_p, R_v and $R_{mr(c)}$ parameters. The first method will employ Kinematical-Geometrical copying (K-G) of the cutting tool geometry onto the machined surface, whereas the second method will consider Design of Experiments (DOE) methodologies, more specifically a nonlinear first-order function. Furthermore, the waviness information of the profile (the W_a parameter) as well as the out-off-roundness of the investigated pieces will be applied as methods to control and verify that the roughness profiles are obtained from a stable hard turning process. The modelling based on kinematical-geometrical copying of the cutting tool geometry onto the machined surface includes a feedback loop dependent on the condition of the processing.

2. Materials, methods, and experimental work

2.1 Kinematical-geometrical (K-G) copying method

Mite *et al.* [32] propose mathematical models for predicting the values of the roughness parameters R_a, R_z, R_p, R_v, $R_{mr(c)}$ as a function of the stability and the conditions of the turning process used to form the surface roughness. The mathematical models indicated in [32] are verified by turning of normal hardness materials (33±1 HRC). This research will use those models to predict the values of the roughness parameters during hard turning. The mathematical models are a function of the angles $\lambda_s, \gamma_o, \kappa_r$, the radius r_ε and the feed *f*. The angles λ_s, γ_o determine whether a circular part or an ellipse will be reflected onto the processed surface, where a circular part is defined when both angles are equal to zero. The angle κ_r additionally determines the position of the ellipse relative to the processed surface. The angles λ_s, γ_o directly impact the process of chip formation.

The maximum height of the roughness profile (R_z) will be calculated as follows [32]:

$$Rz = Rz_{k-g} \cdot e^{3SE} \tag{1}$$

where:

$$Rz_{k-g} = r_\varepsilon \sqrt{t} - \sqrt{r_\varepsilon^2 t - \frac{f^2}{4\cos^2\omega} t^2} \tag{2}$$

$$\varphi = \kappa_r - \text{arctg}\left(\frac{\text{tg}\lambda_s}{\text{tg}\gamma_o}\right) \tag{3}$$

$$\omega = \text{arctg}\left(\frac{\text{tg}\gamma_o}{\cos\left(\text{arctg}\left(\frac{\text{tg}\lambda_s}{\text{tg}\gamma_o}\right)\right)}\right) \tag{4}$$

$$t = 1 - \cos^2\varphi \cdot \sin^2\omega \tag{5}$$

r_ε – nose radius of the inserts, κ_r – entering angle, f – feed rate, λ_s – inclination angle, γ_o – rake angle. The calculation of the parameter of statistic equality of sampling lengths in surface roughness measurement (SE) requires the measuring of the primary surface profile and a determination of the z-coordinates of the primary profile points. Then, SE is calculated as follows [30]:

$$SE = \frac{K_{sm}}{K_s} \tag{6}$$

where:

$$K_{sm} = \frac{s_{max}^2 - s_{min}^2}{s_{max}^2} \tag{7}$$

s_{max} – the maximum standard deviation calculated for primary profile points (z-coordinates) within the sampling lengths, s_{min} – the minimum standard deviation calculated for primary profile points (z-coordinates) within the sampling lengths, and:

$$K_s = \frac{\bar{s}^2}{s_p^2} \tag{8}$$

$\bar{s}$ – the standard deviation calculated as the mean value of the individual standard deviations calculated for primary profile points (z-coordinates) within the sampling length, s_p – the standard deviation calculated for all points of primary profile (z-coordinates) within the evaluation lengths.

The maximum profile peak height of the roughness profile (R_p) will be determined as follows [32]:

$$Rp = Rp_{k-g} \cdot e^{2SE} \tag{9}$$

where:

$$Rp_{k-g} = \left| \frac{r_\varepsilon^2 \cos\omega}{2f} \left(\left(\text{arctg}\frac{Y_2}{X_2\cos\omega} \right) - \left(\text{arctg}\frac{Y_1}{X_1\cos\omega} \right) \right) \right| - \left| \frac{X_1 Y_2 - X_2 Y_1}{2f} \right| \tag{10}$$

$$X_1 = \sin\varphi \sqrt{\frac{r_\varepsilon^2}{t} - \frac{f^2}{4\cos^2\omega}} + \frac{f\cos\varphi}{2} \tag{11}$$

$$X_2 = \sin\varphi \sqrt{\frac{r_\varepsilon^2}{t} - \frac{f^2}{4\cos^2\omega}} - \frac{f\cos\varphi}{2} \tag{12}$$

$$Y_1 = \frac{H - Rz_{k-g}}{\cos\varphi} - \text{tg}\varphi \cdot X_1 \tag{13}$$

$$Y_2 = \frac{H - Rz_{k-g}}{\cos\varphi} - \text{tg}\varphi \cdot X_2 \tag{14}$$

$$H = r_\varepsilon \sqrt{1 - \cos^2\varphi \sin^2\omega} \tag{15}$$

The maximum profile valley depth R_v, according to [32], will be determined as follows:

$$Rv = Rv_{k-g} \cdot e^{3SE} \tag{16}$$

where:

$$Rv_{k-g} = Rz_{k-g} - Rp_{k-g} \tag{17}$$

Arithmetical mean height of the roughness profile Ra will be determined as follows [32]:

$$Ra = Ra_{k-g} \cdot e^{SE} \tag{18}$$

where:

$$Ra_{k-g} = \left| \frac{r_\varepsilon^2 \cos\omega}{f} \left(\left(\text{arctg}\frac{Y_4}{X_4\cos\omega} \right) - \left(\text{arctg}\frac{Y_3}{X_3\cos\omega} \right) \right) \right| - \left| \frac{X_3 Y_4 - X_4 Y_3}{f} \right| \tag{19}$$

$$X_3 = \frac{(H - Rz_{k-g} + Rp_{k-g})\sin\varphi + \cos\varphi \cdot \cos\omega \sqrt{r_\varepsilon^2 t - (H - Rz_{k-g} + Rp_{k-g})^2}}{t} \tag{20}$$

$$X_4 = \frac{(H - Rz_{k-g} + Rp_{k-g})\sin\varphi - \cos\varphi \cdot \cos\omega \sqrt{r_\varepsilon^2 t - (H - Rz_{k-g} + Rp_{k-g})^2}}{t} \tag{21}$$

$$Y_3 = \frac{H - Rz_{k-g} + Rp_{k-g}}{\cos\varphi} - \text{tg}\varphi \cdot X_3 \tag{22}$$

$$Y_4 = \frac{H - Rz_{k-g} + Rp_{k-g}}{\cos\varphi} - \text{tg}\varphi \cdot X_4 \tag{23}$$

Load length ratio of the roughness profile $R_{mr(c)}$ will be determined as follows [32]:

$$Rmr(c) = \frac{Rmr(c)_{k-g}}{e^{SE}} \tag{24}$$

where:

$$Rmr(c)_{k-g} = \left(1 - \frac{2\cos\omega \sqrt{r_\varepsilon^2 t - \left(\sqrt{r_\varepsilon^2 t - \frac{f^2}{4\cos^2\omega} t^2} + c \right)^2}}{f \cdot t} \right) \cdot 100\% \tag{25}$$

The limitations of the mathematical models developed on the basis of kinematical-geometrical copying, stipulated in [32], also apply to this research.

2.2 Design of experiments

This section presents the mathematical models for the R_a, R_z, R_p, R_v, $R_{mr(c)}$, SE and W_a parameters, as nonlinear functions denoted with the Eq. 26. For acquiring the required data for empirical modelling, four-factorial plan experiment of first order was conducted, where the independent input variables comprised cutting speed v, feed f, tool nose radius r_ε and depth of cut a_p, with repetition in the middle point of the investigated hyperspace. Table 1 provides the values of the defined independent variables. The number of experiments is $2^4 = 16$, with additional four experiments for the repetitions in the middle points. Table 2 provides the detailed plan of experiments. The verification of the adequacy of the obtained mathematical models employs the Fisher test with a significance level of $\alpha = 0.05$. The accuracy of the mathematical models is defined at 95 % confidence interval.

$$Parameter = Constant \cdot v^a \cdot f^b \cdot a^c \cdot r_\varepsilon^d \tag{26}$$

2.3. Defining of the investigated hyperspace (input independent variables)

The mathematical models based on kinematical-geometrical copying are a function of the angles $\lambda_s, \gamma_o, \kappa_r$, the radius r_ε and the feed f. The angles $\lambda_s, \gamma_o, \kappa_r$ characterize the cutting tool and they will not change during the experiments, whereas the radius r_ε and the feed f will change. To provide comparability and consistency of the results with the other model, the values of r_ε and f will be kept identical as in the DOE. As aforementioned, the independent variables in the first-order nonlinear mathematical model comprise of the cutting speed v, feed f, depth of cut a_p, and tool nose radius (r_ε), and their values are summarized in Table 1. Considering the cutting tool (insert) that the producer recommends (described in sub-chapter 2.5) for continuous cutting the following parameter ranges should be employed: cutting speed v from 80-250 m/min, depth of cut a_p from 0.05-0.5 mm and feed (f from 0.03-0.2 mm).

Starting from the conclusion stated in the introduction of this paper, that increasing efforts are made to replace grinding with turning, the authors of this paper were attentive to the selection of the values for f and a_p.

In typical industrial applications, the lower limit of the R_a parameter during classical grinding is 0.2 μm. Considering the well-known theoretical equation for determining $Ra = f^2/32r_\varepsilon$ during turning, an insert radius $r_\varepsilon = 1.2$ mm and $R_a = 0.2$ μm yields that the feed is $f = 0.087$ mm/rev. Therefore, this research adopts a lower limit for f of 0.09 mm/rev, while the upper limit reflects the recommendations of the cutting tool producer. When selecting the minimum value for the depth of cut (a_p), the authors assured that the ratio f/a_p is always less than or equal to one. This is crucial since under such circumstances the general "shape" of the chip cross section does not change significantly, which impacts the chip formation process and the geometric structure of the surface. Therefore, the paper adopts a lower limit for a_p of 0.2 mm, and twice as big upper limit.

Table 1 Input parameters and their levels

No.	Parameters	Level 1	Central point	Level 2
1	Cutting speed (v), m/min	100	141.4	200
2	Feed (f), mm/rev	0.09	0.134	0.2
3	Depth of cut (a_p), mm	0.2	0.283	0.4
4	Tool nose radius (r_ε), mm	0.4	0.8	1.2

2.4 Work piece material

This research uses work pieces made of steel EN C55 (AISI 1055). To achieve appropriate hardness of 53±1 HRC, the work pieces were thermally enhanced. The pieces are made into rings to achieve uniform hardness throughout the entire cross-section. The size of the rings is ø100 × ø82 × 20 mm and they are clamped on a special device using a flat key (Fig. 1).

2.5 Machine and cutting tool

The work rings are processed using CNC lathe, shown on Fig. 1, model OKUMA LB 15-II (C-1S). The lathe provides variable spindle speed from 38-3800 rpm, feed rate from 0.001-1000 mm/rev and 15 kW spindle drive motor. From one side the work pieces are clamped in the chuck, while on the other side, they lean on the tailstock (Fig. 1). Before performing the machining experiments, the rings were processed to remove the circular run out from the clamping of the rings. During the machining of the workpieces in accordance with the defined DOE, a coolant (17 % concentration of cutting oil in water) was applied. The pieces were processed using a holder designated ADPNN2525M15-A (Tungaloy), with $\kappa_r = 62.5°$, $\gamma_o = 0°$, $\lambda_s = -10°$ and cutting T-CBN negative inserts designated 2QP-DNGA 150404-BXM20, 2QP-DNGA 150408-BXM20 and 2QP-DNGA 150412-BXM20 (Tungaloy). The angles γ_o and λ_s are defined perpendicularly to the axis of rotation. Every working ring is processed using a new cutting edge of the insert, to eliminate the effect from the wear of the inserts. In models based on the kinematical-geometrical copying principle, the angle γ_o equals –0.0001°, to avoid the mathematical constraints stipulated in [32].

Fig. 1 Experimental equipment

2.6 Measurement equipment and execution of experiment

The out-off-roundness of the work rings is measured using a Roundtest RA-400 (Mitutoyo), Fig. 2. To avoid potential impact of the elastic deformation of the working rings caused by clamping, the authors measured the circularity while the rings remained clamped on the device, as shown on Fig. 2. The primary, roughness and waviness profiles of the processed rings were measured using a Surf test model No. SJ-410 (Mitutoyo), Fig. 3. The considered parameters were measured at five equally spaced locations around the circumference of the work rings to obtain the statistically significant data for the test. The profiles and parameters were measured and calculated in accordance with the ISO standard recommendations, i.e. in accordance with the procedure for obtaining the primary profile, the roughness profile, and the waviness profile presented in [30]. Table 2 provides the measurement conditions when obtaining the primary, roughness, and waviness profiles. The $R_{mr(c)}$ parameter was calculated at a level of 30 % of R_z ($30R_z$) from the highest peak of the roughness profile, i.e. c = 30 % of R_z µm, for all considered roughness profile. A pick-up stylus with top angle of 60° and top radius of 2 µm was utilized, as well as a skidless pick-up. During the measurements, the instrument was mechanically levelled with respect to the measured surface. The measuring system was calibrated using a type C etalon with R_a = 2.97 µm, and was verified using a type C etalon with R_a = 6 µm. The used calibration etalons have a measuring uncertainty of 5 %. The parameter *SE* was calculated for a primary profile in accordance with the conditions listed in Table 2.
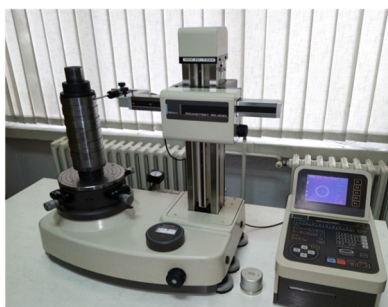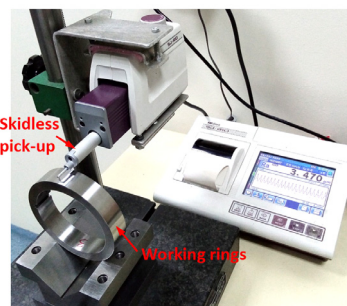

Fig. 2 Roundtest RA-400 (Mitutoyo)

Fig. 3 Surf test model No. SJ-410 (Mitutoyo)

3. Results and discussion

Table 3 shows the entire plan for the realization of the experiments, as well as the measured values for: the roughness parameters R_a, R_z, R_p, R_v and $R_{mr(c)}$, the parameter *SE* determined for the primary profile, the parameter W_a determined for the waviness profile and the out-off-roundness values. The value of all parameters provided in Table 3, except for the out-off-

roundness, are derived as mean values of five measurements. The values for the out-off-roundness in Table 3 are mean values of three measurements. Furthermore, this research includes the parameter W_a that reflects the waviness profile. Constitutionally, according to DIN 4760 and [32], the roughness profile forms as third, fourth and fifth order deviations, while the waviness profile forms as a result of second order deviations. Out of all the second order deviations, off-center clamping can greatly influence waviness. To obtain a comprehensive picture of the conditions for forming the roughness profiles, the parameter W_a and the out-off-roundness of the working rings are also considered and measured. Table 3 shows the values of the out-off-roundness. The out-off-roundness of the work rings is not subject to mathematical modelling. However, a non-linear function of the first order model is established for the W_a parameter.

Table 2 Measurement conditions of roundness, primary, roughness and waviness profiles

Profile/Parameters	Primary profile / P_a / SE	
Experiment No.	All	
Filter	Gaussian	
r_{tip} (μm)	2	
λ_s profile filter (μm)	2.5	
L evaluation length (mm) $L = 1 \times N$ (mm)	8	
Profile/Parameters	Waviness profile / W_a	
Experiment No.	1,2,5,6,9,10,13,14	3,4,7,8,11,12,15,16,17,18,19,20
Filter	Gaussian	
r_{tip} (μm)	2	
λ_c profile filter (mm)	0.25	0.8
λ_f profile filter (mm)	2.5	
L evaluation length (mm)	5 × 2.5 = 12.5	
Profile/Parameters	Roughness profile / R_a	
Experiment No.	1,2,5,6,9,10,13,14	3,4,7,8,11,12,15,16,17,18,19,20
Filter	Gaussian	
r_{tip} (μm)	2	
λ_s profile filter (μm)	2.5	
λ_c profile filter (mm) l_r sampling length (mm)	0.25	0.8
l_n evaluation length (mm) $l_n = N \times l_r$ (mm)	5 × 0.25 = 1.25	5 × 0.8 = 4

Table 3 Experimental plan and results

No.	v (m/min)	f (mm/rev)	a_p (mm)	r_ε (mm)	SE P-profile	R_z (μm)	R_p (μm)	R_v (μm)	R_a (μm)	R_{mr} (30R_z) (%)	W_a (μm)	Out-of-roundness (μm)
1	100	0.09	0.2	0.4	0.036	3.098	1.992	1.106	0.695	14.1	0.055	0.658
2	200	0.09	0.2	0.4	0.047	3.313	2.074	1.239	0.735	15.5	0.049	0.633
3	100	0.2	0.2	0.4	0.033	14.148	9.262	4.886	3.398	14.4	0.078	0.700
4	200	0.2	0.2	0.4	0.044	14.084	9.310	4.774	3.362	13.7	0.094	0.732
5	100	0.09	0.4	0.4	0.033	3.010	1.891	1.120	0.720	14.9	0.076	0.689
6	200	0.09	0.4	0.4	0.041	3.209	2.047	1.162	0.782	14.2	0.055	0.705
7	100	0.2	0.4	0.4	0.038	13.789	9.017	4.771	3.309	14.3	0.080	0.933
8	200	0.2	0.4	0.4	0.051	14.334	9.475	4.932	3.442	13.0	0.101	0.893
9	100	0.09	0.2	1.2	0.147	1.329	0.795	0.534	0.249	10.7	0.045	0.533
10	200	0.09	0.2	1.2	0.078	1.345	0.742	0.603	0.287	18.6	0.054	0.603
11	100	0.2	0.2	1.2	0.047	4.039	2.541	1.498	0.938	15.2	0.036	0.842
12	200	0.2	0.2	1.2	0.047	4.089	2.715	1.375	0.934	14.2	0.040	0.795
13	100	0.09	0.4	1.2	0.115	1.413	0.742	0.671	0.254	15.2	0.042	0.551
14	200	0.09	0.4	1.2	0.141	1.052	0.639	0.413	0.218	12.0	0.041	0.400
15	100	0.2	0.4	1.2	0.039	4.138	2.636	1.498	0.938	13.3	0.035	0.681
16	200	0.2	0.4	1.2	0.054	4.297	2.796	1.501	0.940	12.8	0.036	0.652
17	141.4	0.134	0.283	0.8	0.039	2.962	1.848	1.114	0.699	16.0	0.026	0.433
18	141.4	0.134	0.283	0.8	0.043	3.236	2.005	1.230	0.726	13.4	0.027	0.568
19	141.4	0.134	0.283	0.8	0.032	3.325	2.058	1.309	0.713	14.1	0.028	0.675
20	141.4	0.134	0.283	0.8	0.042	3.362	2.216	1.146	0.781	12.9	0.036	0.500

The reason pertains to the fact that the *SE* parameter determined for the primary profile, as well as the primary profile itself, contain the waviness. From a measurement point of view, the boundary between the waviness profile and the roughness profile is defined by the applied λ_c profile filter. Any deficiencies or inappropriate choices for the applied λ_c profile reflect on the

shape of the roughness profile. In addition, from a constitutional point of view, the selection of the combination of values for cutting speed (v), feed (f), depth of cut (a_p) and tool nose radius (r_ε) can also influence the vibrations on the tool and the machine. The following mathematical models for the considered parameters were obtained based on the values from Table 3 and applying the methodology stipulated in sub-chapter 2.2:

$$R_z = 77.533 \cdot v^{-0.0121541} \cdot f^{1.673} \cdot a^{-0.0322310} \cdot r_\varepsilon^{-0.9691411} \tag{27}$$

$$R_p = 50.514 \cdot v^{0.0145691} \cdot f^{1.775} \cdot a^{-0.0406075} \cdot r_\varepsilon^{-1.026} \tag{28}$$

$$R_v = 26.753 \cdot v^{-0.0516292} \cdot f^{1.515} \cdot a^{-0.0190284} \cdot r_\varepsilon^{-0.8838959} \tag{29}$$

$$R_a = 17.175 \cdot v^{0.0278376} \cdot f^{1.783} \cdot a^{-0.0278446} \cdot r_\varepsilon^{-1.071} \tag{30}$$

$$R_{mr(30Rz)} = 10.732 \cdot v^{0.0202365} \cdot f^{-0.0328251} \cdot a^{-0.0730024} \cdot r_\varepsilon^{-0.0278032} \tag{31}$$

$$SE = 0.0095850 \cdot v^{0.1733292} \cdot f^{-0.5450216} \cdot a^{0.0656300} \cdot r_\varepsilon^{0.5575011} \tag{32}$$

$$W_a = 0.0406614 \cdot v^{0.0491459} \cdot f^{0.1290388} \cdot a^{0.0104809} \cdot r_\varepsilon^{-0.5093038} \tag{33}$$

The mathematical models expressed by the Eq. 27-33 represent first order models without mutual interaction and without factor significance evaluation. Table 5 provides their dispersion analysis together with an adequacy evaluation. The negative sign in the exponent in the term of the model indicates an inverse relationship between that term and the modelled parameter. The *SE* parameter model, Eq. 32, obtained in accordance with the DOE was used to obtain the values necessary to calculate the roughness parameters according to the kinematical-geometrical copying model, Eq. 1,9,16,18,24. The percentage differences between the mean values of the measurements and the theoretically calculated values of the parameters modelled according to K-G and DOE, are systematized in Table 4. The negative sign before the values in Table 4 indicates that the theoretical value is lower than the measured value. The paper presents 3D graphs, Figs. 4 to 20, in order to provide a graphic overview of the obtained mathematical models of the modelled parameters, but also to show the differences between the models obtained using different techniques of the investigated hyperspace. For every roughness parameter, the paper presents three graphs selected in a state with the biggest percentage difference, from Table 4, between the kinematical-geometrical copying model (K-G) and the DOE.

Table 4 Percentage difference between measured average values and calculated values according to the two techniques

No.	R_z (%)		R_p (%)		R_v (%)		R_a (%)		R_{mr} (30Rz) (%)		SE (%)
	K-G	DOE	K-G	DOE	K-G	DOE	K-G	DOE	K-G	DOE	DOE
1	-7.9	7.3	-8.5	3.1	-15.7	13.1	-2.8	6.7	9.8	4.3	16.6
2	-13.5	0.0	-11.8	0.1	-27.5	-0.9	-8.7	3.1	0.3	-3.8	3.2
3	-3.1	-11.4	-3.7	-9.2	-7.5	-14.5	-1.7	-10.0	8.2	-0.5	-17.6
4	-1.5	-11.8	-3.5	-8.7	-3.9	-15.9	-0.6	-6.7	12.1	5.4	-39.9
5	-3.8	7.9	-2.6	5.4	-16.5	10.8	-6.6	1.4	4.1	-6.8	26.2
6	-8.8	0.9	-9.8	-1.4	-18.7	4.2	-15.8	-5.1	8.5	0.0	18.6
7	-0.1	-11.0	-0.7	-9.3	-4.6	-13.3	0.8	-9.2	8.5	-5.3	-30.5
8	-2.9	-16.3	-5.0	-13.7	-6.9	-21.4	-3.1	-11.4	16.7	5.9	-57.6
9	-24.9	-15.4	-21.2	-19.3	-50.6	-10.8	-7.7	-8.7	29.4	25.3	-85.9
10	-22.6	-17.7	-10.9	-10.3	-65.1	-29.7	-23.7	-22.5	-24.5	-28.6	11.8
11	16.5	7.8	17.1	7.5	7.0	7.3	17.0	1.6	1.8	-9.5	8.6
12	17.1	5.9	12.6	2.2	16.3	11.8	17.3	3.8	7.9	-0.6	18.3
13	-31.4	-25.5	-12.4	-14.7	-87.1	-41.0	-9.9	-12.9	-0.9	-11.9	-39.7
14	5.2	5.8	5.2	2.3	-11.6	10.0	5.6	4.8	19.1	12.4	-51.4
15	15.1	3.4	14.4	1.3	7.7	6.1	16.8	-0.4	13.9	-0.8	26.9
16	13.6	-1.1	10.5	-3.6	9.4	2.4	16.6	1.3	16.7	4.5	10.9
17	10.1	9.4	11.2	8.9	-1.4	9.5	7.6	3.0	-3.5	-14.3	28.6
18	1.8	1.1	3.6	1.1	-12.0	0.0	4.0	-0.8	13.1	4.0	22.1
19	-0.9	-1.7	1.1	-1.5	-19.2	-6.4	5.7	1.0	8.9	-0.6	41.1
20	-2.0	-2.8	-6.5	-9.3	-4.4	6.8	-3.3	-8.4	16.4	7.7	23.6

Table 5 Dispersion analysis

		Degrees of freedom f	Sum of squares s	Dispersion s/f	Dispersion ratios fr	Table value ft	Model Adequacy evaluation
R_z	Residual sum	15	0.293426	0.019562			
	Experiment error	3	0.009897	0.003299			
	Model adequacy	12	0.283529	0.023627	7.162	8.740	fr < ft adequate
	Multiple regression coefficient: R = 0.9877						
R_p	Residual sum	15	0.218346	0.014556			
	Experiment error	3	0.016825	0.005608			
	Model adequacy	12	0.201521	0.016793	2.994	8.740	fr < ft adequate
	Multiple regression coefficient: R = 0.9918						
R_v	Residual sum	15	0.475066	0.031671			
	Experiment error	3	0.015825	0.005275			
	Model adequacy	12	0.459240	0.038270	7.255	8.740	fr < ft adequate
	Multiple regression coefficient: R = 0.9762						
R_a	Residual sum	15	0.198609	0.013241			
	Experiment error	3	0.007023	0.002341			
	Model adequacy	12	0.191586	0.015966	6.820	8.740	fr < ft adequate
	Multiple regression coefficient: R = 0.9928						
R_{mr} ($30R_z$)	Residual sum	15	0.231928	0.015462			
	Experiment error	3	0.025964	0.008655			
	Model adequacy	12	0.205964	0.017164	1.983	8.740	fr < ft adequate
	Multiple regression coefficient: R = 0.2649						
SE	Residual sum	15	1.779	0.118613			
	Experiment error	3	0.053990	0.017997			
	Model adequacy	12	1.725	0.143767	7.988	8.740	fr < ft adequate
	Multiple regression coefficient: R = 0.7526						
W_a	Residual sum	15	1.889	0.125933			
	Experiment error	3	0.065015	0.021672			
	Model adequacy	12	1.824	0.151998	7.014	8.740	fr < ft adequate
	Multiple regression coefficient: R = 0.6384						

In the mathematical models for calculating the R_z, R_p, R_v and R_a parameters, Eq. 27-30, obtained using the DOE methodology, the feed (f) and the tool nose radius (r_ε) have a dominant influence. The feed is proportionally correlated, while the tool nose radius is inversely proportional to the values of the parameters. Still, the feed has a bigger impact than the radius. The cutting speed (v) and depth of cut (a_p) have insignificant impacts. Interestingly, in all models, Eq. 27-30, the impact of the depth of cut is inversely proportional. Although insignificant, this means that an increase of the depth of cut will stabilize the process of transforming the removed material into a chip. Due to the fact that, for the $R_{mr(c)}$ parameter, the paper adopts "c" as a function of the R_z parameter, none of the input variables (v, f, a_p, r_ε) in the model have a dominant impact.

The *SE* parameter model, Eq. 32, and Fig. 5, show that the depth of cut has the least impact on the stochastic character of the primary profile, while the feed and the tool nose radius have comparably strong impacts, but with different signs. On one hand, considered on a micro-plan, the radius increase disturbs the deterministic nature of the irregularities along the primary profile, resulting in an increased value of the *SE* parameter. However, on a mezzo-plan, the increase of the radius "irons out" the unevenness which leads to a waviness profile with a smaller W_a, reflected in Eq.33, and Fig. 20. Although to a lesser extent and direction relative to the radius, the feed also influences the value of the W_a parameter. This influence cannot be attributed only to the changes related to the increase of the feed (for example: increased cutting forces), but also to the imperfection of the shape of the middle line generated by the λ_c profile filter. Table 4 shows that the calculated and measured values of the parameters R_p and R_v differ the most, expressed in percent. These parameters directly depend on the position of the roughness profile mean line.

Another conclusion is that the experiments with lower f/r_ε ratios feature bigger deviations. The patterns described above also apply to the percentage differences between the values calculated according to the models based on the kinematical-geometrical copying and the measured values, Table 4. If we compare the percentage difference of both models, we can conclude that the DOE mathematical models yield values slightly closer to the measured values. This is because for the *SE* parameter, responsible for compensating the theoretical values in accordance with the real processing, there are large percentage differences between the values determined in accordance with the SE model, Eq. 32, and the actual measured values, Table 3.

This, in turn, can be attributed to the "sensitive nature" of the *SE* parameter. The graphic comparisons presented in Fig. 5-19, clearly indicate small differences between the values of the modelled roughness parameters obtained in accordance with the two considered mathematical modelling methodologies. More importantly, the change trends along one or the other axis should be followed continuously. The biggest difference in this respect, exists for the parameters $R_{mr(c)}$, where the DOE model, throughout the hyperspace, yields smaller values relative to the kinematical-geometrical copying model, Fig. 16, 18 and 19, without any intersecting lines or overlapping. The measured small values for the out-off-roundness of the working rings, in itself indicates that the entire process of obtaining the roughness profile was implemented under a strictly controlled and stable turning process.
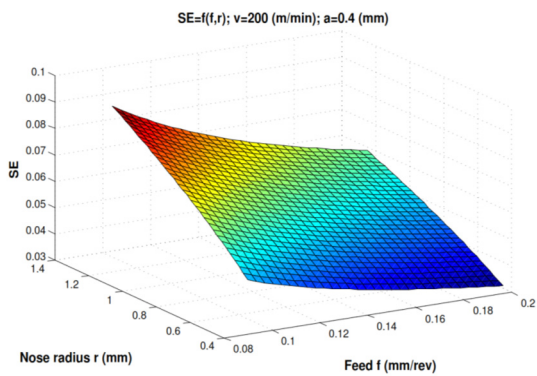
Fig. 4 3D graph for *SE* (v = 200 m/min, a_p=0.4 mm)
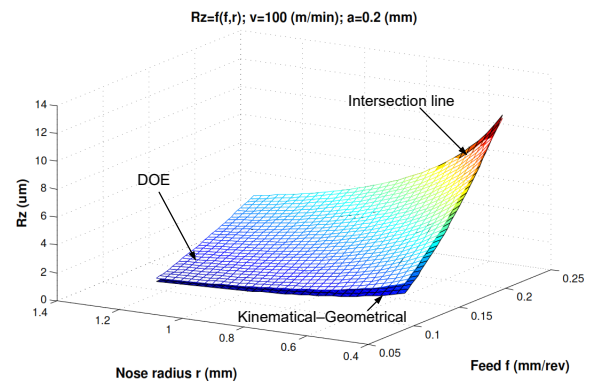
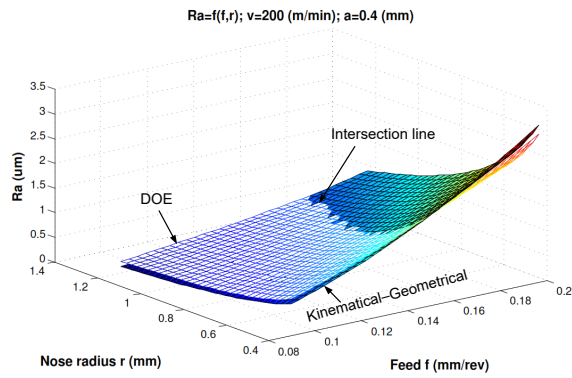**Fig. 5** 3D graphs for R_z (v =100 m/min, a_p = 0.2 mm)
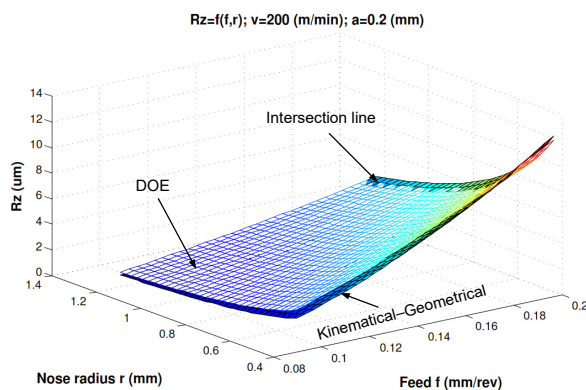
Fig. 6 3D graphs for R_z (v = 200 m/min, a_p = 0.2 mm)
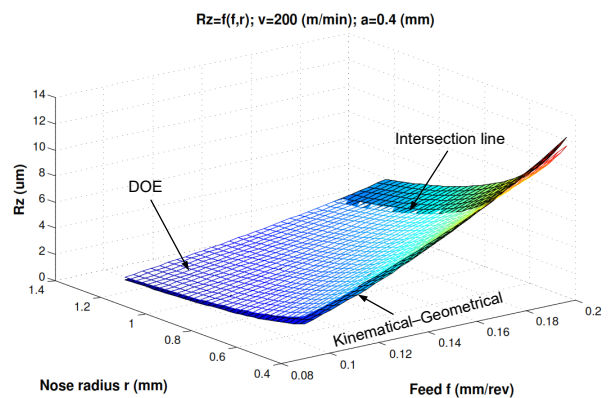
Fig. 7 3D graphs for R_z (v = 200 m/min, a_p = 0.4 mm)
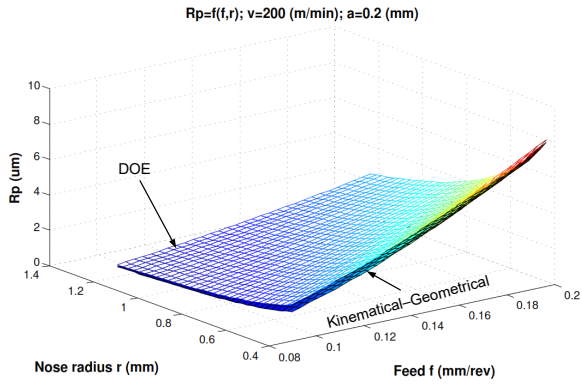
Fig. 8 3D graphs for R_p (v = 200 m/min, a_p = 0.2 mm)
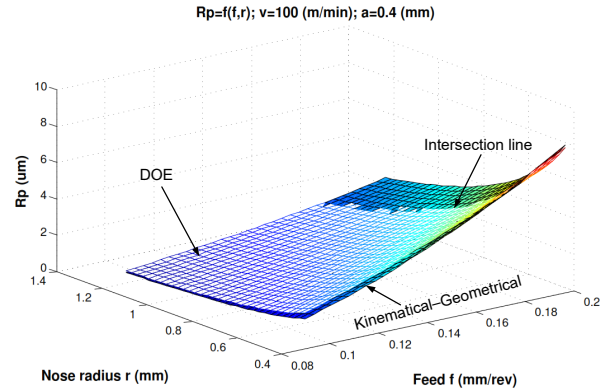
Fig. 9 3D graphs for R_p (v = 100 m/min, a_p = 0.4 mm)
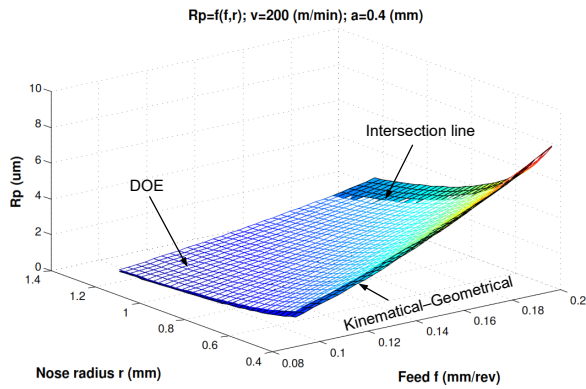
Fig. 10 3D graphs for R_p (v = 200 m/min, a_p = 0.4 mm)
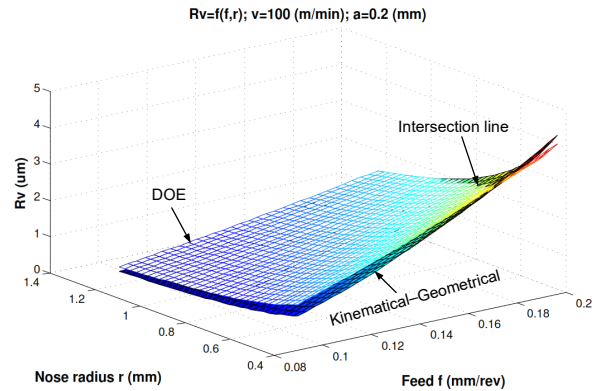
Fig. 11 3D graphs for R_v (v =100 m/min, a_p = 0.2 mm)
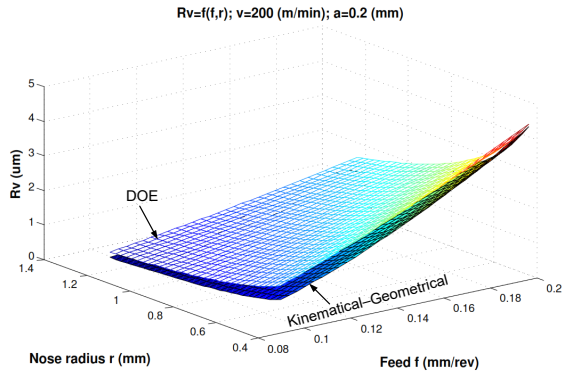
Fig. 12 3D graphs for R_v (v = 200 m/min, a_p = 0.2 mm)
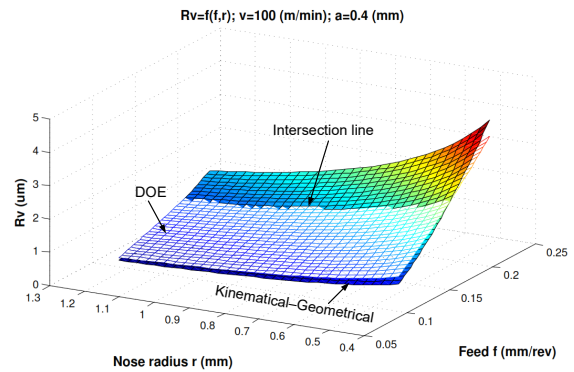
Fig. 13 3D graphs for R_v (v =100 m/min, a_p = 0.4 mm)
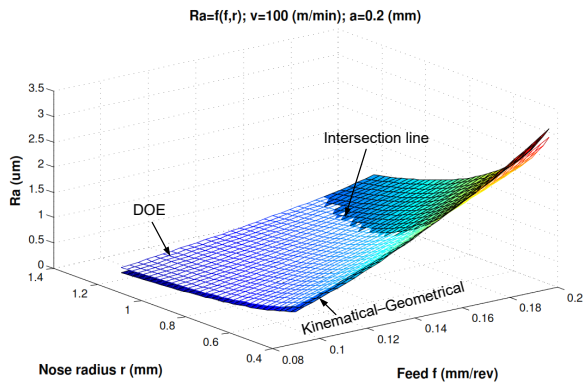
Fig. 14 3D graphs for R_a (v =100 m/min, a_p = 0.2 mm)
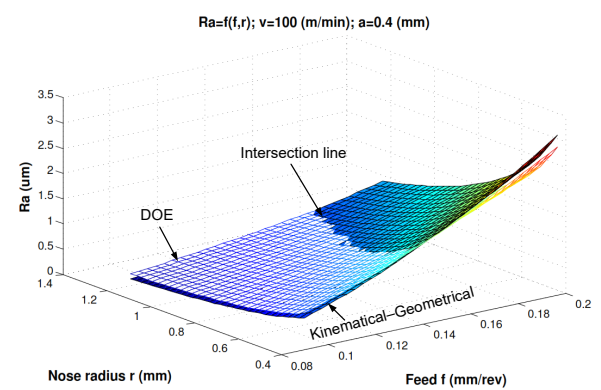
Fig. 15 3D graphs for R_a (v =100 m/min, a_p = 0.4 mm)

Ra=f(f,r); v=200 (m/min); a=0.4 (mm)

Fig. 16 3D graphs for R_a (v = 200 m/min, a_p = 0.4 mm)

Rmr(30Rz)=f(f,r); v=100 (m/min); a=0.2 (mm)
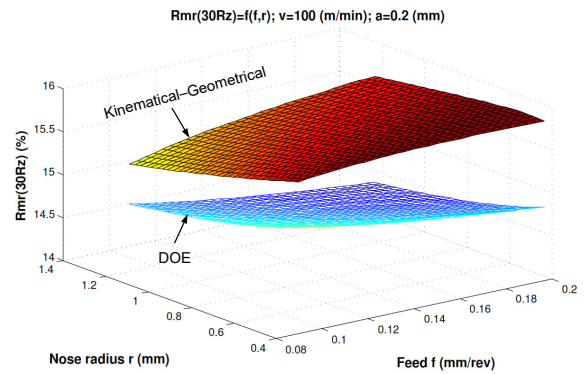
Fig. 17 3D graphs for R_{mr} ($30R_z$)
(v = 100 m/min, a_p = 0.2 mm)

Rmr(30Rz)=f(f,r); v=100 (m/min); a=0.4 (mm)
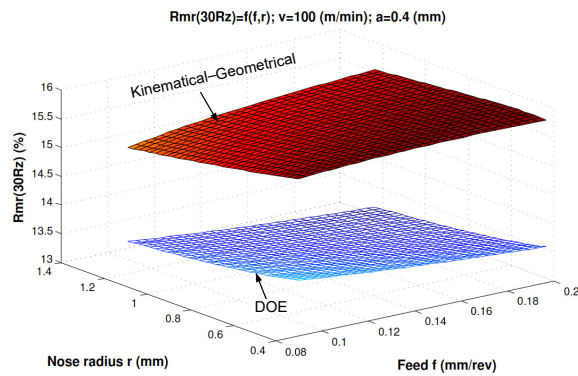
Fig. 18 3D graphs for R_{mr} ($30R_z$)
(v =100 m/min, a_p = 0.4 mm)

Rmr(30Rz)=f(f,r); v=200 (m/min); a=0.4 (mm)
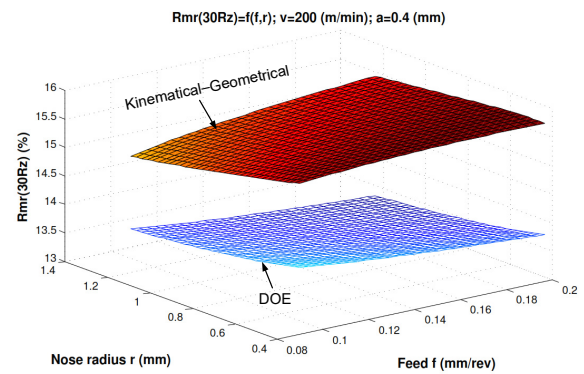
Fig. 19 3D graphs for R_{mr} ($30R_z$)
(v = 200 m/min, a_p = 0.4 mm)

Wa=f(f,r); v=200 (m/min); a=0.4 (mm)
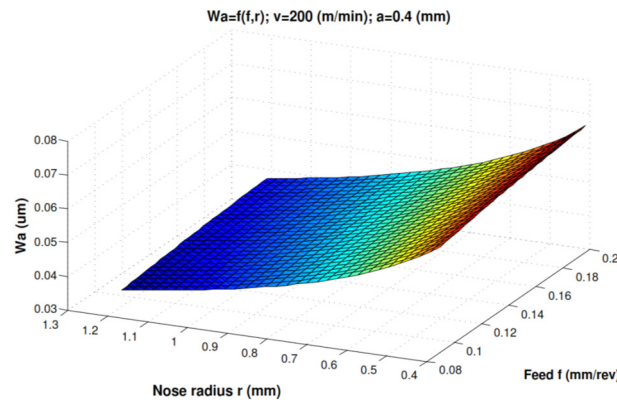
Fig. 20 3D graphs for W_a (v = 200 m/min, a_p = 0.4 mm)

4. Conclusion

The simultaneous modelling of multiple roughness parameters using two different approaches, the kinematical-geometrical copying method and the DOE method, as well as the comparison between the two, clearly showed their strengths and weaknesses.

The mathematical models expressed as a nonlinear first order function can accurately model the roughness parameters during hard turning. This showed that all obtained mathematical models are adequate although they estimate multiple roughness parameters for the same processed surface (the same roughness profile). The difference between the measured values of the roughness parameters compared to the values theoretically calculated with the DOE models is acceptable. However, it should be noted that from the practical point of view, the empirically derived roughness parameter models depict the process accurately solely in the conditions in which they had been obtained. Any changes of machines, clamping methods, working pieces,

different geometry tools etc., means a new model of the roughness parameters needs to be derived referring to those precise machining conditions. The mathematical models of the roughness parameters obtained using the method of kinematical-geometrical copying (K-G) of the cutting tool onto the processed surface, including the *SE* parameter, were shown that likewise successfully model the roughness parameters during hard turning. Their graphical presentations showed a great similarity with the graphical presentations of the DOE models. The SE parameter from these models make the link between the theoretically calculated values and the actual condition of the cutting process. In other words, the *SE* parameter also considers, to an extent, the 'difficult' modelling factors. From a general practical point of view, the models based on the kinematical-geometrical copying of the cutting tool including the *SE* parameter have a broader applicability. It is sufficient to model the *SE* parameter and then to calculate multiple roughness parameters. The measurements of the deviations from out-off-roundness of the working rings, as well as the modelling of the waviness parameter *Wa* showed the stability of the turning process used to obtain the roughness profiles.

Acknowledgement

References

[1] He, C.L., Zong, W.J., Zhang, J.J. (2018). Influencing factors and theoretical modeling methods of surface roughness in turning process: State-of-the-art, *International Journal of Machine Tools and Manufacture*, Vol. 129, 15-26, doi: 10.1016/j.ijmachtools.2018.02.001.

[2] Trung, D.D., Thinh, H.X. (2021). A multi-criteria decision-making in turning process using the MAIRCA, EAMR, MARCOS and TOPSIS methods: A comparative study, *Advances in Production Engineering & Management*, Vol. 16, No. 4, 443-456, doi: 10.14743/apem2021.4.412.

[3] Kramar, D., Cica, Dj. (2021). Modeling and optimization of finish diamond turning of spherical surfaces based on response surface methodology and cuckoo search algorithm, *Advances in Production Engineering & Management*, Vol. 16, No. 3, 326-334, doi: 10.14743/apem2021.3.403.

[4] Savkovic, B., Kovac, P., Rodic, D., Strbac, B., Klancnik, S. (2020). Comparison of artificial neural network, fuzzy logic and genetic algorithm for cutting temperature and surface roughness prediction during the face milling process, *Advances in Production Engineering & Management*, Vol. 15, No. 2, 137-150, doi: 10.14743/apem2020.2.354.

[5] Tamang, S.K., Chandrasekaran, M. (2015). Modeling and optimization of parameters for minimizing surface roughness and tool wear in turning Al/SiCp MMC, using conventional and soft computing techniques, *Advances in Production Engineering & Management*, Vol. 10, No. 2, 59-72, doi: 10.14743/apem2015.2.192.

[6] Heidari, M., Hosseini, S.V., Parvaz, H. (2021). Modelling and optimization of surface roughness and specific tool wear in milling process, *Tehnički Vjesnik – Technical Gazette,* Vol. 28, No. 5, 1626-1633, doi: 10.17559/TV-20200614105300.

[7] Aljinović, A., Bilić, B., Gjeldum, N., Mladineo, M. (2021). Prediction of surface roughness and power in turning process using response surface method and ANN, *Tehnički Vjesnik – Technical Gazette,* Vol. 28, No. 2, 456-464, doi: 10.17559/TV-20190522104029.

[8] Mgwatu, M.I. (2013). Integrated approach for optimising machining parameters, tool wear and surface quality in multi-pass turning operations, *Advances in Production Engineering & Management*, Vol. 8, No. 4, 209-218, doi: 10.14743/apem2013.4.168.

[9] Kang, W.T., Derani, M.N., Ratnam, M.M. (2020). Effect of vibration on surface roughness in finish turning: Simulation study, *International Journal of Simulation Modelling*, Vol. 19, No. 4, 595-606, doi: 10.2507/IJSIMM19-4-531.

[10] Bartarya, G., Choudhury, S.K. (2012). Effect of cutting parameters on cutting force and surface roughness during finish hard turning AISI52100 grade steel, *Procedia CIRP,* Vol. 1, 651-656, doi: 10.1016/j.procir.2012.05.016.

[11] Mohruni, A.S., Yanis, M., Kurniawan, E. (2018). Development of surface roughness prediction model for hard turning on AISI d2 steel using cubic boron nitride insert, *Jurnal Teknologi,* Vol. 80, No. 1, 173-178, doi: 10.11113/jt.v80.10492.

[12] Kumar, S., Singh, D., Kalsi, N.S. (2016). Surface quality evaluation of AISI 4340 steel having varying hardness during machining with TiN-coated CBN inserts, *Proceedings of the Institution of Mechanical Engineers, Part J: Journal of Engineering Tribology*, Vol. 231, No. 7, 925-933, doi: 10.1177/1350650116684243.

[13] Agrawal, A, Goel, S., Rashid, W.B., Price, M. (2015). Prediction of surface roughness during hard turning of AISI 4340 steel (69 HRC), *Applied Soft Computing*, Vol. 30, 279-286, <u>doi: 10.1016/j.asoc.2015.01.059</u>.

[14] Panda, A., Sahoo, A.K., Rout, A.K. (2016). Investigations on surface quality characteristics with multi-response parametric optimization and correlations, *Alexandria Engineering Journal*, Vol. 55, No. 2, 1625-1633, <u>doi: 10.1016/j.aej.2016.02.008</u>.

[15] Xiao, Z., Liao, X., Long, Z., Li, M. (2017). Effect of cutting parameters on surface roughness using orthogonal array in hard turning of AISI 1045 steel with YT5 tool, *International Journal of Advanced Manufacturing Technology*, Vol. 93, 273-282, <u>doi: 10.1007/s00170-016-8933-5</u>.

[16] Das, S.R., Panda, A., Dhupal, D. (2017). Experimental investigation of surface roughness, flank wear, chip morphology and cost estimation during machining of hardened AISI 4340 steel with coated carbide insert, *Mechanics of Advanced Materials and Modern Processes,* Vol. 3, Article No. 9, <u>doi: 10.1186/s40759-017-0025-1</u>.

[17] Jena, J., Panda, A., Behera, A.K., Jena, P.C., Das, S.R., Dhupal, D. (2017). Modeling and optimization of surface roughness in hard turning of AISI 4340 steel with coated ceramic tool, In: Chattopadhyay, J., Singh, R., Prakash, O. (eds.), *Innovation in Materials Science and Engineering,* Springer, Singapore, 151-160, <u>doi: 10.1007/978-981-13-2944-9_15</u>.

[18] Meddour, I., Yallese, M.A., Khattabi, R., Elbah, M., Boulanour, L. (2014). Investigating and modeling of cutting forces and surface roughness when hard turning of AISI 52100 steel with mixed ceramic tool: Cutting conditions optimization, *International Journal of Advanced Manufacturing Technology*, Vol. 77, 1387-1399, <u>doi: 10.1007/s00170-014-6559-z</u>.

[19] Zerti, O., Yallese, M.A., Khettabi, R., Chaoui, K., Mabrouki, T. (2017). Design optimization for minimum technological parameters when dry turning of AISI D3 steel using Taguchi method, *International Journal of Advanced Manufacturing Technology*, Vol. 89, 1915-1934, <u>doi: 10.1007/s00170-016-9162-7</u>.

[20] Khellaf, A., Aouici, H., Smaiah, S., Boutabba, S., Yallese, M.A., Elbah, M. (2017). Comparative assessment of two ceramic cutting tools on surface roughness in hard turning of AISI H11 steel: Including 2D and 3D surface topography, *International Journal of Advanced Manufacturing Technology*, Vol. 89, 333-354, <u>doi: 10.1007/s00170-016-9077-3</u>.

[21] Kacal, A., Yıldırım, F. (2012). Application of grey relational analysis in high-speed machining of hardened AISI D6 steel, *Proceedings of the Institution of Mechanical Engineers, Part C: Journal of Mechanical Engineering Science,* Vol. 227, No. 7, 1566-1576, <u>doi: 10.1177/0954406212466792</u>.

[22] Günay, M., Yücel, E. (2013). Application of Taguchi method for determining optimum surface roughness in turning of high-alloy white cast iron, *Measurement,* Vol. 46, No. 2, 913-919, <u>doi: 10.1016/j.measurement.2012.10.013</u>.

[23] Tang, L., Gao, C., Huang, J., Shen, H., Lin, X. (2015). Experimental investigation of surface integrity in finish dry hard turning of hardened tool steel at different hardness levels, *International Journal of Advanced Manufacturing Technology*, Vol. 77, 1655-1669, <u>doi: 10.1007/s00170-014-6484-1</u>.

[24] Derakhshan, E.D., Akbari, A.A. (2009). Experimental investigation on the effect of workpiece hardness and cutting speed on surface roughness in hard turning with CBN tools, In: *Proceedings of the World Congress on Engineering 2009,* London, United Kingdom.

[25] Mia, M., Dhar, N.R. (2017). Optimization of surface roughness and cutting temperature in high-pressure coolant-assisted hard turning using Taguchi method, *International Journal of Advanced Manufacturing Technology*, Vol. 88, 739-753, <u>doi: 10.1007/s00170-016-8810-2</u>.

[26] Chinchanikar, S., Salve, A.V., Netake, P., More, A., Kendre, S., Kumar, R. (2014). Comparative evaluations of surface roughness during hard turning under dry and with water-based and vegetable oil-based cutting fluids, *Procedia Materials Science*, Vol. 5, 1966-1975, <u>doi: 10.1016/j.mspro.2014.07.529</u>.

[27] Naigade, D.M, Patil, D.K, Sadaiah, M. (2013). Some investigations in hard turning of AISI 4340 alloy steel in different cutting environments by CBN insert, *International Journal of Machining and Machinability of Materials*, Vol. 14, No. 2, 165-193, <u>doi: 10.1504/IJMMM.2013.055736</u>.

[28] Tomov, M., Karolczak, P., Skowronek, H., Cichosz, P., Kuzinovski, M. (2020). Mathematical modelling of core roughness depth during hard turning, In: Królczyk, G., Niesłony, P., Królczyk, J. (eds.), *Industrial Measurements in Machining. IMM 2019. Lecture Notes in Mechanical Engineering,* Springer, Cham, Switzerland, <u>doi: 10.1007/978-3-030-49910-5_1</u>.

[29] Tomov, M., Kuzinovski, M., Cichosz, M. (2016). Modeling and prediction of surface roughness profile in longitudinal turning, *Journal of Manufacturing Processes*, Vol. 24, Part 1, 231-255, <u>doi: 10.1016/j.jmapro.2016.09.010</u>.

[30] Tomov, M., Kuzinovski, M., Cichosz, P (2013). A new parameter of statistic equality of sampling lengths in surface roughness measurement*, Strojniški vestnik - Journal of Mechanical Engineering,* Vol. 59, No. 5, 339-348, <u>doi: 10.5545/sv-jme.2012.606</u>.

[31] Tomov, M., Prangoski, B., Karolczak, P. (2021). Mathematical modelling and correlation between the primary waviness and roughness profiles during hard turning. *Jordan Journal of Mechanical and Industrial Engineering,* Vol. 15, No. 3, 243-249.

[32] Tomov, M., Kuzinovski, M., Cichosz, P. (2016). Development of mathematical models for surface roughness parameter prediction in turning depending on the process condition, *International Journal of Mechanical Sciences*, Vol. 113, 120-132, <u>doi: 10.1016/j.ijmecsci.2016.04.015</u>.

A gold nanoparticles and hydroxylated fullerene water complex as a new product for cosmetics

Rudolf, R.[a,b,*], **Jelen, Ž.**[a], **Zadravec, M.**[a], **Majerič, P.**[a,b], **Jović, Z.**[c], **Vuksanović, M.**[c], **Stankovic, I.**[d], **Matija, L.**[d], **Dragičević, A.**[d], **Miso Thompson, N.**[e], **Horvat, A.**[f], **Koruga, D.**[c,d]

[a]University of Maribor, Faculty of Mechanical Engineering, Slovenia
[b]Zlatarna Celje d.o.o., Celje, Slovenia
[c]TFT Nano Center, Belgrade, Serbia
[d]University of Belgrade, Nano Lab, Faculty of Mechanical Engineering, Serbia
[e]ZeptoHyperTech, Belgrade, Serbia
[f]Zepter-Slovenica d.o.o., Slovenj Gradec, Slovenia

A B S T R A C T

Three types of gold nanoparticles (AuNPs) were synthesised with a custom-made Ultrasonic Spray Pyrolysis (USP) device, from aqueous solutions of gold (III) chloride ($AuCl_3$) and gold (III) acetate ($AuC_6H_{12}O_6$), with an initial concentration of Au 0.5 g/L. AuNPs were collected in suspensions of deionised (D.I.) water with the stabilisers polyvinylpyrrolidone (PVP) or polyethylene glycol (PEG), followed by the process of freeze drying the AuNPs to be useful as a new additive for the cream. The standard cream base was used as a matrix for preparation of three types of cream with AuNPs in the same concentration ratios. The third AuNPs cream was prepared with a patented hydroxylated fullerene water complex (3HFWC-W) matrix. To examine the effect of AuNPs as additive in creams, a six-week study of test creams was conducted on 33 volunteers with no dermatological diseases. During the study three main parameters of the skin where measured: Collagen quality, skin moisturisation and the epidermis-dermis function. The results of the study found improvements of collagen quality between 18-24 %, achieved due to the use of AuNPs in standard creams, while the cream with the combination of 3HFWC-W and AuNPs gave significantly higher improvements with a value of 45.7 %. It was also discovered that hydration of the skin (stratum cornum) increased by 6.4-9.6 % in standard creams with AuNPs, and 73.7 % in the 3HFWC/AuNPs` cream. Similar results were measured by the epidermis-dermis function, where 24-28 % improvement for standard creams with AuNPs was identified, and 38.4 % for the cream 3HFWC-W/AuNPs.

1. Introduction

Personal skin care is an important factor in slowing the appearance of age-related skin symptoms such as wrinkles, pigmented lesions, patchy hypopigmentation, actinic keratoses, thinning skin and exaggerated expression lines, all of which are a result of the internal metabolic ageing processes and external damage caused by the influx of various substances and exposure to UV light [1, 2]. Nanoparticles have recently attracted attention for use in anti-ageing cosmetics as alternatives and synergists to already established anti-ageing substances. One of the main ad-

vantages of nanoparticles is their ability to penetrate the skin barrier [3, 4], which can, potentially, result in higher effectiveness with smaller doses and shorter wear times [5]. Gold nanoparticles (AuNPs) and Hyper Harmonised Hydroxyl Modified Fullerene (3HFWC-W) have garnered special attention for use in cosmetics. AuNPs, luckily, exhibit a high degree of biocompatibility, as evidenced by their use in Cosmetics, Medical imaging and Oncology [6-8], while other metallic nanoparticles, because of their potential toxicity, represent an issue of concern when used on living organisms. The main mechanisms by which AuNPs benefit human skin are acceleration of blood circulation, anti-inflammatory properties, antiseptic properties, improving the firmness and elasticity of skin and vitalising skin metabolic processes [9-11]. 3HFWC-W is a modified form of the third allotrope of carbon – fullerene, and has been proven to offer several benefits when used on skin. The hollow one nanometre surface hydroxide functionalised spheres have increased hydro solubility, and can bond to molecules of water with hydrogen bonds [12, 13]. By establishing hydrogen bonds with the surrounding water molecules and biomolecules, 3HFWC-W improves the moisturisation and moisture retention of skin, which is considered one of the most important anti-ageing skin treatments [14].

AuNPs in suspension can be synthesised through Ultrasonic Spray Pyrolysis (USP), which has many advantages, such as the simplicity of setup and adaptability, continuous operation, relative cost-effectiveness and the possibility of easy capacity increase – i.e. scale up [15, 16]. To obtain AuNPs in dry form, freeze drying was applied for suspensions. Namely, freeze drying is the common method for the preparation of stable formulations with protein drugs, and its use and deeper understanding are becoming increasingly important from the point of view of the preparation of new, patient-friendly dosage forms in pharmaceutical products [17]. In line with the intensive increase of new temperature sensitive products, where standard drying procedure doesn't fit [18, 19], a high-quality, safe and effective nanomaterial can be provided with freeze drying.

The use of 3HFWC-W was targeted due to the fact that the combination with the nano-harmonised substance (NHS) is favourable, resulting in the functionalisation of $the\ C_{60}$ molecule with OH groups – these processes are patented as material made from (C_{60}(OH)x) [20, 21]. The 3HFWC-W substance is based on additional water layers $C_{60}(OH)_{36\pm12}@(H_2O)_{144-2528}$. These water layers give 3HFWC-W a water liquid phase $(H_2O)_{144-2528}$, surrounding the solid phase— hydrogen bonded $C_{60}(OH)_{36\pm12}$ nanostructure. The 3HFWC-W water layers possess similar properties to liquid crystals, and they protect $the\ C_{60}(OH)_{36\pm12}$ complex from environmental influences, and, at the same time, they protect biomolecules from the potentially toxic effects of C_{60}. This structure, whose diameter size ranges between 6-15 nm, is a water-soluble amphiphilic biomolecule with a potential for various applications. Fullerene derivative nano-harmonised $C_{60}(OH)_{36\pm12}$ has shown no toxicity in tests on human dermal fibroblasts (HDF) and liver carcinoma cells [13, 22]. As a cosmetic product ingredient (its INCI name is "hydroxylated fullerene"), it could act as an active compound and a stability factor. Compared to the commercial products and vehiculums, all cosmetic products with 3HFWC-W, except body lotion, have shown significant improvements of the functionality of the basement membrane [23]. While regenerating cream and body lotion with 3HFWC-W have positively affected collagen quality in the dermis, anti-ageing and hand cream with 3HFWC-W have shown positive effects on signal transduction and regeneration of collagen. Results imply that anti-ageing and hand cream with 3HFWC-W, as well as body lotion vehiculum, could improve the properties of the basement membrane and accelerate signal transduction in the dermis, and, finally, enable faster regeneration of the epidermis and rapid reaction of the skin to negative environmental influences [23]. Regenerating cream with 3HFWC-W has shown positive effects on the basement membrane and strength of the collagen supportive structure in the skin. The body lotion with 3HFWC-W and commercial hand cream have improved the mechanical properties of the skin through strengthening collagen fibres in the dermis. The ingredient 3HFWC-W, which acts in a natural, biophysical way on the skin, might open a new era in the way we understand and treat changes in the altered and ageing skin. Depending on the type of cream, the average improvement was 22.5 %, based on the arithmetic value of 12 % (body lotion), 18 % (regenerating cream), 28 % (anti-ageing), and 32 % (hand cream). Based on the presented clinical studies and results, in order to achieve an even

more visible anti-ageing effect, it was hypothesised that an additional effect could be achieved with AuNPs that are highly biocompatible and have some baseline functional properties [24, 25].

The focus in this dermatological study was, therefore, to find the effect of AuNPs not only in cosmetic standard creams, but also in combination with 3HFWC-W, to get a potentially new complex in cosmetics. In the first step creams were prepared, followed by six weeks of testing on volunteers. In order to evaluate the activity of the AuNPs in creams, characterisation of the cream`s ingredients was performed, and real-time analysis of the skin anti-ageing effect was done on the volunteers.

2. Materials and methods

2.1 Materials

The starting materials for the preparation of AuNPs` suspensions were two precursors: Au chloride salt – (gold (III) chloride tetrahydrate – trace metals basis 99.9 %, Acros Organics, Germany) and Au acetate salt – (gold (III) acetate, Alfa Aesar, USA). Collection mediums were prepared with D.I. water and two steric stabilisers: Polyvinylpyrrolidone (PVP40 Sigma Aldrich, Germany) and polyethylene glycol (PEG 6000, Fisher Scientific, UK). Other chemicals were: Sodium hydroxide (NaOH, Fisher Chemicals, Germany) and hydrochloric acid (HCl, 37 %, Sigma Aldrich, Germany). Three types of AuNPs` suspensions were prepared for cosmetic creams with the characteristics shown in Table 1 (these names/abbreviations are used throughout the text). Preparation of the 3HFWC-W took place under controlled conditions. The first step was water purification from tap water to water with 0.1 µS/m conductivity. The main ingredient, fullerol $C_{60}(OH)_{36}$ with purity of 99.99 %, was imported from Solaris Chem in Canada. A specified amount of fullerol was mixed with the purified water in a vessel at temperatures of 33-400 °C. After achieving a satisfying solubility the solution was transferred to another vessel, where it was exposed to an oscillatory magnetic field of 100-250 mT in order to create aqueous layers based on strong hydrogen bonds [20, 21]. The result was 3HFWC-W: $C_{60}(OH)_{36}@(H_2O)_n^l$, size of 6-15 nm, with n-water molecules (600-200) and l-water layers (1-6). 3HFWC-W was mixed in a concentration of 18 % by a standard procedure with 34 % of aqua purificata and 48 % of standard cream base (TFT Nano Center, Belgrade, Serbia).

Table 1 Characteristics for all three types of AuNPs` suspensions

AuNPs` suspension	Type of Stabiliser – concentration in D.I. water (g/L)
AuNC PEG10	PEG – 10 g/L
AuNC PVP5	PVP – 5 g/L
AuNA PEG20	PEG – 20 g/L

Table 2 Composition of 3HFWC-W[Au NP PEG 20] cream

Formula	Product identifier	Quantity (wt. %)
$C_{60}(OH)_{36-48}@(H_2O)_{950-2100}$	3HFWC-W	18.00
AuNPs	AuNPs (AuNA+PEG 20 g/L)	0.05
H_2O	Ultra-pure water (0.055 µS/cm)	32.95
AB	Ambiphilic base	49.00
3HFWC-W[AuNP PEG20]	Nano gold hyperharmonized fullerene water complex	100.00

2.2 Methods

Synthesis of AuNPs` suspensions

AuNPs` synthesis was done on a custom built USP device, located in Zlatarna Celje d.o.o., Slovenia. The device was constructed from a custom aerosol generator based on a 1.6 MHz piezoelectric transducer (Liquifog II, Johnson Matthey Piezo Products GmbH, Germany), which aerosolises the Au precursor solution. The aerosol droplets were transferred by a constant flow of carrier gas (N_2) into a heated multi zone reactor tube made from quartz glass. The first zone facilitates the evaporation of the aerosol droplets and the formation of a solid aerosol. In the second reaction zone the temperature is increased to initiate thermal decomposition in the presence of a

reducing gas (H_2) and continues with the reduction of Au^{+3} into elemental Au^0. The final zone facilitates the sintering of AuNPs, which are finally collected in a system composed of three connected gas wash bottles. The collection medium was with D.I. water, with PVP, or PEG at different concentrations. The detailed parameters of the AuNPs` synthesis and USP device are the subject of a patent for AuNPs` production [26]. The synthesised AuNPs` suspensions are marked AuNC when a chloride precursor was used, and as AuNA in the case of the acetate precursor. The starting concentration of [Au] in all the prepared precursors was 0,5 g/L. The technological USP parameters, such as temperature profiles, gas flows, were also consistent with previous experimental trials [27, 28].

Freeze drying of AuNPs` suspensions

A separation process was applied for AuNPs` suspensions in order to obtain AuNPs in dry form (Fig. 1). As the removal of the liquid phase from the AuNPs` suspensions must be done in a way to retain the AuNPs` size distribution and to keep their properties, they cannot be separated using mechanical processes. Based on this, the use of a thermal process was proposed in the form of freeze drying. In the case of freeze drying, the advantages over other forms of drying methods are in: (i) Preserving the structure, shape, and size of the AuNPs, (ii) Extending the life span of AuNPs, (iii) Rehydration of dry AuNPs is possible, (iv) The sample is placed directly into the container, which can be sealed in-situ in the freeze drier, thus avoiding potential contamination. The idea of the freeze drying process was in freezing the AuNPs` suspension, therefore stabilising the AuNPs` size distribution, which was followed by a rapid decrease of the system pressure to a few Pa, causing sublimation of the carrier liquid phase. In this way, when the frozen liquid was sublimated, all that remained was the AuNPs`/stabiliser powder inside the container. The intensity of the process was controlled by the temperature of the heating shelves and system pressure. Since the synthesis of AuNPs with USP and subsequent freeze drying process for producing dried AuNPs is not yet readily available in literature or otherwise [29], the selection of system pressure and shelf temperature that led to a stable, yet reasonably fast process (allowing the removal of the liquid without AuNPs` entrainment from the process of the drying protocol), had to be aligned to get stable process behaviour. In the case of 3HFWC-W products for cosmetics, the AuNPs` suspension was dried in a Miron glass cosmetic jar, which was later also used as the final cosmetic product envelope.

Freeze drying was performed in a laboratory freeze dryer manufactured by Kambic (LIO 2000LFT, Slovenia). The dryer had a separate drying chamber with two temperature regulated stainless steel shelves, each with a shelf area of about 0.09 m^2, and a condensation chamber with a condenser capacity of 5 kg. The shelf temperature during the freeze drying can be varied between −40 °C and 40 °C, and the temperature of the condenser can be set to −90 °C. The chamber pressure was measured with a Pirani gauge, which was also used to regulate the vacuum pump (see Fig. 1).
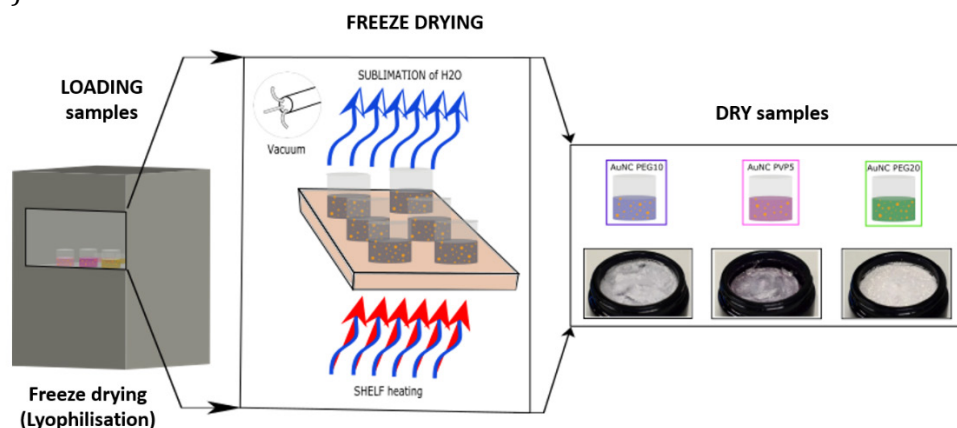

Fig. 1 Prepared and freeze dried AuNPs: AuNC PEG10, AuNC PVP5 and AuNA PEG20

In the drying cycles, 30 Miron glass cosmetic jars were filled with 80 ml of AuNPs` suspensions and placed on the temperature regulated shelves. After filling, every jar was weighed and placed in its corresponding position. To limit the heat gains from the surroundings, arising due to the front plexiglass observation doors, the front door was covered with a styrodure plate enveloped in aluminium foil. To limit the effect of the ice build-up on the condenser surfaces, the condenser was defrosted completely before each drying run. The freezing phase lasted for 15 hours at the shelf temperature –40 °C and atmospheric pressure. This was followed by the primary drying phase at the shelf temperature of –20 °C and the chamber pressure of 12 Pa for 67 h. This was followed by the secondary drying at the same pressure, and shelf temperature of 10 °C for the next 40 hours. The key parameter in the freeze drying phase was to adjust the heat release from the tray to samples during the primary drying phase according to the pressure level in the vacuuming phase, and not to collapse the samples.

Preparation of creams with AuNPs and 3HFWC-W

Creams with dried AuNPs (AuNC PEG10, AuNC PVP5 and AuNA PEG20) were obtained according to the procedure for the preparation of cosmetic creams, by mixing AuNPs in the weight percentage of 12 %, aqua purificata 48 % and standard cream base 40 % [30]. The 3HFWC-W$^{AuNA PEG20}$ cream was obtained by mixing 18 % 3HFWC-W, 0.05 % AuNA PEG20, 32.95 % aqua purificata and 49 % ambiphilic base (standard cream base).

AuNA PEG20 were chosen to be mixed with the 3HFWC-W substance in the ratio 1:10, giving a 3HFWC-W$^{AuNA PEG20}$ complex (Fig. 2). A commercial base ("U", Unichem Pharm) was used, without any active ingredient. In weight, pure water (0.1 µS/cm) was 35 %, the base "U" 45 % and the active ingredient 3HFWC-W$^{AuNA PEG20}$ was 20 %. The creams were prepared by a standard procedure using a mixing machine, the Unguator E/S (Gako International), which is individually programmable. The jar size was 500/600 ml (rated volume/filling volume).
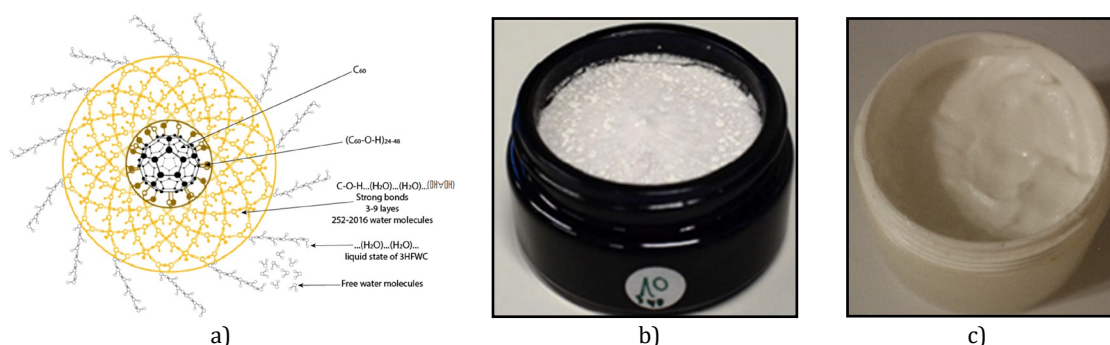

a)   b)   c)

Fig. 2 Schematic presentation of the cream components and cream: a) 3HFWC-W substance, b) Dried AuNA PEG20, and c) 3HFWC-W$^{AuNA PEG20}$ cream

2.3 Characterisation methods

Inductively Coupled Plasma-Mass Spectrometry (ICP-MS)

The concentration of Au in the synthesised AuNPs` suspensions for all three types was measured with Inductively Coupled Plasma-Mass Spectrometry (ICP-MS). The spectrometer used was an HP, Agilent 7500 CE, equipped with a collision cell (Santa Clara, CA, USA). The following conditions were used for the ICP-MS: The power was 1.5 kW, Nebuliser-Meinhard, plasma gas flow was 15 L/min, nebuliser gas flow was 0.85 L/min, make up gas flow was 0.28 L/min and reaction gas flow was 4.0 mL/min. The instrument was calibrated with matrix matched calibration solutions. The relative measurement uncertainty was estimated as ±3 %.

Dynamic Light Scattering (DLS) and measurements of ζ potential

DLS measurements of the hydrodynamic size distribution of AuNPs in aqueous suspension and measurements of ζ potential were performed with a Malvern Zetasizer Nano ZS (Malvern Panalytical, Worcestershire, UK). The hydrodynamic size distribution of AuNPs was measured using disposable plastic cuvettes and ζ potential measurements were done using a closed capillary cell

with electrodes. DLS and ζ potential measurements were performed with the following parameters for AuNP suspensions: Refractive Index (RI) = 0.2, absorption = 3.32; the suspension properties were: Dispersant = water, Refractive Index (RI) = 1.33, viscosity = 0.887 cP, temperature = 25 °C, equilibration time = 30 s, angle of incidence = 173° backscatter, dielectric constant = 78.5. Measurements were performed in 10 series at a time of 10 s per series, and the measurement was repeated 3 times.

Scanning Electron Microscopy (SEM)

A Scanning Electron Microscope, Sirion 400NC (FEI, USA), with an Energy-Dispersive X-ray spectroscope (EDS) INCA 350 (Oxford Instruments, UK), was used for the SEM analysis. The AuNPs` suspensions were put dropwise onto the SEM holders (mesh) with conductive carbon adhesive tape, which allowed better SEM observation. The SEM holders were left to dry in a desiccator for one day before the SEM investigations were carried out. The dried AuNPs were placed directly on conductive carbon adhesive tapes and observed as is.

Transmission Electron Microscopy (TEM)

A JEOL 2100 (JEOL, Japan) and JEOL JEM-2200FS HR (JEOL, Japan), operating at 200 kV, were used for the TEM observations of the cream with AuNPs. All of the samples were first dispersed in ethanol, and then a drop of each of these samples was put on a copper TEM grid with an amorphous carbon film. The grids were then dried before they were used for the TEM investigations.

Opto-Magnetic Imaging Spectroscopy (OMIS)

The effects of the creams with AuNPs were examined using Opto-Magnetic Imaging Spectroscopy (OMIS), a diagnostic method which is based on light-matter interaction, and has been applied to characterise water and skin layers [31, 32], cervical cancer and colon cancer [33], [34], collagen and skin miniaturisation [2, 23]. The OMIS detects reflected diffuse and polarised white light after their interaction with tissue, since the energy of photons of visible light (1.6- 3.0 eV) is the same value as valance electrons. The method of examination is its ability to detect paired (p^-) and unpaired (p^+) electrons as the paramagnetic and diamagnetic properties of the specimen.
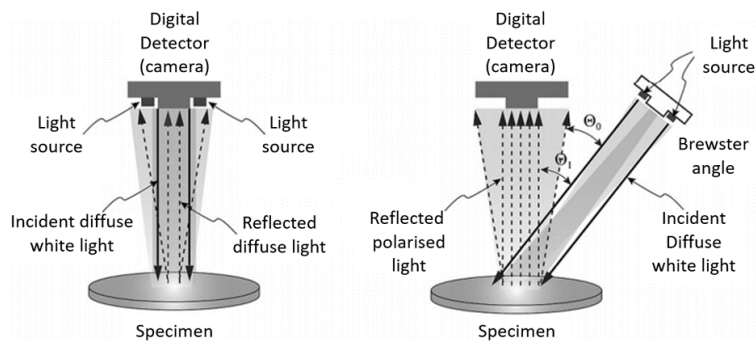

Fig. 3 Schematic representation of the Opto OMIS method [35]

As shown in Fig. 3, the device consists of two light sources, which emit the same light, one at an angle of 90° and the other at an angle of 53° (Brewster angle for the skin) to the sample, and a detector (camera) to collect the reflected light. There are two different types of light after the interaction with the tissue – one being reflected as diffuse (the one coming from the source at a right angle), and one being reflected as polarised (coming from the source at the Brewster angle). When reaching the detector, polarised light contains only its electrical properties, while diffused light contains both magnetic and electrical properties. By subtracting these two lights, the magnetic component is able to determine the paramagnetic and diamagnetic properties of various layers of the tissue of interest. The light source contains light-emitting diodes (LEDs) of different wavelengths (ultraviolet, green, red, infrared and white), and the detector collects the reflected light using three channels: Red, green and blue (all contained in white light). Since

those wavelengths go through skin to different depths (as shown in Fig. 4), it's possible to determine the biophysical properties of its layers. The biophysical skin properties (diamagnetic/paramagnetic) were measured using OMIS as an innovative patented diagnostic method [36]. Fig. 4 shows the second-harmonic function, which is a nonlinear optical process, where two photons with the same frequency interacting with a nonlinear material, are "combined", and generate a new photon with half the wavelength and twice the frequency of the photons, which can serve the coherence of the excitation. It means in the skin, as nonlinear media, a UV photon of 390 nm (omega) will generate as two photons of 780 nm ($2 \times 390 = 780$ nm) and penetrate deeply into the skin. Also, the process could be inversion, two photons of 780 nm may generate a photon of 390 nm if they activate certain nonlinear media.

In the analysis method, Higuchi Fractal Dimension (HFD) was used as one of the parameters for analysis. The Higuchi algorithm is a technique for calculating the fractal dimension of a time series. The usage of the Higuchi method leads to very precise values of the fractal dimension and shows the complexity of the time series studied. HFD is fast, and applicable in real-time calculations. Contrary to the linear methods, HFD can be applied directly to nonlinear time series, and it is suitable for short time series` analysis. HFD needs to be provided with only one input parameter, specifying the maximal distance between the points compared in the time series [38, 39].
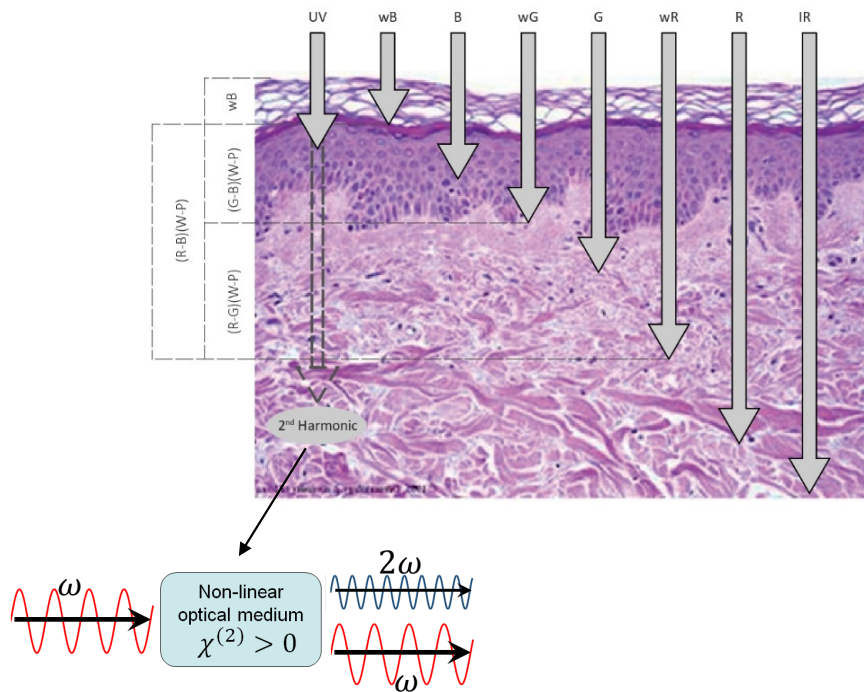

Fig. 4 Skin cross-section and penetration of light of different wavelengths (from UV to IR) (wB – Blue channel of white LED light, B – Blue LED light, wG – Green chanel of white LED light, G – Green LED light, wR – Red channel of white LED light, R – red LED light, (G-B)(W-P) - Green minus Blue channel of white LED light (diffuse) and white polarised, (R-G)(W-P) Red minus Green channel of white LED light (diffuse) and white polarised, (R-B)(W-P) Red minus Blue channel of white LED light (diffuse) and white polarised) [37]

Volunteers` testing

A six-week study was conducted to examine the effects of AuNPs and 3HFWC-W in new creams, as well as their synergistic effects. The volunteers were 33 women with an average age of 37 years, with the oldest participant being 65 and the youngest 21 years old, and they were divided into four groups. Every volunteer was given two cream samples and instructions to apply them twice a day on their forearm. One cream was the base of the standard cream without AuNPs (as control), which was the same for all four groups. Three groups tested creams with a standard base and with AuNPs, while the fourth group tested cream with the new complex AuNPs and 3HFWC-W. During the study two areas on the volunteers` forearms were filmed every seven days. After six weeks we had usable data for 33 volunteers.

3. Results and discussions

3.1 ICP-MS

To ensure consistency between the differently stabilised AuNPs, the Au content of the initial suspensions with ICP-MS was determined, and they were diluted with the appropriate amount of D.I. water. The final measured concentrations of Au in all the prepared AuNPs` suspensions are shown in Table 3.

Table 3 Au concentration in the prepared AuNPs` suspensions

Au suspension	Au concentration (ppm)
AuNC PEG10	120
AuNC PVP5	150
AuNA PEG20	100

3.2 DLS measurements

The principle of size measurement is based on Rayleigh scattering resulting from the Brownian motion of AuNPs whose size is less than the wavelength of the incident light at a fixed scattering angle [40]. The reason for choosing this technique for size distribution was the spherical shape of the AuNPs, which was confirmed by the pronounced colour of all the obtained suspensions. To determine the mean size distribution of AuNPs, DLS measurements were performed on all three suspensions with the presence of the selected stabilisers. The estimated Z-average AuNPs in the AuNC PEG10 suspension was 146.9 nm, in AuNC PVP5 190.9 nm and in AuNA PEG20 342.3 nm. The histogram data for the PDI index and the shape of the size distribution curve are shown in Fig. 5. The curves show a slight difference between the mean hydrodynamic radius of AuNPs in the AuNC suspensions produced from the same AuNC precursor. This difference was most likely caused by the difference between the PEG and PVP stabilisers. AuNPs prepared from the organic AuNA precursor were, on average, much larger than the AuNPs prepared from the inorganic AuNC precursor. The DLS measurements demonstrated somewhat larger AuNPs sizes than expected, while SEM and TEM observations show much smaller sizes of primary AuNPs in groups, and soft agglomerates in the PVP and PEG medium. Soft agglomerate AuNPs are held together by weak, physical van der Waals forces, while hard agglomerates (or aggregates) are usually nanoparticles with stronger chemical or sintering bonds between them [41, 42]. It is difficult to discern between primary nanoparticles and agglomerates with optical mobility measuring techniques [43], such as DLS. The agitation and light mechanical force applied during mixing of the AuNPs in the creams confirmed the presence of soft agglomerates, as they were disrupted into individual AuNPs, seen in the investigations of the prepared creams shown below.
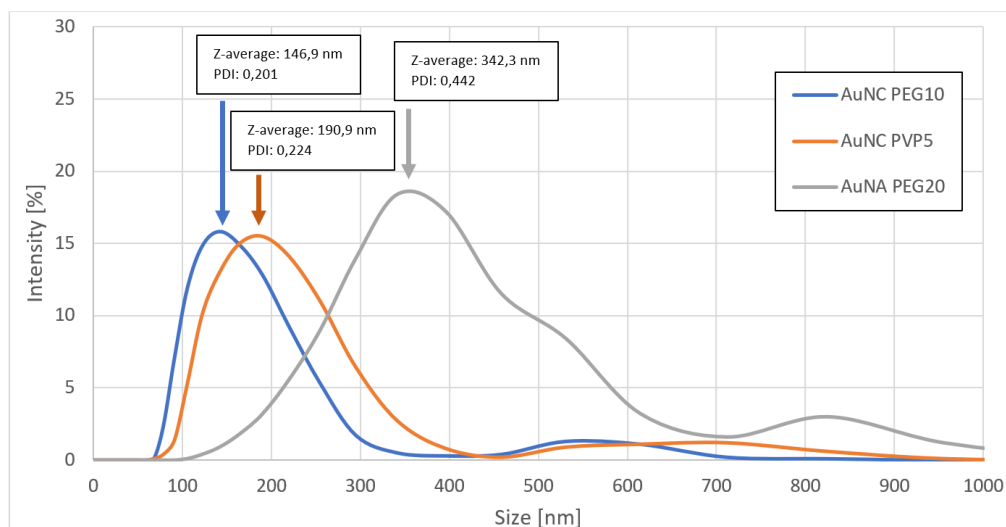

Fig. 5 DLS size distribution of AuNPs in suspensions: AuNC PEG10, AuNC PVP5 and AuNA PEG20

3.3 ζ potential

AuNPs in a suspension of D.I. water synthesised with USP exhibited a slight negative surface charge that was not significant enough to prevent agglomeration. Therefore, the addition of steric stabilisers was needed to ensure a stable suspension. This was achieved with the addition of water-soluble polymers such as PEG or PVP, that physically prevent the AuNPs from coming in close contact with each other, without having a significant effect on the surface charge of the AuNPs. The measured ζ potential of the stabilised AuNPs suspensions is shown in Table 4. Significantly, PVP had the most negative charge. It is a well-established phenomenon that PVP has the ability to reduce the surface charge of AuNPs [44 -46].

Table 4 Results of ζ potential for all AuNPs` suspensions

AuNPs` suspension	Type of Stabiliser concentration in D.I. water [g/L]	ζ potential
AuNC PEG10	PEG – 10 g/L	-1.56 ±8.15 mV
AuNC PVP5	PVP – 5 g/L	-3.12 ±4.66 mV
AuNA PEG20	PEG – 20 g/L	-1.53 ±8.21 mV

3.4 SEM observations

AuNPs in all three suspensions were spherical in shape (see Fig. 6). The average sizes of the smaller AuNPs ranged from 74 nm to about 95 nm. The presence of bigger AuNPs was also confirmed, in the range of about a couple of hundred nanometres. These represent a group of soft agglomerates that are easily dispersed during the redispersion process. Hard agglomerates of connected primary AuNPs were not detected in this study. Several point EDS analyses were performed on the surface of AuNPs to confirm the purity and content of Au. The obtained results showed a high purity of Au, especially for the case of nanoparticles from AuNA (96.10 wt. %). The rest represents O, the origin of which can be attributed to bonds with the stabiliser. No other impurities were detected.
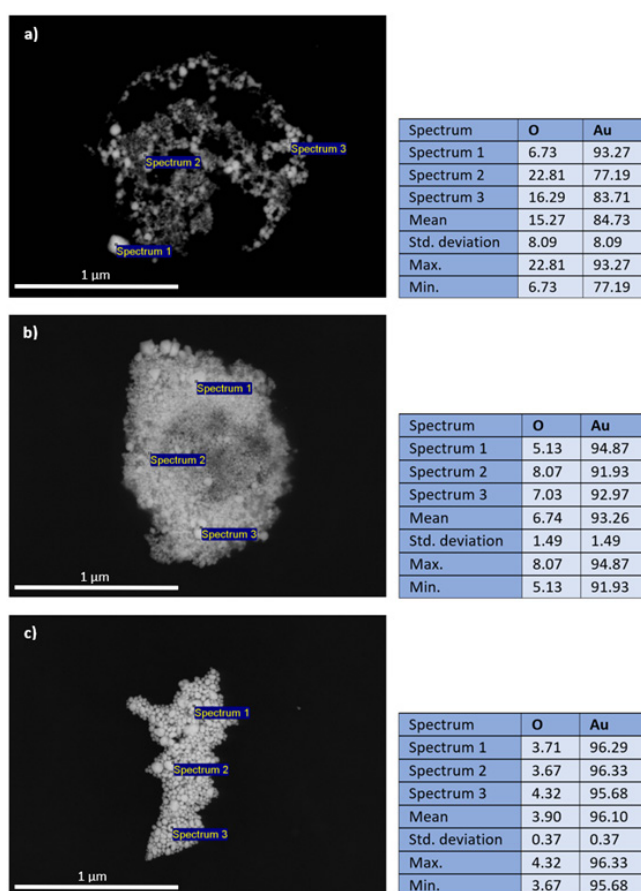

Spectrum	O	Au
Spectrum 1	6.73	93.27
Spectrum 2	22.81	77.19
Spectrum 3	16.29	83.71
Mean	15.27	84.73
Std. deviation	8.09	8.09
Max.	22.81	93.27
Min.	6.73	77.19

Spectrum	O	Au
Spectrum 1	5.13	94.87
Spectrum 2	8.07	91.93
Spectrum 3	7.03	92.97
Mean	6.74	93.26
Std. deviation	1.49	1.49
Max.	8.07	94.87
Min.	5.13	91.93

Spectrum	O	Au
Spectrum 1	3.71	96.29
Spectrum 2	3.67	96.33
Spectrum 3	4.32	95.68
Mean	3.90	96.10
Std. deviation	0.37	0.37
Max.	4.32	96.33
Min.	3.67	95.68

Fig. 6 SEM micrographs and results of EDS point analyses in wt. % for AuNPs: a) AuNC PEG10, b) AuNC PVP5 and c) AuNA PEG20

The chemical composition of the synthesised AuNPs was checked by EDS (see Fig. 6), and the results have shown the presence of a high gold content (more than 85 wt. %) with oxygen originating from the stabilisers (PEG or PVP) at individual sites of the surface AuNPs.

3.5 Circularity and size of AuNPs

The calculated average circularity was 0.9 for all tested AuNPs (with a 0-1 range, 0 signifies an irregular shape and 1 signifies a perfect circle). Table 5 shows the experimentally measured mean AuNPs sizes compared to the theoretically calculated values, which were calculated based on data from literature [47]. There was a difference between the theoretically calculated and experimentally obtained sizes of synthesised AuNPs, which were bigger and not finely dispersed. The synthesised AuNPs had a mixture of different morphologies, which was not taken into account in the theoretical calculations. The aerosol droplets were also generated in a size distribution, rather than a single droplet size. The coalescence of aerosol droplets was also not considered, which is difficult to prevent, as the gas flows in an enclosed system where turbulence effects are to be expected. The microporosity of the AuNPs was not seen after synthesis, the result of which would perhaps be an even greater discrepancy between the experimental and theoretical values. It was observed from the SEM measurements that the AuNPs in suspensions had almost a unimodal size distribution. Namely, the AuNPs in AuNC PEG10 had an average size with a peak at 84.94 nm (in the range 20-100 nm there were 88 % of the total AuNPs), the AuNPs in AuNC PVP5 had an average size with a peak at 97.39 nm (in the range 20-100 nm there were 92 % of the total AuNPs) and AuNPs in AuNA PEG20 had an average size distribution with a peak at 104.25 nm (in the range 20-100 nm there were 93 % of the total AuNPs). The results are not completely consistent with the SEM micrographs, as the SEM images should be considered to show slightly higher AuNPs, due to insufficient high resolution and charge build-up due to stabiliser residues.

Table 5 Experimentally measured average AuNPs` size compared to the theoretically calculated values

Au suspension	Average size of synthesised AuNPs (nm)	Theoretically calculated AuNPs` size (nm)
AuNC PEG10	74.94	94.53
AuNC PVP5	87.39	94.53
AuNA PEG20	94.25	91.55

3.6 TEM observations

The prepared cosmetic creams were observed with TEM to determine how AuNPs were incorporated into the matrix of the base cream. As can be seen in the obtained TEM images (Fig. 7), the AuNPs were quite well integrated with the other components of the base cream, which is the basic requirement for cosmetics` application. The monodispersity and stability of the different AuNPs was achieved and is shown by the red circles in the TEM images for each test cream separately. A more detailed investigation showed that there was no agglomeration of AuNPs, and that they were mixed well with the base substance of the cream.

TEM investigations were also carried out for the cream 3HFWC-W/AuNPs, Fig. 8. Fullerene from 3HFWC-W was found to be in direct contact with the smaller AuNPs (visible with a red arrow). The size of the this fullerene was around 10 nm with completely spherical shapes, which is consistent with the TEM photographs obtained by other authors [48, 49].
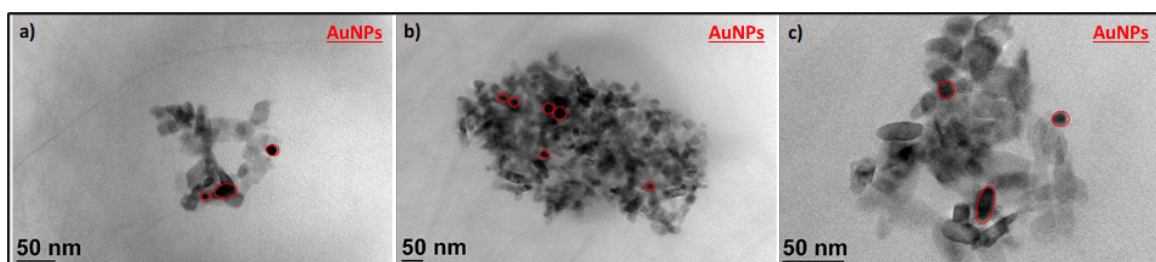

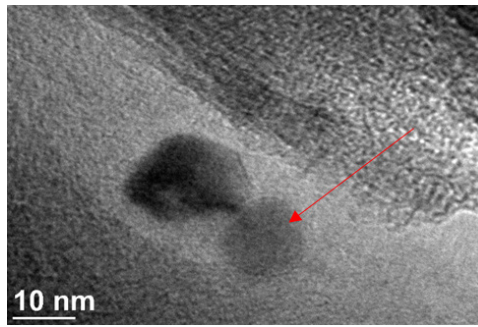**Fig. 7** TEM micrographs of AuNPs taken from cosmetic creams with: a) AuNC PEG10, b) AuNC PVP5 and c) AuNA PEG20

Fig. 8 TEM micrographs of fullerene from 3HFWC-W (red arrow) in contact with AuNPs

3.7 Cream test results

Predispositions and limitations in this study were: In order to obtain information about the epidermis, we had to subtract the values obtained on the blue channel from the values of the reflected light obtained on the green light channel, and, thus, we obtained the w(G-B) convolution of the spectrum. As seen in Fig. 4 wG penetrates to the bottom of the epidermis and wB to the dream stratum corneum, so the w(G-B) convolution gives us complete information about the biophysical characteristics of the epidermis.

In the attached graph of Fig. 9, which represents the average values of all participants, it can be seen that there was a shift in the peak as well as a change in its intensity. The obtained values give us information on the number of paired (p+) and unpaired electrons (p-), i.e. on the paramagnetic and diamagnetic characteristics of the skin.
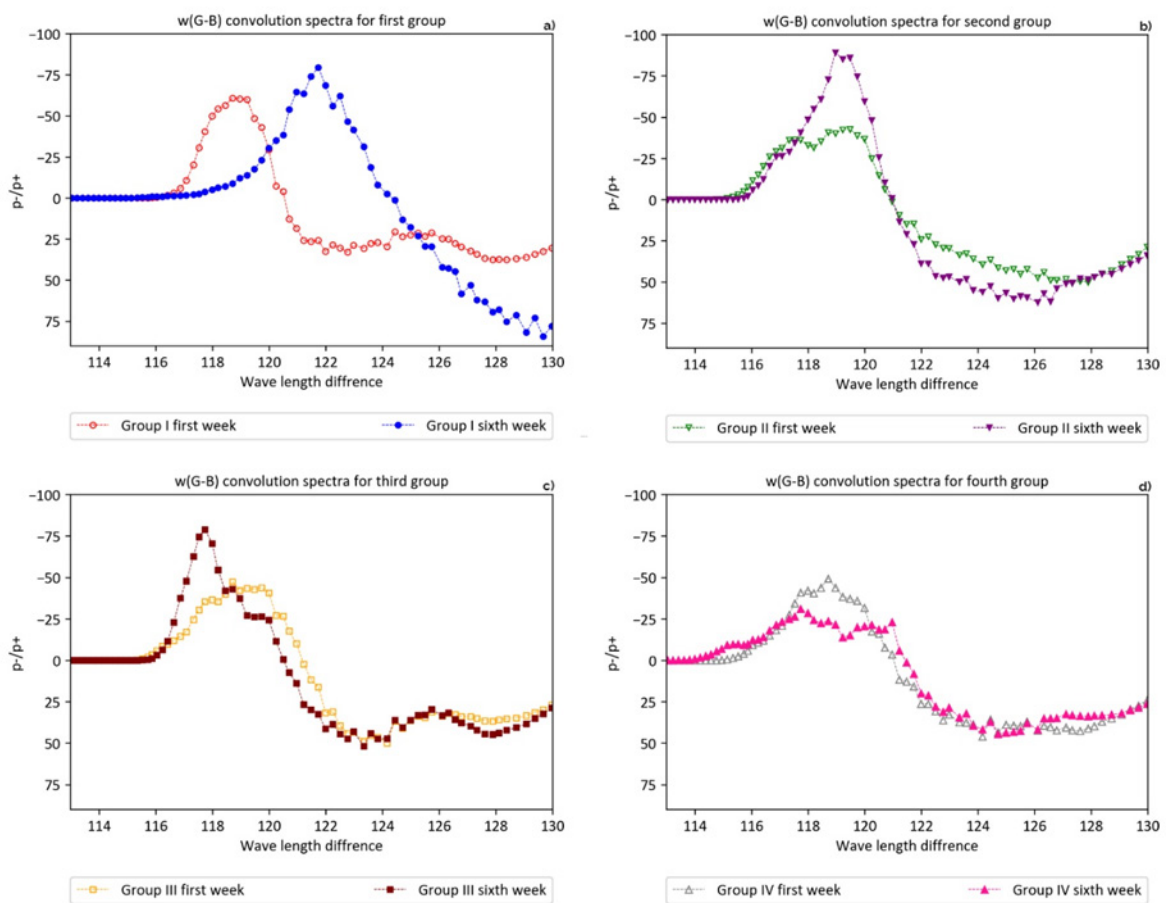
Fig. 9 Change of (p-/p+) electrons in the epidermis before and after using creams with a) AuNC PEG 10, b) AuNC PVP5, c) AuNA PEG20 and d) 3HFWC-W$^{AuNA\ PEG20}$

In Fig. 9a the change in the number of (p-/p+) electrons in the epidermis is visible for a group of participants who used a cream with AuNC PEG 10. In the case of AuNC PVP5 cream, according to the attached graph (Fig. 9b), it can be noticed that there was a change in the intensity of the peak, but not its shifting, which is a possible consequence of the surface energy of AuNPs interacting with the skin [50]. Since these are larger AuNPs compared to the first group, their surface energy is lower. In the values obtained by averaging the data on the biophysical state of the skin, volunteers of the third group, cream with AuNA PEG20, we noticed an even smaller change in the intensity of the peak because their surface energy was the lowest (Fig. 9c). Cream with 3HFWC-W$^{AuNA\ PEG20}$ used by the volunteers of the fourth group represents a symbiosis of AuNPs and 3HFWC-W substances. AuNPs have a negative surface energy [51], which is why hydrogen atoms from aqueous layers in 3HFWC-W are oriented towards them, thus creating a coating around the AuNPs ($2r < 95$ nm). Thanks to this homogeneous structure, the substance neutralises the negative charge of AuNPs, which is why the changes in the intensity of the peak were the smallest in this group (Fig. 9d).
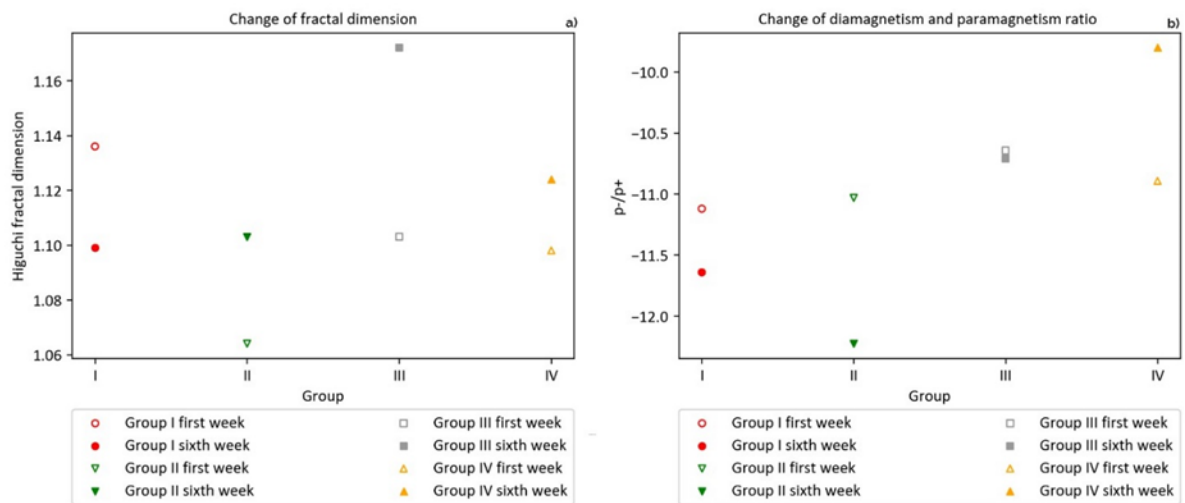
Fig. 10 Diagram of Higuchi fractal dimension (HFD) as one of biophysical parameters of epidermis properties-HFD gives the dynamics of (p-/p+) electrons tissue: a) for all four groups before and after six weeks treatment for different types of light. b) Diagram of the average biophysical properties of the epidermis (p-/p+) electrons for all four groups before and after six weeks of treatment for different types of light

The fractal dimension (see Fig. 10a) of the graph for the first week of the third group is $D_f =$ 1.417, while for the sixth week $D_f = 1.5$, which indicates that there has been a change in the dermis. The change is different with the fourth group, since the fractal dimension for the first week is $D_f = 1.346$, and for the sixth $D_f = 1.235$. When other parameters are taken into consideration, such as the ratio of (p+/p-) electrons, then we see that for group III, for the first week the result equals -95.38, and for the sixth week -96.67, which indicates that the cream with AuNPs did not affect the fibroblasts and collagen synthesis significantly, which is in accordance with the increase in fractal dimension by 6.3 % in group III subjects. In group IV, which for the first week had approximately the same value (p+/p-) = -95.65 as in group III (-95.38), while in the sixth week there was a significant change in collagen synthesis in group IV subjects. The change of diamagnetism and paramagnetism ratio presented in Fig. 10b as value (p+/p) increased significantly for group IV, the change in the sixth week compared to the first was even 73.7 % better. This is in accordance with the change in the fractal dimension of the signal obtained from the dermis because the fractal dimension of the signal spectrum decreased by 8.6 % due to the balanced dynamics of the oscillatory processes in the depth of the dermis, where collagen is dominant.

Next, if we look at the results in Table 6, where the change of biophysical properties of skin for dermis are presented according to the data for red light depending on the difference in wavelength (nm), intensity (n. a. u.), surface ratio (p+/p-) and fractal dimensions, the following findings can be made. In previous studies with a cream containing only the 3HFWC-W substance

(without AuNPs), an improvement in effect by 28 % was achieved, what is comparable to other creams that had the same base as classic bioactive ingredients. When AuNPs with 3HFWC-W were combined in cream, significantly better improvement was achieved by 73.7 % (a difference of 45.7 %), which is an obvious beneficial effect of the new cream. This can be attributed to the result of the new combination of nano-quantum substance and functional properties of AuNPs (AuNPs@3HFWC-W).

Table 6 Change of biophysical properties of skin for dermis according to data of red (R) light for all four groups: 1. (AuNC PEG 10), 2. (AuNC PVP5), 3. (AuNPsPEG20) and group 4. (3HFWC-W[AuNA PEG20])

Light	Week	Unit	1. Group		2. Group		3. Group		4. Group	
			D	P	D	P	D	P	D	P
W (G-B)	1	Int (n.a.u)	-60.85	37.57	-42.62	50.67	-47.48	49.92	-49.38	45.87
		WLD (nm)	118.71	128.37	119.48	127.33	118.71	124.16	118.71	124.16
		(p+/p-)	-11.12		-11.03		-10.64		-10.89	
		D_f	1.136		1.064		1.103		1.098	
	6	Int (n.a.u)	-79.52	84.19	-89.21	62.25	-78.92	51.70	-31.13	44.52
		WLD (nm)	121.73	129.669	118.97	126.10	117.79	123.34	117.73	124.71
		(p+/p-)	-11.64		-12.23		-10.71		-9.80	
		D_f	1.099		1.103		1.172		1.124	

4. Discussion

The perception of gold as an inert material was altered by the discovery that AuNPs are chemically reactive. Their properties can be adapted to certain applications by controlling the size and atomic structure on the surface of the AuNPs. Suspensions with different stabilisers such as PEG and PVP were used during the drying of AuNPs` suspensions with lyophilisation in a laboratory lyophiliser. At the same drying conditions in miron glass cosmetic jars, the dried material with PVP was more stable and no entrainment of dried material was noted, where, on the other hand, with the use of PEG stabiliser, the dried cake was more sensitive to sublimated solvent vapour, which always entrained some fraction of the dried material out of the miron glass cosmetic jars. The use of PVP in cosmetics` application is also beneficial, and exhibits the best performance in binding capacity, solubility, film formation and emulsifying performance [52]. The reduction in surface charge mediated by PVP allows for more positively charged 3HFWC-W to be coordinated around the surface of the AuNPs [44-46]. This allows for an increased transfer of -OH ions.

The proposed binding mechanism between AuNPs and 3HFWC-W is mediated by the stabilising polymers. Specifically, by the oxygen and nitrogen atoms that are present in their macromolecular chains. Here, oxygen and nitrogen atoms act as electron donors to the almost 0 surface charge of the AuNPs [53]. This interaction allows for weak surface binding of the polymers to the surface of the AuNPs [44, 45]. Due to the inherent charge of the polymers being negative, this, in turn, allows for electrostatic attraction between the AuNPs and the polymer stabiliser complex, to attract and coordinate 3HFWC-W around its hydrodynamic radius. Zeta potential measurements suggest that PVP offers more binding locations in comparison to PEG if one looks at the molecular conformation of PVP and PEG, as shown in Fig. 11, with the proposed binding. In PEG the oxygen atoms that interact with AuNPs and 3HFWC-W are in the main macromolecular chain, while, in comparison, the interacting oxygen and nitrogen in PVP are a side functional group. This steric and functional difference most likely enables a closer interaction between the AuNPs` surface and the molecule, causing a higher binding energy. One must also note that the monomer unit (marked by square brackets) of PVP offers two binding points when compared to the one of PEG. Since this coordinated complex is formed in a solution of water and stabiliser, we presume that, due to the creams being emulsions containing a separate aqueous and lipoic phase, that the complex is stable in the aqueous phase.
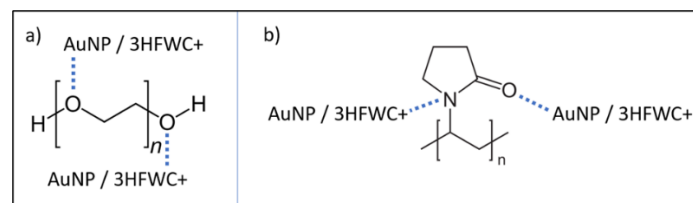
Fig. 11 Presentation of a binding scheme of AuNPs or 3HFWC-W with a) PEG and b) PVP. As there are hydrogen atoms on the surface of the AuNPs or 3HFWC-W complex which carry a positive charge, the interaction of the complex with PEG and PVP will be via hydrogen bonds O⋯H and N⋯H.

Collagen is one of the most abundant proteins in the human body, and, compared to all others, it makes up 40 % of the total mass. In the skin, that percentage is much higher, almost 75 %. The three main amino acids, glycine, proline and lysine participate in its formation. Depending on the order of amino acids, there are about 28 different types of collagen. It is extremely important for the healthy appearance of the skin, because it's a support, together with elastin network, that allows the skin to return to it's original position after being deformed by movement. With age, as the amount of collagen fibres in the skin decreases, and due to the effects of UV and high-energy photons of the sun, pollution, age and so on, skin deteriorates significantly, and constant movement in the same place on the skin leads to changes called wrinkles. Until now to activate collagen and elastin in an optimal way 3HFWC-W substance was used, which acts on the biological structures that are arranged according to the same laws of symmetry (collagen, clathrin, microtubules, centrioles, flagella and processes based on Gibbs free energy), harmonises them, and brings them into a natural functional state. Due to its icosahedral structure, it has appropriate vibrational-rotational states that enable its harmonisation. Namely, 3HFWC-W stimulates the formation of linearly bound water molecules in accordance with icosahedral (Fibonacci) properties. This mechanism takes place in several steps: (i) Establishing the original state with the conformational structure of biomolecules on the water/hydrogen bond and thus achieving the optimal state; (ii) Signal transmission via non-covalent hydrogen bonds in the α-helix via peptide planes; (iii) Reaction of a liquid crystal structure in a cosmetic product applied to the skin; (iv) Creation of a water cluster with icosahedral symmetry, which together with water organised in linear chains, that creates a network of water with properties of icosahedral symmetry [2].

Previous studies have confirmed that 3HFWC-W increases the moisture content and stimulates the regeneration of biomolecules. In comparison with four commercial cosmetic products, the 3HFWC-W based creams showed better effects by 12-32 % [22]. Nanoparticles usually have different physical, catalytic or biological properties from larger materials with the same chemical composition. The key to achieving better nanoparticle performance is increasing the surface to volume ratio of the material, due to reduction to nanometre dimensions. The large and reactive interface is responsible for the catalytic, antimicrobial and many electronic properties that give nanoparticles a significant advantage over bulk materials. The most important difference between basic materials and nanoparticles is that they have a large number of atoms on a small outer surface, which leads to high surface energy and high reactivity. Ease of production and functionalisation have resulted in various applications in many fields of biomedicine, such as nanosensors, targeted drug delivery, medical imaging, but also in the cosmetics industry. The high optical absorption of AuNPs, their scattering properties and low or complete lack of toxicity have made them a promising class of ingredient in cosmetics. Previous research has shown that the main properties of AuNPs in beauty care are accelerating blood circulation, anti-inflammatory properties, antiseptic properties, increasing the firmness and elasticity of the skin, improving the metabolism, and, thus, slowing down the ageing process [54]. Testing of creams with the quantum substance 3HFWC-W based on the double derivative of C_{60} molecules was conducted, in order to investigate the impact of the synergistic effects of C_{60} and AuNPs. To see whether there is a synergistic effect of AuNPs and the substance 3HFWC-W, we monitored changes in the forearms of the subjects (women) in two places every seven days. Wanting to see how the creams with AuNPs (group III) and with the added 3HFWC-W (group IV) affected collagen, we observed red light, because it penetrates to the depths where collagen is formed.

A more detailed mechanism of the 3HFWC-W$^{AuNA\ PEG20}$ substance of the cream in the skin is presented in Fig. 12. The mechanism is as follows:

a) The 3HFWC-W$^{AuNA\ PEG20}$ substance penetrates through the layers of the epidermis up to the basement membrane, where, under the oscillatory processes of collagen in the basement membrane, it is activated and acts on the fibroblasts. Synthesis of new collagen and elastin through water channels takes place, then continues to pass through the epidermis to the skin`s surface, releasing water molecules from the peripheral water layers of the substance.

b) Trans Epidermal Water Loss is being implemented, which affects the length of the segments of lipid layers and regulates the amount of water leaving the epidermis.

c) Regulation of the collagen oscillatory processes occurs in the basement membrane, and, with that, the preservation of its stability is maintained.

d) In the final stage activation of the fibroblasts in the dermis from the basement membrane occurs, using water (organised in water chains), which leads to the synthesis of new collagen and elastin.

Based on the obtained scientific results the new substance 3HFWC-W with AuNPs will be prepared in a cream with the name La Danza-Hyperlight fusion Anti - Ageing essential complex. This will be followed by extensive testing to ensure maximum safety for cosmetic users.
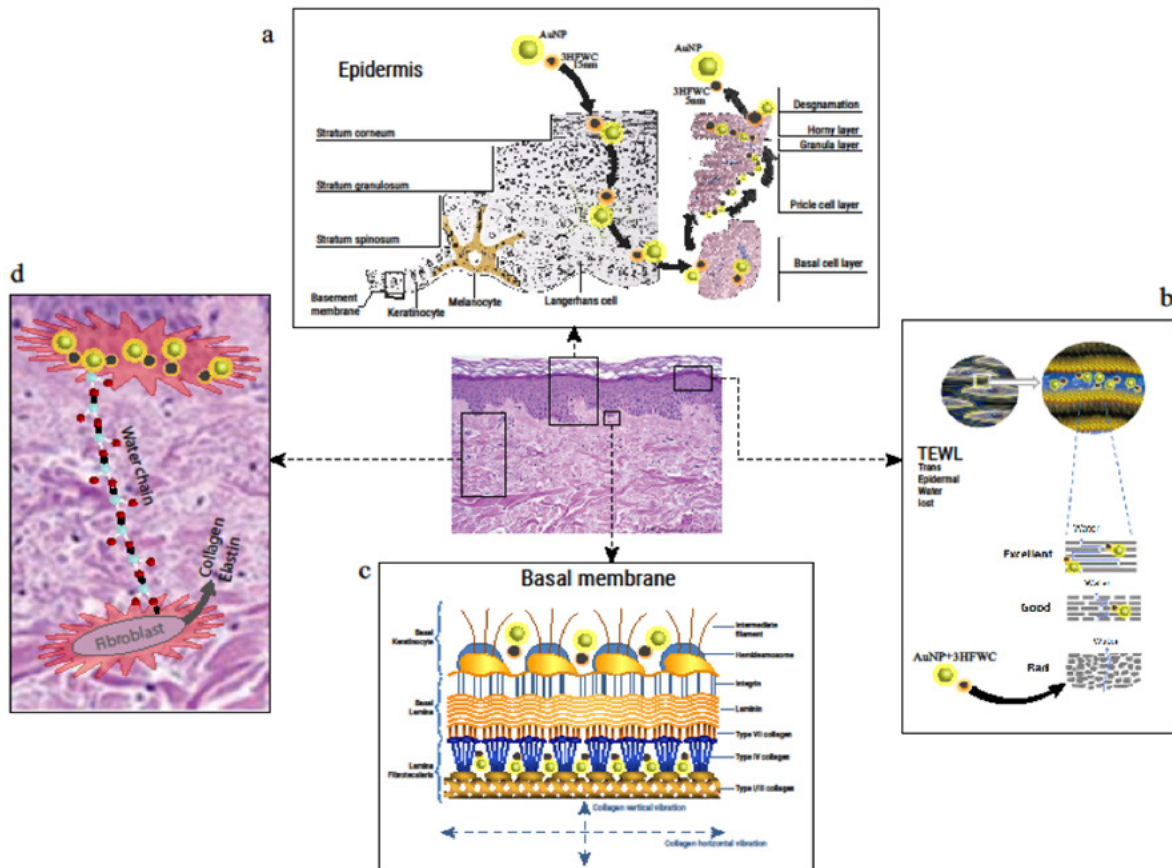
Fig. 12 Schematic representation of the effect of the 3HFWC-W$^{AuNA\ PEG20}$ substance in the epidermis a) and b) on the basement membrane c) and in the dermis, from the basal membrane to fibroblast, via water hydrogen bonds, for d) a new collagen synthesis

5. Conclusion

Within the performed research, we came to the following findings:

- With the use of Ultrasonic Spray Pyrolysis and freeze drying, AuNPs were successfully synthesised, with the selected stabilisers that prevented their agglomeration. Dry AuNPs had the final properties required for the preparation of cosmetic creams.
- The use of a PVP stabiliser in the freeze drying process allowed the formation of a very stable form of dried AuNPs, with a smaller shrinkage observed in the drying Miron glass cosmetic jar compared to the PEG stabiliser. Measurements showed that PVP helped reduce the surface charge of AuNPs in suspension, which allowed for better 3HFWC-W setting around the surface of the AuNPs.
- The results of the six weeks clinical study cream on volunteers found improvements of collagen quality in skin between 18-24 %, achieved due to the use of AuNPs (groups I, II, III) in a standard cream base, while the cream with the combination of 3HFWC-W and AuNPs gave significantly higher improvements with the value of 45.7 %.
- It was also discovered that hydration of the skin (*stratum cornum*) increased by 6.4 -9.6 % in standard creams with AuNPs, and 73.7 % in the 3HFWC-W/AuNPs cream. Similar results were measured by the epidermis-dermis function, where 24-28 % for standard creams with AuNPs was identified, and 38.4 % for the cream 3HFWC-W/AuNPs.

Acknowledgments

References

[1] Krutmann, J. (2003). Hautalterung, *Der Hautarzt,* Vol. 54, No. 9, 803-803, doi: 10.1007/s00105-003-0610-6.

[2] Miljkovic, S., Jeftic, B., Stankovic, I., Stojiljkovic, I., Koruga, D. (2021). Mechanisms of skin moisturization with hyperharmonized hydroxyl modified fullerene substance, *Journal of Cosmetic Dermatology,* Vol. 20, No. 9, 3018-3025, doi: 10.1111/jocd.13965.

[3] Pulit-Prociak, J., Grabowska, A., Chwastowski, J., Majka, T.M., Banach, M. (2019). Safety of the application of nanosilver and nanogold in topical cosmetic preparations, *Colloids and Surfaces B: Biointerfaces,* Vol. 183, Article No. 110416, doi: 10.1016/j.colsurfb.2019.110416.

[4] Gupta, R., Rai, B. (2017). Effect of size and surface charge of gold nanoparticles on their skin permeability: A molecular dynamics study, *Scientific Reports*, Vol. 7, Article No. 45292, doi: 10.1038/srep45292.

[5] Manatunga, D.C., Godakanda, V.U., Herath, H.M.L.P. B, de Silva, R.M., Yeh, C.-Y., Chen, J.-Y., de Silva, A.A.A., Rajapaksha, S., Nilmini, R., de Silva, K.M.N. (2020). Nanofibrous cosmetic face mask for transdermal delivery of nano gold: Synthesis, characterization, release and zebra fish employed toxicity studies, *Royal Society Open Science,* Vol. 7, Article No. 201266, doi: 10.1098/rsos.201266.

[6] Bachelet, M. (2016). Design of pH-responsive gold nanoparticles in oncology, *Materials Science and Technology,* Vol. 32, No. 8, 794-804, doi: 10.1179/1743284715Y.0000000090.

[7] Banstola, A., Emami, F., Jeong, J.-H., Yook, S. (2018). Current applications of gold nanoparticles for medical imaging and as treatment agents for managing pancreatic cancer, *Macromolecular Research,* Vol. 26, No. 11, 955-964, doi: 10.1007/s13233-018-6139-4.

[8] Yupapin, P., Suwandee, P. (2016). Nano-particles for cosmetic use: Particle sizing, cytotoxicity test, and facial gesture monitoring model, *Journal of Cosmetology & Trichology,* Vol. 2, No. 2, Article No. 112, doi: 10.4172/2471-9323.1000112.

[9] Kaul, S., Gulati, N., Verma, D., Mukherjee, S., Nagaich, U. (2018). Role of nanotechnology in cosmeceuticals: A review of recent advances, *Journal of Pharmaceutics,* Vol. 2018, Article ID 3420204, doi: 10.1155/2018/3420204.

[10] Kim, J.-H., Hong, C.-O., Koo, Y.-C., Choi, H.-D., Lee, K.-W. (2012). Anti-glycation effect of gold nanoparticles on collagen, *Biological and Pharmaceutical Bulletin,* Vol. 35, No. 2, 260-264, doi: 10.1248/bpb.35.260.

[11] Fytianos, G., Rahdar, A., Kyzas, G.Z. (2020). Nanomaterials in cosmetics: Recent updates, *Nanomaterials,* Vol. 10, No. 5, Article No. 979, doi: 10.3390/nano10050979.

[12] Lieber, C.M., Chen, C.-C. (1994). Preparation of fullerenes and fullerene-based materials, *Solid State Physics,* Vol. 48, 109-148, doi: 10.1016/S0081-1947(08)60578-0.

[13] Matija, L., Tsenkova, R., Munćan, J., Miyazaki, M., Banba, K., Tomić, M., Jeftić, B. (2013). Fullerene based nanomaterials for biomedical applications: Engineering, functionalization and characterization, *Advanced Materials Research,* Vol. 633, 224-238, doi: 10.4028/www.scientific.net/AMR.633.224.

[14] Milani, M., Sparavigna, A. (2017). The 24-hour skin hydration and barrier function effects of a hyaluronic 1%, glycerin 5%, and Centella asiatica stem cells extract moisturizing fluid: An intra-subject, randomized, assessor-blinded study, *Clinical, Cosmetic and Investigational Dermatology,* Vol. 10, 311-315, doi: 10.2147/CCID.S144180.

[15] Marinković, K., Gomez, L.S., Rabanal, M.E., Mančić, L., Milošević, O. (2010). Aerosol route in processing of nanostructured phosphor materials, *Processing and Application of Ceramics,* Vol. 4, No. 3, 135-145, doi: 10.2298/pac1003135m.

[16] Majerič, P., Rudolf, R. (2020). Advances in ultrasonic spray pyrolysis processing of noble metal nanoparticles–Review, *Materials,* Vol. 13, No. 16, Article No. 3485, doi: 10.3390/ma13163485.

[17] Ravnik, J., Golobič, I., Sitar, A., Avanzo, M., Irman, Š., Kočevar, K., Cegnar, M., Zadravec, M., Ramšak, M., Hriberšek, M. (2018). Lyophilization model of mannitol water solution in a laboratory scale lyophilizer, *Journal of Drug Delivery Science and Technology,* Vol. 45, 28-38, doi: 10.1016/j.jddst.2018.02.015.

[18] Cui, Y., Wu, Q., He, J., Li, M., Zhang, Z., Qiu, Y. (2020). Porous nano-minerals substituted apatite/chitin/pectin nanocomposites scaffolds for bone tissue engineering, *Arabian Journal of Chemistry,* Vol. 13, No. 10, 7418-7429, doi: 10.1016/j.arabjc.2020.08.018.

[19] Chang, Y., Zheng, C., Chinnathambi, A., Alahmadi, T.A., Alharbi, S.A. (2021). Cytotoxicity, anti-acute leukemia, and antioxidant properties of gold nanoparticles green-synthesized using Cannabis sativa L leaf aqueous extract, *Arabian Journal of Chemistry,* Vol. 14, No. 4, Article No. 103060, doi: 10.1016/j.arabjc.2021.103060.

[20] Koruga, D. (2011). *Composition of matter containing harmonized hydroxyl modified fullerene substance,* Patent US 8058483 B52, from *https://patents.google.com/patent/US8058483*, accessed December 18, 2021.

[21] Koruga, D. (2019). *Compositions comprising hyper harmonized hydroxyl modified fullerene substances*, Patent App. No. PCT/EP2019/083307, Int. Pub. No.:WO 2021/110234 A1, 2021, from *https://patents.google.com/patent/WO2021110234A1/en*, accessed December 18, 2021.

[22] Matija, L., Koruga, D., Jovanović, J., Dobrosavljević, D., Ignjatović, N. (2004). In vitro and in vivo investigation of collagen – C60(OH)24 interaction, *Materials Science Forum,* Vol. 453-454, 561-566, doi: 10.4028/www.scientific.net/msf.453-454.561.

[23] Miljković, N., Godman, B., Kovačević, M., Polidori, P., Tzimis, L., Hoppe-Tichy, T., Saar, M., Antofie, I., Horvath, L., De Rijdt, T., Vida, R.G., Kkolou, E., Preece, D., Tubić, B., Peppard, J., Martinez, A., Yubero, C.G., Haddad, R., Rajinac, D., Zelić, P., Jenzer, H., Tartar, F., Gitler, G., Jeske, M., Davidescu, M., Beraud, G., Kuruc-Polje, D., Haag, K.S., Fischer, H., Sviestina, I., Ljubojević, G., Markestad, A., Vujić-Aleksić, V., Nežić, L., Crkvenčič, A., Linnolahti, J., Ašanin, B., Duborija-Kovačević, N., Bochenek, T., Huys, I., Miljković, B. (2020). Prospective risk assessment of medicine shortages in Europe and Israel: Findings and implications, *Frontiers in Pharmacology,* Vol. 11, Article No. 357, doi: 10.3389/fphar.2020.00357.

[24] Rudolf, R., Friedrich, B., Stopić, S., Anžel, I., Tomić, S., Čolić, M. (2012). Cytotoxicity of gold nanoparticles prepared by ultrasonic spray pyrolysis, *Journal of Biomaterials Applications,* Vol. 26, No. 5, 595-612, doi: 10.1177/0885328210377536 .

[25] Rudolf, R., Majerič, P., Tomić, S., Shariq, M., Ferčec, U., Budič, B., Friedrich, B. Vučević, D., Čolić, M. (2017). Morphology, aggregation properties, cytocompatibility, and anti-inflammatory potential of citrate-stabilized AuNPs prepared by modular ultrasonic spray pyrolysis, *Journal of Nanomaterials*, Vol. 2017, Article ID 9365012, doi: 10.1155/2017/9365012.

[26] Rudolf, R., Majerič, P., Štager, B. Albreht, B. (2020). *Process for the production of gold nanoparticles by modified ultrasonic spray pyrolysis:* patent application no. P-202000079. Ljubljana: Office of the Republic of Slovenia for Intellectual Property, Slovenia, Ljubljana: Urad RS za intelektualno lastnino.

[27] Shariq, M., Chattopadhyaya, S., Rudolf, R., Dixit, A.R. (2020). Characterization of AuNPs based ink for inkjet printing of low cost paper based sensors, *Materials Letters,* Vol. 264, Article ID 127332, doi: 10.1016/j.matlet.2020.127332.

[28] Shariq, M., Friedrich, B., Budic, B., Hodnik, N., Ruiz-Zepeda, F., Majerič, P., Rudolf, R. (2018). Successful synthesis of gold nanoparticles through ultrasonic spray pyrolysis from a gold(III) nitrate precursor and their interaction with a high electron beam, *ChemistryOpen,* Vol. 7, No. 7, 533-542, doi: 10.1002/open.201800101.

[29] Abdelwahed, W., Degobert, G., Stainmesse, S., Fessi, H. (2006). Freeze-drying of nanoparticles: Formulation, process and storage considerations, *Advanced Drug Delivery Reviews,* Vol. 58, No. 15, 1688-1713, doi: 10.1016/j.addr.2006.09.017.

[30] Jović, Z. (2020). *Quantum cosmetics – Revolution in skin care,* Nova Galaksija – Zepter's Nanoworld, 86-98.

[31] Koruga, Đ., Miljković, S., Ribar, S., Matija, L., Kojić, D. (2010). Water hydrogen bonds study by opto-magnetic fingerprint technique, *Acta Physica Polonica A,* Vol. 117, No. 5, 777-781, doi: 10.12693/APhysPolA.117.777.

[32] Koruga, Đ., Bandić, J., Janjić, G., Lalović, Č., Munćan, J., Dobrosavljević Vukojević, D. (2012). Epidermal layers characterisation by opto-magnetic spectroscopy based on digital image of skin, *Acta Physica Polonica A,* Vol. 121, No. 3, 606-610, doi: 10.12693/APhysPolA.121.606.

[33] Jeftic, B., Papic-Obradovic, M., Muncan, J., Matija, L., Koruga, D. (2017). Optomagnetic imaging spectroscopy application in cervical dysplasia and cancer detection: Comparison of stained and unstained papanicolaou smears, *Journal of Medical and Biological Engineering,* Vol. 37, No. 6, 936-943, doi: 10.1007/s40846-017-0255-z.

[34] Dragicevic, A., Matija, L., Krivokapic, Z., Dimitrijevic, I., Baros, M., Koruga, D. (2019). Classification of healthy and cancer states of colon epithelial tissues using opto-magnetic imaging spectroscopy, *Journal of Medical and Biological Engineering*, Vol. 39, No. 3, 367-380, doi: 10.1007/s40846-018-0414-x.

[35] Koruga, D., Tomic, A. (2009). *System and method for analysis of light-matter interaction based on spectral convolution,* Int. App. NoL. PCT/US2009/030347, Int. Pb. No.: WO 2009/089292 A1, 2009.

[36] Bandic, J., Koruga, D., Marinkovich, S., Mehendale, R. (2007). *Analytic methods of tissue evaluation,* Patent US 10,085,643 B2, 2018.

[37] Jacques, S.L. (2013). Optical properties of biological tissues: A review, *Physics in Medicine & Biology,* Vol. 58, No. 11, R37-61, doi: 10.1088/0031-9155/58/11/R37.

[38] Higuchi, T. (1988). Approach to an irregular time series on the basis of the fractal theory, *Physica D: Nonlinear Phenomena,* Vol. 31, No. 2, 277-283, doi: 10.1016/0167-2789(88)90081-4.

[39] Klonowski, W. (2002). Chaotic dynamics applied to signal complexity in phase space and in time domain, *Chaos, Solitons & Fractals,* Vol. 14, No. 9, 1379-1387, doi: 10.1016/S0960-0779(02)00056-5.

[40] Lin, P.-C, Lin, S., Wang, P.C., Sridhar, R. (2014). Techniques for physicochemical characterization of nanomaterials, *Biotechnology Advances,* Vol. 32, No. 4, 711-726, doi: 10.1016/j.biotechadv.2013.11.006.

[41] Tsantilis, S., Pratsinis, S.E. (2004). Soft- and hard-agglomerate aerosols made at high temperatures, *Langmuir,* Vol. 20, No. 14, 5933-5939, doi: 10.1021/la036389w.

[42] Yeap, S.P. (2018). Permanent agglomerates in powdered nanoparticles: Formation and future prospects, *Powder Technology,* Vol. 323, 51-59, doi: 10.1016/j.powtec.2017.09.042.

[43] Teleki, A., Wengeler, R., Wengeler, L, Nirschl, H., Pratsinis, S.E. (2008). Distinguishing between aggregates and agglomerates of flame-made TiO2 by high-pressure dispersion, *Powder Technology,* Vol. 181, No. 3, 292-300, doi: 10.1016/j.powtec.2007.05.016.

[44] Behera, M., Ram, S. (2013). Spectroscopy-based study on the interaction between gold nanoparticle and poly(vinylpyrrolidone) molecules in a non-hydrocolloid, *International Nano Letters,* Vol. 3, Article No. 17, doi: 10.1186/2228-5326-3-17.

[45] Seoudi, R. Fouda, A.A., Elmenshawy, D.A. (2010). Synthesis, characterization and vibrational spectroscopic studies of different particle size of gold nanoparticle capped with polyvinylpyrrolidone, *Physica B: Condensed Matter,* Vol. 405, No. 3, 906-911, doi: 10.1016/j.physb.2009.10.012.

[46] Tiyyagura, H.R., Majerič, P., Bračič, M., Anžel, I, Rudolf, R. (2021). Gold inks for inkjet printing on photo paper: Complementary characterisation, *Nanomaterials,* Vol. 11, No. 3, Article No. 599, doi: 10.3390/nano11030599.

[47] Majerič, P. (2016). *Synthesis of gold nanoparticles with a modified ultrasonic spray pyrolysis,* Doctoral dissertation, University of Maribor, Faculty of Mechanical Engineering.

[48] Sumi, N., Chitra, K.C. (2019). Impact of fullerene C_{60} on behavioral and hematological changes in the freshwater fish, Anabas testudineus (Bloch, 1792), *Applied Nanoscience,* Vol. 9, No. 8, 2147-2167, doi: 10.1007/s13204-019-01041-1.

[49] Wang, X., Tang, F., Qi, X., Lin, Z., Battocchi, D., Chen, X. (2019). Enhanced protective coatings based on nanoparticle fullerene C_{60} for oil & gas pipeline corrosion mitigation, *Nanomaterials,* Vol. 9, No. 10, Article No. 1476, doi: 10.3390/nano9101476.

[50] Holec, D., Löfler, L., Zickler, G.A., Vollath, D., Fischer, F.D. (2021). Surface stress of gold nanoparticles revisited, *International Journal of Solids and Structures,* Vol. 224, Article No. 111044, doi: 10.1016/j.ijsolstr.2021.111044.

[51] Rudolf, R., Majerič, P., Golub, D., Tiyyagura, H.R. (2020). Testing of novel nano gold ink for inkjet printing, *Advances in Production Engineering & Management,* Vol. 15, No. 3, 358-368, doi: 10.14743/apem2020.3.371.

[52] Gawade, R.P., Chinke, S.L., Alegaonkar, P.S. (2020). Chapter 17 - Polymers in cosmetics, *Polymer Science and Innovative Applications,* Elsevier, Amsterdam, Netherlands, 545-565, doi: 10.1016/B978-0-12-816808-0.00017-2.

[53] Al-Johani, H., Abou-Hamad, E., Jedidi, A., Widdifield, C.M., Viger-Gravel, J., Sangaru, S.S., Gajan, D., Anjum, D.H., Ould-Chikh, S., Hedhili, M.N., Gurinov, A., Kelly, M.J., El Eter, M., Cavallo, L., Emsley, L., Basset, J.-M. (2017). The structure and binding mode of citrate in the stabilization of gold nanoparticles, *Nature Chemistry,* Vol. 9, 890-895, doi: 10.1038/nchem.2752.

[54] Prajapati, P. (2011). Overview on applications of nanoparticles in cosmetics, *Asian Journal of Pharmaceutical and Clinical Research,* Vol. 1, Article No. 40.

Appendix A

List of abbreviations

AuNC PEG10	AuNPs prepared by USP, with a chloride precursor with a concentration 0.5 g/L Au and collected in a suspension of D.I. water with 10 g/L PEG
AuNA PEG20	AuNPs prepared by USP, with an acetate precursor with a concetration 0.5 g/L Au and collected in a suspension of D.I. water with 20 g/L PEG
AuNC PVP5	AuNPs prepared by USP, with a chloride precursor with a concentration 0.5 g/L Au and collected in a suspension of D.I. water with 5 g/L PVP
AuNPs	Gold nanoparticles
D.I. water	Deionised water
DLS	Dynamic Light Scattering
EDS	Energy-Dispersive X-ray Spectroscopy
HFD	Higuchi Fractal Dimension

HDF	Human dermal fibroblasts
ICP-MS	Inductively Coupled Plasma-Mass Spectrometry
LED	Light-Emitting Diode
NHS	Nano-harmonised substance
OMIS	Opto-Magnetic Imaging Spectroscopy
PEG	Polyethylene glycol
PVP	Polyvinylpyrrolidone
RI	Refractive Index
SEM	Scanning Electron Microscopy
TEM	Transmission Electron Microscopy
USP	Ultrasonic Spray Pyrolysis
wB	Blue channel of white LED light
wG	Green channel of white LED light
WLD	wavelength difference
wR	Red channel of white LED light
w(G-B)	Green minus Blue channel of white LED light (diffuse)
w(R-B)	Red minus Blue channel of white LED light (diffuse)
w(R-G)	Red minus Green channel of white LED light (diffuse)
3HFWC-W	Hyper Harmonised Hydroxyl Modified Fullerene

The influence of artificial intelligence technology judicial decision reasoning on contract performance in manufacturing supply chain: A simulation analysis using Evolutionary Game approach

Zhao, G.[a], Shi, H.B.[a,*], Wang, J.F.[a]

[a]School of Management, Shenyang University of Technology, Shenyang, P.R. China

ABSTRACT

Today's world revolves around technology, which has a total impact not only on human life but also on manufacturing companies. Many companies have embraced artificial intelligence (AI) in the form of powerful computers, applications, or software that can screen job applicants, alert when a machine is about to break down, and read legal contracts. However, the rapid expansion of AI and its use in legal settings, such as contract performance, in a company is a major challenge on the judicial side. This article, thus, establishes an evolutionary game model of whether manufacturing suppliers are performing contracts or not when the court chooses to use artificial intelligence (AI) technology. Considering the complexity of choosing manufacturers' AI strategy, the method constructs a simulation analysis model of manufacturers' contract enforcement behaviour with the participation of several subjects. We can simulate the influence of the factors selected on the strategy chosen by both parties (manufacturers and court) by changing the different influence factors and studying the evolutionary law of different court guidance and regulation strategies on the production behaviour of green products. The results show that the choice of the court and manufacturers to use the AI technology strategy or not is based on the rate of error reduction, through the computational implementation of multi-subject modelling.

1. Introduction

Over time, the problems and expectations of human life have become increasingly complex. Solving these problems has brought us into the current technological era, where there are constant attempts to make machines smarter than humans, or at least to make them at the same level of intelligence as humans [1]. This is how AI was born, which can be defined as the branch of advanced engineering that allows inducing intelligence in computers, mainly to improve those sectors of activity that lag in providing services to consumers. It is also a branch of computer science that focuses on the development of intelligent machines that think and work like humans. In today's business world, AI has become a serious topic. Hence, as predicted to be the next technological disruption, AI is redefining business growth strategies [2]. In this regard, many

companies have already followed suit and are recognizing the benefits of AI within their operations. With the implementation of additive manufacturing technologies, manufacturing executives will make a strategic decision based on the ability to predict the impact of this investment on improving the company's competitive advantage [3]. AI is emerging as a competitive advantage, while some areas of information technology are reduced to a position of competitive necessity [4]. Blockchain technology enables organisations to develop a more responsible and flexible supply chain and to overcome internal and external challenges at all levels [5]. Production in manufacturing companies has been optimized thanks to machine learning, which allows robots to perform all kinds of calculations in real-time to adapt the production rate, increase the occupancy rate of the machines, support an operator on the production line, and optimally manage inventory [6]. Briefly speaking, AI increases productivity, accelerates production, reduces costs and delays. Therefore, many manufacturing companies have moved from remote monitoring to AI-based control, optimization, and advanced autonomous systems to improve their functionality [7]. In [8], the LMDI (logarithmic mean divisia index) decomposition model was used to decompose the influencing factors of carbon emission from five aspects: energy structure, energy intensity, economic efficiency, industrial structure, and employee scale. AI offers solutions for generating content, predicting sales, and also optimizing advertising strategies. The ability to deliver content, or personalized advertising to a target market, allows sales/marketing teams to centralize their efforts to better follow the customer through the buying process. Thus, by integrating AI into customer relationship management (CRM), service and product companies benefit from improved sales and financial performance. Future releases of CRM systems such as salesforce will enable sales, marketing, and digital managers to meet and exceed their goals. In addition, AI, combined with big data, which generates data on purchase history, consumption habits, etc., allows a company's prospects to be better identified and thus optimize qualified leads. Artificial intelligence provides faster, simpler, and more accurate solutions. More recently, AI is also being used in the judicial field. Using AI in law, decision support systems have been developed and decisions are now easier for legal professionals to make. AI is also used to manage risk and perform heavy legal research tasks [9]. As future research has many potential benefits for existing and new businesses, companies should not lose sight of the future of AI [10].

The significant opportunities, realistic impact assessment, challenges, and potential research agenda posed by the rapid emergence of AI in several areas: business and management, government, public sector, and science and technology are presented in [11]. However, it is limited to an overview of AI technology and its impact on the future of industry and society based on the societal and industrial influence on the pace and direction of AI development. It did not take into consideration the impact of AI on the core workforce of the company. The importance of decision support systems and the application of AI in supply chain risk management is presented in [12], but it limited its research in the domain that manages risks that affect the supply chain. The literature [13] outlines the key challenges and their analysis, as well as the opportunities presented by AI, IoT, and blockchain, but has specifically considered the cooperation of legislators, developers, and businesspeople to grow businesses in the face of this technological boom. How the practice of law will be affected by artificial intelligence is proposed in [14]. Here, recent developments in artificial intelligence that have enabled lawyers to make objective and accurate predictions on discrete legal issues have been demonstrated. However, the limitations that lawyers face have not been highlighted, and the predictions made have not proven to be 100 % reliable. A contractual control in the supply chain is described in [15]. It examines the legal steps that a limited number of multinationals are taking in practice to govern their supply chains in terms of CSR, providing valuable insights into which companies are aiming to improve the CSR performance of their supply chains and acting accordingly. However, technology, i.e., AI, has not been integrated into this research, not only at the contractual level but also at the judicial level.

The objective of this paper is to demonstrate the influence of artificial intelligence technology judicial decision reasoning on contract performance in manufacturing supply chain. An evolutionary game model between the court and manufacturers is constructed to determine whether manufacturing suppliers will choose to enforce contracts or not when the court uses AI or not. Section 2 presents the literature review of the evolutionary game model. Section 3 presents the

problem description by pointing out the basic assumptions of the evolutionary game model and an analysis of the evolutionary game of the court choice. The research method describing the phase diagram of the evolutionary game is presented in Section 4. The simulation results and discussion are shown in Section 5, while the conclusion is presented in Section 6.

2. Literature review: Analysis of the evolutionary game of AI

The benefits of AI include the improvement of quality, faster response, and reduction of costs [16]. It has been shown that the neural network model can handle the production management and control problem of a discrete manufacturing job shop, based on ant colony optimisation (ACO) [17]. Artificial intelligence companies continue to find ways to develop technologies that can handle laborious tasks in different industries with greater speed and accuracy. AI, in the legal profession, has already found its place in helping lawyers and clients. Thus, the judicial method chose and the manufacturer's decision have different responsibilities in the choice of the final strategy that will be adopted by the judge, and the relationship between them is an evolutionary game, promoting the integration of AI into the judicial system [18]. However, the decision focus of both, the court and the manufacturers, is different. Courts typically focus on reducing error rates, while companies aim to improve their key performance indicators (KPIs) and maximize their profit. The relationship between the two parties is a kind of competition to achieve good performance. Therefore, the court and companies are in a state of competition and cooperation when deciding whether to implement AI or not. Both the court and the companies need AI technology. AI helps the court system automate, increasing efficiency within an affordable budget [19]. In many industries, AI has helped reduce costs, increase revenues and improve assets. It also helps companies optimize R&D and increase lower cost, higher quality manufacturing, achieve 100 % accurate customer demand projections and forecasts. AI enables supply chain managers to ensure real-time tracking and error-free production, achieve efficient designs to eliminate waste, and facilitate process cycle time reduction [20]. The implementation of an AI system in the supply chain can synchronize the production rates and sales. It also allows firms to improve their profits by acting on the sharing contract [21].

The use of AI in the courts involves the application of mathematical and computational techniques to make the law more manageable, predictable, understandable, and accessible. This makes judicial decisions more reliable. Thus, the implementation of AI in court decisions attracts many manufacturers to submit individual cases or issues to the AI-driven court. Today, smart contracts are the future of contract analysis. There is no doubt that AI is highly beneficial in reviewing, comparing, and writing contracts, saving time, money, and effort. An integrated knowledge-based system including rule-based reasoning and cases for acquisition or transfer of real estate according to the Indian legal domain using Win Prolog VisiRule IDE was developed. It can help build a large knowledge base system with a mix of rules that is useful to practicing lawyers and ordinary people for making legal decisions [22]. Case analysis of numerous companies such as Adam Nguyen, Ned Gannon, and LawGeex shows that these companies are using artificial intelligence technology that dramatically reduces costs and saves time, making it easier to summarize, review, manage, and compare [23]. For the environment of an economic system, the quality of judicial procedures determines the level of the business environment favourable to the development of entrepreneurship and the acceleration of economic growth. Overall, the quality of legal procedures influences the investment attractiveness of the economy [24]. Therefore, they have a cooperative relationship and are interdependent.

3. Problem description

3.1 Model assumptions

The basic assumptions of the evolutionary game model between manufacturers and the court in the use of AI technology for contract performance are as follows:

- R_c represents the court benefit of using AI technology; R_M represents manufacturers' revenues from the use of AI in court; D represents the company's deposits for the use of AI technology in court; $-D$ represents the company's deposits for not using AI technology in the court;
- T_{ai} is the cost of using AI technology in the courtroom; P is the penalty given to manufacturers by the court for breach of contract for using AI technology; L represents losses due to wrongful conviction cases as a result of not using AI technology;
- B is the court's gain from the default when manufacturers breach the contract; H represents the manufacturers' gain in credit enhancement due to the court's use of AI technology.
- α symbolizes the error reduction rate in the AI technology approach; the probability of default not being detected when the AI technology is used by the court is symbolized by β, where $0 \leq \alpha \leq 1$, $0 \leq \beta \leq 1$.
- Suppose x represents the proportion of the court to use AI technology, 1-x represents the proportion of the court that decides not to use AI technology, y represents the proportion of manufacturers that have decided to breach a contract, 1-y represents the proportion of manufacturers that have decided to implement AI technology, with $0 \leq x \leq 1$, $0 \leq y \leq 1$.
- The payment matrix for courts and manufacturing based on the above assumptions is presented in Table 1.

Table 1 Courts and manufacturing companies payment matrix

Court \ Manufacturer	Manufacturer Contract breach	Manufacturer implementation
Use of AI	$R_c - T_{ai} - D + P - \alpha * L, R_M + D - P + \beta * B$	$R_c - T_{ai} - D, R_M + D + H$
No use of AI	$R_c - L, R_M + B$	$R_c, R_M + H$

3.2 Matrix game pay-off

According to the above assumptions described, the analysis of the evolutionary game of court choice is as follows:

(1) Payment when the court chooses to use AI technology strategy:

$$W_1 = y(R_c - T_{ai} - D + P - \alpha * L) + (1 - y)(R_c - T_{ai} - D) \tag{1}$$

Payment when the court chooses to NOT use AI technology strategy:

$$W_2 = y(R_c - L) + (1 - y)(R_c) \tag{2}$$

Average payment of the court:

$$\overline{W} = xW_1 + (1 - x)W_2 \tag{3}$$

Thus, the equation presented below represents the dynamic differential equation of the court:

$$\frac{dx(t)}{dt} = x(W_1 - \overline{W}) = x(1 - x)\{[(1 - \alpha)L + P]y - T_{ai} - D\} \tag{4}$$

and

$$F(x) = x(1 - x)\{[(1 - \alpha)L + P]y - T_{ai} - D\} \tag{5}$$

Therefore,

$$F'(x) = (1 - 2x)\{[(1 - \alpha)L + P]y - T_{ai} - D\} \tag{6}$$

Based on the stability principle: If $F'(x*) < 0$, $x*$ will be in a stable state.

$$\frac{dx(t)}{dt} = 0 \Rightarrow x_1 = 0, \ x_2 = 1, \ y = \frac{T_{ai}+D}{(1-\alpha)L+P}$$

Then, an evolutionary stable state analysis is performed for the three points:

a) When $y = \frac{T_{ai}+D}{(1-\alpha)L+P}$, $\frac{dx(t)}{dt}$ is always zero (0), meaning that x doesn't change over time;

b) When $y > \frac{T_{ai}+D}{(1-\alpha)L+P}$, $F'(x) < 0$, $x = 1$. This is an evolutionary stable state, which means that through continuous imitation and learning, the proportion of the AI technology strategy chosen by the court tends to be 100 %.

c) When $y < \frac{T_{ai}+D}{(1-\alpha)L+P}$, $F'(x) < 0$, $x = 0$. This is an evolutionary stable state, which means that through continuous imitation and learning, the proportion of the court's decision not to choose AI technology strategy tends to be 100 %.

(2) Payment when the manufacturer chooses to breach the contract:

$$U_1 = x[(R_M + D - P + \beta * B] + (1 - x)(R_M + B) \tag{7}$$

Payment when the manufacturer chooses to implement AI technology strategy:

$$U_2 = x[R_M + D + H] + (1 - x)(R_M + H) \tag{8}$$

The manufacturer average payment:

$$\bar{U} = yU_1 + (1 - y)U_2 \tag{9}$$

Thus, the manufacturer enterprise dynamic differential equation:

$$\frac{dx(t)}{dt} = y(U_1 - \bar{U}) = y(1 - y)\{[(\beta - 1)B - P]x + B - H\} \tag{10}$$

and

$$F(y) = y(1 - y)\{[(\beta - 1)B - P]x + B - H\} \tag{11}$$

So,

$$F'(y) = (1 - 2y)\{[(\beta - 1)B - P]x + B - H\} \tag{12}$$

Based on the principle of stability: If $F'(y^*) < 0$, y^* is a stable state.

$$\frac{dy(t)}{dt} = 0 \Rightarrow y_1 = 0, \ y_2 = 1, \ x = \frac{H-B}{(\beta-1)B-P}$$

Then, an evolutionary stable state analysis is performed for the three points:

a) When $x = \frac{H-B}{(\beta-1)B-P}$, $\frac{dx(t)}{dt}$ is always zero (0), meaning that y does not change over time;

b) When $x > \frac{H-B}{(\beta-1)B-P}$, $F'(x) < 0$, $y = 1$. This is an evolutionary stable state, which means that through continuous imitation and learning, the proportion of manufacturer enterprise that chooses to breach the contract tends to be 100 %.

c) When $x < \frac{H-B}{(\beta-1)B-P}$, $F'(x) < 0$, $y = 0$. This is an evolutionary stable state, which means that through continuous imitation and learning, the proportion of manufacturer enterprise that chooses to implement the AI technology strategy tends to be 100 %.

(3) Stability strategy of the evolutionary game system

By combining Eq. 4 and Eq. 10, a system of differential Eq. 13 is obtained, which represents the whole system game evolution process:

$$\begin{cases} \dfrac{dx(t)}{dt} = x(1-x)\{[(1-\alpha)L+P]y - T_{ai} - D\} \\ \dfrac{dy(t)}{dt} = y(1-y)\{[(\beta-1)B-P]x + C - H\} \end{cases} \qquad (13)$$

Make $\begin{cases} \dfrac{dx(t)}{dt} = 0 \\ \dfrac{dy(t)}{dt} = 0 \end{cases}$ to obtain the possible equilibrium point of the system K($0,0$), L($0,1$), M($1,0$), N($1,1$), O$\left(\dfrac{H-B}{(\beta-1)B-P}, \dfrac{T_{ai}+D}{(1-\alpha)L+P}\right)$, which is the Evolutionary Stable Strategy (ESS) point. Based on the method of how to calculate the local stability of the system created by Friedman in 1991, in this paper, the Jacobi matrix of the equations of evolutionary systems can be analyzed [25].

The partial derivatives of the two equations, from Eq. 13, are obtained as shown in Eq. 14.

$$J = \begin{vmatrix} \dfrac{\partial F(x)}{\partial x} & \dfrac{\partial F(x)}{\partial y} \\ \dfrac{\partial F(y)}{\partial x} & \dfrac{\partial F(y)}{\partial y} \end{vmatrix} \qquad (14)$$

$$\frac{\partial F(x)}{\partial x} = (1\text{-}2x)\{[(1-\alpha)L+P]y - T_{ai} - D\} \qquad (15)$$

$$\frac{\partial F(x)}{\partial y} = x(1\text{-}x)[(1-\alpha)L+P] \qquad (16)$$

$$\frac{\partial F(y)}{\partial x} = y(1-y)[(\beta-1)B-P] \qquad (17)$$

$$\frac{\partial F(y)}{\partial y} = (1-2y)\{[(\beta-1)B-P]x + B - H\} \qquad (18)$$

K, L, M, N, and O, the local equilibrium points, are put into the Jacobi matrix and det J and tr J can be obtained to get the Evolutionary Stable Strategy (ESS) of the system.

The matrix determinant is:

$$\det J = \left(\frac{\partial F(x)}{\partial x} \times \frac{\partial F(y)}{\partial y} - \frac{\partial F(y)}{\partial x} \times \frac{\partial F(x)}{\partial y}\right) > 0 \qquad (19)$$

The matrix trace is:

$$\text{tr} J = \left(\frac{\partial F(x)}{\partial x} + \frac{\partial F(y)}{\partial y}\right) < 0 \qquad (20)$$

4. Research method: The evolutionary game phase diagram

The above five points (K, L, M, N, and O) are respectively put into the trace and determinant of the matrix, and further, analyze the strategy behaviour trend and system stability state of the evolutionary game system according to the symbol of sum:

- As shown in Fig. 1, when $x = 0$, $y = 0$, the determinant and trace of matrix J is:

$$\begin{cases} \det J = (-T_{ai} - D)(-1)(B-H) \\ \text{tr} J = (-T_{ai} - D) - (B-H) \end{cases} \qquad (21)$$

and the result is presented in Table 2.

Table 2 Result of (0,0)

$-T_{ai} - D > 0, B - H > 0$	$\det J > 0$，$\operatorname{tr} J > 0$	Instability
$-T_{ai} - D > 0, B - H < 0$	$\det J < 0$，$\operatorname{tr} J$ not sure	Saddle point
$-T_{ai} - D > 0, B - H > 0$	$\det J < 0$，$\operatorname{tr} J$ not sure	Saddle point
$-T_{ai} - D > 0, B - H < 0$	$\det J > 0$，$\operatorname{tr} J < 0$	Stability (ESS)

When the model parameters respectively take the following values: α = 0.5, L = 5, P = 1, T_{ai} = 2, D = 2, β = 1, B = 0.3, H = 2, when the losses due to wrongful convictions are high, and the cost of using AI in court is also slightly high, this gives manufacturers an incentive to breach the contract with the court. The court then tends not to use AI technology. At this time, the ESS point is (contract breach, no use of AI).
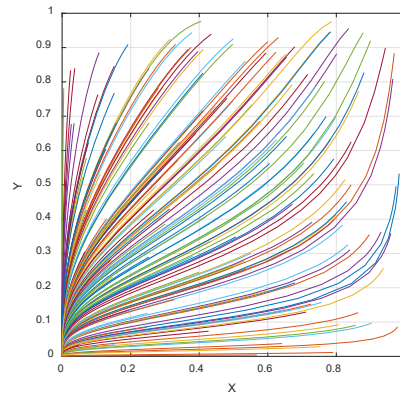
Fig. 1 (0, 0) Evolutionary equilibrium

- As shown in Fig. 2, when $x = 0, y = 1$, the determinant and trace of matrix J is:

$$\begin{cases} \det J = (-1)([(1-\alpha)L + P] - T_{ai} - D)(B - H) \\ \operatorname{tr} J = (B - H) - ([(1-\alpha)L + P] - T_{ai} - D) \end{cases} \tag{22}$$

and the result is presented in Table 3.

Table 3 Result of (0,1)

$[(1-\alpha)L + P] - T_{ai} - D$，$(B - H) > 0$	$\det J < 0$，$\operatorname{tr} J$ Instability	Saddle point
$[(1-\alpha)L + P] - T_{ai} - D > 0$，$(B - H) < 0$	$\det J > 0$，$\operatorname{tr} J > 0$	Instability
$[(1-\alpha)L + P] - T_{ai} - D < 0$，$(B - H) > 0$	$\det J < 0, \operatorname{tr} J < 0$ not sure	Stability (ESS)
$[(1-\alpha)L + P] - T_{ai} - D < 0$，$(B - H) < 0$	$\det (J) > 0, \operatorname{tr} J$ Instability	Saddle point

When the model parameters respectively take the following values: α = 0.7, L = 2, P = 1, T_{ai} = 3, D = 4, β = 1, B = 0.3, H = 1, when the cost of using AI in court is high, and the company's deposits are also high, this tends to force the manufacturers to breach the contract with the court. The court, therefore, chooses not to use AI technology. At this time, the ESS point is (contract breach, no use of AI).
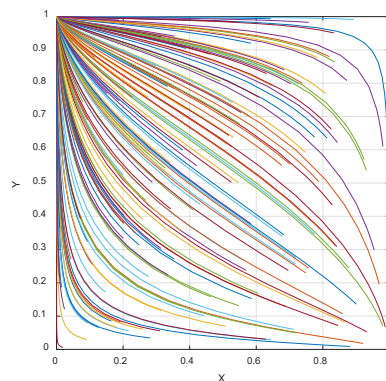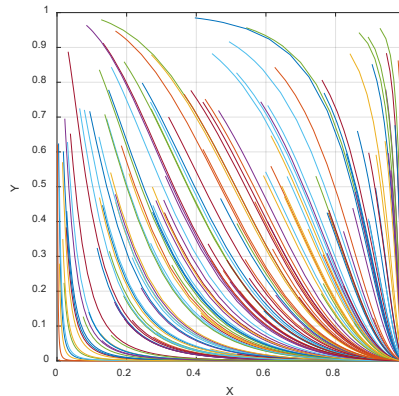

Fig. 2 (0, 1) Evolutionary equilibrium

- As shown in Fig. 3, when $x = 1, y = 0$， the determinant and trace of matrix J is:

$$\begin{cases} \det J = (-1)(-T_{ai} - D)\{[(\beta - 1)B - P] + B - H\} \\ \operatorname{tr} J = \{[(\beta - 1)B - P] + B - H\} - (-T_{ai} - D) \end{cases} \tag{23}$$

and the result is presented in Table 4.

Table 4 Result of (1,0)

$(-T_{ai} - D) > 0$， $\{[(\beta - 1)B - P] + B - H\} > 0$	$\det J < 0, \operatorname{tr} J$ not sure	Saddle point
$(-T_{ai} - D) > 0$， $\{[(\beta - 1)B - P] + B - H\} < 0$	$\det J > 0$， $\operatorname{tr} J < 0$	Stability (ESS)
$(-T_{ai} - D) < 0$， $\{[(\beta - 1)B - P] + B - H\} > 0$	$\det J > 0$， $\operatorname{tr} J > 0$	Instability
$(-T_{ai} - D) < 0$， $\{[(\beta - 1)B - P] + B - H\} < 0$	$\det J < 0, \operatorname{tr} J$ not sure	Saddle point

When the model parameters respectively take the following values: $\alpha = 0.7$, $L = 2$, $P = 1$, $T_{ai} = 1$, $D = 1$, $\beta = 0$, $B = 4$, $H = 6$, the cost of using AI in court is low, which tends to encourage manufacturers to choose implementation. With the low cost of using AI, the court chooses not to use AI technology. At this time, the ESS point is (implementation, no use of AI).

Fig. 3 (1, 0) Evolutionary equilibrium

- As shown in Fig. 4, when $x = 1, y = 1$, the determinant and trace of matrix J is:

$$\begin{cases} \det J = \{[(1 - \alpha)L + P] - T_{ai} - D\}\{[(\beta - 1)B - P] + B - H\} \\ \operatorname{tr} J = (-1)\{[(1 - \alpha)L + P] - T_{ai} - D\} + (-1)\{[(\beta - 1)B - P] + B - H\} \end{cases} \tag{24}$$

and the result is presented in Table 5.

Table 5 Result of (1,1)

$\{[(1 - \alpha)L + P] - T_{ai} - D\} > 0$， $\{[(\beta - 1)B - P] + B - H\} > 0$	$\det J > 0$， $\operatorname{tr} J < 0$	Stability (ESS)
$\{[(1 - \alpha)L + P] - T_{ai} - D\} > 0$， $\{[(\beta - 1)B - P] + B - H\} < 0$	$\det J < 0$， $\operatorname{tr} J$ not sure	Saddle point
$\{[(1 - \alpha)L + P] - T_{ai} - D\} < 0$， $\{[(\beta - 1)B - P] + B - H\} > 0$	$\det J < 0$， $\operatorname{tr} J$ not sure	Saddle point
$\{[(1 - \alpha)L + P] - T_{ai} - D\} < 0$， $\{[(\beta - 1)B - P] + B - H\} < 0$	$\det J > 0$， $\operatorname{tr} J > 0$	Instability

When the model parameters respectively take the following values: $\alpha = 0.5$, $L = 4$, $P = 1$, $T_{ai} = 0.5$, $D = 0.5$, $\beta = 0.5$, $B = 4$, $H = 1$, the cost of using AI in court is low, which tends to encourage manufacturers to choose implementation. The losses due to wrongful convictions and the court's gain from default are high, encouraging the court to choose to use AI technology to improve courtroom efficiency. At this time, the ESS point is recorded (implementation, use of AI).
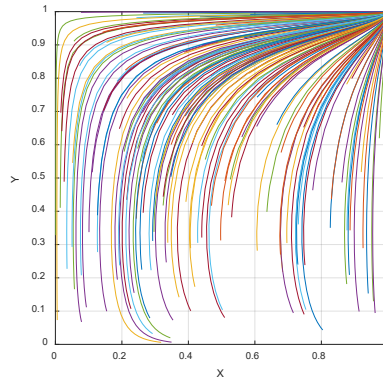
Fig. 4 (1, 1) Evolutionary equilibrium

- Then, since tr $J = 0$, at point O, there is no stable point.

5. Simulation results and discussion

- The influence of the error reduction rate in the AI technology approach on the evolutionary game between both sides is given in Fig. 5.
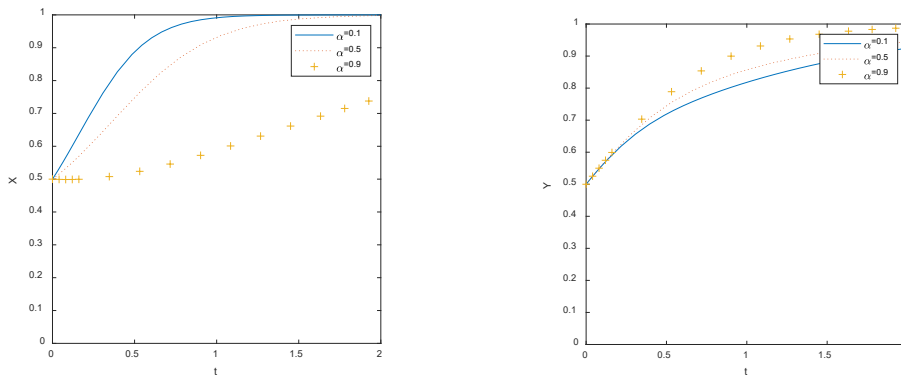

Fig. 5 Different error reduction rates of the court

Figure 5 shows that compared to manufacturers, the value of the error reduction rate has an impact on the court. When the value of the error reduction rate increases, the cost of using AI increases, and the value of the error reduction rate may induce manufacturers to maintain the status quo. However, the court tends to reduce the value of the error reduction rate due to the existence of a speculative effect; manufacturers are stimulated by the value of the error reduction rate, and the lack of use of AI technology tends to slow down.

- The influence of the losses due to wrongful conviction cases on the evolutionary game between both sides is given in Fig. 6.
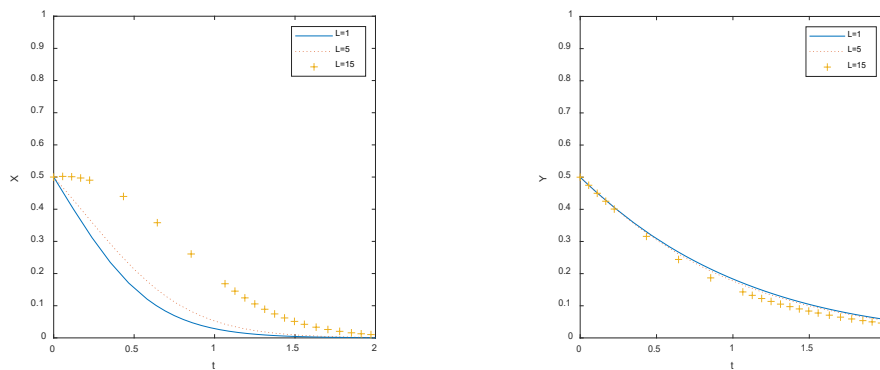
Fig. 6 Different losses due to error conviction cases of the court

Fig. 6 shows that as the value of error conviction cases increases, the court will choose to use AI technology to resolve cases. However, the increase in the value of wrongful conviction losses will not have as much of an effect on the choice of manufacturers who will still choose to breach the contract to reduce their risk of lost profits.

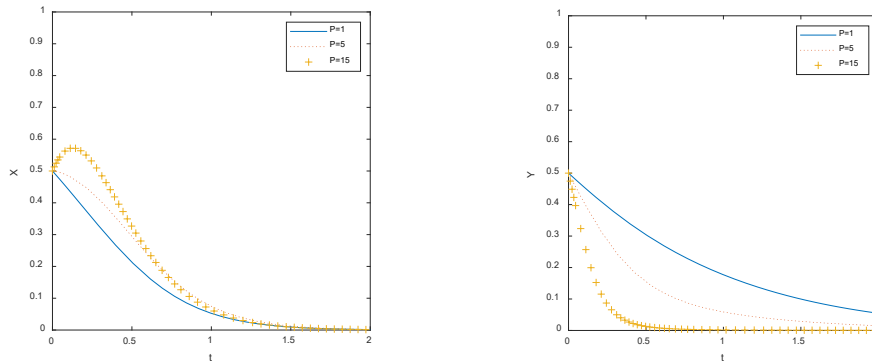- The influence of the penalty for breach of contract on the evolutionary game between both sides is given in Fig. 7.

Fig. 7 Different penalties for breach of contract of manufacturers

From Fig. 7, it can be seen that the increase in the value of the penalties for breach of contract will induce the court to choose the use of AI technology, and after a long time, it will choose not to use AI technology; At the same time, the increase in the value of the penalties for breach of contract will have a slight effect on the decision of the manufacturers but will not make them change their decision on whether to breach the contract.

- The influence of the cost of using AI technology in the courtroom on the evolutionary game between both sides is given in Fig. 8.
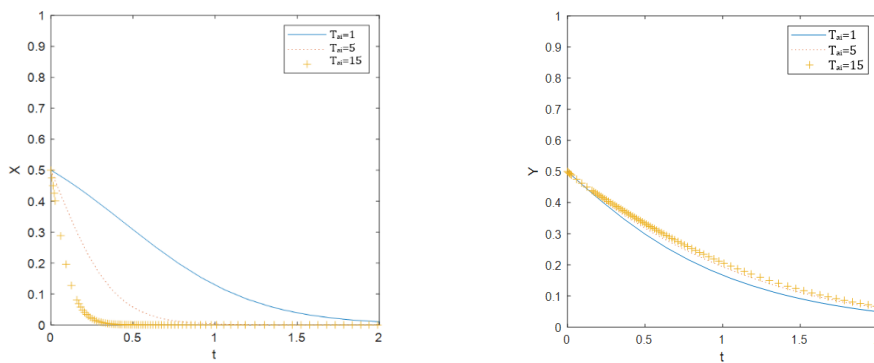
Fig. 8 Different costs of using AI technology of the court

Fig. 8, shows that the increase in the value of the cost of using AI technology will lead manufacturers to breach the contract. With the increase in the value of the cost of using AI technology, the court chooses not to use the AI technology strategy.

- The influence of the cost of using AI technology in the courtroom on the evolutionary game between both sides is given in Fig. 9.

From Fig. 9, it can be seen that the increase in company's deposits will induce manufacturers to implement the use of AI technology, but after a period, they will choose to breach the contract, while the increase in company's deposits will not affect the choice of the court's to not use AI technology strategy.
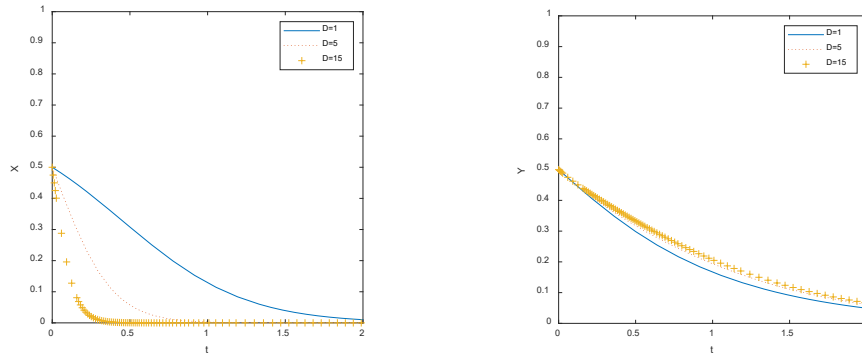
Fig. 9 Different company's deposits

- The influence of the probability of default not being detected on the evolutionary game between both sides is given in Fig. 10.
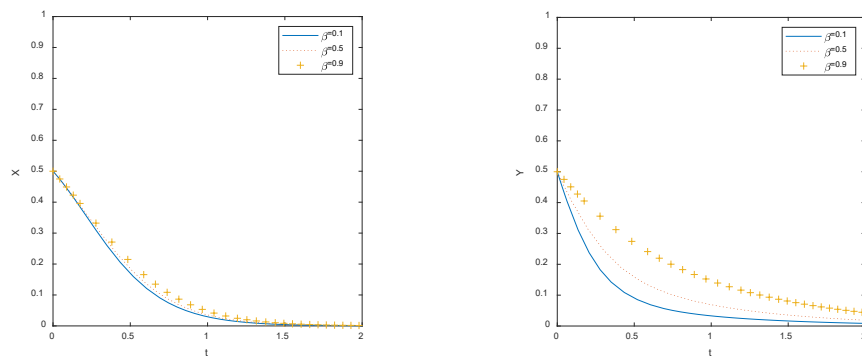

Fig. 10 Different error not being detected probabilities

From Fig. 10, it shows that, with the increase of possibility β of the court's default not being detected, the court tends not to use the strategy of AI technology to avoid losses due to error conviction cases, but the change of the intensity of this measure is not obvious. With the improvement of β, manufacturers will choose to breach the contract, to reduce the possible error penalty.

- The influence of the court's gain from the default on the evolutionary game between both sides is given in Fig. 11.
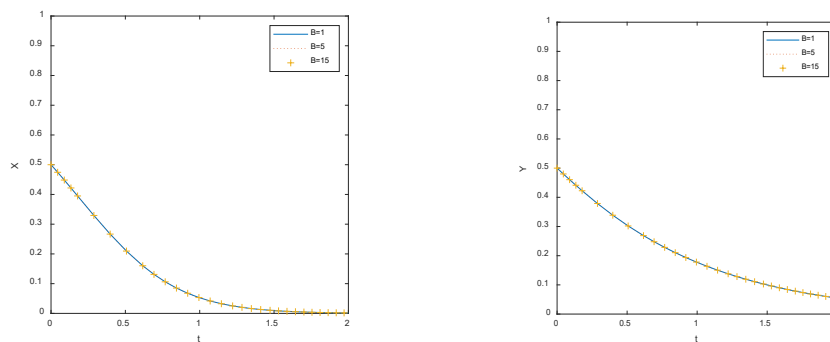

Fig. 11 Different error gains of the court

From Fig. 11, it shows that, with the increase of the error gains (B), the court tends not to use the strategy of AI technology, so that it may get more benefits from the error. With the improvement of B, manufacturers choose to breach the contract.

- The influence of the benefit from credit enhancement on the evolutionary game between both sides is given in Fig. 12.
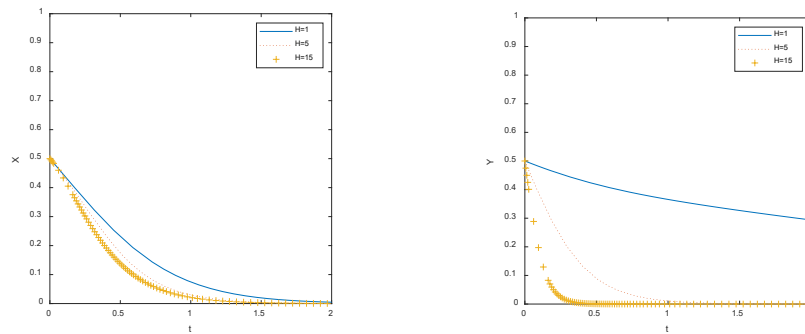
Fig. 12 Different benefits of credit enhancement of manufacturers

It can be seen from Fig. 12 that the increase in credit enhancement benefits for manufacturers will slow down manufacturers' strategy to implement the AI technology strategy, while it will cause the court not to adopt the AI technology strategy.

6. Conclusion

We can see that through the simulation, the evolutionary equilibrium points (0,0) and (1,1) are crossed by the parameter adjustment. The increase in losses due to wrongful convictions shows the determination of the court to use the AI technology strategy. The increase in error reduction rates will stimulate the willingness of manufacturers to choose the AI technology strategy, while the increase in losses due to wrongful convictions and penalties will encourage manufacturers to break the contract. The increased costs of using AI technology and the value of the company's deposits influence manufacturers' decisions and also influence the court's decision whether to use the AI technology strategy to resolve cases. For manufacturers, the increase in the probability of the default not being detected and the increase in the gain from the default do not influence their decision to breach the contract. The evolution of the benefits of credit enhancement plays a role in the court's strategic decision to use AI technology or not, and also influences the decision of manufacturers.

Therefore, by proving that by choosing AI technology to solve problems, the error rate will be minimized, manufacturers will be able to implement this strategy because only the reduction of the error rate has a significant impact on both parties.

Acknowledgement

References

[1] Schutzer, D. (1990). Business expert systems: The competitive edge, *Expert Systems with Applications,* Vol. 1, No. 1, 17-21, doi: 10.1016/0957-4174(90)90065-3.

[2] Park, W., Seo, K.-K. (2020). A study on cloud-based software marketing strategies using cloud marketplace, *Journal of Logistics, Informatics and Service Science,* Vol. 7, No. 2, 1-13, doi: 10.33168/JLISS.2020.0201.

[3] Patalas-Maliszewska, J., Topczak, M. (2021). A new management approach based on Additive Manufacturing technologies and Industry 4.0 requirements, *Advances in Production Engineering & Management,* Vol. 16, No. 1, 125-135, doi: 10.14743/apem2021.1.389.

[4] Thow-Yick, L., Huu-Phuong, T. (1990). Management expert systems for competitive advantage in business, *Information & Management,* Vol. 18, No. 4, 195-201, doi: 10.1016/0378-7206(90)90040-O.

[5] Goyat, R., Kumar, G., Rai, M.K., Saha, R. (2019). Implications of blockchain technology in supply chain management, *Journal of System and Management Sciences,* Vol. 9, No. 3, 92-103.

[6] Sethi, N.A., Karnawat, S.N. (2018). Real time reporting of inventory: An innovation in inventory management, *Journal of Logistics, Informatics and Service Science,* Vol. 5, No. 2, 1-10.

[7] Kohtamäki, M., Parida, V., Oghazi, P., Gebauer, H., Baines, T. (2019). Digital servitization business models in ecosystems: A theory of the firm, *Journal of Business Research,* Vol. 104, 380-392, doi: 10.1016/J.JBUSRES.2019.06.027.

[8]   Zhang, L., Yan, Y., Xu, W., Sun, J., Zhang, Y. (2022). Carbon emission calculation and influencing factor analysis based on industrial big data in the "double carbon" era, *Computational Intelligence and Neuroscience,* Vol. 2022, Article ID 2815940, doi: 10.1155/2022/2815940.

[9]   McKeown, T., Mustafina, J., Magizov, R., Gataullina, C. (2020). AI in law practices, In: *Proceedings of 13th International Conference on Developments in eSystems Engineering (DeSE),* Liverpool, United Kingdom, 27-32, doi: 10.1109/DESE51703.2020.9450780.

[10]   Bai, S.A. (2011). Artificial intelligence technologies in business and engineering, In: *Proceedings of International Conference on Sustainable Energy and Intelligent Systems (SEISCON 2011),* Chennai, India, 856-859, doi: 10.1049/CP.2011.0486.

[11]   Dwivedi, Y.K., Hughes, L., Ismagilova, E., Aarts, G., Coombs, C., Crick, T., Duan, Y., Dwivedi, R., Edwards, J., Eirug, A., Galanos, V., Ilavarasan, P.V., Janssen, M., Jones, P., Kar, A.K., Kizgin, H., Kronemann, B., Lal, B., Lucini, B., Medaglia, R., Le Meunier-FitzHugh, K., Le Meunier-FitzHugh, L.C., Misra, S., Mogaji, E., Sharma, S.K., Singh, J.B., Raghavan, V., Raman, R., Rana, N.P., Samothrakis, S., Spencer, J., Tamilmani, K., Tubadji, A., Walton, P., Williams, M.D. (2019). Artificial Intelligence (AI): Multidisciplinary perspectives on emerging challenges, opportunities, and agenda for research, practice and policy, *International Journal of Information Management,* Vol. 57, Article No. 101994, doi: 10.1016/j.ijinfomgt.2019.08.002.

[12]   Baryannis, G., Dani, S., Validi, S., Antoniou, G. (2019). Decision support systems and artificial intelligence in supply chain risk management, In: Zsidisin, G., Henke, M. (eds.), *Revisiting supply chain risk,* Springer series in supply chain management, Vol 7, Springer, Cham, Switzerland, 53-71, doi: 10.1007/978-3-030-03813-7_4.

[13]   Nehme, E., Salloum, H., Bou Abdo, J., Taylor, R. (2021). AI, IoT, and blockchain: Business models, ethical issues, and legal perspectives, In: Kumar, R., Wang, Y., Poongodi, T., Imoize, A.L. (eds.), *Internet of things, artificial intelligence and blockchain technology,* Springer, Cham, Switzerland, 67-88, doi: 10.1007/978-3-030-74150-1_4.

[14]   Alarie, B., Niblett, A., Yoon, A.H. (2018). How artificial intelligence will affect the practice of law, *University of Toronto Law Journal,* Vol. 68, No. 1, 106-124, doi: 10.3138/UTLJ.2017-0052.

[15]   Vytopil, A.L. (2015). *Contractual control in the supply chain. on corporate social responsibility, codes of conduct, contracts and (avoiding) liability,* Eleven International Publishing, Hague, Netherlands.

[16]   Kim J.B. (2019). Implementation of artificial intelligence system and traditional system: A comparative study, *Journal of System and Management Sciences,* Vol. 9, No. 3, 135-146, doi: 10.33168/JSMS.2019.0309.

[17]   Huo, H., Wang, H.B., Zhang, D.D. (2021). Production management and control based on ant colony optimization and neural network, *International Journal of Simulation Modelling,* Vol. 20, No. 1, 158-169, doi: 10.2507/IJSIMM20-1-CO1.

[18]   Cui, Y. (2020). AI–An effective way to judicial modernization, In: *Artificial intelligence and judicial modernization,* Springer, Singapore, 33-40, doi: 10.1007/978-981-32-9880-4_3.

[19]   Sil, R., Roy, A., Bhushan, B., Mazumdar, A.K. (2019). Artificial intelligence and machine learning based legal application: The state-of-the-art and future research trends, In: *Proceedings of 2019 International Conference on Computing, Communication, and Intelligent Systems (ICCCIS),* Greater Noida, India, 57-62, doi: 10.1109/ICCCIS48478.2019.8974479.

[20]   Dash, R., McMurtrey, M., Rebman, C., Kar, U.K. (2019). Application of artificial intelligence in automation of supply chain management, *Journal of Strategic Innovation and Sustainability,* Vol. 14, No. 3, 43-53, doi: 10.33423/jsis.v14i3.2105.

[21]   De Giovanni, P. (2021). Smart supply chains with vendor managed inventory, coordination, and environmental performance, *European Journal of Operational Research,* Vol. 292, No. 2, 515-531, doi: 10.1016/J.EJOR.2020.10.049.

[22]   Sharma, S., Chaturvedi, (2021). Ethical and legal issues of AI technology and its applications, *International Journal of Law and Legal Jurisprudence Studies,* Vol. 6, No. 1, 49-72.

[23]   Rusakova, E.P., Inshakova, A.O. (2021). Industrial and manufacturing engineering in digital legal proceedings in the asia-pacific region: A new level of quality based on data, blockchain and AI, *International Journal for Quality Research,* Vol. 15, No. 1, 273-290, doi: 10.24874/IJQR15.01-16.

[24]   Naik, M.V., Mohanty, R. (2014). An expert system approach for legal reasoning in acquire immovable property, In: *Proceedings of 2014 First International Conference on Networks & Soft Computing (ICNSC2014),* Guntur, India, 370-374, doi: 10.1109/CNSC.2014.6906664.

[25]   Friedman, D. (1991). Evolutionary games in economics, *Econometrica,* Vol. 59, No. 3, 637-666, doi: 10.2307/2938222.

A two-stage construction heuristic approach for vehicle routing problem with split deliveries and pickups: Case studies and performance comparison

Jin, C.[a], Lu, L.J.[a,b], Min, J.N.[a,*]

[a]School of Economics and Management, Taihu University of Wuxi, Jiangsu, P.R. China
[b]School of Management, Nanjing University, Nanjing 210093, Jiangsu, P.R. China

A B S T R A C T

The vehicle routing problem with split deliveries and pickups is a hot research topic in recent years, where a customer can be served multiple times with split deliveries and pickups. The objective is to minimize the travel distance, use the fewest number of vehicles and increase the load rate, which will further reduce the carbon emissions that damage the environment. In this paper, we use a two-stage construction heuristic approach to solve this problem. First, partitioning algorithms based on the multi-restart-iterative sweep algorithm are adopted to partition the customer domain into sub-domains according to the vehicle capacity, and to determine the split points and the corresponding values. Second, a modified Clarke-Wright savings algorithm is used to check the possibility of each point in each route based on the load of each point and the vehicle load limitation. The three case studies with 12 instances per each from the reconstructed Solomon benchmark datasets were conducted to evaluate the effectiveness and feasibility of the proposed approaches-Unsplit, Both-Split and Enhanced-Both-Split. The comparison among these approaches reveals that the splits reduce the total travel cost and vehicles used, and increase the average loading rate considerably, especially when customers have larger demand values. Our computation results proves that the vehicle routing problem with split deliveries and pickups is highly beneficial for transportation and logistics enterprises.

1. Introduction

1.1 General

The vehicle routing problem (VRP) plays an important role in modern logistics. The vehicle route optimization has a considerable impact on reducing transport distance, the number of transport vehicles and carbon emissions that damage the environment [1-3]. The VRP with simultaneous delivery and pickup (VRPSDP) [4] can reduce the energy consumption that results from the empty return trips of vehicles under the single vehicle delivery or pickup system. It can reduce not only the transport costs that benefit enterprises, but also increase the protection of environments. Therefore, the VRPSDP and its variants have become a popular research topic in logistics. With the relaxation of the constraint imposed on the classic VRPSDP in which each customer can be visited once and only once [5], the delivery and pickup demands of customers can be split (i.e., each customer is allowed to be visited multiple times), and greater vehicle reduction and path

savings can be achieved [6, 7]. Therefore, the VRPs concerning split demands have received increasing attention from researchers. The corresponding problem with only the split delivery is called the split delivery VRP (SDVRP); the corresponding problem splitting both delivery and pickup demands is called the split VRP with deliveries and pickups (SVRPDP). The SVRPDP has three models based on the sequence of deliveries and pickups [8]. In the first model, all pickups are done on the backhaul way after all deliveries, which is similar the VRP with backhauling. In the second model, deliveries and pickups can occur in any sequence on a vehicle route, which is similar to the VRP with mixed deliveries and pickups. In the third model called the VRP with split deliveries and pickups (VRPSPDP), both the delivery and the pickup occur simultaneously (similar to the VRPSDP). This study focuses on this third model and its solution, also on the performance comparisons between the VRPSDP and the VRPSPDP in terms of transportation distances, vehicles used and the load rates which are the important factors affecting transportation costs and environmental costs [9, 10].

In the SDVRP, which was introduced by Dror and Trudeau [5] in 1989, a customer point can be visited multi-times by vehicles via the split deliveries. Therefore, numerous researchers have focused on solutions to the SDVRP problem because this model reduces the distance travelled and the number of vehicles used by splitting customer demands [11-13]. A lengthy article would be needed to present the survey of all researchers in the area; nonetheless, typical theoretical analysis and experimental results can be glimpsed from the previous articles [14-23].

In the VRPSPDP, which was introduced by Mitra [24] in 2005, a vehicle carrying goods within its load-carrying capacity, departs from the depot, delivers the loads to customers en route, and picks up their returnable items; finally, the vehicle returns to the depot with these items within its load-carrying capacity. The VRPSPDP allows an unlimited number of deliveries and pickings up, which means that each customer can be serviced multiple times by the same vehicle or by different vehicles. The goal of [24] is to determine a group of vehicle paths that minimizes the total travel distance under the premise that the load of each path does not exceed the vehicle's load-carrying capacity. To address this problem, a mixed-integer linear programming formulation was proposed [24], and a route construction heuristic was developed based on the cheapest insertion criterion with the fewest vehicles. Subsequently, better solutions have been proposed [25] that employ a parallel clustering technique and a new route construction heuristic. Based on [24, 25], Wang [26, 27] designed two heuristics (viz., the farthest node split load algorithm and competitive decision algorithm) for the VRPSPDP model without the vehicle number limitation and two heuristics (viz., the farthest node full split algorithm and nearest node full split algorithm) for the VRPSPDP model with the vehicle number limitation. Yin *et al.* [28] proposed a VRPSPDP model with two special preconditions: a maximum travel distance constraint and a restriction that each customer's demand should be split only once. Wang *et al.* [29] developed a two-stage heuristic method that integrated the initial heuristic algorithm and a hybrid heuristic algorithm to solve the VRPSPDP. Polat [30] proposed a parallel approach based on the variable neighbourhood search to solve the VRP with divisible deliveries and pickups. Qiu *et al.* [31] developed a tabu search algorithm based on specially designed batch combinations and item creations for the VRPSPDP.

So far, the focus has been mainly on SDVRP solutions, and there have been only few articles on VRPSPDP. Consequently, there is considerable room for improvements in terms of the comprehensive optimization effect, methods and the time spent in solving the VRPSPDP. With these in mind, we propose a two-stage approach based on the principle "clustering first, routing later." The proposed approach will solve the VRPSPDP in as little as possible computation time to reduce the travel distance, the number of vehicles used and increase the loading rate. In the first stage, partitioning algorithms based on the multi-restart-iterative sweep algorithms (MRISA) are adopted to cluster customers into sub-domains and to determine the split points and the corresponding values. In the second stage, a modified Clarke-Wright (C-W) savings algorithm is applied to optimize the travel distance of each route in each cluster. The three case studies with 12 instances per each from the reconstructed Solomon benchmark datasets were adopted to evaluate the effectiveness and feasibility of the proposed approaches, which are used for un-splitting customer demands, splitting both customer deliveries and pickups and fine-tuning splitting both customer deliveries and pickups. The computational results present that the VRPSPDP model is more effective in the

transportation and logistics enterprises than the VRPSDP because of the reduced the total travel distances, the reduced number of vehicles used, and the increased the loading rate.

2. Problem statement

The VRPSPDP mentioned in this paper refers to n customers and m vehicles with the same model in the problem domain. Each vehicle leaves the depot $i = 0$ carrying only the delivery goods that are within its load-carrying capacity $\sum_{i=1}^{n} d_i \leq Q$. Each vehicle delivers d_i and picks up (e.g., recycles) p_i simultaneously along the route for the customers $i \mid i = (1, 2,..., n)$. Finally, the vehicle returns to the depot with only the picked-up goods that are within its load-carrying limit $\sum_{i=1}^{n} p_i \leq Q$. At each customer location, there may be a mixture of goods (deliveries and pickups), and the load on the vehicle may increase or decrease because of simultaneous loading and unloading. Therefore, the load feasibility needs to be checked for each point along a route. The distance between the customers i and j is c_{ij}; there is no $c_{ii} = 0$ loop, and the path is undirected $c_{ij} = c_{ji}$. The quantity of deliveries between the customers i and j is $0 \leq d_{ij} \leq Q$, and the quantity of pickups between the customers i and j is $0 \leq p_{ij} \leq Q$. Each customer may have both delivery and pickup demands, either of which may exceed the vehicle's load-carrying capacity. Each customer's deliveries and pickups can be split; that is, each customer can be visited by multiple vehicles or by the same vehicle multiple times. If the vehicle k travels from the customer i to j, then x_{ijk} is equal to 1; otherwise $x_{ijk} = 0$. If the customer i is served by the vehicle k, then y_{ik} is equal to 1; otherwise, $y_{ik} = 0$. The minimum number of vehicles used is $\lceil max (\sum_{i=1}^{n} d_i , \sum_{i=1}^{n} p_i)/Q \rceil$, where x denotes the smallest integer that is equal to or greater than x [24, 25]. For the sake of simplicity, we assume that there is no time window limit and no limit on the maximum driving time and distance. The goal is to minimize the total driving distance using few vehicles and keeping a high load rate to meet the demands of all the customers.

The formulation [32] is given as:

$$min \sum_{i=0}^{n} \sum_{j=0}^{n} \sum_{k=1}^{m} c_{ij} \, x_{ijk} \tag{1}$$

s. t.

$$\sum_{k=1}^{m} d_{0j} \, y_{jk} = d_j, j = 1,2, \dots , n; \tag{2}$$

$$\sum_{k=1}^{m} p_{j0} \, y_{jk} = p_j, j = 1,2, \dots , n; \tag{3}$$

$$\sum_{i=1}^{n} d_{0i} \, y_{ik} \leq Q, k = 1,2, \dots , m; \tag{4}$$

$$\sum_{i=1}^{n} p_{i0} \, y_{ik} \leq Q, k = 1,2, \dots , m; \tag{5}$$

$$\sum_{i=0}^{\theta} p_i \, y_{ik} + \sum_{i=\theta+1}^{n} d_i \, y_{ik} \leq Q, i = 0,1, \dots \theta, \theta + 1, \dots , n; \; k = 1,2, \dots , m; \tag{6}$$

$$\sum_{i=0}^{n} d_{i0} = 0; \tag{7}$$

$$\sum_{i=0}^{n} p_{0i} = 0; \tag{8}$$

$$\sum_{i=1}^{n-1} \sum_{j=i+1}^{n} (x_{ijk} - x_{j(j+1)k}) = 0, k = 1,2,\dots,m; \tag{9}$$

$$\sum_{j=0}^{n} x_{0jk} = 1, \sum_{j=0}^{n} x_{j0k} = 1, \ k = 1,2,\dots,m; \tag{10}$$

Eq. 1 is the objective function to minimize the total travel distance. Eq. 2 and 3 are the customer demand constraints to ensure that the delivery/pickup demands of the customer j are satisfied by multiple visits. Eq. 4 and 5 are the vehicle-loading constraints to ensure that the delivery/pickup quantities of a vehicle in one tour do not exceed the vehicle's load-carrying capacity. Eq. 6 is the real-time vehicle-loading constraint [32], which is used to check the fluctuating load on every point of each route; this constraint ensures that the gross load of both the delivery and pickup at any node will not exceed the vehicle capacity in one tour. The sum of the picked-up quantity at the customer node θ (including node θ) and the delivery quantity after the customer node θ (starting from node $\theta + 1$) along the route of the vehicle k cannot exceed the vehicle capacity. Eq. 7 and 8 are the depot load-type constraints to ensure that no delivery loads are directed to the depot and no pickup loads come from the depot. Eq. 9 is the vehicle access conservation constraint to ensure that a vehicle that arrives at the customer location j also leaves this location. Eq. 10 states the depot access restriction that each vehicle enters/exits the depot only once per tour.

3. A two-stage approach

A two-stage approach based on "clustering first and routing later" is proposed to solve the VRP-SPDP. In the first stage, partitioning algorithms based on the MRISA are employed to partition customers into some clusters and to ascertain the split points and the corresponding values. In the second stage, a modified C-W savings algorithm that satisfies the customer particular double requirements is adopted to optimize the travel distance.

3.1 Initialization of the coordinate system

A sweep algorithm proposed by Gillett and Miller in 1974 [33] groups the nearest points into a cluster under certain preconditions. It is performed in a polar coordinate system, so that the rectangular coordinate system needs to be transformed into a polar coordinate system, all points have to be sorted in ascending or/and descending order [34], and a set of variables *optimal* should be defined to store the best distance and the corresponding customer points (i.e., the points and their deliveries and pickups) and the split points (i.e., the split points and the corresponding values) in each cluster.

3.2 Sweep algorithm for the VRPSDP

The sweep algorithm for the VRPSDP (SA-VRPSDP), which satisfies the delivery/pickup double demands, is the modification of the basic sweep algorithm. In the VRPSDP, a vehicle visits a point only once; therefore, the customer demands cannot be split. Thus, SA-VRPSDP is also called SA-Unsplit. In addition, before the clustering, the delivery or pickup demand of each point needs to be checked to ensure that this demand is less than the vehicle's load-carrying capacity Q. If $d_i, p_i \geq Q$, the quantity Q would be individually delivered or picked-up. The remaining part would participate in SA-VRPSDP. The SA-Unsplit procedure is described as follows.

Step 1: Specify one point as the first starting point.
Step 2: SA-Unsplit (Partitioning of the customer area).
a) Sweep points gradually into an initial cluster in one direction (clockwise or anticlockwise). Three possible cases arise at point i.
Case 1: When (($MCV_d^i < Q$) and ($MCV_p^i < Q$)), continue to sweep points gradually into this cluster.

Case 2: When $((MCV_d^i = Q)$ or $(MCV_p^i = Q))$, the point i becomes the last point lp of this cluster, and record lp and this cluster. There are following three situations:

- If $((MCV_d^i = Q)$ and $(MCV_p^i = Q))$, then denote as $((MCV_d^{lp} = Q)$ and $(MCV_p^{lp} = MCV_p^i))$.
- If $((MCV_d^i = Q)$ and $(MCV_p^i < Q))$, then denote as $((MCV_d^{lp} = Q)$ and $(MCV_p^{lp} = MCV_p^i))$.
- If $((MCV_d^i < Q)$ and $(MCV_p^i = Q))$, then denote as $((MCV_d^{lp} = MCV_d^i)$ and $(MCV_p^{lp} = Q))$.

Case 3: When $((MCV_d^i > Q)$ or $(MCV_p^i > Q))$, the point preceding i becomes the lp of this cluster, and record lp and this cluster. The following three situations are possible:

- If $((MCV_d^i > Q)$ and $(MCV_p^i > Q))$, then denote as $((MCV_d^{lp} = MCV_d^i - d_i)$ and $(MCV_p^{lp} = MCV_p^i - p_i))$.
- If $((MCV_d^i > Q)$ and $(MCV_p^i < Q))$, then denote as $((MCV_d^{lp} = MCV_d^i - d_i)$ and $(MCV_p^{lp} = MCV_p^i - p_i))$.
- If $((MCV_d^i < Q)$ and $(MCV_p^i > Q))$, then denote as $((MCV_d^{lp} = MCV_d^i - d_i)$ and $(MCV_p^{lp} = MCV_p^i - p_i))$.

b) Taking the next point of lp as the first starting point of the next cluster, repeat Step 2 a) until the endpoint is swept.

c) Calculate the total travel distance ttd of every cluster based on the spatial distribution of the points.

d) Compare the ttd with the value in the *optimal*, and store the smaller value and the corresponding points (the customer points and the split points) into the *optimal* variables.

Step 3: End the SA-Unsplit procedure.

3.3 Sweep algorithm for the VRPSPDP

In the VRPSPDP, the constraint imposed on the VRPSDP that a customer point can be visited only once for both delivery and pickup, is relaxed. Therefore, a point can be visited more than once, and the customer demands of both delivery and pickup can be split. The sweep algorithm for VRPSPDP (SA-VRPSPDP) is then employed to determine the split points and the split values in each cluster of the VRPSPDP. It is also called SA-Both-Split. The SA-Both-Split procedure of is described in the following.

Step 1: Specify one point as the first starting point.
Step 2: SA-Both-Split (Partitioning of the customer area).

a) Sweep points gradually into an initial cluster in one direction (clockwise or anticlockwise) until $\lceil max(\sum_{i=1}^i d_i, \sum_{i=1}^i p_i) \geq Q \rceil$ reaches point i, the point i becomes the last point lp of this cluster. The following four cases can arise:

Case 1: When $((MCV_d^i = Q)$ or $(MCV_p^i = Q))$, record lp and this cluster. There are three situations.

- If $((MCV_d^i = Q)$ and $(MCV_p^i = Q))$, then denote as $((MCV_d^{lp} = Q)$ and $(MCV_p^{lp} = Q))$.
- If $((MCV_d^i = Q)$ and $(MCV_p^i < Q))$, then denote as $((MCV_d^{lp} = Q)$ and $(MCV_p^{lp} = MCV_p^i))$.
- If $((MCV_p^i = Q)$ and $(MCV_d^i < Q))$, then denote as $((MCV_d^{lp} = MCV_d^i)$ and $(MCV_p^{lp} = Q))$.

Case 2: When $((MCV_d^i > Q)$ and $(MCV_p^i < Q))$, split lp into $lp1$ and $lp2$, and end the grouping at the point $lp1$. Then, there are $MCV_d^{lp1} = Q$, $d_{lp2} = MCV_d^{lp} - Q$, $MCV_p^{lp1} = $

MCV_p^i and $p_{lp2} = 0$. Record lp, d_{lp1}, d_{lp2}, p_{lp1}, p_{lp2} and this cluster; $lp2$ becomes the starting point of the next clustering.

Case 3: When $((MCV_d^i < Q)$ and $(MCV_p^i > Q))$, split lp into $lp1$ and $lp2$, and end the grouping at the point $lp1$. Then, there are $MCV_d^{lp1} = MCV_d^i$, $d_{lp2} = 0$, $MCV_p^{lp1} = Q$ and $p_{lp2} = MCV_p^{lp} - Q$. Record lp, d_{lp1}, d_{lp2}, p_{lp1}, p_{lp2} and this cluster; $lp2$ becomes the starting point of the next clustering.

Case 4: When $((MCV_d^i > Q)$ and $(MCV_p^i > Q))$, split lp into $lp1$ and $lp2$, and end the grouping at the point $lp1$. Then, $MCV_d^{lp1} = Q$, $d_{lp2} = MCV_d^i - Q$, $MCV_p^{lp1} = Q$, and $MCV_p^{lp2} = MCV_p^i - Q$. Record lp, d_{lp1}, d_{lp2}, p_{lp1}, p_{lp2} and this cluster; $lp2$ becomes the starting point of the next clustering.

b) Taking $lp2$ (with the demand d_{lp2} and p_{lp2}) as the starting point of the next cluster, repeat Step 2 until the endpoint is swept.

c) Calculate the total travel distance *ttd* of every cluster based on the spatial distribution of points.

d) Compare the *ttd* with the value in *optimal* variables, and store the smaller values and the corresponding points (the customer points and the split points) in the *optimal* variables.

Step 3: End the SA-Both-Split procedure.

3.4 Multi-restart-iterative mode

When SA-Unsplit and SA-Both-Split are performed in the multi-restart-iterative (MRI) mode, the operations are called MRISA-Unsplit and MRISA-Both-Split, respectively.

- MRISA-Unsplit: Execute the SA-Unsplit procedure from each customer point (0-*n*) successively in the clockwise and anticlockwise directions to partition the customer area.
- MRISA-Both-Split: Execute the SA-Both-Split procedure from each customer point (0-*n*) successively in the clockwise and anticlockwise directions to partition the customer area.

The smallest *ttd* in the *optimal* is extracted, and the corresponding cluster becomes the most appropriate customer sub-domains.

3.5 Route optimization in a cluster

After the operations described above, there is one route in each cluster, and each customer point has both delivery and pickup demands simultaneously. Therefore, the routing problem becomes a VRPSDP. A modified C-W algorithm is adopted as follows [32]:

Step 1: Form an initial solution set $L = \{L_i\}$, $\forall i \in \{1, 2, 3, ..., n\}$, where L_i states one point i.

Step 2: Compute the distance-saving degree of point-pair (i, j) $\Delta c_{ij} = c_{0i} + c_{0j} - \Delta c_{ij}$. Sort Δc_{ij} $(i, j = 1, 2, ..., n)$ in descending order Dc_{ij}.

Step 3: Initialize the new route set $L_0' = \emptyset$ and the load quantity set $R_0' = 0$ for both the delivery demands d_i and pickup demands p_i.

Step 4: Scan the descending order Dc_{ij} from the top to the bottom and stop at the bottom.

Step 5: Look for the merge possibility of point-pairs according to the following discriminant conditions during scanning.

a) Go to the next point-pair in the descending order Dc_{ij} if both points i and j are not on the route, that is, $L_i \not\subset L_0'$ and $L_j \not\subset L_0'$.

b) Go to the next point-pair in the descending order Dc_{ij} if both points i and j are on the route, that is, $L_i \subseteq L_0'$ and $L_j \subseteq L_0'$.

c) Merge one point i or j, which is not in L_0', that is, $(L_i \cup L_0')$ or $(L_j \cup L_0')$, and calculate the route distance if one point j or i is on the route, that is, $L_j \subseteq L_0'$ or $L_i \subseteq L_0'$. This can give rise to four scenarios:

- Merging point j behind point i if i is the end of the route.
- Merging point j before point i if i is the beginning of the route.

- Merging point i behind point j if j is the end of the route.
- Merging point i before point j if j is the beginning of the route.

d) Check the load feasibility for every point of each route because the gross load of the vehicle fluctuates with increasing or decreasing loads along the route. If the load in the current route meets the following conditions, go to the next point-pair; otherwise, delete all operations in Step 5 and return to Step 4. This leads to the following scenarios:

- The load quantity at the starting point is equal to $R'_{s0} = \sum_{i=1}^{n} d_i\, y_{ik} \leq Q$.
- The load quantity at the end point is equal to $R'_{e0} = \sum_{i=1}^{n} p_i\, y_{ik} \leq Q$.
- The load quantity at the current point i is equal to $R'_{0,i} = R'_{0,i} - d_i + p_i + R'_{(i+1),0} \leq Q$, that is $R'_{0,i} = R'_{s0} - \sum_{i=1}^{i-1} d_i\, y_{ik} - d_i + \sum_{i=1}^{i-1} p_i\, y_{ik} + p_i \leq Q$.

4. Case studies

Computational experiments were performed to verify the feasibility and effectiveness of the proposed algorithms in reducing travel distances and the number of vehicles used, and increasing the loading rates. The executed results of the VRPSPDP and the VRPSDP were compared to determine which heuristic performs better than others. The 25-, 50-, and 100-customer datasets were chosen from the Solomon datasets of VRP Web [35]. However, the Solomon datasets cannot be used directly in the VRPSPDP model because they do not include the pickup demand data. The delivery and pickup demands in a new constructed dataset come from two different original datasets. For example, for the new constructed dataset CR101, the delivery is from C101, and the pickup is from R101. The experiments were implemented using C in a 64-bit Windows 7 machine with an Intel (R) Core processor of 2.50 GHz speed and 8 GB memory as in [32].

4.1 Execution on the constructed Dataset 1

Our initial experiment was performed on the constructed Dataset 1. The results of MRISA-Both-Split + Modified C-W (hereinafter B-Split) for the VRPSPDP and MRISA-Unsplit + Modified C-W (hereinafter Unsplit) for the VRPSDP are shown in Table 1. Here, the distance reduction (ΔDist. %) and the route reduction (ΔRt. %) are respectively given as follows:

$$\Delta_{\text{B-Split to Unsplit}} \text{Dist. \%} = |(\text{Dist. of B-Split} - \text{Dist. of Unsplit})|/(\text{Dist. of Unsplit}) \times 100\ \% \qquad (11)$$

$$\Delta_{\text{B-Split to Unsplit}} \text{Rt. \%} = |(\text{Rt. of B-Split} - \text{Rt. of Unsplit})|/(\text{Rt. of Unsplit}) \times 100\ \%. \qquad (12)$$

The results do not show any benefits for B-Split as compared with Unsplit. We note the following points:

- The average ΔDist % of the B-Split is 1.95 %, and ΔDist % is between 0.0 % and 3.76 %.
- The average ΔRt. % of the B-Split is 0.0 %.

Table 1 Results for the constructed Dataset 1 (Q = 200 kg)

Instance	Demands (D/P) kg	B-Split				Unsplit	
		Distance (m)	Route	ΔDist. %	ΔRt. %	Distance (m)	Route
CR101-25	460/332	236	3	3.28	0	244	3
CR201-25	460/332	266	3	2.21	0	272	3
R_C101-25	332/460	395	3	2.95	0	407	3
RCR101-25	540/332	311	3	2.81	0	320	3
CR101-50	860/721	488	5	0.61	0	491	5
CR201-50	860/721	633	5	2.91	0	652	5
R_C101-50	721/860	677	5	0.00	0	677	5
RCR101-50	970/721	580	5	0.68	0	584	5
CR101-100	1810/1458	976	10	3.27	0	1009	10
CR201-100	1810/1458	1034	10	0.48	0	1039	10
R_C101-100	1458/1810	1032	10	0.39	0	1036	10
RCR101-100	1724/1458	1406	9	3.76	0	1461	9
Average	—	—	—	1.95	0	—	—

Note: Demand (D/P) denotes Deliveries/Pickups.

These results might be the consequence of the average demand values being too small in the original constructed dataset with average values being 8.96 %, 8.53 %, and 8.50 % of the vehicle capacity for the deliveries and 7.28 %, 7.56 %, and 7.73 % of the vehicle capacity for the pickups in the 25-, 50-, and 100-customer cases, respectively. All these values are below 9 % of the vehicle capacity.

4.2 Execution on the constructed Dataset 2

To verify the benefits of splitting, we constructed Dataset 2 from the Dataset 1. We retained the data locations but changed the delivery and pickup values by multiplying all the values by 4 and adding $0.1 \times Q$ to all the points; here, Q denotes the capacity of the vehicle. Thus, Dataset 2 had delivery and pickup values between 12 % and 110 % of the vehicle capacity with average values of 45.84 %, 44.11 %, and 44.01 % of the vehicle capacity for the deliveries, and 39.12 %, 40.23 %, and 40.92 % of the vehicle capacity for the pickups in the 25-, 50-, and 100- customer cases, respectively.

The results of applying B-Split and Unsplit to the Dataset 2 are shown in Table 2. Here, the load rate increase (Δ Lr. %) is given as follows:

$$\Delta_{\text{B-Split to Unsplit}} \text{Lr. \%} = |(\text{Lr. of B-Split} - \text{Lr. of Unsplit})| / (\text{Lr. of Unsplit}) \times 100\% \qquad (13)$$

The results show that B-Split has obvious advantages over Unsplit:

- The ΔDist.% of the B-Split lies between 3.71 % and 16.66 %, with an average of 11.64 %. This distance reduction directly decreases the transportation cost.
- The ΔRt. % of the B-Split lies between 12.50 % and 25.40 %, with an average of 20.71 %. Thus, the vehicle start up fee, manpower costs and the transportation cost will decrease with the reduction of the number of vehicles required.
- The ΔLr. % of the B-Split lies between 14.46 % and 33.80 %, with an average of 26.72 %. Therefore, the number of vehicles used will decrease with increasing load rate, and the transportation cost will be also reduced.
- The resulting routes are shaped like a petal around the depot. The beginning and end points of most routes are split.

Table 2 Results obtained for Dataset 2 (Q = 200 kg)

Instance	Demand (D/P), kg	B-Split						Unsplit		
		Dist., m	Rt.	Lr.	ΔDist. %	ΔRt. %	ΔLr. %	Dist., m	Rt.	Lr.
CR101-25	2340/1828	643	12	0.98	10.57	14.29	16.67	719	14	0.84
CR201-25	2340/1828	782	12	0.98	4.98	14.29	16.67	823	14	0.84
R_C101-25	1828/2340	831	12	0.98	8.98	25.00	34.25	913	16	0.73
RCR101-25	2660/1828	1246	14	0.95	3.71	12.50	14.46	1294	16	0.83
CR101-50	4440/3884	1356	23	0.97	14.93	20.69	25.97	1594	29	0.77
CR201-50	4440/3884	1592	23	0.97	10.66	20.69	25.97	1782	29	0.77
R_C101-50	3884/4440	1685	24	0.93	8.32	20.00	25.68	1838	30	0.74
RCR101-50	4880/3884	2354	25	0.98	16.61	21.88	28.95	2823	32	0.76
CR101-100	9240/7832	3437	48	0.96	16.66	25.00	33.33	4124	64	0.72
CR201-100	9240/7832	3648	48	0.96	15.73	25.00	33.33	4329	64	0.72
R_C101-100	7832/9240	3280	48	0.96	12.88	23.81	31.51	3765	63	0.73
RCR101-100	8896/7832	4021	47	0.95	15.60	25.40	33.80	4764	63	0.71
Average	—	—	—	—	11.64	20.71	26.72	—	—	—

Note: Demand (D/P) denotes Deliveries/Pickups; Dist. denotes Distance; Rt. denotes Route; Lr. denotes Load rate.

4.3 Execution on the constructed Dataset 3

We constructed Dataset 3 from Dataset 1 to better show the benefits of the splitting. We retained the locations from Dataset 1 but changed the delivery and pickup values by adding $0.75 \times Q$ and $0.2 \times Q$ to the delivery and pickup at each odd point and adding $0.2 \times Q$ and $0.75 \times Q$ to the delivery and pickup at each even point [32]. Thus, Dataset 3 had demand values for either delivery or pickup between 20.5 % and 100 % of the vehicle capacity. In the 25-, 50-, and 100-customer cases, the average values were 57.56 %, 56.03 %, and 56.00 % of the vehicle capacity for the deliveries and 53.68 %, 55.06 %, and 55.23 % of the vehicle capacity for the pickups, respectively.

Further, in Cases 2 and 3 of the B-Split, the split of the last point lp depends only on max ($\sum_{i=1}^{i} d_i$, $\sum_{i=1}^{i} p_i$), regardless of how much min ($\sum_{i=1}^{i} d_i$, $\sum_{i=1}^{i} p_i$) differs from Q. This may affect the vehicle load rate, resulting in an increase in the number of vehicles used. Therefore, a coefficient of fine-tuning is introduced to control the "difference," and to form an Enhanced Both-Split (hereinafter E-B-Split). If ($\sum_{i=1}^{i} X_i < coef \times Q$), where X indicates min ($\sum_{i=1}^{i} d_i$, $\sum_{i=1}^{i} p_i$), then the clustering does not terminate on X at the point i and the sweeping continues; If ($\sum_{i=1}^{i} X_i \geq coef \times Q$), then the clustering terminates on X at the point i and the sweeping stops. This implies that d (delivery) and p (pickup) could have separate partition termination points. In E-Both-Split, Cases 2 is given as follows:

*Case 2: When (($MCV_d^i > Q$) and ($MCV_p^i < Q$)) at point i,
- If (($MCV_d^i > Q$) and ($MCV_p^i = ef \times Q$)), and point i is the last point lp for both deliveries and pickups, then split lp into $lp1$ and $lp2$, end the current cluster on both the deliveries and pickups, and start the next clustering at $lp2$. Therefore, $MCV_d^{lp1} = Q$; $d_{lp2} = MCV_d^{lp} - Q$; $d_{lp1} = d_{lp} - d_{lp2}$; $MCV_p^{lp1} = MCV_p^i = ef \times Q$ and $p_{lp2} = 0$.
- If (($MCV_d^i > Q$) and ($MCV_p^i < ef \times Q$)), and point i is the last point lp on the deliveries, split the delivery into $lp1$ and $lp2$, and end the current cluster on delivery. There are $MCV_d^{lp1} = Q$; $d_{lp2} = MCV_d^{lp} - Q$ and $d_{lp1} = d_{lp} - d_{lp2}$. Go to the next i and continue to sweep. Three situations can arise on ($MCV_p^i + p_{i+1}$):
  - If (($MCV_p^i + p_{i+1}) > ef \times Q$), and point $i + 1$ is the lp on the pickup, split the point, and end the cluster on the pickup. Then, $MCV_p^{lp1} = Q$; $p_{lp2} = (MCV_p^i + p_{i+1}) - Q = MCV_p^{lp} - Q$ and $p_{lp1} = p_{lp} - p_{lp2}$.
  - If (($MCV_p^i + p_{i+1}) = ef \times Q$), then point $i + 1$ is the lp on the pickup, and the current cluster is ended on the pickup. Thus, $MCV_p^{lp1} = MCV_p^{lp} = Q$ and $p_{lp2} = 0$.
  - If (($MCV_p^i + p_{i+1}) < ef \times Q$), then continue to sweep.
*Case 3 has the same operations as *Case 2, but only d and p are swapped.

Table 3 shows the results of applying the MRISA-E-Both-Split + Modified C-W (hereinafter E-B-Split), B-Split, and Unsplit to Dataset 3. Table 4 presents the comparisons among the results of E-B-Split, B-Split, and Unsplit.

The results prove that the E-B-Split has significant advantages over the other two algorithms (especially as compared with Unsplit). The main advantages are as follows:

- The ∆Dist. % of the E-B-Split as compared with the Unsplit lies between 30.65 % and 38.35 %, with an average of 33.92%. The ∆Dist. % of the E-B-Split as comparison with the B-Split lies between 12.53 % and 24.23 %, with an average of 17.38 %. The ∆Dist. % of the B-Split relative to the Unsplit lies between 11.66 % and 26.85 %, with an average of 19.89 %. This distance reduction shown as Fig. 1 would directly decrease the transportation cost.
- The average load rate obtained by the E-B-Split, B-Split, and Unsplit are 0.96, 0.89, and 0.57, respectively. The ∆Lr. % of the E-B-Split as compared with the Unsplit lies between 65.52 % and 73.21 %, with an average of 68.83 %. The ∆Lr. % of the E-B-Split in comparison with the B-Split lies between 0.0 % and 13.79 %, with an average of 8.65 %. The ∆Lr. % of the B-Split relative to Unsplit lies between 47.46 % and 66.07 %, with an average of 55.53 %. This load rate increase shown as Fig. 2 would directly decrease the number of vehicles used.
- The number of routes in Unsplit is equal to the number of points, that is, one route corresponds to one point. The number of routes in the E-B-Split is reduced by approximately 40.75 % on the average as compared with the number of routes in Unsplit. The number of routes in B-Split is reduced by approximately 36 % on average as compared with the number of routes in Unsplit shown as Fig. 3. Therefore, by applying the E-B-Split, the number of vehicles and manpower costs can be reduced, which will substantially decrease the transportation cost.

- The resulting routes are shaped like a petal around the depot, and a point splitting often occurs at the beginning or the end of sub-domains in the sweeping procedure.
- When the E-B-Split is applied, there might be two splitting points between two adjacent routes: one for deliveries and another for pickups.

Table 3 Results obtained for Dataset 3 (Q = 200 kg)

Instance	Demand (D/P), (kg)	E-B-Split			B-Split			Unsplit		
		Dist. (m)	Rt.	Lr.	Dist. (m)	Rt.	Lr.	Dist. (m)	Rt.	Lr.
CR101-25	2890/2652	734	0.96	15	891	0.90	16	1132	0.58	25
CR201-25	2890/2652	880	0.96	15	1091	0.90	16	1275	0.58	25
R_C101-25	2762/2780	859	0.93	15	982	0.93	15	1246	0.56	25
RCR101-25	2970/2652	1217	0.99	15	1485	0.87	17	1887	0.59	25
CR101-50	5610/5471	1555	0.97	29	1807	0.91	31	2411	0.56	50
CR201-50	5610/5471	1778	0.97	29	2250	0.88	32	2679	0.56	50
R_C101-50	5471/5610	1757	0.94	30	2319	0.83	34	2625	0.56	50
RCR101-50	5720/5471	2503	0.95	30	2970	0.87	33	4060	0.57	50
CR101-100	11310/10958	3724	0.98	58	4455	0.90	63	5771	0.57	100
CR201-100	11310/10958	3942	0.98	58	4773	0.88	64	5943	0.57	100
R_C101-100	10958/11310	3460	0.96	59	4156	0.87	65	4989	0.57	100
RCR101-100	11224/10958	4372	0.94	60	5182	0.88	64	6618	0.56	100
Average	—	—	0.96	34.42	—	0.89	38	—	0.57	58

Note: Demand (D/P) denotes Deliveries/Pickups; Dist. denotes Distance; Rt. denotes Route; Lr. denotes Load rate.

Table 4 Comparisons of E-B-Split, B-Split and Unsplit

Instance	E-B-Split to Unsplit (%)			E-B-Split to B-Split (%)			B-Split to Unsplit (%)		
	ΔDist.	ΔLr.	ΔRt.	ΔDist.	ΔLr.	ΔRt.	ΔDist.	ΔLr.	ΔRt.
CR101-25	35.16	65.52	40	17.62	6.67	6.25	21.29	55.17	36
CR201-25	30.98	65.52	40	19.34	6.67	6.25	14.43	55.17	36
R_C101-25	31.06	66.07	40	12.53	0	0.00	21.19	66.07	40
RCR101-25	35.51	67.80	40	18.05	13.79	11.76	21.30	47.46	32
CR101-50	35.50	73.21	42	13.95	6.59	6.45	25.05	62.50	38
CR201-50	33.63	73.21	42	20.98	10.23	9.38	16.01	57.14	36
R_C101-50	33.07	67.86	40	24.23	13.25	11.76	11.66	48.21	32
RCR101-50	38.35	66.67	40	15.72	9.2	9.09	26.85	52.63	34
CR101-100	35.47	71.93	42	16.41	8.89	7.94	22.80	57.89	37
CR201-100	33.67	71.93	42	17.41	11.36	9.38	19.69	54.39	36
R_C101-100	30.65	68.42	41	16.75	10.34	9.23	16.70	52.63	35
RCR101-100	33.94	67.86	40	15.63	6.82	6.25	21.70	57.14	36
Average	33.92	68.83	40.75	17.38	8.65	7.81	19.89	55.53	36
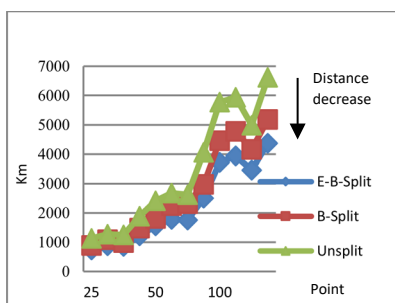
Fig. 1 Distance reduction of E-B-Split
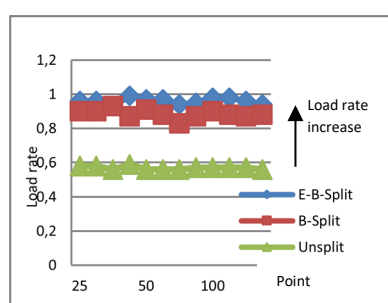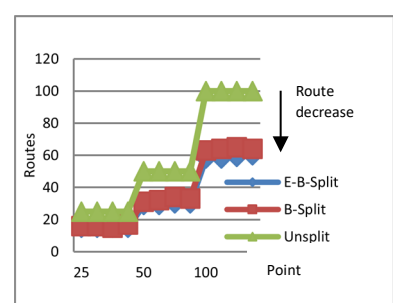

Fig. 2 Load rate increase of E-B-Split

Fig. 3 Routes reduction of E-B-Split

5. Conclusion

In this study, we developed a mathematical formulation to model the VRPSPDP problem. A two-stage construction heuristic approach was used under the strategy of "clustering first and routing later." In the first stage, the partitioning algorithms (B-Split and E-B-Split) based on MRISA and the coefficient of fine-tuning were employed to divide the customer domain into sub-domains. The minimum number of vehicles used was decided by the number of sub-domains. The split points and the corresponding values in each sub-domain were determined after the partitioning

algorithms. In the second stage, a modified C-W savings algorithm was adopted to check the load feasibility for every point of each route and to optimize the route distance in each sub-domain. Three cases studies with 12 instances per each from the reconstructed three Solomon datasets were employed to verify the feasibility and effectiveness of the proposed approaches (Unsplit, Both-Split and Enhanced-Both-Split). Our computation results proves that the vehicle routing problem with split deliveries and pickups is highly beneficial for transportation and logistics enterprises. The results of the comparison among these approaches reveal the following:

- The proposed algorithms of E-B-Split and B-Split for the VRPSPDP considerably reduce the total travel distance and the number of vehicles used, and increase the average loading rate.
- Particularly, the E-B-Split applied to the constructed Dataset 3 shows significant advantages over Unsplit. E-B-Split reduced the travel distance by 33.92 % on average, and increased the loading rate by 68.83 % on average. In addition, the number of vehicles used also decreased by 40.75 % on average. When compared with the results [9-11] of SDVRP, where the optimal route length and the optimal number of vehicles may be as little as half of the corresponding VRP, the results of the E-B-Split performed on Dataset 3 showed trends similar to those of SDVRP.
- The E-B-Split applied to the constructed Dataset 3 has some advantages over the B-Split. The travel distance was reduced by 17.38 % on average; the loading rate was increased by 8.65 % on average, and the number of vehicles used was decreased by approximately 10.50 % on average. These results prove that the E-B-Split can get more optimization results than the B-Split.
- The B-Split applied to the Dataset 3 can provide greater benefits than when it is applied to the Dataset 2 because Dataset 3 has larger customer demand values (about 55 % on average) than Dataset 2 (about 40 % on average).
- Routes are shaped similar to petals around the depot, and point splitting often occurs at the start or end of the sub-domains in the sweep.

The approaches used in this study could achieve the better computational results with a little time. But more work would be done in future to improve the accuracy and the extrapolation of the partitioning algorithms. The intelligent algorithms would be used to focus on obtaining more optimized solution in a bearable time to fit more complexity of problems.

In this study, time-depended problems (such as, customer service time windows, travel speeds, travel start time, etc.) were not considered. These are the very important factors of effecting the transportation fuel consumption and the carbon emission [36-38]. Therefore, multi-objective vehicle routing problem will be our next research target as well.

Acknowledgement

References

[1] Awaga, A.L., Xu, W., Liu, L., Zhang, Y. (2020). Evolutionary game of green manufacturing mode of enterprises under the influence of government reward and punishment, *Advances in Production Engineering & Management*, Vol. 15, No. 4, 416-430, doi: 10.14743/apem2020.4.375.

[2] Cucchiella, F., D'Adamo, I., Gastaldi, M., Koh, S.C.L., Santibanez-Gonzalez, E.D.R. (2020). Assessment of GHG emissions in Europe: Future estimates and policy implications, *Environmental Engineering and Management Journal*, Vol. 19, No. 1, 131-142, doi: 10.30638/eemj.2020.014.

[3] Sadati, M.E.H., Çatay, B. (2021). A hybrid variable neighborhood search approach for the multi-depot green vehicle routing problem, *Transportation Research Part E: Logistics and Transportation Review*, Vol. 149, Article No. 102293, doi: 10.1016/j.tre.2021.102293.

[4] Parragh, S.N., Doerner, K.F., Hartl, R.F. (2008). A survey on pickup and delivery problems, *Journal für Betriebswirtschaft,* Vol. 58, No. 1, 21-51, doi: 10.1007/s11301-008-0033-7.

[5] Dror, M., Trudeau, P. (1989). Savings by split delivery routing, *Transportation Science*, Vol. 23, No. 2, 141-145, doi: 10.1287/trsc.23.2.141.

[6] Dror, M., Trudeau, P. (1990). Split delivery routing, *Naval Research Logistics*, Vol. 37, No. 3, 383-402, doi: 10.1002/nav.3800370304.

[7] Dror, M., Laporte, G., Trudeau, P. (1994). Vehicle routing with split deliveries, *Discrete Applied Mathematics*, Vol. 50, No. 3, 239-254, doi: 10.1016/0166-218X(92)00172-I.

[8] Nagy, G., Wassan, N.A., Speranza M.G., Archetti, C. (2015). The vehicle routing problem with divisible deliveries and pickups, *Transportation Science*, Vol. 49, No. 2, 271-294, doi: 10.1287/trsc.2013.0501.

[9] Bektaş, T., Laporte, G. (2011). The pollution-routing problem, *Transportation Research Part B: Methodological,* Vol. 45, No. 8, 1232-1250, doi: 10.1016/j.trb.2011.02.004.

[10] Zhu, X., Zhao, Z., Yan, R. (2020). Low carbon logistics optimization for multi-depot CVRP with backhauls – Model and solution, *Tehnički Vjesnik – Technical Gazette,* Vol. 27, No. 5, 1617-1624, doi: 10.17559/TV-20200809211109.

[11] Archetti, C., Savelsbergh, M.W.P., Speranza, M.G. (2006). Worst-case analysis for split delivery vehicle routing problems, *Transportation Science*, Vol. 40, No. 2, 226-234, doi: 10.1287/trsc.1050.0117.

[12] Archetti, C., Savelsbergh, M.W.P., Speranza, M.G. (2008). To split or not to split: That is the question, *Transportation Research Part E: Logistics and Transportation Review,* Vol. 44, No. 1, 114-123, doi: 10.1016/j.tre.2006.04.003.

[13] Archetti, C., Speranza, M.G. (2008). The split delivery vehicle routing problem: A survey, In: Golden, B., Raghavan, S., Wasil, E. (eds.), *The vehicle routing problem: Latest advances and new challenges,* Springer, Boston, USA, 103-122, doi: 10.1007/978-0-387-77778-8_5.

[14] Archetti, C., Speranza, M.G. (2012). Vehicle routing problems with split deliveries, *International Transactions in Operational Research*, Vol. 19, No. 1-2, 3-22, doi: 10.1111/j.1475-3995.2011.00811.x.

[15] Archetti, C., Speranza, M.G., Hertz, A. (2006). A tabu search algorithm for the split delivery vehicle routing problem, *Transportation Science*, Vol. 40, No. 1, 64-73, doi: 10.1287/trsc.1040.0103.

[16] Archetti, C., Speranza, M.G., Savelsbergh, M.W.P. (2008). An optimization-based heuristic for the split delivery vehicle routing problem, *Transportation Science*, Vol. 42, No. 1, 22-31, doi: 10.1287/trsc.1070.0204.

[17] Belenguer, J.M., Martinez, M.C., Mota, E. (2000). A lower bound for the split delivery vehicle routing problem, *Operations Research*, Vol. 48, No. 5, 801-810, doi: 10.1287/opre.48.5.801.12407.

[18] Wilck IV, J.H., Cavalier, T.M. (2012). A construction heuristic for the split delivery vehicle routing problem, *American Journal of Operations Research*, Vol. 2, No. 2, 153-162, doi: 10.4236/ajor.2012.22018.

[19] Liu, W., Yang, F., Li, M., Chen, P. (2012). Clustering algorithm for split delivery vehicle routing problem, *Control and Decision*, Vol. 27, No. 4, 535-541, doi: 10.13195/j.cd.2012.04.57.liuwsh.017.

[20] Archetti, C., Bianchessi, N., Speranza, M.G. (2015). A branch-price-and-cut algorithm for the commodity constrained split delivery vehicle routing problem, *Computers & Operations Research,* Vol. 64, 1-10, doi: 10.1016/j.cor.2015.04.023.

[21] Ozbaygin, G., Karasan, O., Yaman, H. (2018). New exact solution approaches for the split delivery vehicle routing problem, *EURO Journal on Computational Optimization*, Vol. 6, No. 1, 85-115, doi: 10.1007/s13675-017-0089-z.

[22] Min, J., Jin, C., Lu, L. (2018). A three-stage approach for split delivery vehicle routing problem solving, In: *Proceedings of 8th International Conference on Logistics, Informatics and Service Sciences (LISS),* Toronto, Canada, 1-6, doi: 10.1109/LISS.2018.8593226.

[23] Min, J.N., Jin, C., Lu, L.J. (2019). Maximum-minimum distance clustering method for split delivery vehicle routing problem: Case studies and performance comparisons, *Advances in Production Engineering & Management*, Vol. 14, No. 1, 125-135, doi: 10.14743/apem2019.1.316.

[24] Mitra, S. (2005). An algorithm for the generalized vehicle routing problem with backhauling, *Asia-Pacific Journal of Operational Research*, Vol. 22, No. 2, 153-169, doi: 10.1142/S0217595905000522.

[25] Mitra, S. (2008). A parallel clustering technique for the vehicle routing problem with split deliveries and pickups, *Journal of the Operational Research Society*, Vol. 59, No. 11, 1532-1546, doi: 10.1057/palgrave.jors.2602500.

[26] Wang, K.F. (2012). *Research of vehicle routing problem with nodes having double demands*, Doctoral dissertation, University of Shanghai for Science and Technology, Shanghai, China.

[27] Wang, K., Ye, C., Ning, A. (2015). Achieving better solutions for vehicle routing problem involving split deliveries and pickups using a competitive decision algorithm, *Asia-Pacific Journal of Operational Research,* Vol. 32, No. 4, Article No.1550022, doi: 10.1142/S0217595915500220.

[28] Yin, C., Bu, L., Gong, H. (2013). Mathematical model and algorithm of split load vehicle routing problem with simultaneous delivery and pickup, *International Journal of Innovative Computing, Information and Control*, Vol. 9, No. 11, 4497-4508.

[29] Wang, Y., Ma, X.-L., Lao, Y.-T., Yu, H.-Y., Liu, Y. (2014) A two-stage heuristic method for vehicle routing problem with split deliveries and pickups, *Journal of Zhejiang University SCIENCE C*, Vol. 15, No. 3, 200-210, doi: 10.1631/jzus.C1300177.

[30] Polat, O. (2017). A parallel variable neighborhood search for the vehicle routing problem with divisible deliveries and pickups, *Computers & Operations Research,* Vol. 85, 71-86, doi: 10.1016/j.cor.2017.03.009.

[31] Qiu, M., Fu, Z., Eglese, R., Tang, Q. (2018). A tabu search algorithm for the vehicle routing problem with discrete split deliveries and pickups, *Computers & Operations Research,* Vol. 100, 102-116, doi: 10.1016/ j.cor. 2018. 07. 021.

[32] Min, J., Lu, L., Jin, C. (2022). A two-stage heuristic approach for split vehicle routing problem with deliveries and pickups, In: Shi, X., Bohács, G., Ma, Y., Gong, D., Shang, X. (eds.), *LISS 2021. Lecture Notes in Operations Research,* Springer, Singapore, 479-490, doi: 10.1007/978-981-16-8656-6_43.

[33] Gillett, B.E., Miller, L.R. (1974). A heuristic algorithm for the vehicle-dispatch problem, *Operations Research*, Vol. 22, No. 2, 340-349, doi: 10.1287/opre.22.2.340.

[34] Min, J.N., Jin, C., Lu, L.J. (2019). Split-delivery vehicle routing problems based on a multi-restart improved sweep approach, *International Journal of Simulation Modeling*, Vol. 18, No. 4, 708-719, doi: 10.2507/IJSIMM8(4)CO19.

[35] Díaz, B.D. VRP Web, from *http://www.bernabe.dorronsoro.es/vrp/*, accessed May 12, 2019.

[36] Zhao, P.X., Luo, W.H., Han, X. (2019). Time-dependent and bi-objective vehicle routing problem with time windows, *Advances in Production Engineering & Management*, Vol. 14, No. 2, 201-212, doi: 10.14743/apem2019.2.322.

[37] Barros, L., Linfati, R., Escobar, J.W. (2020). An exact approach for the consistent vehicle routing problem (ConVRP), *Advances in Production Engineering & Management*, Vol. 15, No. 3, 255-266, doi: 10.14743/apem2020.3.363.

[38] Liu, M.L., Zhang, C., Wu, Q.L., Meng, B.R. (2021). Vehicle routing problem with soft time windows of cargo transport O2O platforms, *International Journal of Simulation Modelling*, Vol. 20, No. 2, 351-362, doi: 10.2507/IJSIMM20-2-564.

Appendix A

Whole-word-descriptions of all the abbreviations used in the paper

VRP	Vehicle Routing Problem
SDVRP	Split Delivery Vehicle Routing Problem
VRPSDP	Vehicle Routing Problem with Simultaneously Delivery and Pickups
VRPSPDP	Vehicle Routing Problem with (Simultaneously) Split Delivery and Pickups
SA-VRP	Sweep Algorithm for VRP
SA-SDVRP	Sweep Algorithm for SDVRP
SA-VRPSDP	Sweep Algorithm for VRPSDP
SA-VRPSPDP	Sweep Algorithm for VRPSPDP
MRI	Multi Restart Iterative
MRISA	MRI +SA Multi Restart Iterative Sweep Algorithm
MRISA-Unsplit	Unsplit based on MRI +SA
MRISA-B-Split	B-Split based on MRI +SA
MRISA-E-B-Split	E-B-Split based on MRI +SA
Unsplit	Non split
B-Split	Split for Both Deliveries and Pickups
E-B-Split	Enhanced Both Split (Fine-Turning Split for Both Deliveries and Pickups)
C-W savings	Clarke-Wright savings

Calendar of events

- 9th International Engine Congress 2022, February 22-23, Baden-Baden, Germany, (hybrid event).

- 7th International Conference on Manufacturing, Material and Metallurgical Engineering, March 18-20, 2022, Osaka, Japan.

- The 10th IIAE International Conference on Industrial Application Engineering, March 26-30, 2022, Matsue, Japan (hybrid event).

- 50th SME North American Manufacturing Research Conference, June 27 to July 1, 2022, West Lafayette, USA.

- 16th International Conference on Micromachining Technology, October 17-18, 2022, Dubai, United Arab Emirates.

Notes for contributors

General

Articles submitted to the *APEM journal* should be original and unpublished contributions and should not be under consideration for any other publication at the same time. Manuscript should be written in English. Responsibility for the contents of the paper rests upon the authors and not upon the editors or the publisher. The content from published paper in the *APEM journal* may be used under the terms of the Creative Commons Attribution 4.0 International Licence (CC BY 4.0). For most up-to-date information please see the APEM journal homepage *apem-journal.org*.

Submission of papers

A submission must include the corresponding author's complete name, affiliation, address, phone and fax numbers, and e-mail address. All papers for consideration by *Advances in Production Engineering & Management* should be submitted by e-mail to the journal Editor-in-Chief:

Miran Brezocnik, Editor-in-Chief
UNIVERSITY OF MARIBOR
Faculty of Mechanical Engineering
Chair of Production Engineering
Smetanova ulica 17, SI – 2000 Maribor
Slovenia, European Union
E-mail: editor@apem-journal.org

Manuscript preparation

Manuscript should be prepared in *Microsoft Word 2010* (or higher version) word processor. *Word .docx* format is required. Papers on A4 format, single-spaced, typed in one column, using body text font size of 11 pt, should not exceed 12 pages, including abstract, keywords, body text, figures, tables, acknowledgements (if any), references, and appendices (if any). The title of the paper, authors' names, affiliations and headings of the body text should be in *Calibri* font. Body text, figures and tables captions have to be written in *Cambria* font. Mathematical equations and expressions must be set in *Microsoft Word Equation Editor* and written in *Cambria Math* font. For detail instructions on manuscript preparation please see instruction for authors in the *APEM journal* homepage *apem-journal.org*.

The review process

Every manuscript submitted for possible publication in the *APEM journal* is first briefly reviewed by the editor for general suitability for the journal. Notification of successful submission is sent. After initial screening, and checking by a special plagiarism detection tool, the manuscript is passed on to at least two referees. A double-blind peer review process ensures the content's validity and relevance. Optionally, authors are invited to suggest up to three well-respected experts in the field discussed in the article who might act as reviewers. The review process can take up to eight weeks on average. Based on the comments of the referees, the editor will take a decision about the paper. The following decisions can be made: accepting the paper, reconsidering the paper after changes, or rejecting the paper. Accepted papers may not be offered elsewhere for publication. The editor may, in some circumstances, vary this process at his discretion.

Proofs

Proofs will be sent to the corresponding author and should be returned within 3 days of receipt. Corrections should be restricted to typesetting errors and minor changes.

Offprints

An e-offprint, i.e., a PDF version of the published article, will be sent by e-mail to the corresponding author. Additionally, one complete copy of the journal will be sent free of charge to the corresponding author of the published article.

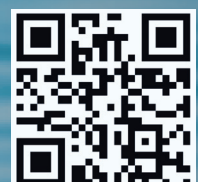# APEM *journal*

Advances in Production Engineering & Management

Contents

apem-journal.org